

Ion-Exchange and Charge Transport in Films of Conducting Polymer and Composite

Thesis submitted for the degree of

Doctor of Philosophy

at the University of Leicester

by

Asuman UNAL

Department of Chemistry

University of Leicester

2017

Ion-Exchange and Charge Transport in Films of Conducting Polymer and Composite

Asuman UNAL

Abstract

This thesis was concerned with the improvement of novel modified electrodes based on polyaniline (Pani) and its copolymers with *o*-aminophenol (*o*-AP) and *o*-toluidine (*o*-OT) and the investigation of their defluoridation properties, and further with the enhancement of the charge transport of Pani and polypyrrole (PPy) via multiwall carbon nanotubes (MWCNTs) in Ethaline. The principle of electrochemical ion-exchange modified electrodes is based on the doping/dedoping process of conducting polymer films. This feature makes it possible to remove undesirable ions, such as fluoride, from aqueous solution. The fabrication of Pani and its copolymers with *o*-AP/*o*-OT, carried out under optimal conditions by EQCM, gave an excellent opportunity to test for the removal of fluoride ions at pH 6.60 from water without chemical contamination of the copolymer. Pani, and its copolymers with *o*-AP/*o*-OT, poly(aniline-co-*o*-aminophenol) (Pani-PAP) and poly(aniline-co-*o*-toluidine) (Pani-POT), can theoretically take up about **91.2 mg g⁻¹** fluoride ions per redox site of polymer film. Experiments indicated that the Pani, Pani-PAP and Pani-POT films removed **51.6 ± 1.0 mg g⁻¹**, **65.0 ± 0.6 mg g⁻¹** and **66.8 ± 1.8 mg g⁻¹**, respectively, of fluoride ions per redox site of each (co)polymer film. This demonstrates that the copolymerisation of aniline with its derivatives enhanced the defluoridation properties of Pani. Pani and PPy are also promising materials for energy storage devices. The presence of MWCNTs to some extent enhanced both the electrochemical properties and mechanical stability in Ethaline, which maintains high efficiency and high-quality depositions through the use of the EQCM technique. The specific mass capacitances of these composite films were determined to be **1170.1 ± 44.7 F g⁻¹** and **120.5 ± 5.4 F g⁻¹** for Pani/MWCNTs and PPy/MWCNTs, respectively.

Acknowledgements

I express my deep sense of gratitude to my supervisor Prof. A. Robert Hillman for his guidance, patience, encouragement, kind endless help, and support throughout my PhD course. It was a great honour to work under his supervision. I am also thankful to Prof. Karl S. Ryder, whose expertise and support made this project possible for me.

I am also thankful to Salih Cihangir, Abdulcabbar Yavuz, and Hani Ismail for their kind co-operation, excellent inspiration, being good friends, and useful discussions.

I also would like to thank to all the other faculty of University of Leicester & staff members of Department of Chemistry for their support. It was a pleasure working with them.

Special thanks to my parents, Erdal and Nergiz Unal, for being a source motivation. This course cannot be accomplished without the inspiration, continuous support, tolerance, and good advice they have offered me.

Last, but not least, I also wish to express my deep sense of gratitude to the Ministry of National Education in Turkey for providing financial support throughout my PhD project.

Contents

Chapter I: Introduction	1
1.1. Introduction	1
1.2. Electronically Conducting Polymers	2
1.2.1. Overview	2
1.2.2. Polyaniline	3
1.2.2.1. Overview	3
1.2.2.2. Synthesis of polyaniline	5
1.2.3. Polypyrrole	9
1.2.3.1. Overview	9
1.2.3.2. Synthesis of polypyrrole	10
1.2.4. Poly-<i>o</i>-aminophenol	11
1.2.4.1. Overview	11
1.2.5. Poly-<i>o</i>-toluidine	11
1.2.5.1. Overview	11
1.3. Copolymerization of Electronically Conducting Polymers	12
1.4. Composite Materials of Electronically Conducting Polymers	13
1.4.1. Composite Materials of Conductive Polymers with CNTs	13
1.5. Ion and Solvent Transfer of Electronically Conducting Polymers	15
1.6. Deep Eutectic Solvents	16
1.7. Project Objectives	18
1.8. References	19

Chapter II: Methodology	33
2.1. Introduction	33
2.2. Electrochemistry and Electrochemical Techniques	33
2.2.1. Mass Transfer	35
2.3. Cyclic Voltammetry	36
2.3.1. Overview	36
2.3.2. Data Interpretation	37
2.4. Chronoamperometry	39
2.4.1. Overview	39
2.4.2. Data Interpretation	40
2.5. Quartz Crystal Microbalance (QCM)	40
2.5.1. Overview	40
2.5.2. The Piezoelectric Effect	41
2.5.3. The Quartz Crystal Orientation of Cut	42
2.5.4. Sauerbrey Equation	43
2.5.5. The Effect of Excess Mass and the Surface Roughness	46
2.5.6. Electrochemical Quartz Crystal Microbalance (EQCM)	46
2.5.7. The Effect of Viscosity	47
2.6. Scanning Electron Microscopy	48
2.7. FTIR	49
2.8. References	50

Chapter III: Experimental and Data Analysis Process	52
3.1. Introduction	52
3.2. Materials and Reagents	52
3.2.1. Storage Conditions	52
3.2.2. Preparation of Ethaline	54
3.2.3. Preparation of MWCNT-COOH	55
3.2.4. Preparation of Monomer Solutions	55
3.3. Techniques and Procedures	57
3.3.1. Electrochemical Techniques	59
3.3.1.1. Cyclic voltammetry	60
3.3.1.2. Electrochemical crystal microbalance	61
3.3.2. Procedures	63
3.3.2.1. The deposition of conductive films	63
3.3.2.2. The electroactive characterisation of the conductive films	64
3.3.2.3. The characterisation of the ion-Exchange Properties of the conductive Films	64
3.3.3. Surface Characterisation Techniques	65
3.3.3.1. Scanning electron microscopy and 3D Profiler	65
3.3.4. FTIR	65
3.3.5. Data Analysis	65
3.3.5.1. Surface coverage and thickness of the final films	65
3.3.5.2. The apparent molar mass (M_{app}) of the final films and the species transferred during redox cycling	66
3.3.5.3. The ohmic resistance of the polymer films	68
3.3.5.4. Mass specific capacitance from cyclic voltammetry	68
3.4. References	68

Chapter IV: The growth dynamic of poly(aniline-co-o-aminophenol) copolymer film and the investigation of its defluoridation properties by means of EQCM	70
4.1. Introduction	70
4.1.1. Overview	70
4.1.2. Defluoridation of Water by Conducting Polymer Films	71
4.1.3. Aims and Objectives	73
4.1. Results and Discussions	73
4.2.1. The Growth Dynamic of Pani and PAP Films	73
4.2.1.1. Polyaniline film	73
4.2.1.2. Poly(o-aminophenol) film	77
4.2.1.3. Comparison of the Pani and the PAP polymer films	79
4.2.2. The Copolymerization of Pani-PAP Copolymer Films	80
4.2.2.1. Copolymerization of Pani-PAP copolymer films by chronoamperometry	80
4.2.2.2. The growth of Pani-PAP copolymer films by means of EQCM	81
4.2.2.3. Characterisation of the Pani-PAP (90:10) copolymer film	86
4.2.3. The Removal of Fluoride Ions	87
4.2.3.1. Removal by the Pani Polymer film	88
4.2.3.2. Removal by the Pani-PAP (90:10) copolymer film	89
4.2.4. Regeneration of the Polymer and the Copolymer Films	94
4.2.4.1. The Pani film	94
4.2.4.2. The Pani-PAP (90:10) copolymer film	96
4.2.5. The Surface Characterisation of the Polymer and the Copolymer Films	97
4.2.5.1. Scanning electron microscopy	97
4.2.6. FTIR	98
4.3. Conclusion	100

4.4. References	103
------------------------	------------

Chapter V: The electrochemical deposition of poly(aniline-co-o-toluidine) copolymer film and film population changes in neutral medium	106
---	------------

5.1. Introduction	106
--------------------------	------------

5.1.1. Overview	106
-----------------	-----

5.1.2. Aims and Objectives	107
----------------------------	-----

5.2. Results and Discussion	107
------------------------------------	------------

5.2.1. Electrochemical Deposition of the Poly(o-toluidine) Film	107
---	-----

5.2.1.1. Comparison of the Pani, the PAP and the POT polymer films	111
--	-----

5.2.2. Copolymerization of the Pani-POT	113
---	-----

5.2.2.1. The copolymerization of the Pani-POT by chronoamperometry	113
--	-----

5.2.2.3. The electrochemical deposition of the Pani-POT copolymer films by means of EQCM	114
--	-----

5.2.2.4. Characterisation of the Pani-POT copolymer films	119
---	-----

5.2.3. The Removal of Fluoride Ions	121
-------------------------------------	-----

5.2.3.1. Using the POT polymer film	121
-------------------------------------	-----

5.2.3.2. Using the Pani-POT copolymer film	121
--	-----

5.2.4. Regeneration of the Pani-POT Copolymer Film	128
--	-----

5.2.5. The Surface Characterisation of the Polymer and the Copolymer Films	129
--	-----

5.2.5.1. Scanning electron microscopy	129
---------------------------------------	-----

5.2.6. FTIR	130
-------------	-----

5.2.7. Comparison of the Pani-PAP and the Pani-POT copolymer films	132
--	-----

5.3. Conclusion	133
------------------------	------------

5.4. References	136
------------------------	------------

Chapter VI: The electrochemical deposition of Pani film in the presence of MWCNTs and its redox switching in Ethaline_ 137

6.1. Introduction	137
6.1.1. Overview	137
6.1.2. Aims and Objectives	138
6.2. Results and Discussions	139
6.2.1. Electrochemical Deposition of the Pani Film in the Presence of MWCNTs in Aqueous Solution	139
6.2.1.1. Cyclic voltammetry experiments	139
6.2.1.2. EQCM experiments on the electrochemical deposition of the Pani/MWCNTs films	140
6.2.1.3. Characterisation of the Pani/MWCNTs composite films	145
6.2.1.4. Surface characterisation of the Pani and the Pani/MWCNTs films	147
6.2.2. Electrochemical Deposition of the Pani/MWCNTs in Ethaline	149
6.2.2.1. Charge and discharge characterisation of Pani/MWCNTs films	159
6.2.3.2. Surface characterisation of the Pani and the Pani/MWCNTs films	163
6.2.3. FTIR	165
6.3. Conclusion	167
6.4. References	169

Chapter VII: The enhancement of electrochemical stability of PPy with MWCNTs in aqueous and non-aqueous media ___ 172

7.1. Introduction	172
7.1.1. Overview	172
7.1.2. Aims and Objectives	173
7.2. Results and Discussions	173

7.2.1. Electrochemical deposition of PPy films in the presence of MWCNTs in aqueous medium	173
7.2.1.1. Characterisation of the PPy/MWCNTs composite films	178
7.2.1.2. Surface characterisation of the PPy and the PPy/MWCNTs films	180
7.2.2. Electrochemical deposition of PPy film in the presence of MWCNTs in Ethaline	181
7.2.2.1. Characterisation of the PPy and the PPy/MWCNTs films	187
7.2.2.2. Surface Characterisation of the PPy and the PPy/MWCNTs Films	189
7.2.3. FTIR	191
7.3. Conclusion	193
7.4. References	194
Chapter VIII: Conclusions and Future Work	196
8.1. Conclusions	196
8.2. Future Work	201
8.3. References	202

Abbreviations

A	The electrode surface area (cm^2)
α	The solvent molecules transferred
c	A constant for AT-cut crystals
D	The diffusion coefficient ($\text{cm}^2 \text{s}^{-1}$)
Δf	The frequency change of the quartz crystal (Hz)
Δm	The mass change of the quartz crystal (g)
Δw	The damping (Hz)
ΔV	The voltage variation during redox reaction (V)
E	The electrode potential (V)
E_{oxi}	The oxidation potential (V)
E_{red}	The reduction potential (V)
E_{poly}	The polymerisation potential (V)
$E_e - E_s$	The driving force (V)
$E_s - E_{ref}$	The potential drop (V)
F	Faraday constant ($96\,485 \text{ C mol}^{-1}$)
f_o	The resonance frequency of a quartz crystal (Hz)
h	Thickness of polymer film (μm)
i	Current (A)
i_p	The peak current (A)
j	Current density (A cm^{-2})
M_{app}	The apparent molar mass (g mol^{-1})

m	The mass density ($\mu \text{ cm}^{-2}$)
μ_q	The crystal shear modulus (g cm^{-1})
MSC	Mass specific capacitance (F g^{-1})
N	Harmonic number
n_L	The viscosity of the liquid
v	The scan rate (V s^{-1})
ρ_q	The crystal density (g cm^{-3})
ρ_L	The density of the product (g cm^{-3})
ρ	density of a polymer (g cm^{-3})
Q	The charge density (C cm^{-2})
Q_{anodic}	The charge passed upon oxidation (C)
$Q_{cathodic}$	The charge passed upon reduction (C)
t	Time (s)
Γ	The surface coverage of a polymer film (mol cm^{-2})
V	The volume of the product (cm^3)
Y_{peak}	The admittance of the quartz crystal (mS)
Z_{peak}	The ohmic resistance of a polymer film (Ω)
$3D$	3D profiler
An	Aniline
$Ag/AgCl$	Silver/silver chloride reference electrode
AP	<i>o</i> -aminophenol
A_{oxi}	The oxidized form of the electroactive species
B_{red}	The reduced form of the electroactive species
$ChCl$	Choline Chloride

<i>CNTs</i>	Carbon Nanotubes
<i>DESs</i>	Deep eutectic solvents
<i>EQCM</i>	Electrochemical quartz microbalance
<i>ETH200</i>	Ethaline 200
<i>ETH400</i>	Ethaline 400
<i>FTIR</i>	Fourier transform infrared spectroscopy
<i>HBD</i>	Hydrogen bond donor
<i>ILs</i>	Ionic liquids
<i>MWCNTs</i>	Multiwall carbon nanotubes
<i>OT</i>	<i>o</i> -toluidine
<i>Pani</i>	Polyaniline
<i>Pani-PAP</i>	Poly(aniline-co- <i>o</i> -aminophenol)
<i>Pani-POT</i>	Poly(aniline-co- <i>o</i> -toluidine)
<i>PPy</i>	Polypyrrole
<i>PAP</i>	Poly- <i>o</i> -aminophenol
<i>POT</i>	Poly- <i>o</i> -toluidine
<i>QCM</i>	Quartz crystal microbalance
<i>RE</i>	Reference electrode
<i>RTILs</i>	The room temperature ionic liquids
<i>SEM</i>	Scanning electron microscopy
<i>SWCNTs</i>	Singlewall carbon nanotubes
<i>TSM</i>	Thickness shear mode
<i>WE</i>	Working electrode

Chapter I:

Introduction

1.1. Introduction

A “Chemically modified electrode” was initially identified by Murray and co-workers¹ in 1975, who described that a variety of material can be immobilized onto an electrode surface to enhance its chemical and physical properties. It was also called a “surface modified electrode”.² This modification can be performed by adsorption³⁻⁵ and chemical or covalent⁶⁻¹⁰ bonding. Other early studies regarding modified electrodes were carried out by Lane and Hubbard,^{11,12} who defined the modified surface effects for electrochemical reactions at the electrode surfaces. Among such modified electrodes, electron-conducting polymer-modified electrodes are commonly preferred, with unique electroactivity towards oxidation and reduction of molecules on the electrode surface.^{13,14} Electron-conducting polymers do not only modify the surface of the electrode material but also provide an electrochemically stable surface.^{15,16} In addition to these benefits, the modified polymers maintain their physical characteristics when immobilized on the electrode surface.^{2, 14}

The pioneer studies of polymer-modified electrodes were conducted by Miller and van de Mark,^{15,16} who adsorbed poly-*p*-nitrostyrene onto platinum, and the 3,5-dinitrobenzoyl moiety onto a polypeptide layer on platinum, respectively. Bard and co-workers performed subsequent research,^{17,18} who synthesized polyvinyl ferrocene (PVF) on platinum and poly(methacryl chloride) on platinum and SnO₂ electrodes with corresponding anodic oxidation of polymers. The latter research highlighted the characteristic properties of polymers needed to allow their use with modified electrodes across a wide range of applications.

Electron-conducting polymers are classified into two groups based on the mode of electron transfer; redox polymers, and electronically conducting polymers.¹⁹ Redox polymers are identified by the presence of electrostatically- and spatially- localized redox sites that can be oxidised and reduced, and electrons can be transferred between neighbouring redox sites by an electron exchange reaction.¹⁹ In contrast to redox

polymers, electronically conducting polymers have a conjugated backbone, with the motion of the delocalized electrons, along with the backbone chain.²⁰ We deal with electronically conducting polymers in the research presented in this thesis.

1.2. Electronically Conducting Polymers

1.2.1. Overview

The story of electronically conducting polymers began in 1977 with the discovery by Heeger, MacDiarmid and Shirakawa that polyacetylene has a high electronic conductivity.²¹ This discovery earned these researchers the Nobel Prize in Chemistry 23 years later.²¹ Furthermore, the discovery of polyacetylene as a conducting polymer led to the emergence of a new class of conducting polymer, examples, such as polyaniline,²² polypyrrole,²³ poly-*o*-toluidine, poly-*o*-aminophenol, polythiophene,²⁴⁻²⁶ polyfluorene,²⁷ poly(5-aminoquinoline)²⁸ and poly[bis(phenylamino)disulphide],²⁹ are shown in figure 1.1. Electronically conducting polymers have a wide range of application in sensors,³⁰⁻³² electrochromic devices,³⁰ corrosion protection,³³⁻³⁷ energy storage,^{30,38} capacitors and artificial muscles.^{19,39}

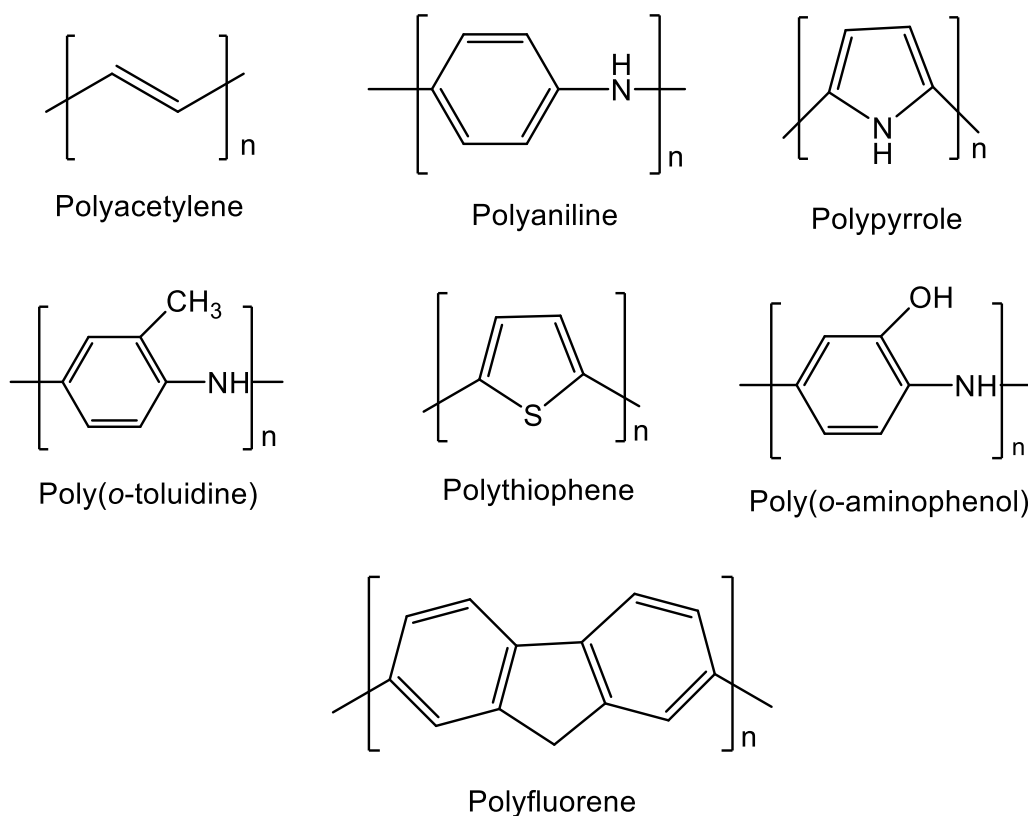


Figure 1.1. The chemical structure of various conducting polymers

Conducting polymers can in an insulating form.⁴⁰ They can be converted to the conducting form through electrochemical redox reactions.¹³ During such a redox reaction, the conducting polymer is charged in its oxidation state (*p-doping*) or discharged in its reduced state (*de-doping*).²⁰ Charging/discharging through the polymer chain enhances its conductivity. This charge transfer processing takes place through the π -electron systems of the polymer. By applying an oxidation (or reduction) potential, conducting polymers can easily be changed between their insulating and conducting forms.²⁰ This electron transfer takes place on the surface of a modified electrode and is accompanied the insertion/expulsion of counter ion in or out of the film to maintain electroneutrality with the polymer matrix. The movement of counter ion can be the results of the ingress/egress of neutral species such as solvent molecules.⁴⁰

Conducting polymers can be prepared by both chemical and electrochemical redox reactions from their corresponding monomers.^{41,42} Electrochemical polymerization is preferable, particularly in the acquisition of, for example, polymer-modified electrodes and thin-layer sensors because of the potential, and thus the deposition characteristic can be controlled during the reaction.¹⁹ Chemical polymerization is preferable when a large amount of polymer is required.⁴²

It is generally agreed in the literature that the electrochemical polymerization of conducting polymers is a three-step process. In the first step, monomers are oxidized at the anode resulting in the formation of reactive cationic radicals and soluble oligomers, this takes place in the diffusion layer. The second step includes the deposition of oligomers, which occurs through a nucleation and growth process. The last step is the propagation of the polymer chain by solid-state polymerization.^{40, 41} The polymerization of conducting polymers is mostly affected by the solvent⁴³ used, the nature of counter ions, the temperature, and the nature of the polymer itself.¹⁴

1.2.2. Polyaniline

1.2.2.1. Overview

Polyaniline (Pani) is the most considered one of the most promising materials among conducting polymers in terms of excellent reversibility it shows for oxidation-reduction

reactions., its ease of preparation, high conductivity, environmental stability, and its existence in different oxidation states.⁴⁴ The presence of a sterically flexible -NH- group in the polymer backbone makes Pani particularly favourable because it contributes to a π -bond formation, which provides environmental stability in addition to stabilizing the protonation and deprotonation of Pani.⁴⁵ Although the conducting properties of Pani were discovered in the early 1980s, it had been known as ‘aniline black’ as far back as the 1830s.⁴⁶ The promising properties of Pani lead to the emergence of important applications in rechargeable batteries, electrode surface modifications, electrochromic devices, display devices, corrosion protection, chemical and biosensors, and supercapacitors.⁴⁶

Unlike other known conducting polymers, Pani can be found in three different forms depending on its oxidation state. They are leucoemeraldine, its fully reduced form (all nitrogen atoms are amine groups, -NH-); emeraldine, its half-oxidized form, which consists of equal amounts of amine and imine groups, and pernigraniline, its fully oxidized form (all the nitrogen atoms are imine, =NH-).^{41,45} The last form is unstable in an aqueous medium and the polymer easily degrades to benzoquinone and various oligomers. Benzoid and quinoid units (the oxidized forms of the benzoid structure) exist in certain oxidation states of Pani.⁴⁶ The conductivity and colour of Pani are changed with the transitions between its various forms. The conducting form of Pani, emeraldine salt (green), is oxidized to the pernigraniline salt (dark blue). The pernigraniline salt can be converted to a pernigraniline base by treatment with a base. The emeraldine salt can be converted to emeraldine base form by an alkaline solution or its yellow leucoemeraldine form by a decrease in conductivity.⁴¹

Among the various Pani forms, emeraldine exhibits high conductivity when doped with a salt or protonated with acid, which provides protonated imine nitrogen atoms in the polymer chain,²⁹ whereas other known conducting polymers have a radical cation at the carbon atom. The involvement of the nitrogen atoms in the formation of a radical cation increases the conjugation of the polymer. This protonation also contributes to the conductivity of polymer, in addition to the oxidation of the aniline itself.⁴¹ The conductivity of Pani is increased by doping from $\sigma \leq 10^{-10}$ S cm⁻¹ in its insulating form to $\sigma \geq 1$ S cm⁻¹ in its doped form.^{41,47} The doping process affects not only conductivity but also the morphology of the polymers.

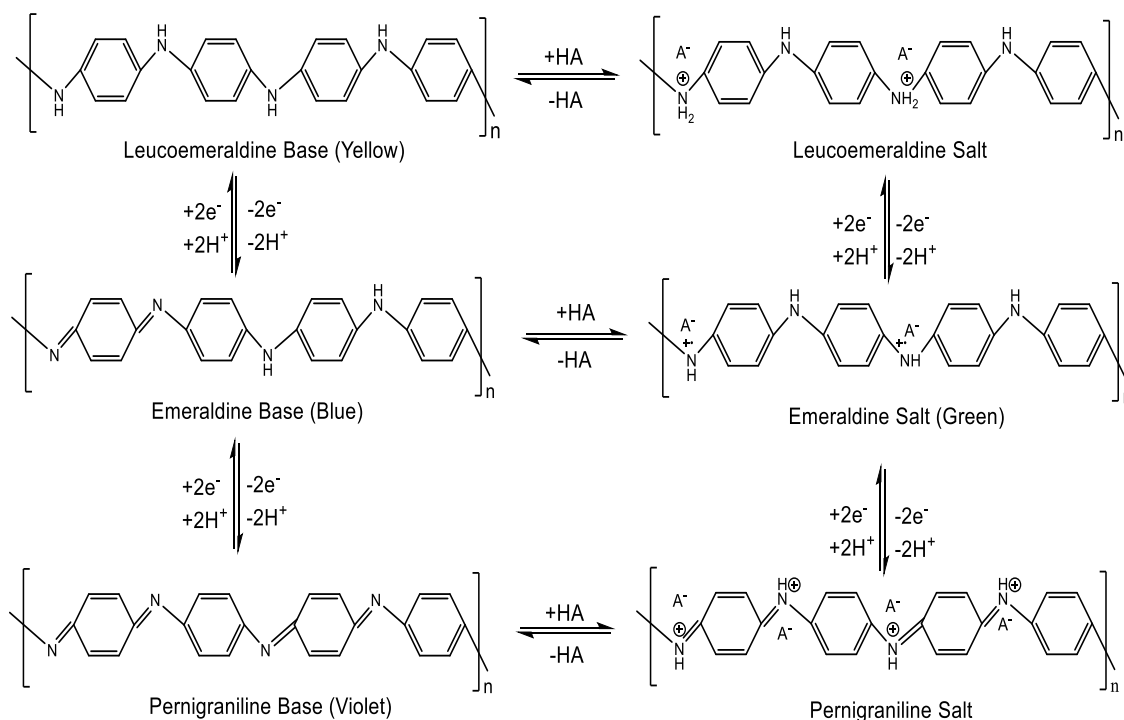


Figure 1.2. The structures of Pani forms in different oxidation states

Pani can be readily switched between its base and salt forms by treatment with acidic or basic solutions as illustrated in figure 1.2. Imine sites of the emeraldine base can be doped to form the conducting form of Pani, an emeraldine salt.^{41, 46}

1.2.2.2. Synthesis of polyaniline

There are various polymerization techniques reported in the literature regarding the synthesis of Pani from aniline monomers, which can be classified as chemical polymerization,^{46,48} electrochemical polymerization,⁴⁸ vapour-phase deposition, photochemically-initiated polymerization, enzyme-catalysed polymerization, and polymerization using an electron acceptor. However, among them, electrochemical polymerization is the most attractive method of producing Pani because of the ability to control the describe properties of Pani-modified electrodes (e.g. morphology, thickness, and electrical properties) by suitable choice of optimal conditions.^{41, 46}

The polymerization of aniline in acidic medium is suitable, although there are several reports in the literature to indicate that polymerization in neutral⁴⁹ and alkali media are also possible. When the pH is elevated (pH>4), conjugated oligomeric materials tend to form in larger amounts, which is undesirable. Contrary to basic medium, acidic medium

increases the solubility of aniline in aqueous solutions, which is favourable for the productions of the emeraldine form via electrochemical techniques. The formation of the emeraldine salt does not occur at higher pH, indicating that a non-electroactive polymer will have been synthesized.⁴⁴⁻⁴⁶

The electrochemical polymerization of aniline can be also performed in organic solvents and ionic liquids⁵⁰ although it has been routinely carried out in aqueous electrolytes.⁴¹ It has recently been reported in the literature that the polymerization of aniline in ionic liquid provides for the synthesis of conductive and high-quality films on the electrode surface.⁴¹

A wide range of studies on the polymerization of aniline has been reported in the literature. They have found that apart from the necessity of a strongly acidic medium, the nature of the counter ion⁵¹⁻⁵³ and electrode material⁵⁴ and electrolyte composition⁵⁵⁻⁵⁷ also have a significant effect on the electrochemical polymerization of aniline. They also affect the electrochemical properties and morphology of the Pani film and the degradation process.⁴⁶ The presence of 'large' counter ions, such as sulphate and nitrate, produce more swollen and open-structure films, unlike 'small' counter ions, such as ClO_4^- and BF_4^- , which results in films that are more compact.⁴¹ Additionally, it has been reported that the nature of the acid itself can also influence the properties of the polymeric films. Sulphuric acid increases the growth rate of the Pani by a factor of 2.7-2.8 and provides a smooth morphology in comparisons with perchloric, nitric and hydrochloric acid, which give porous and granular structures.⁴⁶

The electrochemical polymerization mechanism and kinetics of aniline have been extensively investigated. It is generally acknowledged that the initial step of the polymerization of aniline is the formation of aniline cation radicals by applying an anodic oxidation potential.⁴¹ The aniline cation radicals have three resonance forms,^{41,45,46} as shown in figure 1.3.

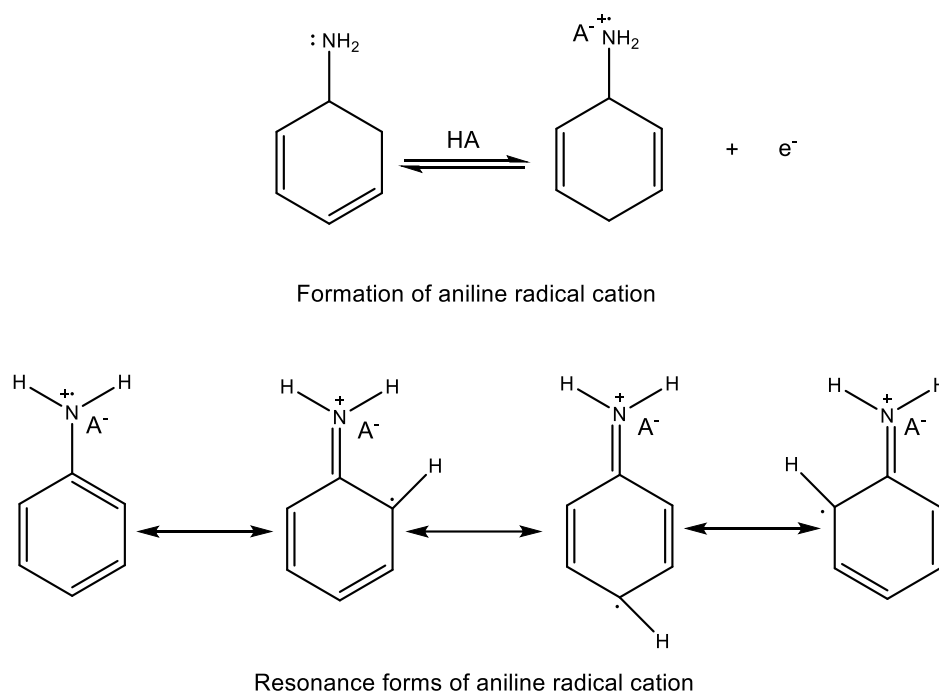


Figure 1.3. The aniline radical cation and its resonance form

In the subsequent step, the aniline radical cation reacts with a second radical cation, producing a dimer by eliminating two protons. The stereochemistry of the aniline cations radical favours para-directed, substitution, rather than ortho- and meta-substituents. In the final step, the oxidation of the dimeric radical cation occurs on the electrode surface, resulting from the formation of aniline oligomers and propagation of the Pani chain.^{41, 46} During this process, electroneutrality is maintained by the transfer of counter ions from the electrolyte, and the solution can become quite colourful due to the formation of soluble oligomers.^{44,46} The schematic representation of these steps is presented in figure 1.4

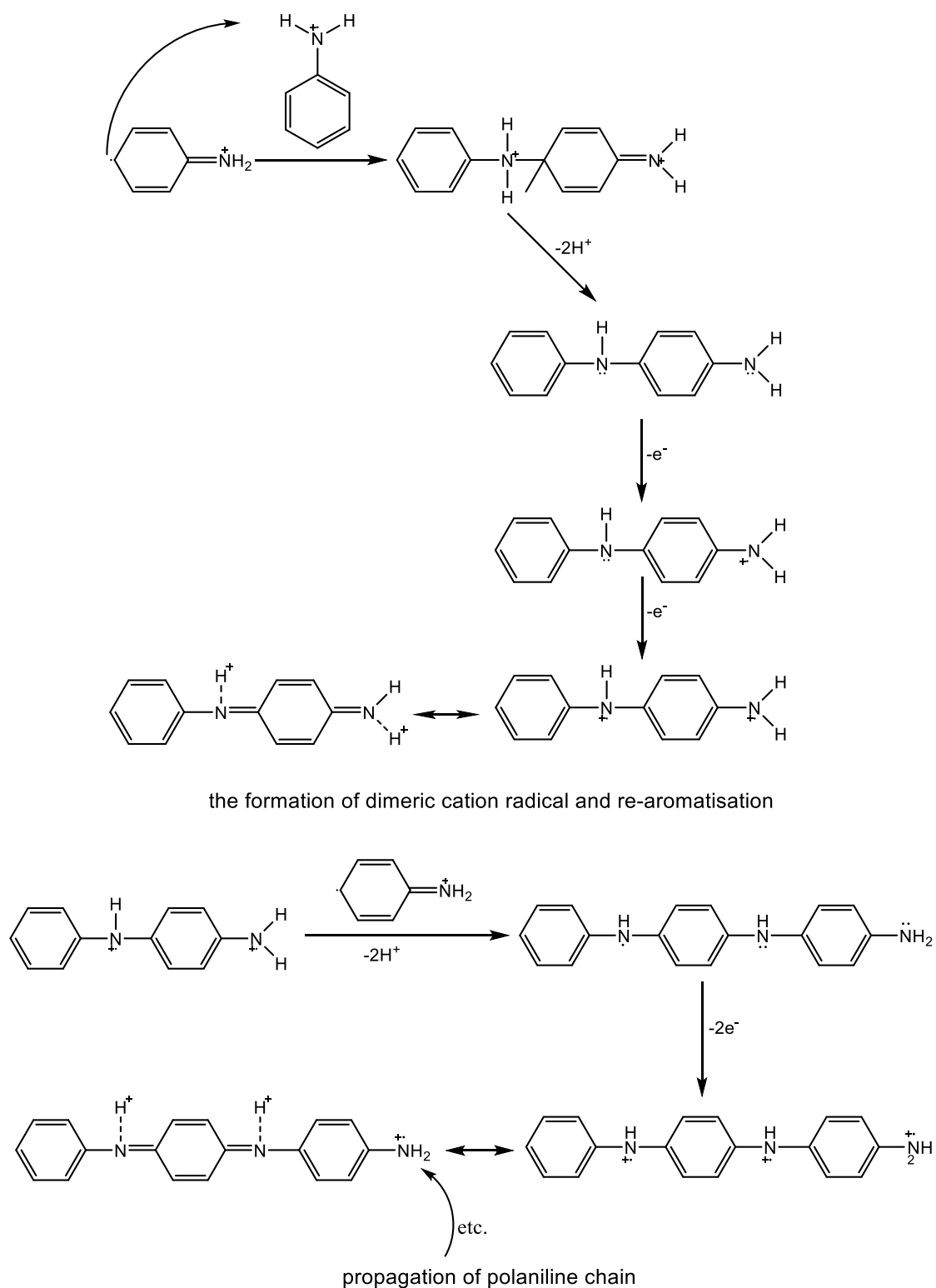


Figure 1.4. The formation of the aniline radical cation and propagation of the Pani chain

The oxidation potential of aniline should be lower than 1.0 V to avoid the degradation of Pani, which was observed in many studied in the literature. In the case of degradation, the Pani film would lose electroactive sites, resulting in a non-conductive

film. Degradation initially causes the brooding and the subsequent gradually disappearance of the associated redox peaks seen in cyclic voltammetry.⁴⁶ Furthermore, Lippe *et al.* studied the effect of several counter anions, such as ClO_4^- , SO_4^{2-} , Cl^- and NO_3^- , on the overoxidation Pani, the only ClO_4^- anions show a specific effect decreasing the overoxidation of Pani at higher potential.⁵³

Although Pani has been a material of choice because of the excellent properties discussed above, there are some limitations on its practical application due to its pH dependence. Pani has a little redox activity and low conductivity at $\text{pH} > 4$. In this case, Pani almost behaves as an insulator, without redox activity. This problem can be overcome by copolymerization of aniline with its derivatives, such as *o*-aminophenol⁵⁸⁻⁶¹ and *o*-toluidine. This topic will be discussed in detail further in this chapter.

Cyclic voltammetry (potentiodynamic), galvanotactic and potentiostatic techniques are mostly used for the electrochemical polymerization of aniline. Cyclic voltammetry is switched via the electrode potential, resulting in the change between the conducting and insulating forms of Pani,^{41,46} generating a polymer film that adheres strongly to the electrode surface.⁴⁰ Detailed information on electrochemical polymerization techniques will be discussed in chapter 2.

1.2.3. Polypyrrole

1.2.3.1. Overview

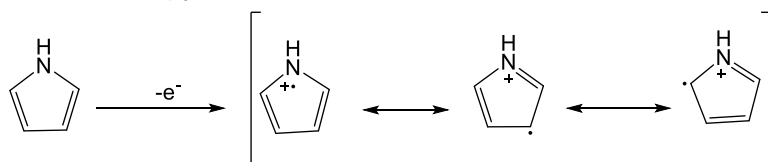
The other preferred conducting polymer used in this research is polypyrrole (PPy) due to its high electroactivity, its excellent reversibility between its conducting and insulating states,⁶² its great environmental stability, its thermal stability, and its ease of synthesis.^{52, 63} The polymerization of the pyrrole monomer was initially performed by Diaz and co-workers⁶³⁻⁶⁹ and Baker and Reynolds followed the polymerization of PPy via EQCM and reported the formation of a highly conductive, strongly adhering polymer film on the electrode surface.⁷⁰ The high application potential of PPy in rechargeable batteries,⁷¹⁻⁷⁵ supercapacitors⁷⁶⁻⁸² and electronic devices⁸³ has led to a significant increase in related research in order to understand its properties in the presence of different counter ions in the electrolyte.⁸⁴⁻⁸⁶ The research in the literature

indicates that the electroactivity and chemical stability of PPy, as well as physical properties such as morphology, mostly depend on the conditions used during electrosynthesis.^{52, 84, 86} PPy is also favoured for the production of composite films in presence of CNTs because it is soluble in pH neutral medium in contrast to aniline monomers.⁵²

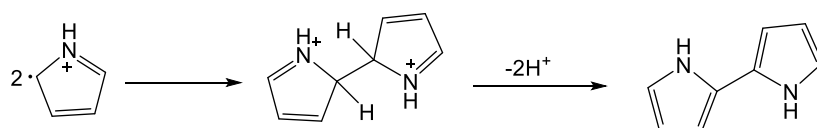
1.2.3.2. Synthesis of polypyrrole

Pyrrole has a heteroaromatic backbone, as shown in figure 1.1. PPy can be easily synthesized by chemical or electrochemical polymerization of the pyrrole monomer from aqueous or organic solutions.^{63, 68, 70, 87} Figure 1.5 displays the electrochemical polymerization of the pyrrole monomer.

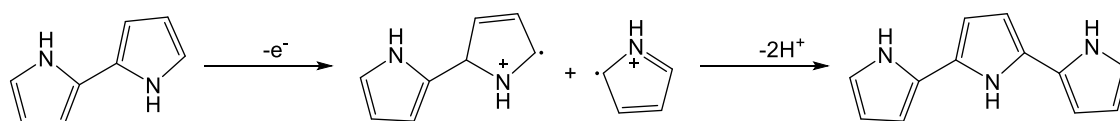
Formation of pyrrole radical cation



Formation of dimer



Coupling of radical cations and re-aromatization



Propagation of polypyrrole chain

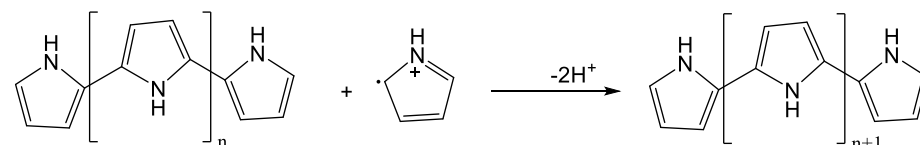


Figure 1.5. The oxidation mechanism of PPy

The conductivity of PPy can be increased with doping, which contributes to an increase in the conductivity of PPy in comparison to its insulating form.⁶⁸

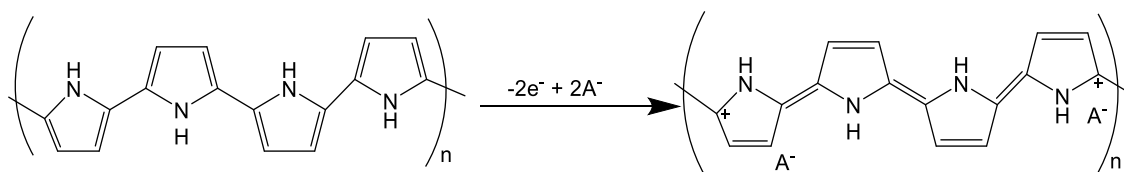


Figure 1.6. Electrochemical doping mechanism of PPy

1.2.4. Poly-*o*-aminophenol

1.2.4.1. Overview

Poly-*o*-aminophenol (PAP) is formed by the oxidation of *o*-aminophenol (see the chemical formula in figure 1.1), showing its high electroactivity with the potential range $-0.2 \text{ V} < E < 0.5 \text{ V}$ (vs SCE) at lower pH values during cyclic voltammetry.⁸⁸ The charge transfer mechanism of PAP has been studied by a variety of techniques⁵⁸ in different media, both aqueous and non-aqueous solutions, and with a variety of electrodes materials.⁵⁹ According to these studies, there are several advantageous of PAP compared to most aniline derivatives; PAP has a self-limiting growth, providing the control of film thickness as being between 10-100 nm, and also allowing for regeneration after use.^{88, 89} In addition to these characteristics, the presence of the -OH group increases the density of imine sites. PAP was synthesized in alkali medium⁵⁹ (pH 12) and the final film acts as a protective film for copper exposed in NaCl.⁹⁰

1.2.5. Poly-*o*-toluidine

1.2.5.1. Overview

Poly-*o*-toluidine (POT), shown in figure 1.1, is an aniline derivative. It is obtained from *o*-toluidine monomers in a strongly acidic medium like Pani. POT exhibits good stability. It was reported that a POT film is protective against corrosion for copper in chloride medium.⁹¹ POT has been found to have an additional advantage over Pani due to its fast switching time between the oxidized and reduced states. Also, the switching behaviour from insulator to conductor of POT films synthesized by the electrochemical method has been extensively studied.⁹²

1.3. Copolymerization of Electronically Conducting Polymers

In some cases, the electroactivity of polymers can suffer depending on the pH of the electrolyte solution. Specifically, the electroactivity of Pani depends on the pH of the electrolyte solution; it has a poor electroactivity at raised pH. In the case of Pani, ring- or N-substituted aniline derivatives, such as *o*-aminophenol and *o*-toluidine, have gained considerable attention in the literature regarding the preparation of substituted conducting Pani.⁴¹ However, it seems that the conductivity of substituted Pani is lower than pure Pani. One approach to addressing this problem is copolymerization, which suppresses these less desirable characteristics and enhances the physical and chemical properties of conducting polymers. Copolymerization consists of polymerization of at least two different monomers species. There are a great number of studies on copolymerization that has been undertaken by both chemical⁹³⁻⁹⁵ and electrochemical methods.⁹⁶ In most cases, having a functional group such as -SO₃H and -OH is preferable because these groups adjust the pH of the surrounding solution.

As a pioneer of such studies, Wei *et al.*⁹⁷ was reported both chemical and electrochemical copolymerization of aniline with *o*-toluidine and *m*-toluidine. The results of this study indicated that the electroactivity of the copolymers could be controlled a wide range of systems. Kumar⁹⁸ and Savitha *et al.*⁹⁹ studied the solubility of the copolymer, poly(aniline-co-*o*-toluidine), in common organic solvents and Borole *et al.*¹⁰⁰⁻¹⁰² reported the copolymerization rate of aniline with *o*-toluidine in organic sulphonic acids. The results of these latter studies showed excellent solubility of the resultant copolymers in organic solvents compared to pure Pani.

Another copolymer of aniline with *o*-aminophenol was studied by Mu, who described that the electroactivity of poly(aniline-co-*o*-aminophenol) (Pani-PAP) copolymer is a high electroactivity as the pH value increases in the range from 5.0 to 7.1 while Pani does not show electroactivity when pH > 4.¹⁰³ In addition to this study, Mu¹⁰⁴ also used the copolymer, Pani-PAP, for construction of a Zn-copolymer battery, showing 39.8 % a high energy density.

These results promoted research into the production of a variety of copolymers between various monomer such as aniline and 3-aminophenol,¹⁰⁵ aniline and *o*-aminophenol,¹⁰⁶

aniline and phenylenediamine,^{107, 108} aniline and thiophene,¹⁰⁹ aniline and *o*-toluidine,⁹⁴ aniline and 2-fluoroaniline,¹¹⁰ aniline and 2-chloroaniline,¹¹⁰ aniline and pyrrole,¹¹¹ *o*-toluidine and *o*-phenylenediamine,¹¹² *o*-toluidine and pyrrole,⁹¹ and most recently *o*-toluidine and *o*-aminophenol.⁹²

1.4. Composite Materials of Electronically Conducting Polymers

According to studies in the literature, the interaction between polymers and other species such as carbon nanotubes (CNTs),¹¹³⁻¹¹⁵ graphene, metals,¹¹⁶⁻¹¹⁸ and inorganic compounds¹¹⁹⁻¹²¹ have enhanced the mechanical and electrical properties of the resultant composites. Particularly CNTs composites have received considerable interest due to their unique molecular structure, electronic, mechanical and thermal properties.^{115, 122-130} The studies reported in the literature show that the presence of small amounts of CNTs in a polymer matrix enhance electrical conductivity and electrostatic charging behaviour of the polymer.¹³¹⁻¹³³ In addition to this, Guo *et al.*,¹³⁴ contributed to this finding with a modified electrode obtained from CNTs and Pani, indicating a higher response from that obtained from a pure Pani-modified electrode. Liu *et al.*,¹³⁵ also found that Pani/CNTs multilayer films shift the electroconductivity of Pani towards a neutral environment.¹³⁶

1.4.1. Composite Materials of Conductive Polymers with CNTs

CNTs have gained widespread recognition due to their electrical, mechanical, thermal, and chemical stability since they were discovered by Iijima in 1991.^{137, 138} These promising properties have led to a huge amount of activity in many areas of science, such as in nanoelectronics, nanocomposites, and biomedical applications.^{139, 140} There are two different types of CNTs; single wall carbon nanotubes (SWCNTs) with a diameters of the order of 1 nm and a length that can be up to centimetres, and multiwall carbon nanotubes (MWCNTs) with a diameters between 2 nm and 100 nm, and length of tens of microns.^{137, 141} SWCNTs have a single graphene sheet while MWCNTs have more than one graphene sheet. The morphologies of both are that of a cylinder. CNTs can also be produced in high purity and a cost-effective manner. Among CNTs, in a mechanical sense, MWCNTs are better than SWCNTs in thermal and electronic applications because SWCNTs show a tendency to form large bundles due to Van der

Waals forces and high surface energies.¹³⁸ The separation of such bundles is extremely difficult in some applications.¹³⁷

In the last few decades, there has been a growing interest in CNTs, which are excellent candidates for the preparation of composite materials with conducting polymers. This increases their electrical and thermal properties as well as increasing their surface area due to their small dimensions.^{142, 143} Even a small amount of CNTs in a polymer matrix can considerably enhance the electrical and mechanical properties.¹⁴⁴ Several studies have been undertaken to explore the influence of CNTs in different polymer matrices, such as in Pani,^{124, 145} PPy,¹⁴⁶ polythiophene, and their derivatives. The results show that CNTs not only act as a filler but also behave as a dopant in the polymer matrix.^{147, 148} These studies have been performed in both aqueous solution¹⁴⁹⁻¹⁵¹ and non-aqueous media, which indicates a more uniform dispersion of CNTs in non-aqueous solutions (such as ILs) than in aqueous medium.^{139, 152, 153}

The preparation of conducting polymers with CNTs is an important issue in the production of a homogenous material.^{133,154} A number of strategies have been developed to produce polymer-composite films, such as direct mixing,¹⁵⁵ chemical surface modification of CNTs,^{148, 156-159} the contribution of third components,¹⁶⁰ chemical,¹⁶¹ and electrochemical^{124, 162} polymerization, covalent bonding, Van der Waals bonding, etc. Among these techniques, electrochemical polymerization is a preferable technique as it exhibits a uniform material.¹⁶³ The CNT/conducting polymers composite materials have been prepared as a gel¹⁶⁴ because it is otherwise difficult to process because of the infusibility and insolubility of Pani. The nanocomposites of gels exhibit better mechanical properties than the others. The second process is covalent bonding^{159, 165} though this resulted in poor electrical and mechanical properties.¹⁶⁶ The third process is non-covalent Conducting polymer/CNT composite preparation, providing for the wrapping of the CNTs with high molecular weight polymer. The results showed a uniform dispersion of CNTs in the desired polymer matrix.¹⁶⁷ A neutral aqueous solution of Pani with CNTs was used to form a composite material, but it showed poor mechanical and electrical properties because of the poor solubility of aniline.¹³⁵ The last formation method is the deposition of Pani onto CNT-layer whiskers, which resulted in a non-uniform distribution of CNT in the polymer matrix

and poor adherence of the composite film to the desired electrode material. It is also synthesized through interfacial polymerization.¹⁶⁸

These preparation methods have low efficiency because of the inert structure of CNTs in polymer matrices, although properties will be enhanced past a certain point. This problem can be overcome by the addition of a functional group on the wall of the CNTs. Doing so allows CNT to be dissolved in aqueous and indeed non-aqueous media. There are a variety of techniques used to functionalize CNTs chemically^{169,170} and electrochemically.¹⁷¹⁻¹⁷³

The enhancement of the properties of conducting polymers in the presence of CNTs allows their use in a wide range of application areas such as batteries, biosensors (with Pani/CNT composites),¹⁷⁴ energy storage devices,¹⁷⁵ corrosion protections (with PPy/CNTs composites),¹⁴⁶ high-strength artificial muscles³⁹ and capacitors.¹⁷⁵

1.5. Ion and Solvent Transfer of Electronically Conducting Polymers

The electrochemical oxidation and reduction reactions of polymers also result in the transfer of counter ions as well as the transfer of electrons. This occurs between the polymer film and bath solution in terms of the charge of the polymer, the mobility of the ions in the electrolyte solution, and the charge of the ions. This illustrates the basic principles of the development of electrochemically ion-exchange techniques¹⁷⁶⁻¹⁷⁸ for charged species. This technique makes possible the selective, reversible, controlled removal of counter ions from the copolymer film. Depending upon the polymerization conditions, both anions and cations can be exchanged with the polymer.⁸⁴

The development of conducting polymer-based ion-exchange techniques led to the use of common conducting polymers such as PPy and Pani in these techniques. In the case of PPy, although early studies showed the ion-exchange behaviour of PPy in an aqueous KCl electrolyte solution,^{179, 180} it can be managed in both aqueous solutions¹⁸¹⁻¹⁸⁴ and non-aqueous solutions,^{84,185,186} demonstrating the possible use of either anions *or* cations in maintaining electroneutrality in the polymer film. Pani has a positive charge in its oxidized state, and thus it can interact with a negative in charge a counter ion.

Ultimately, ion-exchange properties depend mostly on the pH of the surrounding medium.¹⁸⁷

There are two explanations for the movement of ions in or out of the polymer film upon redox, which are the thermodynamic argument and the kinetic argument. By the thermodynamic argument, positively-charged polymer film should be an anion exchanger. On the other hand, the kinetic argument suggests that the ion that moves *fastest* through the electrolyte will be the one to maintain electroneutrality. Both theories show, agreement in the anion exchanger, in that anions are usually small and mobile. In the case of a large anion (immobile) the cation should be transferred, while the anion transfer will take longer.¹⁸⁸ Some papers reported that the solvent transfer takes places with ions transfer between the anionic and cathodic species in order to maintain electroneutrality when the anionic radius is relatively large.^{189, 190}

There are a number of electrochemical ion-exchange techniques which were developed for the extraction of chromium (VI) by Pani,¹⁹¹ and the extraction of silver ions,¹⁹² and the removal of perchlorate anions using Pani-PAP.¹⁹³

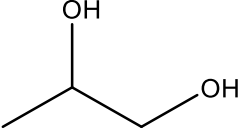
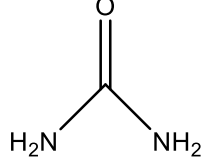
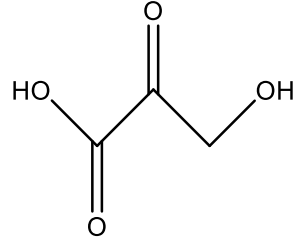
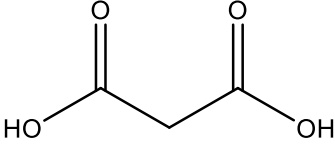
1.6. Deep Eutectic Solvents

The Ionic liquids (ILs) are a new class of solvents which consists of organic cations and anions without any molecular solvent, as opposed to the conventional means of being formed in the presence of a solvent.¹⁹⁴ These salt solutions can be melted thermally and have lower melting points, generally below 100 °C, than either of the individual components¹⁹⁵ and they can exist as liquids at room temperature. In this context, they are also called room temperature ionic liquids (RTILs). Their good thermal and chemical stability, negligible volatility, and solubility in a wide range of ionic liquid solvents has led to them receiving considerable attention for a range of approaches.¹⁶³ Both the promising solvent properties and the suitability for charge storage systems provide a wide range of potential applications in batteries and capacitors.^{196, 197} ILs are suitable solvents with high ionic activities and wide electrochemical windows for the polymerization of conducting polymers,^{96,198,199} such as PPy,²⁰⁰⁻²⁰² polyarene, polythiophene,²⁰³ and particularly Pani^{195, 204-208} which provide higher potentials without degradation.^{50, 209}

Deep eutectic solvents (DESs) have also been categorized as an attractive type of ionic liquid,¹⁵² which are the mixture of cationic compounds such as ammonium salts (e.g., choline chloride, ChCl) and neutral organic hydrogen bond donors (e.g., acids, amides, and carboxylic acids).^{153, 210} DESs exhibits similar characteristics to ILs; however, DESs have their own advantage, such as being inexpensive and having simple preparation across a range of components.¹⁵³ DESs have prepared from a eutectic mixture of [Brønsted-Lowry] acids and bases with a large number of non-symmetric ionic species. There is a delocalisation during hydrogen bonding arising from the anion and hydrogen bond donor (HBD). This delocalisation lowers the melting point of the mixture compared to that of the individual components.²¹¹ Table 1.1 shows the combination of DESs with common hydrogen bond donors and choline chloride.

In recent times, there has been a growing interest in the use of DESs in the deposition of high-quality electroactive polymer films because they provide a remarkable enhancement in the electroactivity of films such as Pani,²¹² PPy²¹³ and poly(3,4-ethylenedioxythiophene).^{214, 215} Furthermore, DESs are useful medium for the dispersion of CNTs through the solution, resulting in a much better interaction between the monomer and CNTs in contrast to aqueous medium because of their higher viscosity.

Table 1.1. The combination of DESs with a hydrogen bond donors (HBDs) and Choline Chloride

<i>DES</i>	<i>HBD name</i>	<i>HBD structure</i>
Ethaline	Ethylene glycol	
Propaline	Propylene glycol	
Reline	Urea	
Oxaline	Oxalic acid	
Maline	Malonic acid	

In this thesis, we have used Ethaline, which is composed of choline chloride and ethylene glycol, as shown in table 1.1, this research is discussed in detail in chapter 7.

1.7. Project Objectives

The research presented in this thesis has two main objectives. The first is the improvement of both electroactivity and ionic-activity of Pani in higher pH solutions with the copolymerization of aniline in the presence of *o*-aminophenol and *o*-toluidine, respectively and their redox switching in monomer-free NaF electrolyte solutions. The second introduces the polymerization of the conducting polymers, aniline, and pyrrole,

in the presence of MWCNT-COOH in both aqueous and Ethaline media to enhance the charge transport of Pani film.

In the first section, the electrochemical deposition of Pani, PAP, and POT is dealt with in detail to identify their growth dynamics. Then, the conditions for the copolymerization of aniline with *o*-aminophenol and *o*-toluidine are optimised. The electrochemical properties of the resultant polymer and copolymer films were characterized in 1 M H₂SO₄ monomer-free electrolyte solutions. In the last stage, the defluoridation properties of these polymer and copolymer film were examined in monomer-free NaF solutions in order to improve a novel method to remove fluoride ions from drinking water.

In the last section, the growth dynamics of the conducting polymers, Pani and PPy, will be performed in the presence /absence of MWCNTs. The goal of these studies is to improve the charge transferred and mechanical properties of the conducting polymers, Pani and PPy, in aqueous and Ethaline media.

1.8. References

- 1 P. R. Moses, L. Wier and R. W. Murray, *Analytical Chemistry*, 1975, **47**, 1882-1886 (DOI:10.1021/ac60362a043).
- 2 K. D. Snell and A. G. Keenan, *Chemical Society Review*, 1979, **8**, 259-282 (DOI:10.1039/cs9790800259).
- 3 A. P. Brown, C. Koval and F. C. Anson, *Journal of Electroanalytical Chemistry*, 1976, **72**, 379-387 (DOI:10.1016/S0022-0728(76)80324-5).
- 4 K. S. V. Santhanam, N. Jespersen and A. J. Bard, *J. American Chemical Society*, 1977, **99**, 274-276 (DOI:10.1021/ja00443a063).
- 5 R. F. Lane and A. T. Hubbard, *Journal of Physical Chemistry*, 1975, **79**, 808-815 (DOI:10.1021/j100575a008).
- 6 J. R. Lenhard and R. W. Murray, *Journal of Electroanalytical Chemistry*, 1977, **78**, 195-201 (DOI:10.1016/S0022-0728(77)80442-7).
- 7 C. M. Elliott and R. W. Murray, *Analytical Chemistry*, 1976, **48**, 1247-1254 (DOI:10.1021/ac50002a046).

- 8 P. R. Moses and R. W. Murray, *Journal of Electroanalytical Chemistry*, 1977, **77**, 393-399 (DOI:10.1016/0368-1874(77)80140-8).
- 9 I. Haller, *Journal of American Chemical Society*, 1978, **100**, 8050-8055 (DOI:10.1021/ja00494a003).
- 10 R. J. Burt, G. J. Leigh and C. J. Pickett, *Journal of the Chemical Society-Chemical Communications*, 1976, , 940-941 (DOI:10.1039/c39760000940).
- 11 R. F. Lane and A. T. Hubbard, *Journal of Physical Chemistry*, 1973, **77**, 1401-1410 (DOI:10.1021/j100630a018).
- 12 R. F. Lane and A. T. Hubbard, *Journal of Physical Chemistry*, 1973, **77**, 1411-1421 (DOI:10.1021/j100630a019).
- 13 H. Bagheri, Z. Ayazi and M. Naderi, *Analytica Chimica Acta*, 2013, **767**, 1-13 (DOI:10.1016/j.aca.2012.12.013).
- 14 G. Inzelt, *Electrochimica Acta*, 1989, **34**, 83-91 (DOI:10.1016/0013-4686(89)87071-9).
- 15 D. C. Miller, J. P. Walter, D. F. Guthaner and J. B. D. Mark, *Chest*, 1978, **74**, 218-220 (DOI:10.1378/chest.74.2.218).
- 16 M. A. Miller, G. J. Mark and D. Kanarek, *American Journal of Medicine*, 1978, **65**, 373-378 (DOI:10.1016/0002-9343(78)90835-5).
- 17 K. Itaya and A. J. Bard, *Analytical Chemistry*, 1978, **50**, 1487-1489 (DOI:10.1021/ac50033a026).
- 18 A. Merz and A. J. Bard, *Journal of American Chemical Society*, 1978, **100**, 3222-3223 (DOI:10.1021/ja00478a049).
- 19 G. Inzelt, M. Pineri, J. W. Schultze and M. A. Vorotyntsev, *Electrochimica Acta*, 2000, **45**, 2403-2421 (DOI:10.1016/S0013-4686(00)00329-7).
- 20 S. M. Park and H. J. Lee, *Bulletin of the Korean Chemical Society*, 2005, **26**, 697-706.
- 21 R. Menon, *Current Science*, 2000, **79**, 1632-1635.
- 22 A. F. Diaz and J. A. Logan, *Journal of Electroanalytical Chemistry*, 1980, **111**, 111-114 (DOI:10.1016/S0022-0728(80)80081-7).
- 23 R. A. Bull, F. R. Fan and A. J. Bard, *Journal of The Electrochemical Society*, 1983, **130**, 1636-1638 (DOI:10.1149/1.2120053).
- 24 G. Tourillon and F. Garnier, *Journal of The Electrochemical Society*, 1983, **130**, 2042-2044 (DOI:10.1149/1.2119517).

- 25 K. Kaneto, K. Yoshino and Y. Inuishi, *Solid State Communications*, 1983, **46**, 389-391 (DOI:10.1016/0038-1098(83)90454-4).
- 26 R. J. Waltman, J. Bargon and A. F. Diaz, *Journal of Physical Chemistry*, 1983, **87**, 1459-1463 (DOI:10.1021/j100231a035).
- 27 G. Schiavon, G. Zotti and G. Bontempelli, *Journal of Electroanalytical Chemistry*, 1985, **186**, 191-199 (DOI:10.1016/0368-1874(85)85765-8).
- 28 H. A. A. ElRahman and J. W. Schultze, *Journal of Electroanalytical Chemistry*, 1996, **416**, 67-74 (DOI:10.1016/S0022-0728(96)04718-3).
- 29 Y. Z. Su, Y. P. Niu, Y. Z. Xiao, M. Xiao, Z. X. Liang and K. C. Gong, *Journal of Polymer Science Part A-Polymer Chemistry*, 2004, **42**, 2329-2339 (DOI:10.1002/pola.20072).
- 30 T. K. Das and S. Prusty, *Polymer-Plastics Technology and Engineering*, 2012, **51**, 1487-1500 (DOI:10.1080/03602559.2012.710697).
- 31 U. Lange, N. V. Roznyatouskaya and V. M. Mirsky, *Analytica Chimica Acta*, 2008, **614**, 1-26 (DOI:10.1016/j.aca.2008.02.068).
- 32 X. Li, Y. Wang, X. Yang, J. Chen, H. Fu and T. Cheng, *TrAC Trends in Analytical Chemistry*, 2012, **39**, 163-179 (DOI:10.1016/j.trac.2012.06.003).
- 33 J. L. Camalet, J. C. Lacroix, S. Aeiayach, K. ChaneChing and P. C. Lacaze, *Journal of Electroanalytical Chemistry*, 1996, **416**, 179-182 (DOI:10.1016/S0022-0728(96)01012-1).
- 34 D. E. Tallman, G. Spinks, A. Dominis and G. G. Wallace, *Journal of Solid State Electrochemistry*, 2002, **6**, 73-84 (DOI:10.1007/s100080100212).
- 35 V. Brusic, M. Angelopoulos and T. Graham, *Journal of Electrochemical Society*, 1997, **144**, 436-442 (DOI:10.1149/1.1837428).
- 36 D. Sazou and C. Georgolios, *Journal of Electroanalytical Chemistry*, 1997, **429**, 81-93 (DOI:10.1016/S0022-0728(96)05019-X).
- 37 R. Racicot, R. Brown and S. C. Yang, *Synthetic Metals*, 1997, **85**, 1263-1264 (DOI:10.1016/S0379-6779(97)80232-9).
- 38 K. Gurunathan, A. V. Murugan, R. Marimuthu, U. P. Mulik and D. P. Amalnerkar, *Materials Chemistry Physics*, 1999, **61**, 173-191 (DOI:10.1016/S0254-0584(99)00081-4).
- 39 G. Spinks, V. Mottaghitlab, M. Bahrami-Saniani, P. Whitten and G. Wallace, *Advanced Materials*, 2006, **18**, 637-640 (DOI:10.1002/adma.200502366).
- 40 J. Heinze, B. A. Frontana-Urbe and S. Ludwigs, *Chemical Reviews.*, 2010, **110**, 4724-4771 (DOI:10.1021/cr900226k).

- 41 M. Gvozdenovic, B. Jugovic, J. Stevanovic, T. Trisovic and B. Grgur, in *Electropolymerization*, ed. E. Schab-Balcerzak and Rijeka, inTech, 2011, pp.77-96.
- 42 G. Inzelt, in *Conducting Polymers*, ed. nonymous 2012, pp.149-170.
- 43 B. Meana-Esteban, F. Sundfors, R. Espindola, C. Kvarnstrom, J. Heinze and A. Ivaska, *Electrochimica Acta*, 2008, **53**, 7988-7994 (DOI:10.1016/j.electacta.2008.06.004).
- 44 G. Ciric-Marjanovic, *Synthetic Metals*, 2013, **177**, 1-47 (DOI:10.1016/j.synthmet.2013.06.004).
- 45 N. Gospodinova and L. Terlemezyan, *Progress in Polymer Science*, 1998, **23**, 1443-1484 (DOI:10.1016/S0079-6700(98)00008-2).
- 46 A. A. Syed and M. K. Dinesan, *Talanta*, 1991, **38**, 815-837 (DOI:10.1016/0039-9140(91)80261-W).
- 47 J. Huang and R. B. Kaner, in *Conjugated Polymers: Theory, Synthesis, Properties and Characterization*, ed. Skotheim, T.A., Reynolds, R.J., CRL PressTaylor and Francis Group, 6000 Broken Sound Parkway NW, Suite 300 Boca Raton, FL 33487-2742, 2007, pp.1-40.
- 48 H. N. Dinh and V. I. Birss, *Journal of Electroanalytical Chemistry*, 1998, **443**, 63-71 (DOI:10.1016/S0022-0728(97)00470-1).
- 49 M. Matsushita, H. Kuramitz and S. Tanaka, *Environmental Science and Technology*, 2005, **39**, 3805-3810 (DOI:10.1021/es040379f).
- 50 Ren Dandan, J. Xu, Xi Lingling and Z. Yan, *Journal of Chromatographic Science*, 2011, **49**, 612-616.
- 51 A. M. P. Hussain and A. Kumar, *Bulletin of Material Science*, 2003, **26**, 329-334 (DOI:10.1007/BF02707455).
- 52 Y. Wang, J. Zhang, D. Sheng and C. Sun, *Journal of Chromatography*, 2010, **1217**, 4523-4528 (DOI:10.1016/j.chroma.2010.04.075).
- 53 J. Lippe and R. Holze, *Journal of Electroanalytical Chemistry*, 1992, **339**, 411-422 (DOI:10.1016/0022-0728(92)80465-G).
- 54 S. K. Mondal, K. Barai and N. Munichandraiah, *Electrochimica Acta*, 2007, **52**, 3258-3264 (DOI:10.1016/j.electacta.2006.09.067).
- 55 V. V. Abalyaeva and O. N. Efimov, *Russian Journal of Electrochemistry*, 2011, **47**, 1307-1316 (DOI:10.1134/S1023193511110036).
- 56 M. C. Li, C. A. Ma, B. Y. Liu and Z. M. Jin, *Electrochemistry Communications*, 2005, **7**, 209-212 (DOI:10.1016/j.elecom.2004.12.012).

- 57 G. Zotti, S. Cattarin and N. Comisso, *Journal of Electroanalytical Chemistry*, 1988, **239**, 387-396 (DOI:10.1016/0022-0728(88)80293-6).
- 58 C. Barbero, J. J. Silber and L. Sereno, *Journal of Electroanalytical Chemistry*, 1989, **263**, 333-352 (DOI:10.1016/0022-0728(89)85103-4).
- 59 A. Guenbour, A. Kacemi, A. Benbachir and L. Aries, *Progress in Organic Coatings*, 2000, **38**, 121-126 (DOI:10.1016/S0300-9440(00)00085-0).
- 60 R. Tucceri, *The Open Physical Chemistry Journal*, 2010, **4**, 45-61.
- 61 O. Levin, V. Kondratieva and V. Malev, *Electrochimica Acta*, 2005, **50**, 1573-1585 (DOI:10.1016/j.electacta.2004.10.028).
- 62 C. Ehrenbeck and K. Juttner, *Electrochimica Acta*, 1996, **41**, 511-518 (DOI:10.1016/0013-4686(95)00337-1).
- 63 A. F. Diaz, K. K. Kanazawa and G. P. Gardini, *Journal of the Chemical Society-Chemical Communications*, 1979, , 635-636 (DOI:10.1039/c39790000635).
- 64 A. Diaz, J. M. V. Vallejo and A. M. Duran, *Ibm Journal of Research and Development*, 1981, **25**, 42-50.
- 65 A. F. Diaz and J. I. Castillo, *Journal of the Chemical Society-Chemical Communications*, 1980, , 397-398 (DOI:10.1039/c39800000397).
- 66 A. F. Diaz, W. Y. Lee, A. Logan and D. C. Green, *Journal of Electroanalytical Chemistry*, 1980, **108**, 377-380 (DOI:10.1016/S0022-0728(80)80348-2).
- 67 A. F. Diaz and M. Salmon, *Abstracts of Papers of the American Chemical Society*, 1981, **182**, 74-INOR.
- 68 A. F. Diaz, J. I. Castillo, J. A. Logan and W. Y. Lee, *Journal of Electroanalytical Chemistry*, 1981, **129**, 115-132 (DOI:10.1016/S0022-0728(81)80008-3).
- 69 A. F. Diaz and B. Hall, *Ibm Journal of Research and Development*, 1983, **27**, 342-347.
- 70 C. K. Baker and J. R. Reynolds, *Journal of Electroanalytical Chemistry*, 1988, **251**, 307-322 (DOI:10.1016/0022-0728(88)85192-1).
- 71 J. Tanguy and N. Mermillodthevenin, *Molecular Crystals and Liquid Crystals*, 1985, **121**, 374-374.
- 72 N. V. Bhat and S. Yasmin, *Journal of Applied Polymer Science*, 1995, **55**, 1827-1835 (DOI:10.1002/app.1995.070551313).
- 73 Y. Zhang, Z. Bakenov, Y. Zhao, A. Konarov, The Nam Long Doan, M. Malik, T. Paron and P. Chen, *Journal of Power Sources*, 2012, **208**, 1-8 (DOI:10.1016/j.jpowsour.2012.02.006).

- 74 X. Cao, J. Zhang and L. Zhu, *Journal of Nanoscience and Nanotechnology*, 2015, **15**, 7081-7086 (DOI:10.1166/jnn.2015.10546).
- 75 J. Huang and Z. Yang, *Royal Society of Chemistry Advances*, 2014, **4**, 19205-19209 (DOI:10.1039/c4ra01322k).
- 76 Q. Qu, Y. Zhu, X. Gao and Y. Wu, *Advanced Energy Materials*, 2012, **2**, 950-955 (DOI:10.1002/aenm.201200088).
- 77 B. Muthulakshmi, D. Kalpana, S. Pitchumani and N. G. Renganathan, *Journal of Power Sources*, 2006, **158**, 1533-1537 (DOI:10.1016/j.jpowsour.2005.10.013).
- 78 D. Zhang, X. Zhang, Y. Chen, P. Yu, C. Wang and Y. Ma, *Journal of Power Sources*, 2011, **196**, 5990-5996 (DOI:10.1016/j.jpowsour.2011.02.090).
- 79 A. Davies, P. Audette, B. Farrow, F. Hassan, Z. Chen, J. Choi and A. Yu, *Journal of Physical Chemistry C*, 2011, **115**, 17612-17620 (DOI:10.1021/jp205568v).
- 80 L. Z. Fan and J. Maier, *Electrochemistry Communications*, 2006, **8**, 937-940 (DOI:10.1016/j.elecom.2006.03.035).
- 81 H. Mi, X. Zhang, X. Ye and S. Yang, *Journal of Power Sources*, 2008, **176**, 403-409 (DOI:10.1016/j.jpowsour.2007.10.070).
- 82 K. Jurewicz, S. Delpeux, V. Bertagna, F. Beguin and E. Frackowiak, *Chemical Physics Letters*, 2001, **347**, 36-40 (DOI:10.1016/S0009-2614(01)01037-5).
- 83 M. Satoh and E. Hasegawa, *Macromolecular Symposia*, 1996, **105**, 211-216 (DOI:10.1002/masy.19961050130).
- 84 M. A. Vorotyntsev, E. Vieil and J. Heinze, *Journal of Electroanalytical Chemistry*, 1998, **450**, 121-141 (DOI:10.1016/S0022-0728(97)00623-2).
- 85 D. Orata and D. A. Buttry, *Journal of American Chemical Society*, 1987, **109**, 3574-3581 (DOI:10.1021/ja00246a013).
- 86 U. Johanson, A. Marandi, T. Tamm and J. Tamm, *Electrochimica Acta*, 2005, **50**, 1523-1528 (DOI:10.1016/j.electacta.2004.10.016).
- 87 H. S. Lee and J. Hong, *Synthetic Metals*, 2000, **113**, 115-119.
- 88 R. Tucceri, *Journal of New Materials for Electrochemical Systems*, 2005, **8**, 305-317.
- 89 T. Ohsaka, M. Ohba, M. Sato, N. Oyama, S. Tanaka and S. Nakamura, *Journal of Electroanalytical Chemistry*, 1991, **300**, 51-66 (DOI:10.1016/0022-0728(91)85383-Z).
- 90 A. Guenbour, A. Kacemi and A. Benbachir, *Progress in Organic Coatings*, 2000, **39**, 151-155 (DOI:10.1016/S0300-9440(00)00141-7).

- 91 S. Yalcinkaya, T. Tueken, B. Yazici and M. Erbil, *Progress in Organic Coatings*, 2008, **63**, 424-433 (DOI:10.1016/j.porgcoat.2008.07.002).
- 92 Q. Yang, Y. Zhang, H. Li, Y. Zhang, M. Liu, J. Luo, L. Tan, H. Tang and S. Yao, *Talanta*, 2010, **81**, 664-672 (DOI:10.1016/j.talanta.2009.12.051).
- 93 X. Wang, H. Li and P. Liu, *Electrochimica Acta*, 2014, **125**, 630-636 (DOI:10.1016/j.electacta.2014.02.015).
- 94 S. Shreepathi and R. Holze, *Journal of Applied Polymer Science*, 2009, **113**, 700-708 (DOI:10.1002/app.30104).
- 95 M. A. Shenashen, M. M. Ayad, N. Salahuddin and M. A. Youssif, *Reactive & Functional Polymers*, 2010, **70**, 843-848 (DOI:10.1016/j.reactfunctpolym.2010.07.005).
- 96 S. Mu, *Journal of Physical Chemical B*, 2008, **112**, 6344-6349 (DOI:10.1021/jp7117828).
- 97 Y. Wei, R. Hariharan and S. A. Patel, *Macromolecules*, 1990, **23**, 758-764 (DOI:10.1021/ma00205a011).
- 98 D. Kumar, *Synthetic Metals*, 2000, **114**, 369-372 (DOI:10.1016/S0379-6779(00)00270-8).
- 99 P. Savitha and D. N. Sathyanarayana, *Polymer International*, 2004, **53**, 106-112 (DOI:10.1002/pi.1316).
- 100 D. D. Borole, U. R. Kapadi, P. P. Mahulikar and D. G. Hundiwale, *Mater Lett*, 2006, **60**, 2447-2452 (DOI:10.1016/j.matlet.2006.01.014).
- 101 D. D. Borole, U. R. Kapadi, P. P. Mahulikar and D. G. Hundiwale, *Material Letters*, 2004, **58**, 3816-3822 (DOI:10.1016/j.matlet.2004.07.035).
- 102 D. Borole, U. Kapadi, P. Mahulikar and D. Hundiwale, *Designed Monomers and Polymers*, 2005, **8**, 107-116 (DOI:10.1163/1568555053603242).
- 103 S. L. Mu, *Synthetic Metals*, 2004, **143**, 259-268 (DOI:10.1016/j.synthmet.2003.12.008).
- 104 S. L. Mu, *Synthetic Metals*, 2004, **143**, 269-275 (DOI:10.1016/j.synthmet.2003.12.009).
- 105 F. J. Hua and E. Ruckenstein, *Macromolecules*, 2004, **37**, 6104-6112 (DOI:10.1021/ma040070g).
- 106 M. Liu, M. Ye, Q. Yang, Y. Zhang, Q. Xie and S. Yao, *Electrochimica Acta*, 2006, **52**, 342-352 (DOI:10.1016/j.electacta.2006.05.013).
- 107 H. Q. Tang, A. Kitani, S. Maitani, H. Munemura and M. Shiotani, *Electrochimica Acta*, 1995, **40**, 849-857 (DOI:10.1016/0013-4686(94)00370-G).

- 108 R. Mazeikiene and A. Malinauskas, *Synthetic Metals*, 1998, **92**, 259-263 (DOI:10.1016/S0379-6779(98)80094-5).
- 109 N. P. Ozcicek, K. Pekmez, R. Holze and A. Yildiz, *Journal of Applied Polymer Science*, 2003, **90**, 3417-3423 (DOI:10.1002/app.13035).
- 110 Y. Sahin, S. Percin, M. Sahin and G. Ozkan, *Journal of Applied Polymer Science*, 2004, **91**, 2302-2312 (DOI:10.1002/app.13367).
- 111 H. R. Wasniki and D. S. Kelkar, *International Conference on Materials Science and Technology (Icmst 2012)*, 2015, **73**, 012026 (DOI:10.1088/1757-899X/73/1/012026).
- 112 S. Bilal and R. Holze, *Journal of Electroanalytical Chemistry*, 2006, **592**, 1-13 (DOI:10.1016/j.jelechem.2006.03.039).
- 113 R. Singh, R. Verma, G. Sumana, A. K. Srivastava, S. Sood, R. K. Gupta and B. D. Malhotra, *Bioelectrochemistry*, 2012, **86**, 30-37 (DOI:10.1016/j.bioelechem.2012.01.005).
- 114 J. Zhang, S. Yang, H. Wang and S. Wang, *Electrochimica Acta*, 2012, **85**, 467-474 (DOI:10.1016/j.electacta.2012.08.089).
- 115 Y. H. Lin and X. L. Cui, *Journal of Materials Chemistry*, 2006, **16**, 585-592 (DOI:10.1039/b510947g).
- 116 U. Lange and V. M. Mirsky, *Electrochimica Acta*, 2011, **56**, 3679-3684 (DOI:10.1016/j.electacta.2010.08.092).
- 117 H. Lian, W. Qian, L. Estevez, H. Liu, Y. Liu, T. Jiang, K. Wang, W. Guo and E. P. Giannelis, *Sensors and Actuators B-Chemical*, 2011, **156**, 187-193 (DOI:10.1016/j.snb.2011.04.012).
- 118 D. Pathania, G. Sharma, A. Kumar and N. C. Kothiyal, *Journal of Alloys and Compounds*, 2014, **588**, 668-675 (DOI:10.1016/j.jallcom.2013.11.133).
- 119 A. A. Khan and L. Paquiza, *Synthetic Metals*, 2014, **190**, 66-71 (DOI:10.1016/j.synthmet.2014.02.001).
- 120 N. P. Berezina, N. A. Kononenko, A. A. -. Sytcheva, N. V. Loza, S. A. Shkirskaya, N. Hegman and A. Pungor, *Electrochimica Acta*, 2009, **54**, 2342-2352 (DOI:10.1016/j.electacta.2008.10.048).
- 121 A. A. Khan and L. Paquiza, *Synthetic Metals*, 2011, **161**, 899-905 (DOI:10.1016/j.synthmet.2011.02.022).
- 122 M. Trojanowicz, *Trac-Trends in Analytical Chemistry*, 2006, **25**, 480-489 (DOI:10.1016/j.trac.2005.11.008).
- 123 P. M. Ajayan, *Chemical Review*, 1999, **99**, 1787-1799 (DOI:10.1021/cr970102g).

- 124 Z. Wang, J. Yuan, M. Li, D. Han, Y. Zhang, Y. Shen, L. Niu and A. Ivaska, *Journal of Electroanalytical Chemistry*, 2007, **599**, 121-126 (DOI:10.1016/j.jelechem.2006.09.021).
- 125 I. -. P. Chen, P. Cottinet, S. Tsai, B. Foster, R. Liang, B. Wang and C. Zhang, *Sensors and Actuators B-Chemical*, 2012, **171**, 515-521 (DOI:10.1016/j.snb.2012.05.022).
- 126 Q. Zhu, A. N. A. Sujari and S. Ab Ghani, *Journal of Solid State Electrochemistry*, 2012, **16**, 3179-3187 (DOI:10.1007/s10008-012-1749-9).
- 127 R. B. Mathur, S. Chatterjee and B. P. Singh, *Composites Science and Technology*, 2008, **68**, 1608-1615 (DOI:10.1016/j.compscitech.2008.02.020).
- 128 A. Y. Cao, L. J. Ci, D. J. Li, B. Q. Wei, C. L. Xu, J. Liang and D. H. Wu, *Chemical Physics Letters*, 2001, **335**, 150-154 (DOI:10.1016/S0009-2614(01)00003-3).
- 129 R. Gangopadhyay and A. De, *Chemistry of Materials*, 2000, **12**, 2064-2064 (DOI:10.1021/cm002002o).
- 130 G. Inzelt, in *Chemical and Electrochemical Synthesis of Conducting Polymers*, ed. nonymous 2012, pp.53-60.
- 131 X. Y. Gong, J. Liu, S. Baskaran, R. D. Voise and J. S. Young, *Chemistry of Materials*, 2000, **12**, 1049-1052 (DOI:10.1021/cm9906396).
- 132 V. Mottaghitlab, G. M. Spinks and G. G. Wallace, *Synthetic Metals*, 2005, **152**, 77-80 (DOI:10.1016/j.synthmet.2005.07.154).
- 133 C. Dhand, S. K. Arya, S. P. Singh, B. P. Singh, M. Datta and B. D. Malhotra, *Carbon*, 2008, **46**, 1727-1735 (DOI:10.1016/j.carbon.2008.07.028).
- 134 M. L. Guo, J. H. Chen, J. Li, B. Tao and S. Z. Yao, *Analytica Chimica Acta*, 2005, **532**, 71-77 (DOI:10.1016/j.aca.2004.10.045).
- 135 J. Y. Liu, S. J. Tian and W. Knoll, *Langmuir*, 2005, **21**, 5596-5599 (DOI:10.1021/la0501233).
- 136 X. Luo, A. J. Killard, A. Morrin and M. R. Smyth, *Analytica Chimica Acta*, 2006, **575**, 39-44 (DOI:10.1016/j.aca.2006.05.064).
- 137 J. N. Coleman, U. Khan, W. J. Blau and Y. K. Gun'ko, *Carbon*, 2006, **44**, 1624-1652 (DOI:10.1016/j.carbon.2006.02.038).
- 138 H. Miyagawa, M. Misra and A. K. Mohanty, *Journal of Nanoscience and Nanotechnology*, 2005, **5**, 1593-1615 (DOI:10.1166/jnn.2005.181).
- 139 S. H. Hong, T. T. Tung, L. K. H. Trang, T. Y. Kim and K. S. Suh, *Colloid and Polymer Science*, 2010, **288**, 1013-1018 (DOI:10.1007/s00396-010-2229-3).

- 140 M. F. L. De Volder, S. H. Tawfick, R. H. Baughman and A. J. Hart, *Science*, 2013, **339**, 535-539 (DOI:10.1126/science.1222453).
- 141 J. Leis, A. Perkson, M. Arulepp, M. Kaarik and G. Svensson, *Carbon*, 2001, **39**, 2043-2048 (DOI:10.1016/S0008-6223(01)00020-3).
- 142 X. Xie, L. Gao, J. Sun, Y. Liu, H. Kajiura, Y. Li and K. Noda, *Carbon*, 2008, **46**, 1145-1151 (DOI:10.1016/j.carbon.2008.04.014).
- 143 A. Krishna, C. Laslau, G. I. N. Waterhouse, Z. D. Zujovic and J. Travas-Sejdic, *Chemical Papers*, 2013, **67**, 995-1001 (DOI:10.2478/s11696-013-0327-7).
- 144 J. Thomassin, X. Lou, C. Pagnouille, A. Saib, L. Bednarz, I. Huynen, R. Jerome and C. Detrembleur, *Journal of Physical Chemistry C*, 2007, **111**, 11186-11192 (DOI:10.1021/jp0701690).
- 145 P. Gajendran and R. Saraswathi, *Pure and Applied Chemistry*, 2008, **80**, 2377-2395 (DOI:10.1351/pac200880112377).
- 146 A. A. Ganash, *Journal of Composite Materials*, 2014, **48**, 2215-2225 (DOI:10.1177/0021998313495904).
- 147 H. Zengin, W. S. Zhou, J. Y. Jin, R. Czerw, D. W. Smith, L. Echegoyen, D. L. Carroll, S. H. Foulger and J. Ballato, *Advanced Materials*, 2002, **14**, 1480-1483 (DOI:10.1002/1521-4095(20021016)14:203.0.CO;2-O).
- 148 D. Wei, C. Kvarnstrom, T. Lindfors and A. Ivaska, *Electrochemistry Communications*, 2007, **9**, 206-210 (DOI:10.1016/j.elecom.2006.09.008).
- 149 S. S. Karajanagi, H. C. Yang, P. Asuri, E. Sellitto, J. S. Dordick and R. S. Kane, *Langmuir*, 2006, **22**, 1392-1395 (DOI:10.1021/la0528201).
- 150 Y. Sabba and E. L. Thomas, *Macromolecules*, 2004, **37**, 4815-4820 (DOI:10.1021/ma049706u).
- 151 B. Fei, H. F. Lu, Z. G. Hu and J. H. Xin, *Nanotechnology*, 2006, **17**, 1589-1593 (DOI:10.1088/0957-4484/17/6/010).
- 152 M. C. Gutierrez, F. Rubio and F. del Monte, *Chemistry of Materials*, 2010, **22**, 2711-2719 (DOI:10.1021/cm9023502).
- 153 H. Maka, T. Szychaj and K. Kowalczyk, *Journal of Applied Polymer Science*, 2014, **131** (DOI:10.1002/app.40401).
- 154 C. Park, Z. Ounaies, K. A. Watson, R. E. Crooks, J. Smith, S. E. Lowther, J. W. Connell, E. J. Siochi, J. S. Harrison and T. L. S. Clair, *Chemical Physics Letters*, 2002, **364**, 303-308 (DOI:10.1016/S0009-2614(02)01326-X).
- 155 J. Sandler, M. S. P. Shaffer, T. Prasse, W. Bauhofer, K. Schulte and A. H. Windle, *Polymer*, 1999, **40**, 5967-5971 (DOI:10.1016/S0032-3861(99)00166-4).

- 156 B. Fragneaud, K. Masenelli-Varlot, A. Gonzalez-Montiel, M. Terrones and J. Y. Cavaille, *Chemical Physics Letters*, 2006, **419**, 567-573 (DOI:10.1016/j.cplett.2005.12.011).
- 157 S. Banerjee, T. Hemraj-Benny and S. S. Wong, *Advanced Materials*, 2005, **17**, 17-29 (DOI:10.1002/adma.200401340).
- 158 B. Yu, F. Zhou, G. Liu, Y. Liang, W. T. S. Huck and W. Liu, *Chemical Communications*, 2006, , 2356-2358 (DOI:10.1039/b603878f).
- 159 M. Baibarac, I. Baltog, C. Godon, S. Lefrant and O. Chauvet, *Carbon*, 2004, **42**, 3143-3152 (DOI:10.1016/j.carbon.2004.07.030).
- 160 H. Chen, H. Muthuraman, P. Stokes, J. Zou, X. Liu, J. Wang, Q. Huo, S. I. Khondaker and L. Zhai, *Nanotechnology*, 2007, **18**, 415606 (DOI:10.1088/0957-4484/18/41/415606).
- 161 W. Feng, X. D. Bai, Y. Q. Lian, J. Liang, X. G. Wang and K. Yoshino, *Carbon*, 2003, **41**, 1551-1557 (DOI:10.1016/S0008-6223(03)00078-2).
- 162 D. J. Guo and H. L. Li, *Journal of Solid State Electrochemistry*, 2005, **9**, 445-449 (DOI:10.1007/s10008-004-0589-7).
- 163 J. D. Mota-Morales, M. C. Gutierrez, M. Luisa Ferrer, R. Jimenez, P. Santiago, I. C. Sanchez, M. Terrones, F. Del Monte and G. Luna-Barcenas, *Journal of Materials Chemistry a*, 2013, **1**, 3970-3976 (DOI:10.1039/c3ta01020a).
- 164 A. Garai and A. K. Nandi, *Synthetic Metals*, 2009, **159**, 1710-1716 (DOI:10.1016/j.synthmet.2009.05.011).
- 165 J. Chen, M. A. Hamon, H. Hu, Y. S. Chen, A. M. Rao, P. C. Eklund and R. C. Haddon, *Science*, 1998, **282**, 95-98 (DOI:10.1126/science.282.5386.95).
- 166 Z. Yang, X. Chen, C. Chen, W. Li, H. Zhang, L. Xu and B. Yi, *Polymer Composites*, 2007, **28**, 36-41 (DOI:10.1002/pc.20254).
- 167 A. Star, J. F. Stoddart, D. Steuerman, M. Diehl, A. Boukai, E. W. Wong, X. Yang, S. W. Chung, H. Choi and J. R. Heath, *Angewandte Chemie-International Edition*, 2001, **40**, 1721-1725 (DOI:10.1002/1521-3773(20010504)40:93.0.CO;2-F).
- 168 R. V. Salvatierra, M. M. Oliveira and A. J. G. Zarbin, *Chemistry of Materials*, 2010, **22**, 5222-5234 (DOI:10.1021/cm1012153).
- 169 V. Georgakilas, K. Kordatos, M. Prato, D. M. Guldi, M. Holzinger and A. Hirsch, *Journal of Americal Chemical Society*, 2002, **124**, 760-761 (DOI:10.1021/ja016954m).
- 170 J. L. Bahr and J. M. Tour, *Journal of Materials Chemistry*, 2002, **12**, 1952-1958 (DOI:10.1039/b201013p).

- 171 S. Bhattacharyya, E. Kymakis and G. A. J. Amaratunga, *Chemistry of Materials*, 2004, **16**, 4819-4823 (DOI:10.1021/cm0496063).
- 172 E. Kymakis and G. A. J. Amaratunga, *Applied Physical Letters*, 2002, **80**, 112-114 (DOI:10.1063/1.1428416).
- 173 G. M. A. Rahman, D. M. Guldi, R. Cagnoli, A. Mucci, L. Schenetti, L. Vaccari and M. Prato, *Journal of American Chemical Society*, 2005, **127**, 10051-10057 (DOI:10.1021/ja050396k).
- 174 W. J. Liou, T. Y. Yang, K. N. Lin, C. H. Yang and H. M. Lin, *Semiconductor Materials for Sensing*, 2005, **828**, 85-95.
- 175 C. Peng, S. Zhang, D. Jewell and G. Z. Chen, *Progress in Natural Science-Materials International*, 2008, **18**, 777-788 (DOI:10.1016/j.pnsc.2008.03.002).
- 176 M. A. Lilga, R. J. Orth, J. P. H. Sukamto, S. D. Rassat, J. D. Genders and R. Gopal, *Separation and Purification Technology*, 2001, **24**, 451-466 (DOI:10.1016/S1383-5866(01)00145-9).
- 177 S. D. Rassat, J. H. Sukamto, R. J. Orth, M. A. Lilga and R. T. Hallen, *Separation and Purification Technology*, 1999, **15**, 207-222 (DOI:10.1016/S1383-5866(98)00102-6).
- 178 Y. H. Lin and X. L. Cui, *Chemical Communications*, 2005, , 2226-2228 (DOI:10.1039/b500417a).
- 179 P. Burgmayer and R. W. Murray, *Journal of Physical Chemistry*, 1984, **88**, 2515-2521 (DOI:10.1021/j150656a017).
- 180 Y. H. Lin, X. L. Cui and J. Bontha, *Environmental Science and Technology*, 2006, **40**, 4004-4009 (DOI:10.1021/es052148u).
- 181 V. M. Schmidt and J. Heitbaum, *Electrochimica Acta*, 1993, **38**, 349-356 (DOI:10.1016/0013-4686(93)85150-W).
- 182 C. Lopez, M. F. M. Viegas, G. Bidan and E. Vieil, *Synthetic Metals*, 1994, **63**, 73-78 (DOI:10.1016/0379-6779(94)90252-6).
- 183 Q. X. Zhou, C. J. Kolaskie and L. L. Miller, *J Electroanalytical Chemistry*, 1987, **223**, 283-286 (DOI:10.1016/0022-0728(87)85267-1).
- 184 Q. J. Xie, S. Kuwabata and H. Yoneyama, *Journal of Electroanalytical Chemistry*, 1997, **420**, 219-225 (DOI:10.1016/S0022-0728(96)04777-8).
- 185 H. Lee, H. Yang and J. Kwak, *Journal of Electroanalytical Chemistry*, 1999, **468**, 104-109 (DOI:10.1016/S0022-0728(99)00037-6).
- 186 M. D. Levi, C. Lopez, E. Vieil and M. A. Vorotyntsev, *Electrochimica Acta*, 1997, **42**, 757-769 (DOI:10.1016/S0013-4686(96)00340-4).

- 187 F. B. Diniz, K. C. S. deFreitas and W. M. deAzevedo, *Electrochimica Acta*, 1997, **42**, 1789-1793 (DOI:10.1016/S0013-4686(96)00378-7).
- 188 S. Bruckenstein, K. Brzezinska and A. R. Hillman, *Electrochimica Acta*, 2000, **45**, 3801-3811 (DOI:10.1016/S0013-4686(00)00467-9).
- 189 A. Bund and S. Neudeck, *Journal of Physical Chemistry B*, 2004, **108**, 17845-17850 (DOI:10.1021/jp0469721).
- 190 S. Bruckenstein, K. Brzezinska and A. R. Hillman, *Physical Chemistry Chemical Physics*, 2000, **2**, 1221-1229 (DOI:10.1039/a908719b).
- 191 R. Zhang, H. Ma and B. Wang, *Industrial and Engineering Chemistry Research*, 2010, **49**, 9998-10004 (DOI:10.1021/ie1008794).
- 192 A. Fedorczyk and M. Skomska, *Electrochimica Acta*, 2013, **99**, 62-68 (DOI:10.1016/j.electacta.2013.03.087).
- 193 Y. Zhang, S. Mu, B. Deng and J. Zheng, *Journal of Electroanalytical Chemistry*, 2010, **641**, 1-6 (DOI:10.1016/j.jelechem.2010.01.021).
- 194 T. Welton, *Chem. Rev.*, 1999, **99**, 2071-2083 (DOI:10.1021/cr980032t).
- 195 P. C. Innis, J. Mazurkiewicz, T. Nguyen, G. G. Wallace and D. MacFarlane, *Current Applied Physics*, 2004, **4**, 389-393 (DOI:<http://dx.doi.org.ezproxy3.lib.le.ac.uk/10.1016/j.cap.2003.11.056>).
- 196 C. Nanjundiah, S. F. McDevitt and V. R. Koch, *Journal of Electrochemistry Society*, 1997, **144**, 3392-3397 (DOI:10.1149/1.1838024).
- 197 D. R. Macfarlane, M. Forsyth, P. C. Howlett, J. M. Pringle, J. Sun, G. Annat, W. Neil and E. I. Izgorodina, *Accounts of Chemical Research*, 2007, **40**, 1165-1173 (DOI:10.1021/ar7000952).
- 198 S. Ahmad, M. Deepa and S. Singh, *Langmuir*, 2007, **23**, 11430-11433 (DOI:10.1021/la702442c).
- 199 K. Sekiguchi, M. Atobe and T. Fuchigami, *Journal of Electroanalytical Chemistry*, 2003, **557**, 1-7 (DOI:10.1016/S0022-0728(03)00344-9).
- 200 P. G. Pickup and R. A. Osteryoung, *Journal of American Chemical Society*, 1984, **106**, 2294-2299 (DOI:10.1021/ja00320a014).
- 201 P. G. Pickup and R. A. Osteryoung, *Journal of Electroanalytical Chemistry*, 1985, **195**, 271-288 (DOI:10.1016/0022-0728(85)80048-6).
- 202 T. A. Zawodzinski, L. Janiszewska and R. A. Osteryoung, *Journal of Electroanalytical Chemistry*, 1988, **255**, 111-117 (DOI:10.1016/0022-0728(88)80008-1).

- 203 L. Janiszewska and R. A. Osteryoung, *Journal of Electrochemical Society*, 1987, **134**, 2787-2794 (DOI:10.1149/1.2100288).
- 204 Z. J. Miao, Y. Wang, Z. M. Liu, J. Huang, B. X. Han, Z. Y. Sun and J. M. Du, *Journal of Nanoscience and Nanotechnology*, 2006, **6**, 227-230 (DOI:10.1166/jnn.2006.054).
- 205 N. Koura, H. Ejiri and K. Takeishi, *Denki Kagaku*, 1991, **59**, 74-75.
- 206 N. Koura, H. Ejiri and K. Takeishi, *Journal of Electrochemical Society*, 1993, **140**, 602-605 (DOI:10.1149/1.2056128).
- 207 S. Mu, *Electrochimica Acta*, 2007, **52**, 7827-7834 (DOI:10.1016/j.electacta.2007.06.053).
- 208 D. Wei, C. Kvarnstrom, T. Lindfors and A. Ivaska, *Electrochemistry Communications*, 2006, **8**, 1563-1566 (DOI:10.1016/j.elecom.2006.07.024).
- 209 F. F. C. Bazito, L. T. Silveira, R. M. Torresi and S. I. Cordoba de Torresi, *Physical Chemistry Chemical Physics*, 2008, **10**, 1457-1462 (DOI:10.1039/b714458j).
- 210 Q. Zhang, K. D. O. Vigier, S. Royer and F. Jerome, *Chemical Society Reviews*, 2012, **41**, 7108-7146 (DOI:10.1039/c2cs35178a).
- 211 E. L. Smith, A. P. Abbott and K. S. Ryder, *Chemical Reviews*, 2014, **114**, 11060-11082 (DOI:10.1021/cr300162p).
- 212 P. M. V. Fernandes, J. M. Campina, C. M. Pereira and F. Silva, *Journal of Electrochemical Society*, 2012, **159**, G97-G105 (DOI:10.1149/2.059209jes).
- 213 M. A. Skopek, M. A. Mohamoud, K. S. Ryder and A. R. Hillman, *Chemical Communications*, 2009, , 935-937 (DOI:10.1039/b819084d).
- 214 K. P. Prathish, R. C. Carvalho and C. M. A. Brett, *Electrochemistry Communications*, 2014, **44**, 8-11 (DOI:10.1016/j.elecom.2014.03.026).
- 215 A. R. Hillman, K. S. Ryder, V. C. Ferreira, C. J. Zaleski and E. Vieil, *Electrochimica Acta*, 2013, **110**, 418-427 (DOI:10.1016/j.electacta.2013.07.120).

Chapter II:

Methodology

2.1. Introduction

This chapter gives a comprehensive introduction to electrochemical measurement techniques, and the surface and structure characterisation techniques used in this research.

Electrochemical techniques are so widely used for characterisation of polymer-modified electrodes. Electrochemical techniques are used to monitor not only the film response to their electrolyte but also the deposition mechanisms of films. Among these techniques, although cyclic voltammetry is the most popular, the electrochemical quartz crystal microbalance (EQCM) is preferable for monitoring small mass changes when combined with cyclic voltammetry.¹⁻³ A large number of studies have reported on the use of the quartz crystal microbalance in different fields.⁴⁻⁷

Non-electrochemical techniques were also used in this research to define the characteristics of the prepared polymer-modified electrodes. Scanning electron microscopy (SEM) and 3D microscopy have been used to define the characteristics of the modified electrodes in high resolution while FTIR has provided for structural analysis of the prepared modified electrodes.

2.2. Electrochemistry and Electrochemical Techniques

Electrochemistry can be defined as the study of chemical reactions by applying electrical potential/current across the interface between electrodes (commonly metallic but not always) and an electrolyte solution. There are two types of electrochemical methods, which are the interfacial and bulk methods. In interfacial methods, the electrochemical reaction takes place between the electrode surfaces, while in bulk methods it occurs within the bulk of the solution.³ We have focused on interfacial methods in this research.

Interfacial methods are classified into two main categories as per the absence or presence of a current, which are referred to as the static and dynamic methods, respectively. Static methods include potentiometric measurements. The basis of dynamic methods is the flow of a current throughout the electrochemical cell, which provides information about the concentration and other properties of electroactive species.⁸ Cyclic voltammetry and chronoamperometry are the most common dynamic interfacial methods used in this research.

The electrochemical cell used in dynamic interfacial techniques is a simple system consisting of a working electrode and a reference electrode. The electrochemical reaction takes place at the working electrode while the reference electrode provides a constant, fixed potential. Thus, the acquired response can only originate from electrochemical reactions on the surface of the working electrode. However, to measure the increase in any current requires a typical three-electrode system, as shown in figure 2.1.^{2, 9, 10} In the three-electrode system, there is a counter electrode in addition to a working electrode and a reference electrode.

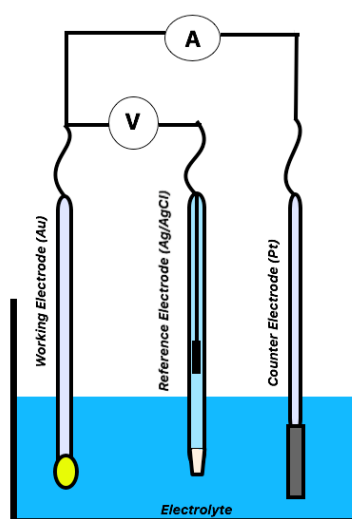
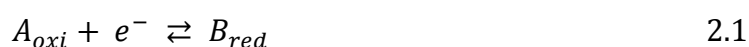


Figure 2.1. A schematic representation of a typical three-electrode system

The electrochemical reaction on the surface of a conventional working electrode can be illustrated by the following equation:



A_{oxi} and B_{red} in equation 2.1 are the oxidized and reduced forms of the electroactive species, respectively. This reaction is driven a continuous electron transfer and the

accompanying the mass transport of mobile species at the electrode/solution interface.^{1, 2, 10}

If a voltage, E , is applied between a working electrode and reference electrode, a current would be flowed between them, then:

$$E = E_e - E_s + iR + E_s - E_{ref} \quad 2.2$$

In equation 2.2, E originates from three terms. $E_e - E_s$ is the driving force for electrochemical reactions at the working electrode/solution interface; $E_s - E_{ref}$ is the potential drop at the reference electrode; iR is the potential drop in the solution due to the current flowing between two electrodes; lastly, R is the resistance of the bulk solution. In the case of microelectrodes, iR can be neglected and the current can be measured as a function of the applied potential ($E_e - E_s$) at a fixed potential ($E_s - E_{ref}$). On the other hand, iR cannot be neglected and the addition of a counter electrode is required in the electrochemical cell to account for this.^{1, 2, 10}

In the case of conductive polymer-modified electrodes, two or more interfaces can appear, which are at the electrode/polymer interface (electron exchange takes place) and at the polymer/solution interface (ion/solvent exchange occurs).¹¹⁻¹⁴

2.2.1. Mass Transfer

For an electrochemical reaction to occur at the surface of an electrode, the transport of the mobile ions is necessary. This transfer can proceed in any of three ways, by diffusion, convection or migration. Diffusion originates from the difference in concentration of the electroactive species in the bulk solution and the electrode surface, which drives the dispersion of the redox species throughout the system. In contrast to diffusion, convection occurs when applying a mechanical force. This mechanical force can be generated not only through the involvement of external sources (stirring, pumping, etc.) but also through natural means such as thermal gradients and/or differences in density. The last mass transport, migration, is derived from an external electric field. The drop in electrical potential results in an electric field (i.e., a gradient)

at the electrode/solution interface, which induces the movement of ions to or from the electrode.^{1, 10}

2.3. Cyclic Voltammetry

2.3.1. Overview

Cyclic voltammetry (CV) is a highly useful technique that provides a wide range of information about the mechanism and rates of electrochemical reactions that occur at the electrode surface/solution interface during the generation of modified electrodes.

Cyclic voltammetry is based on sweeping the potential applied to the working electrode between a starting and finishing potential, E_1 and E_2 , respectively, at a constant scan rate, v ($V s^{-1}$). This gives a triangular potential waveform as a function of time, as shown in figure 2.2.^{1, 10}

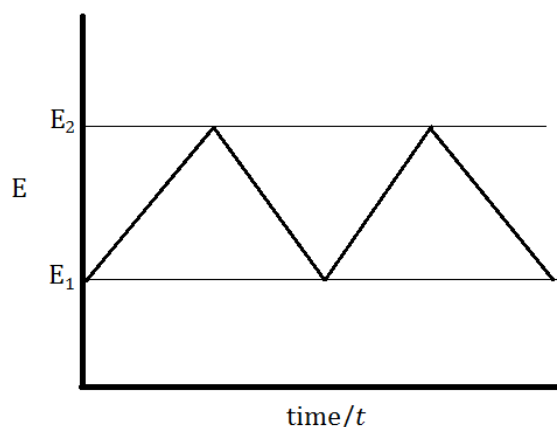


Figure 2.2. The response of the applied potential as a function of time in a cyclic voltammetry experiment

Although there is no chemical reaction at the electrode surface at the initial value, E_1 , the electrochemical reactions of the electroactive species will take place at the final value, E_2 . While a potentiostat monitors the change in potentials between the working and reference electrodes, the current flowing between the working electrode and counter electrode is also measured. Valuable information about the electrochemical reactions of electroactive species at electrode surface/solution interface can be derived from this current measurement. The integration current flow with regards to time allows for the

calculation of the total charge passed during the experiment, which is associated with a number of electroactive species present.¹

In cyclic voltammetry measurements, varying the scan rate also produces kinetic data about the electrochemical reactions.¹

2.3.2. Data Interpretation

When the potential, E_1 , is applied, the formation of B_{red} species occurs at the electrode surface during the forward scan. With the application of the potential E_2 , A_{oxi} species will be formed on the electrode surface along the reverse scan. The E_1 and E_2 potentials are called switching potentials, which are selected with respect to the electrochemical properties of the sample.^{1, 10}

The initial scan can be negative or positive depending on the characteristics of the sample. Figure 2.3 illustrates a negative scan. The current as a function of applied potential initially increases due to the formation of B_{red} species being preferable while the potential becomes more positive. In the reverse scan, the B_{red} species is transformed to A_{oxi} species and the current drops to zero.

The shape of the CV is dependent on the reversibility or irreversibility of the electrochemical reaction (A_{oxi}/B_{red} from equation 2.1) at the electrode surface/solution interface during the forward and reverse scans. The kinetic behaviour of the electroactive species determines the reversible and irreversible behaviour. The amount of A_{oxi} and B_{red} species present at any given moment changes according to electron and mass transfer rates.^{1, 2, 15}

A typical cyclic voltammogram for a reversible electroactive species (A_{oxi}/B_{red}) is presented in figure 2.3. The current flows with the sweeping potential in the forward and reverse scans.

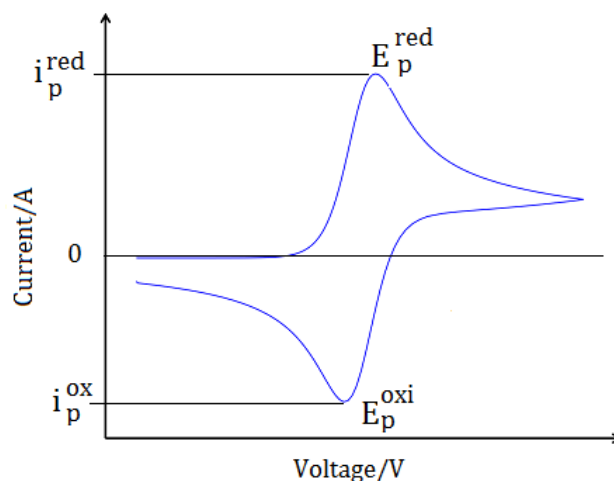


Figure 2.3. A typical cyclic voltammogram for a reversible redox reaction

In a reversible system, the size of the peak produced in the forward and reverse directions are almost identical. The difference in magnitude of these peaks is 59 mV (at 25°C) neglecting the effect of scan rate. Assuming the transfer of n electrons during the electrochemical reactions:

$$|E_p^{ox} - E_p^{red}| = 2.218 \frac{RT}{nF} \quad 2.3$$

In irreversible electrochemical reactions, no definite anodic peak will be obtained, while the cathodic peak appears at a more negative potential to contrary the reversible systems. This can be an indication of the necessarily higher potential required to observe the anodic peak in the forward scan.

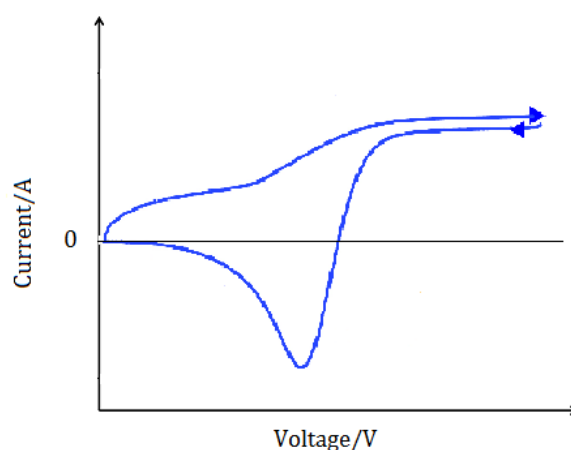


Figure 2.4. Cyclic voltammogram for an irreversible redox reaction

The scan rate has no influence on the reversible/irreversible nature of electroactive species, but it does affect the magnitude of the peak currents of the anodic and cathodic peaks. The relationship between the changes in magnitude of the peak current, i_p , as a function of $v^{1/2}$ is linear, as shown in figure 2.5.¹

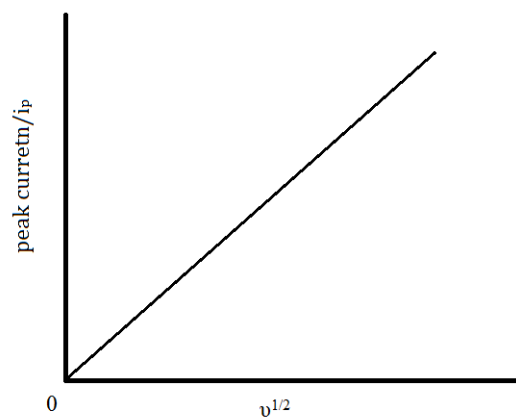


Figure 2.5. Variation of peak current, i_p , as a function of voltage scan rate, $v^{1/2}$

2.4. Chronoamperometry

2.4.1. Overview

Chronoamperometry measures the current-time response (shown in figure 2.6) of the electroactive species during an electrochemical reaction, which allows the measurement of the rate of the reaction.^{1, 10}

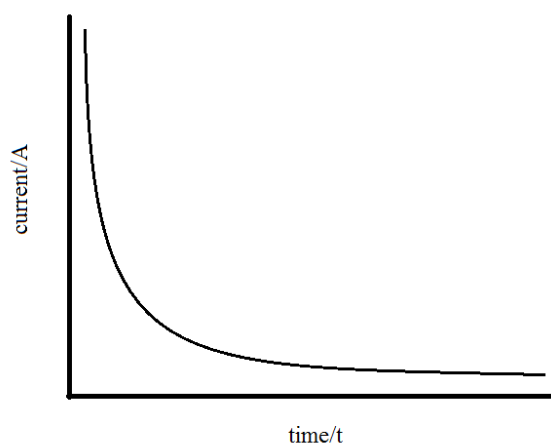


Figure 2.6. The current response in a potential step experiment

2.4.2. Data Interpretation

Initially, the current is very large, as shown in Figure 2.6, but then consistently decreases with time. This is due to the depletion of the electroactive species (A) that occurs with the formation of the diffusion layer. This current ultimately tends towards zero, as is also illustrated in figure 2.6. In this case, the Cottrell equation can be useful to define the current response as function of time;¹

$$|i| = \frac{nFAD_A^{\frac{1}{2}}[A]_{bulk}}{\pi^{\frac{1}{2}}t^{\frac{1}{2}}} \quad 2.4$$

In this equation, F is the Faraday constant (96485 C s^{-1}), n is the number of transferred electrons, D is the diffusion coefficient, and I is the current. According to this equation, it is possible to measure the diffusion coefficient with potential swept experiments.^{1, 10}

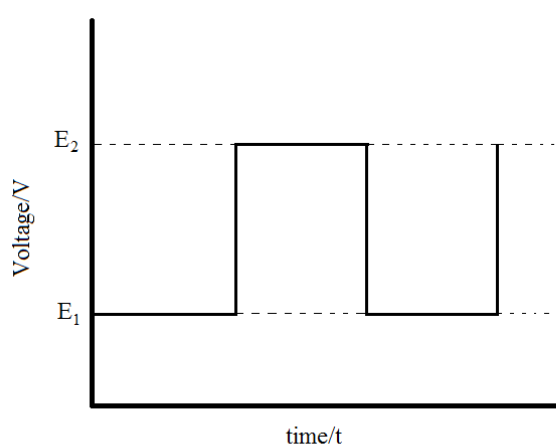


Figure 2.7. The variation of applied potential in a potential step experiments

2.5. Quartz Crystal Microbalance (QCM)

2.5.1. Overview

The quartz crystal microbalance (QCM) serves as a gravimetric sensor, providing high sensitivity while allowing for the observation of small mass changes in electroactive species on the electrode surface during electrochemical reactions via the changes in resonant frequency of a quartz crystal as mass is deposited.¹⁶ The principle of this

technique is based on the piezoelectric effect of the quartz crystal, as will be explained in the following section. The QCM method is an absolute method, which means it does not require any prior calibration.¹⁷

2.5.2. The Piezoelectric Effect

The piezoelectric effect can be generated in two ways: (i) when a quartz crystal is exposed to a mechanical force, a potential difference occurs across its surface, which is called the “direct piezoelectric effect”; (ii) when a potential is applied across a quartz crystal, it causes a mechanical shear stress known as the “converse piezoelectric effect”. The mechanical shear stress is proportional to the applied potential.³ Figure 2.8 illustrated the piezoelectric effect.

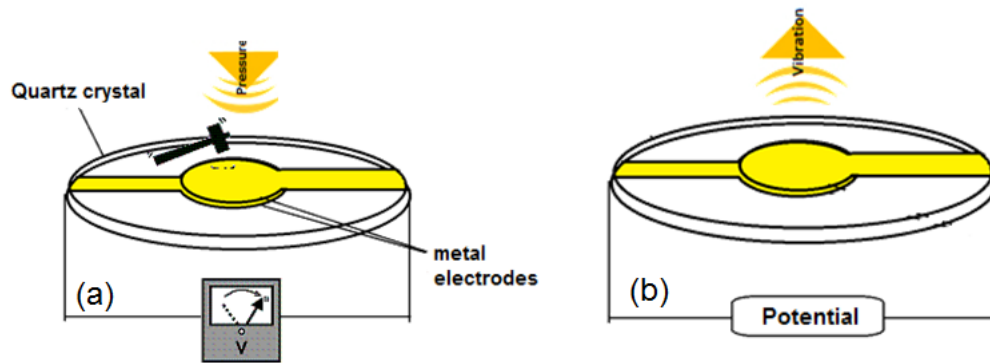


Figure 2.8. (a) pizoelectric effect (b) converse piezoelectric effect

The connection between the piezoelectric effect and crystal structure was primarily described by the Curie Brothers in 1880,¹⁸ whose studies showed the formation of an electric potential between the faces of a quartz crystal when an applying a stress to its two faces. This electric field, which is proportional to the applied stress, is called the direct piezoelectric effect. The discovery of the direct piezoelectric effect leads directly to the development of the mathematical model of the converse piezoelectric effect by Lippmann.¹⁸ According to this model, a potential difference applied to the surfaces of the crystal will produce a distortion in the lattice of the crystal that results in mechanical strain at its surface. This model was proved experimentally by the Curies in 1881¹⁸ but there was little further research into piezoelectric devices until 1917. The development of first ultrasonic detector in 1917 stimulated considerable interest in piezoelectric devices.

On the other words, if there is an oscillation in the quartz crystal, there is always a resonance frequency (abbreviated to f_o). This oscillation occurs with minimum impedance in conjunction with the maximal admittance. The resonance frequency of the quartz crystal depends on its dimensions and certain physical properties, generally its density and shear modulus. It can vibrate at other frequencies when the admittance decreases until the point where the vibration can no longer be detected.³ This change in resonance frequency is relevant with loading or removing the mass or during its interaction with a liquid, which can be determined with high accuracy.³

2.5.3. The Quartz Crystal Orientation of Cut

The chemical, thermal and mechanical stability, and indeed cost efficiency, of a quartz crystal has led to its use in a wide range of frequency-controlled devices. On the other hand, there are many types of the vibrational mode in its natural form, which are commonly longitudinal (extensional), lateral (flexural and shear) and torsional (twist). This can be complicated when a particular mode is required. For these cases, the quartz crystal is cut at a specific orientation and shape in order to avoid other modes. Both the AT- and BT-cut angles (shown in figure 2.9) provide vibrations in one direction of the thickness-shear mode of the quartz crystals. Thus, QCM resonators are occasionally referred to as thickness shear mode (TSM) resonators. Also, this vibrational mode is sensitive to any mass change of the quartz crystal, and further the AT-cut quartz crystal shows almost zero temperature dependence at room temperature.¹⁹ Thus, AT-cut crystals have become the preferred cut for quartz crystal microbalance (besides their low cost).

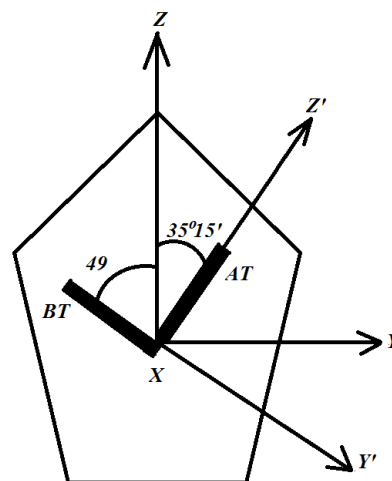


Figure 2.9. Images of AT-cut and BT-cut quartz crystals

2.5.4. Sauerbrey Equation

The first introduction of the principle of the QCM technique was performed by Sauerbrey in 1959 while observing the deposition of thin films on the first quartz crystal resonators in ultra-high vacuum conditions. According to this introduction, the resonance frequency is proportional to the mass change of the quartz crystal.¹⁷

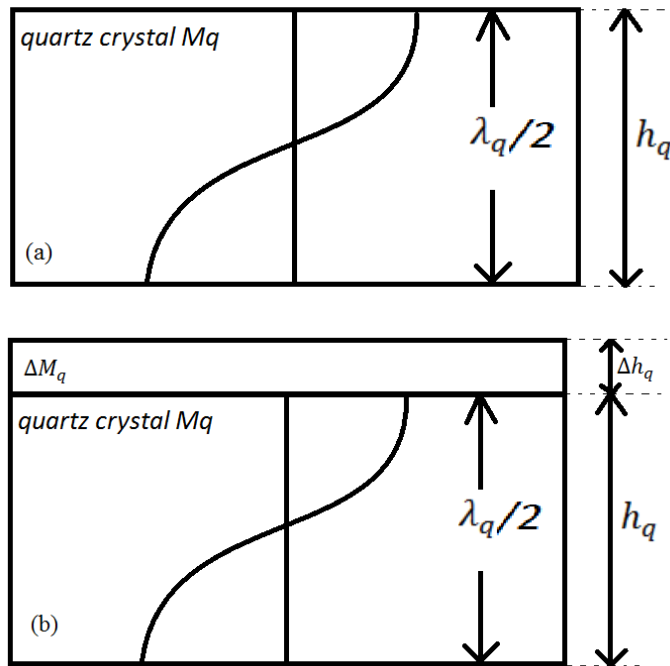


Figure 2.10. (a) the thickness of a QCM as relevant to acoustic wavelength (b) a rigid mass results in an increase in h_q and therefore an increase in λ

The acoustic wavelength during oscillation is related to the thickness of the quartz crystal, as shown in figure 2.10. The change in the thickness, h_q , of the quartz crystal by addition of mass causes an increase in the acoustic wavelength, λ :

$$h_q = \frac{\lambda_q}{2} \tag{2.5}$$

The relationship between the shear wave velocity, v_q , and the fundamental resonance frequency, f_o , of the quartz crystal is stated in the following equation:

$$f_o = \frac{v_q}{\lambda_q} \tag{2.6}$$

By combining equation 2.5 and equation 2.6:

$$h_q = \frac{1}{2} N \lambda = \frac{1}{2} N \left(\frac{v_q}{f_o} \right) \quad 2.7$$

Equation 2.7 shows that the resonance frequency of the quartz crystal is inversely proportional to its thickness. N is an odd integer ($N = 1, 3, 5, \dots$). The shear wave velocity can be calculated from the crystal shear modulus, μ_q ($\mu_q = 2.947 \times 10^{11} \text{ g cm}^{-1} \text{ s}^{-2}$) and the crystal density, ρ_q ($\rho_q = 2.648 \text{ g cm}^{-3}$):

$$v_s = \left(\frac{\mu_q}{\rho_q} \right)^{\frac{1}{2}} \quad 2.8$$

If equation 2.7 is inserted into equation 2.8:

$$h_q = \frac{1}{2} \frac{N}{f_o} \left(\frac{\mu_q}{\rho_q} \right)^{1/2} = \frac{N}{f_o} \left(1.7 \frac{\text{nm}}{\text{s}} \right) \quad 2.9$$

Equation 2.9 shows the direct relationship between the thickness and the resonance frequency of the quartz crystal. The measurements in QCM mostly employ 5 and 10 MHz frequencies, which correspond to h_q values of 0.0334 and 0.0167 cm, respectively, for AT-cut crystals.

The thickness of the quartz crystal is changed with loading mass, which leads to a decrease in resonance frequency, as expressed in equation 2.10:

$$\frac{\Delta f}{f_o} = - \frac{\Delta h}{h_q} \quad 2.10$$

The negative sign of in equation 2.10 illustrates that the resonance frequency and the thickness of the quartz crystal is inversely proportional. The density, ρ_q , and piezoelectric active area, A , of the quartz crystal help to determine the change in thickness via equation 2.11:

$$\Delta h = \Delta m / A_q \rho_q \quad 2.11$$

When equation 2.11 is inserted into equation 2.10, equation 2.12 can be derived as follows:

$$\frac{\Delta f}{f_o} = - \frac{\Delta m}{h_q A_q \rho_q} \quad 2.12$$

The combination and rearrangement of equations 2.9 and 2.12 gives:

$$\Delta f = - \frac{2f_o^2}{(\mu_q \rho_q)} \frac{\Delta m}{A_p} N \quad 2.13$$

The obtained equation 2.13 is the basic form of the Sauerbrey Equation. The abbreviation of equation 2.13 is given by equation 2.14.

$$\Delta f = -C_1 \Delta m \quad 2.14$$

In equation 2.14, C_1 is a constant, with a value of $C_1 = 2.26 \times 10^8 \text{ Hz cm}^2 \text{ g}^{-1}$ for AT-cut crystals ($N = 1$). According to this equation, a 1 Hz change in frequency of the quartz crystal for 10 MHz AT-cut crystals corresponds to a ca. 1 ng change in mass of the quartz crystal.¹⁷

The Sauerbrey equation is valid only for a small, rigid and uniform mass gain to the quartz crystal so that the frequency change is directly proportional to the gain in mass. In addition to these, the QCM technique can be used in vacuum and gaseous environments. These limitations of the QCM application have led to the emergence of several studies in order to utilise QCM as a gravimetric tool.¹⁷

In the 1980s, it was shown that the QCM technique can be performed in a liquid²⁰. In this case, the resonance frequency change of the quartz crystal is not only due to mass change but also the density and viscosity of the liquid, and the Sauerbrey Equation can then be expressed as follows:

$$\Delta f = -f_o^{3/2} \left(\frac{\rho_L \eta_L}{\pi \rho_q \mu_q} \right)^{1/2} \quad 2.15$$

In equation 2.15, ρ_L is the density of the product and η_L is the viscosity of the liquid. In ideal conditions, the product and liquid remain constant while any experiments are

ongoing. Then, the Sauerbrey Equation remains applicable for the liquid medium, as shown in equation 2.16, where μ_q and ρ_q are the shear modulus and density of quartz with values of $2.947 \times 10^{11} \text{ g cm}^{-1} \text{ s}^{-2}$ and 2.65 g cm^{-3} , respectively.

$$\Delta f = -2.26 \times 10^{-6} f_o^2 \Delta m \quad 2.16$$

2.5.5. The Effect of Excess Mass and the Surface Roughness

The other limitation of the Sauerbrey Equation is in circumstances of high mass loading, resulting in a failure of the Sauerbrey Equation. Reported studies show that the validity of the Sauerbrey Equation extends up to around 10% mass gain of the quartz crystal. If there is further mass gain, then the density and the shear modulus of the film must be taken into account.

A smooth surface for QCM applications is favourable, providing a direct relationship between the frequency change and the square root of the viscosity-density product of the solution²¹. With a rough surface, the liquid can partially or completely fill in the surface, restricting the behaviour of the surface. In this case, a perfectly polished quartz crystal can help minimise the effects of roughness.

Harmonic oscillation; the higher oscillating frequency of the quartz crystal increases its sensitivity to mass change. However, the oscillating frequency can be increased by decreasing the thickness of a crystal, resulting in a fragile, thin crystal. The other way is to stimulate higher harmonics.

$$f_N = \frac{Nv_q}{2h_q} \quad 2.17$$

In equation 2.17, f_N is the resonance frequency and N (an integer) is the harmonic number. The sensitivity shows a linear increase with higher harmonic numbers. However, it indicates a squared relationship with the fundamental frequency.

2.5.6. Electrochemical Quartz Crystal Microbalance (EQCM)

The quartz crystal resonator has been used in a wide variety of areas such as electrochemistry after the contributions by Kanazawa and Bruckenstein.^{6, 7, 12, 20, 22} The

QCM contains a piece of quartz with a vacuum-deposited electrode (commonly gold, or platinum) on either side. While one surface of the quartz crystal is in direct contact with the electrolyte solution, the other surface remains exposed to air. The surface in contact with the solution is used as the working electrode for electrochemical experiments. The EQCM technique produces not only frequency changes (mass changes) but also current density change as a function of the applied potential.

The EQCM technique can be used in a wide range of studies because it has a high sensitivity to mass change and a short data acquisition time (commonly < 1 s). Among these studies, it has been generally preferred in studies of the electrodeposition and charge/mass transfer processes of conducting polymers.^{5, 14, 23-28} This is because it is capable of quantitative analysis of rigid films owing to its gravimetric operation.²⁹

2.5.7. The Effect of Viscosity

In polymer-modified electrodes, the characterisation of specific ions and molecules during electrochemical experiments can be carried out by EQCM when the mass loading on the quartz crystal is deposited. The relationship between the frequency change and mass change during the deposition is illustrated in the following statement:

$$\Delta f = \frac{CF^2\Delta m}{A} \quad 2.18$$

In equation 2.18, Δm and Δf are the mass and frequency change of the quartz crystal during the deposition, respectively. F is the Faraday constant, A is the piezoelectric active area and C is a constant of proportionality. This equation is useful for the acoustically thin film of polymer formation on the surface of electrode, which can measure the mass change with high accuracy. However, the polymer-modified electrodes commonly form a thick film, which can result in a certain viscosity of the polymer film on the electrode surface. To overcome this problem, a new model that accounts for these parameters is presented in equation 2.19.¹⁴

$$\Delta f^* = \Delta f + \frac{i\Delta w}{2(i^2 = -1)} \quad 2.19$$

In the equation 2.19, Δw is the damping. According to this equation, there is not only a decrease in frequency but also an increase in damping. The damping can be defined as fwhm (full width at half-maximum) of the resonance crystal in Hz. Thus, the shear modulus and the surface roughness of the films can be characterised.¹⁴

2.6. Scanning Electron Microscopy

Scanning electron microscopy (SEM) is the most common technique in order to characterise the properties of the polymer-modified electrodes. In doing so, information on the growth mechanism and structural changes of the polymers can be obtained, besides the surface physical properties themselves.

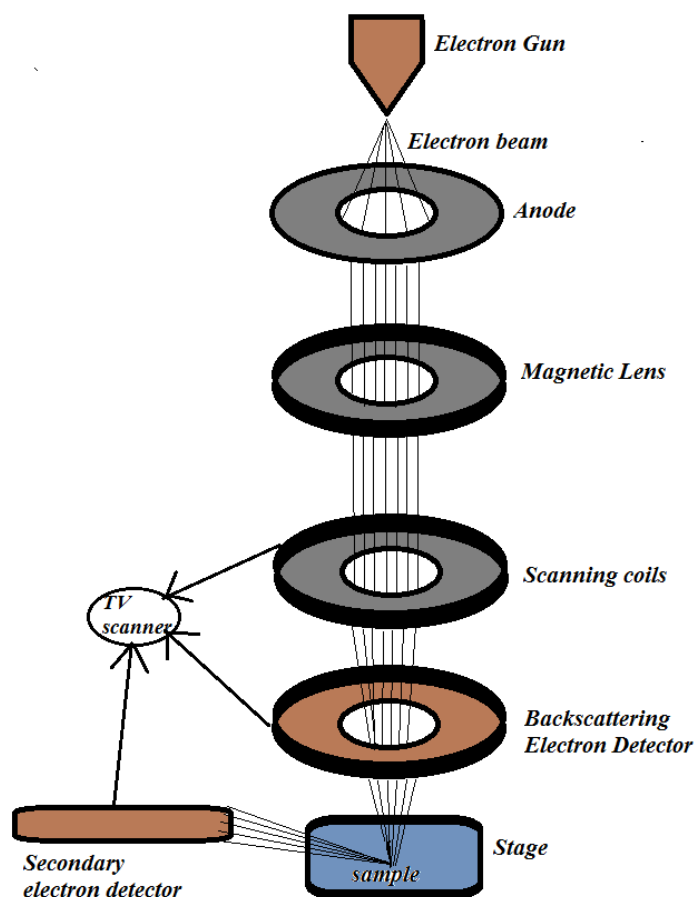


Figure 2.11. The schematic representation of a typical SEM technique

Figure 2.11 shows a schematic representation of the SEM technique, which contains an electron gun for the production a beam of electrons. The energies of these electrons can be varied between 1 keV to 30 keV by the anode. There are several condenser lenses in order to adjust the area of the electron beam from between 0.4 nm to 100 nm in diameter. When the electron beam hits each spot of the sample, secondary electrons are

removed from the surface and the resultant current of secondary electrons reaches the detector, producing an image of the sample surface.^{15, 30}

In the SEM technique, a beam of electrons is scanned across the surface to acquire an image instead of light. The surface of the sample is scanned with the electron beam. This interaction between the atoms and the beam results in various types of the signal from the surface. These signals involve the emission of secondary, backscattered and Auger electrons, as well as X-ray fluorescence photons.¹⁶ All of these signal types have been utilised for the characterisation of surface properties, but backscattered and secondary electrons form the basis of scanning electron microscopy. These give the opportunity to characterise of a large amount of the sample at one time, in high resolution with high magnification of images.^{15, 30}

In the SEM technique, the measurements are applied to a conductive sample in a low vacuum so that the electron beam can travel in straight lines. However, some samples do not display any conductivity. Therefore, they require sputtering with an inert, but conductive, material. By doing so, non-conductive solids also can be investigated with the SEM technique.^{15, 30}

2.7. FTIR

The defining structural changes of modified electrodes at the atomic and molecular level can be acquired through several spectroscopic techniques. The most common spectroscopic technique is Fourier Transform Infrared Spectroscopy (FTIR) for the study of modified electrodes, allowing data acquisition in less than one second. The light reflected from the surface layer provides valuable information at high sensitivity. FTIR also offers improved signal-to-noise at a high resolution because of its analysis the entire spectrum rather than small wavebands from a monochromator with better accuracy.^{15, 30} In this chapter, the significance of the FTIR technique for the characterisation of modified electrodes will be discussed in detail.

The basis of the FTIR technique is the same as for IR spectroscopy; it is the study of the vibrational motions of the conducting polymers at the molecular level. Thus, specific information on molecular orientation and surface properties can be obtained.^{15, 30}

Illumination with infrared radiation excites the characteristic vibrational motions of the polymer-modified layer. In this technique, the sample between the interferometer and the detector absorbs at specific wavelengths.^{15, 30}

2.8. References

- 1 A. C. Fisher, *Electrode Dynamics*, Oxford University Press Inc., United States, 1996.
- 2 D. C. Harris, in *Quantitative Chemical Analysis*, ed. J. Fiorillo, Michelle Russel Julet, USA, 2003, pp.284.
- 3 E. Gileadi, *Physical Electrochemistry*, by Wiley-VCH, Germany, 2011.
- 4 O. Schneider, A. Bund, A. Ispas, N. Borissenko, S. Z. El Abedin and F. Endres, *Journal of Physical Chemistry B*, 2005, **109**, 7159-7168 (DOI:10.1021/jp044892r).
- 5 M. A. Shenashen, M. M. Ayad, N. Salahuddin and M. A. Youssif, *Reactive & Functional Polymers*, 2010, **70**, 843-848 (DOI:10.1016/j.reactfunctpolym.2010.07.005).
- 6 S. Bruckenstein, K. Brzezinska and A. R. Hillman, *Electrochimica Acta*, 2000, **45**, 3801-3811 (DOI:10.1016/S0013-4686(00)00467-9).
- 7 S. Bruckenstein, K. Brzezinska and A. R. Hillman, *Physical Chemistry Chemical Physics*, 2000, **2**, 1221-1229 (DOI:10.1039/a908719b).
- 8 Brett, C.M.A., Brett, A.M.O., in *Electroanalysis*, ed. Compton, R.G., Davies, S.G., Evans, J., Gladden, L.F., 2005, pp.48-49,50,51.
- 9 R. Compton and C. Banks, in *Understanding Voltammetry*, ed. nonymous 2009, pp.107-108,111.
- 10 C. H. Hamann, *Electrochemistry*, Wiley-VCH, New York, 1998.
- 11 Q. Hao, W. Lei, X. Xia, Z. Yan, X. Yang, L. Lu and X. Wang, *Electrochimica Acta*, 2010, **55**, 632-640 (DOI:10.1016/j.electacta.2009.09.018).
- 12 S. Bruckenstein and A. R. Hillman, *Journal of Physical Chemistry*, 1988, **92**, 4837-4839 (DOI:10.1021/j100328a008).
- 13 D. Orata and D. A. Buttry, *Journal of American Chemical Society*, 1987, **109**, 3574-3581 (DOI:10.1021/ja00246a013).
- 14 A. Bund and S. Neudeck, *Journal of Physical Chemistry B*, 2004, **108**, 17845-17850 (DOI:10.1021/jp0469721).
- 15 A. D. Skoog, *Principles of Instrumental Analysis*, 1971.

- 16 A. D. Skoog, F. J. Holler and A. T. Nieman, in *Principles of Instrumental Analysis*, ed. J. Vondeling, Thomson Learning, USA, 1971, pp.10.
- 17 A. R. Hillman, *Journal of Solid State Electrochemistry*, 2011, **15**, 1647-1660.
- 18 S. Katzir, *Archive for History of Exact Sciences*, 2003, **57**, 61-91 (DOI:10.1007/s00407-002-0059-5).
- 19 C. R. Dauwalter, *26th Annual Symposium on Frequency Control*, Atlantic City, USA, 1972, 108-112 (DOI: 10.1109/FREQ.1972.199899).
- 20 S. Bruckenstein and M. Shay, *Electrochimica Acta*, 1985, **30**, 1295-1300 (DOI:10.1016/0013-4686(85)85005-2).
- 21 R. Schumacher, G. Borges and K. K. Kanazawa, *Surface Science*, 1985, **163**, L621-L626.
- 22 S. Bruckenstein, J. Chen, I. Jureviciute and A. R. Hillman, *Electrochimica Acta*, 2009, **54**, 3516-3525 (DOI:10.1016/j.electacta.2008.11.061).
- 23 R. Roto and G. Villemure, *Journal of Electroanalytical Chemistry*, 2006, **588**, 140-146 (DOI:10.1016/j.jelechem.2005.12.014).
- 24 E. P. Cintra, R. M. Torresi, G. Louarn and S. I. C. de Torresi, *Electrochimica Acta*, 2004, **49**, 1409-1415 (DOI:10.1016/j.electacta.2003.11.005).
- 25 K. Kim, I. Jureviciute and S. Bruckenstein, *Electrochimica Acta*, 2001, **46**, 4133-4140 (DOI:10.1016/S0013-4686(01)00707-1).
- 26 B. D. Vogt, E. K. Lin, W. L. Wu and C. C. White, *Journal of Physical Chemistry B*, 2004, **108**, 12685-12690 (DOI:10.1021/jp0481005).
- 27 C. Brosseau, M. Maurice, S. Bearne and S. Roscoe, *Electrochimica Acta*, 2005, **50**, 1289-1297 (DOI:10.1016/j.electacta.2004.08.019).
- 28 C. Yim, M. Yun, N. Jung and S. Jeon, *Analytical Chemistry*, 2012, **84**, 8179-8183 (DOI:10.1021/ac3013785).
- 29 M. Grzeszczuk and M. Chmielewski, *Journal of Electroanalytical Chemistry*, 2012, **681**, 24-35 (DOI:10.1016/j.jelechem.2012.05.025).
- 30 D. C. Harris, *Quantitative Chemical Analysis*, 2002.

Chapter III:

Experimental and Data Analysis Process

3.1. Introduction

This chapter describes the general procedures regarding materials and reagents, and techniques and procedures. Additionally, data analysis results from experimental work will be undertaken.

Methods of synthesis of conducting polymers are dealt with first in this chapter. The second part of the chapter will be concerned with the preparation of the conducting polymer, copolymer, and composite films. The last part of the chapter will deal with the investigation of the electroactive and ionic activities of the prepared films via EQCM.

3.2. Materials and Reagents

Table 3.1 shows the material with properties and area of usage during experimental studies. All aqueous solutions were prepared using doubly distilled water. In Chapter 6 and 7, studies were conducted using ionic liquid instead of an aqueous solution, namely Ethaline, as shown in table 3.1.

3.2.1. Storage Conditions

Of the solutions used, *o*-toluidine and aniline monomer solutions can be affected by air and light, which results in oxidation of the monomers. To counter this, aniline and *o*-toluidine monomer solutions were kept in a dark and cold room. Ethaline prepared from choline chloride and ethyl glycol in various ratios (mentioned in the following section) was kept at 50 °C in sealed containers in an oven to avoiding water absorption. The other reagent solutions and acid solutions were kept in dark containers. It was considered that only fresh solutions would be suitable for use in these studies; for this reason, solutions were usually prepared daily.

Table 3.1. List of materials and reagents utilised during the experimental studies for the research presented in this thesis

<i>Chemical</i>	<i>Abbreviation /formula of Chemical</i>	<i>Source</i>	<i>Purity %</i>	<i>Utilization</i>
Aniline monomer	An	Sigma-Aldrich	99	The monomer of conducting polymer/copolymer synthesis
Pyrrrole monomer	PPy	Sigma-Aldrich	98	The monomer of conducting polymer/composite synthesis
<i>o</i> -aminophenol monomer	AP	Sigma-Aldrich	99	The monomer of conducting polymer/copolymer synthesis
<i>o</i> -toluidine monomer	OT	Sigma-Aldrich	99	The monomer of conducting polymer/copolymer synthesis
Sulphuric acid	H ₂ SO ₄	Fisher Chemical	99.9	Supporting electrolyte
Nitric acid	HNO ₃	Fisher Scientific	99.9	The media to add the functional group to MWCNT and for cleaning electrode surfaces impurities
Hydrogen chloride	HCl	Aldrich	99.9	Cleaning Ag wire electrode and supporting electrolyte for
Sodium fluoride	NaF	Analar	99.0	Electrolyte for ion-exchange experiments
Sodium chloride	NaCl	Analar	99.8	Electrolyte for ion-exchange experiments
Multiwall carbon nanotube	MWCNT	Sigma-Aldrich	98.0	As a filler for the polymer matrix
Choline chloride	ChCl	Sigma-Aldrich	98	Quaternary ammonium salt
Ethylene glycol	C ₂ H ₆ O ₂	Sigma-Aldrich	99.8	Hydrogen bond donor (HBD)
Potassium ferricyanide	K ₃ [Fe(CN) ₆]	Across Organics	98	Standardization for the reference electrode
Potassium chloride	KCl	Fisher Scientific	99	For Ag/AgCl reference electrode

3.2.2. Preparation of Ethaline

The ethaline was prepared as from choline chloride (ChCl) (see figure 3.2a) and ethylene glycol (C₂H₆O₂) (figure 3.2b)^{1, 2} mixed in 1:2 (ETH200) and 1:4 (ETH400) molar ratios at 60 °C until a colourless liquid was achieved, as shown in figure 3.3. This colourless liquid is called Ethaline, which has different characteristics depending on the composition of the mixture.

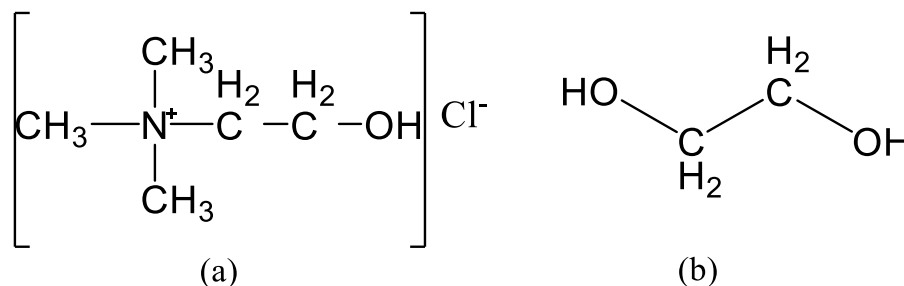


Figure 3.1. The molecular formula of (a) choline chloride and (b) ethylene glycol

Ethaline was used as the electrolyte for the polymerization of aniline and pyrrole in the presence of MWCNT, as presented in chapters 6 and 7, respectively. ETH200 is the most common form of Ethaline used for coating studies, which exists as a liquid after preparation at room temperature, contrary to the majority of ionic liquids such as Propaline and Glyceline, which crystallise at room temperature.^{1, 2} On the other hand, the solution of aniline monomer in ETH200 itself crystallised at room temperature, while this did not occur for the pyrrole solution (figure 3.2a). To overcome this problem, ETH400, which was comprised of a 1:4 choline chloride and ethylene glycol mix, was used to prepare the monomer solution of aniline under identical conditions. The prepared solution remained a liquid at room temperature (figure 3.2b). In doing so, the electrochemical polymerization studies of aniline in the presence of MWCNT were applied in ideal electrolyte medium.

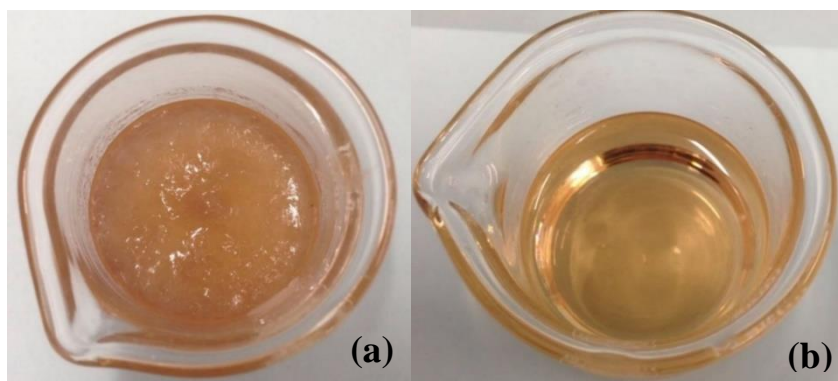


Figure 3.2. The aniline monomer solutions formed in (a) ETH200 (b) ETH400

3.2.3. Preparation of MWCNT-COOH

The MWCNTs used in this study had outside and inside diameters of 10 ± 1 nm and 4.5 ± 0.5 nm, respectively, and lengths of around 3-6 μm .

MWCNT have no functional groups on their wall so behaves as an inert material in any solution. For this reason, it is necessary to add functional groups (such as the $-\text{COOH}$ group) to achieve an active material. To add functional groups to the wall of the MWCNTs, 300 mL concentrated nitric acid was added to 2 g of MWCNT powder. This mixture was heated in a paraffin oil bath instead of direct placement on a hotplate to control temperature, as shown in figure 3.6. This is because the boiling point of the paraffin oil is approximately 370 $^{\circ}\text{C}$, which higher than water and this setup makes it possible to gain control over temperature. The mixture was refluxed for 36 hours keeping the temperature a 120 $^{\circ}\text{C}$. After refluxing, the mixture left to cool for a few hours at room temperature. The mixture was transferred to a beaker (1 L) and was then diluted to 500 mL with distilled water. The mixture was filtered using filter paper (200 nm porosity). This washing process was repeated several times to reach a neutral pH value. After the washing process, it was placed in an oven at 60 $^{\circ}\text{C}$ until dry.^{3,4} With the treatment of the MWCNTs in concentrated HNO_3 , the CNTs not only gain a functional group (figure 3.3) but also become soluble in neutral and alkaline aqueous media.

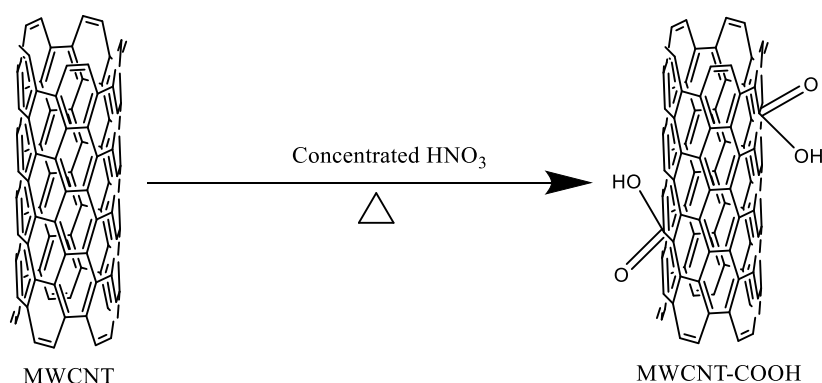


Figure 3.3. The predicted mechanism to add functional groups to the walls of the MWCNTs

3.2.4. Preparation of Monomer Solutions

In the first part of the research presented in chapter 4 and chapter 5, monomer solutions of aniline were prepared from either 0.1 M aniline or 0.2 M aniline in 1 M H_2SO_4 . The

other monomer solutions, *o*-aminophenol, and *o*-toluidine, were prepared with 0.1 M monomer in 1 M H₂SO₄. The studies of the copolymer film were performed at different ratios of between 0.1 M and 0.2 M total monomer concentration.



Figure 3.4. The images of monomer solutions of aniline, *o*-aminophenol, and *o*-toluidine in aqueous solutions, respectively

In the latter sections of the research presented in chapter 6 and chapter 7, the monomer solutions of aniline and pyrrole were used. The monomer solutions of aniline were prepared from 0.1 M aniline and 0.1 M H₂SO₄ in an aqueous medium, and 1.0 M aniline and 0.5 M H₂SO₄ in Ethaline (ETH400), respectively. The acid concentrations were kept at fixed values in both solutions considering the requirement of aniline polymerization and the good dispersion of MWCNTs in the monomer solution.^{5, 6} The other monomer solutions were prepared from 0.1 M pyrrole and 0.1 NaCl in aqueous media, and 0.7 M pyrrole in Ethaline (ETH200). The concentration of the monomer was apparently increased because of the higher viscosity of Ethaline with respect to water. This is because the higher viscosity slows the transportation of monomers toward the electrode surface.^{2, 7}

To study composite films with MWCNT-COOH in an aqueous medium, the concentrations of both aniline and pyrrole were fixed 0.1 M in the presence of various amounts of MWCNT-COOH, which were 1, 3, 6, 10 and 15 wt%. Similarly, the monomer solutions of aniline and pyrrole in Ethaline were prepared in the presence of varying amounts of MWCNT-COOH, which were 4, 8, 12, 16 and 20 wt%. Each of the prepared solutions was sonicated in an ultra-sonication bath for 5 hours. The monomer solutions of aniline and pyrrole with/without MWCNT-COOH are shown as examples in figure 3.5.



Figure 3.5. The images of monomer solutions of aniline and pyrrole with/without MWCNT-COOH in both aqueous and Ethaline media

The different colour of the same monomer solutions can be originated the presence of the higher monomer concentration in the Ethaline medium.

3.3. Techniques and Procedures

All the electrochemical experiments were carried out in a conventional three-electrode system. During the copolymer studies, a platinum flag with a 2 cm² surface area as a counter electrode and an Ag/AgCl electrode as a reference electrode were employed. The larger surface area makes it possible to avoid the current being limited by the reaction on the surface of the counter electrode. The counter electrode was immersed in concentrated HNO₃ solution before every electrochemical experiment to remove impurities and was then washed with tap water, distilled water, and acetone, sequentially. The counter electrode was placed in the electrochemical cell parallel to the working electrode to provide a uniform electric field, which enables a uniform film synthesis on the working electrode surface. All the potential values were referred to

Ag/AgCl reference electrode⁸ during the electrochemical experiments conducted in aqueous medium whilst Ag wire was used all electrochemical experiments in Ethaline medium. The reference electrodes were discussed in detail in Chapter 2. The distance between the reference electrode and the working electrode was minimised to minimise the electrolytic ohmic drop.

In the Ag/AgCl reference electrode, Ag wire was coated with AgCl and placed in a glass tube, which had a porous bottom. This glass tube was then filled with saturated potassium chloride. Although this reference electrode is commonly preferable in an aqueous medium, it is not useful in ionic liquids due to the liquid junction potential that arises from the difference in viscosity between the aqueous and DES solutions. Also, there is a possible diffusion either of salts from the electrolyte to the frit or water and chloride ions through the frit. On the other hand, the Ag wire reference electrode that is suitable to study in a DES consists of a high concentration of Cl⁻ ions (approximately 4.2 M in ETH200). These ions surround the Ag wire reference electrode were immersed in the Ethaline solution. The possible reaction here is similar to that of the Ag/AgCl reference electrode in an aqueous medium. Their potentials are also different, causing a change in peak potential positions.

Two types of working electrode were used for cyclic voltammetry experiments during the research presented in this thesis. In the first part of this research, chapters 4 and 5, a gold working electrode was used for cyclic voltammetry experiments while a platinum working electrode was used for the research presented in chapters 6 and 7 experiments, as the ionic liquid requires a higher potential for the polymerization of the aniline monomer. The surface area of these gold and platinum working electrodes was determined as 0.018 cm². For the EQCM experiments, three types of AT-cut crystals were used as working electrodes, unpolished gold for chapters 4 and 5, and polished platinum quartz crystals for chapters 6 and 7.

Both AT-cut quartz crystals, polished and unpolished, were purchased from International Crystal manufacturing (ICM) Co. Ltd. (Oklahoma City, USA). The electrochemical surface areas and piezoelectric active areas were stated as 0.23 cm² and 0.21 cm², respectively, by the supplier. This difference (0.02 cm²) arises due to the connecting tab of the electrode. A thin slice of AT-cut quartz (ca. 0.18 mm) was

positioned between the vacuum-deposited gold electrodes/platinum electrodes on either side was available for experiments.

The polished crystal had a surface finish of less than 0.1 μm , compared to the unpolished crystal which had a surface finish of about 0.3 μm , because there was a chromium layer under the layer of gold. Pani and its derivatives were deposited onto the unpolished surface. The EQCM experiments were performed with an unpolished crystal in aqueous solution. Unpolished crystals were suitable in this instance because of the gold surfaces, which oxidize easily at higher potentials. Thus, the polished crystal with a platinum surface was used in all the EQCM experiments reported in chapters 6 and 7.

Two types of electrochemical cell were employed in these studies. One of these was a home-made cell consisting of a small beaker, a counter electrode, a working electrode and an Ag/AgCl reference electrode. The other electrochemical cell was made as a Teflon cell, with the AT-cut quartz crystal placed at the bottom of this cell, as shown in figure 3.6.

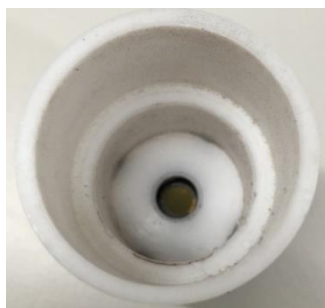


Figure 3.6. An image of the Teflon cell used with a quartz crystal in the centre of it

The surface of the AT-cut quartz crystal exposed to the solution behaves as a working electrode in the Teflon cell. The Teflon cell is constructed so as not to allow any leakage of the solution outside the cell.

3.3.1. Electrochemical Techniques

During the electrochemical experiments, the raw electrochemical data from cyclic voltammetry and chronoamperometry, and the gravimetric data from the EQCM were collected. The first motivation to this was the synthesis of an acoustically thin electroactive polymer, copolymer, and composite films and also, the describing of the

electro and ion activity of the resultant polymer, copolymer, and composite films. All electrochemical experiments during the EQCM study were performed near the fundamental vibrational mode (10 MHz).

In cyclic voltammetry, the ideal copolymer ratio and conditions were determined for the copolymers (see chapters 4 and 5) and the composite films (chapters 6 and 7). In the EQCM studies, the ideal ratios for the copolymers and composite films were investigated gravimetrically. This was followed by electroactivity and ion-exchange studies using various monomer-free electrolyte solutions.

Before use, the gold and platinum working electrodes were polished with Al_2O_3 , providing a mirror-like surface.⁹ In doing so, any possible contamination could be removed from the surface, and the roughness of the working electrode was decreased, reflecting the subsequent decrease in the resistance of the working electrode. The polished working electrode was washed initially with distilled water, then acetone.

3.3.1.1. Cyclic voltammetry

Cyclic voltammetry is the most common electrochemical technique used to obtain useful information about conducting polymers. Detail information about this technique was presented in chapter 2.

In chapters 4 and 5, the electrochemical deposition of aniline, *o*-aminophenol, and *o*-toluidine monomers, respectively, were carried out in the presence of 0.1 M/0.2 M monomer and 1 M H_2SO_4 with repetitive potential cycling at room temperature. After deposition of the films, they were transferred to 1 M H_2SO_4 and 0.1 M NaF solutions to characterise the electrochemical properties of the synthesised films.

In chapter 6, the electrochemical deposition of composite films of Pani/MWCNT-COOH was studied in an aqueous medium using a solution consisting of 0.1 M monomer and 0.1 M H_2SO_4 with various concentrations of MWCNT-COOH, while a 1 M aniline and 0.5 M H_2SO_4 using different concentrations of MWCNT-COOH were used in ETH400. In the meantime, the electrochemical experiments on PPy/MWCNT-COOH were performed using 0.1 M monomer and 0.1 M NaCl in an aqueous medium

and 0.7 M pyrrole monomer in ETH200. The deposition experiments were applied using a wide range of scan rates and cycle numbers to determine optimal conditions.

3.3.1.2. Electrochemical crystal microbalance

The electrochemical quartz microbalance experiments were conducted using an Autolab PGSTAT12 potentiostat (Ecochemie, Holland; controlled with GPES2 software). A Hewlett Packard HP8751A network analyser was connected through a 50 Ω coaxial cable in the vicinity of the fundamental mode ($f_0 = 10$ MHz). The gravimetric data were acquired simultaneously in addition to electrochemical data.

10 MHz AT-cut crystals with Au electrodes (ca. 100nm) and with Pt electrodes (ca. 100nm) were supplied from Oklahoma. The electroactive area for each type of electrodes was 0.23 cm² facing the solution, which was controlled with an EG&G 263 A potentiostat, whilst the other electrode faced the air. All potentials were measured against an Ag/AgCl reference electrode in an aqueous medium.

3.3.1.2.1. Data Fitting

Acquired raw data was fitted automatically to an admittance spectrum as shown in figure 3.7. This file was used as a matrix for fitting relevant spectra of the acquired data. For this, an initial admittance spectrum was converted to a csv file and two columns (A and B) were copied, and then pasted into columns A and B in the admittance spectrum template. The variations in L(inductance), R (resistance), an (a baseline value) and f_0 (the resonant frequency) values to adjust for a matching the measured and theoretical response were determined. Afterwards, the [Fit/Solve] command was proceeded and recorded the file for the consecutive calculation for all data.

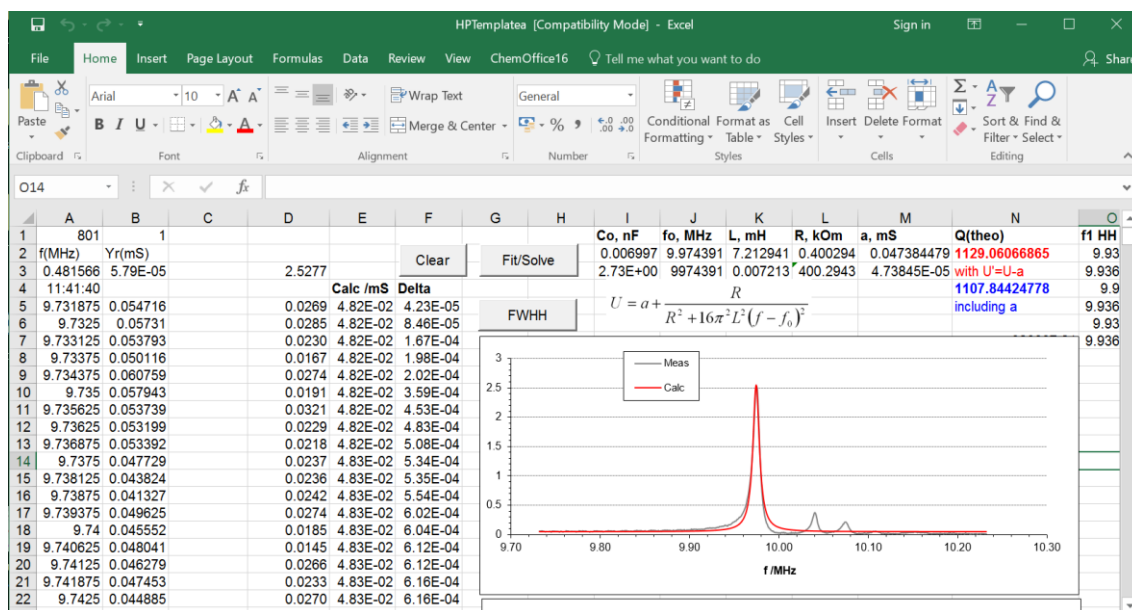


Figure 3.7. Admittance spectrum fitting template

The fitting of admittance spectra data was conducted using in-house developed software (KSR 200, based on the Sauerbrey Equation) as shown in figure 3.8. The remaining admittance spectrum was fitted using an excel-based macro programme. The [Copy/Fit 2] command was used to fit the remaining admittance spectra. The fitting was continued for the calculated data from each corresponding spectrum. At the end of the [Copy/fit 2] function, the [results] command was applied, which provides a spread of data acquired from the fitted admittance spectra.

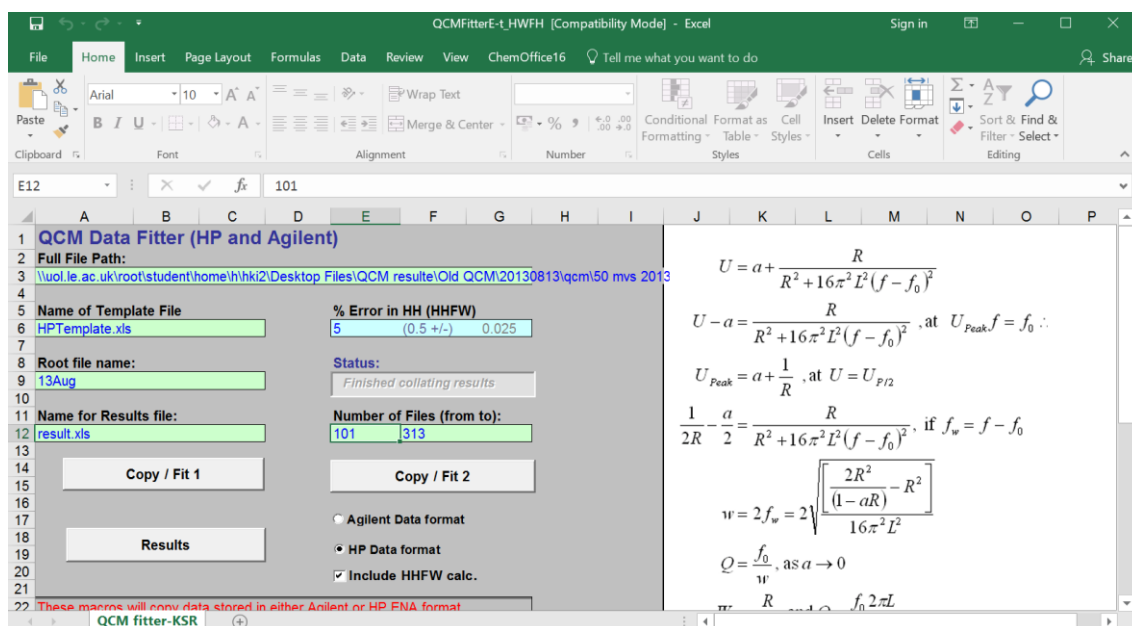


Figure 3.8. Admittance spectrum fitting programme

3.3.2. Procedures

3.3.2.1. The deposition of conductive films

The first deposition studies were applied in 0.1 M aniline monomer and 0.1 M *o*-aminophenol monomer solutions, respectively, in 1 M H₂SO₄ at 10 mV s⁻¹ in the range -0.2 and 1.0 V with continued cycling on a gold working electrode. Later, the copolymers of those monomers from solutions consisting different ratios of these monomers (total concentration of monomers remain 0.1 M), aniline and *o*-aminophenol, in 1 M H₂SO₄ were performed under otherwise identical conditions, from which aniline and *o*-aminophenol were deposited. The poly-*o*-toluidine was deposited from a 0.1 M *o*-toluidine and 1 M H₂SO₄ solution at 10 mV s⁻¹ between -0.2 to 1.0 V over 20 cycles. Similarly, the copolymer deposition of poly(aniline-*o*-toluidine) was employed with different ratios of those monomers under identical conditions, from which *o*-toluidine was deposited. The results acquired from the copolymerization studies show that the lower monomer concentration of *o*-aminophenol and *o*-toluidine, respectively, make copolymer formation possible, which have different electrochemical and physical characteristics to their respective monomers. Therefore, the electrochemical deposition of poly(aniline-co-*o*-aminophenol) and poly(aniline-co-*o*-toluidine) was performed between 0.1 M and 0.2 M monomer concentrations; also, the potential window was chosen as -0.20 to 0.90 V to avoid the degradation of the copolymer film.

Further studies focused on the deposition of composite films of polyaniline/MWCNT-COOH and polypyrrole/MWCNT-COOH in different media, aqueous and non-aqueous, in the presence of different concentrations of MWCNT-COOH. In the case of Pani/MWCNT-COOH, the monomer solutions in aqueous medium consisted of 0.1 M aniline and 0.1 M H₂SO₄ using different concentrations of MWCNT-COOH, which were 1, 3, 6, 10, and 15 wt%, while 1 M aniline and 0.5 M H₂SO₄ with different ratios of MWCNT-COOH, which were 4, 8, 12, 16, and 20 wt%, respectively, for experiments in Ethaline. Using these monomer solutions, the electrochemical deposition of Pani/MWCNT-COOH was performed at different scan rates of 5, 10, and 100 mV s⁻¹.

Lastly, PPy/MWCNT-COOH composite films were deposited from a solution consisting of 0.1 M pyrrole and 0.1 M NaCl in an aqueous medium between -0.6 and

0.7 V at 10 mV s^{-1} , whilst it was deposited from 0.1 M pyrrole in ETH200 between -0.3 and 1.3 V at 5 and 100 mV s^{-1} .

3.3.2.2. The electroactive characterisation of the conductive films

The characterisation of the synthesized polymer and copolymer films was studied in 1 M H_2SO_4 monomer-free background solutions at different scan rates of 100, 50, 40, 30, 20, 10, and 5 mV s^{-1} , respectively. The acquired cyclic voltammograms presented clear information as to the oxidation and the reduction peak positions of the synthesized polymer and copolymer films.

Moreover, the electrochemical properties of Pani/MWCNT-COOH and PPy/MWCNT-COOH composite films were examined in monomer-free electrolyte solutions at 5 mV s^{-1} . Pani/MWCNT-COOH and PPy/MWCNT-COOH generated in aqueous medium were studied in 1 M H_2SO_4 and in 0.1 M NaF monomer-free solutions, respectively. The other composite films of Pani/MWCNT-COOH and PPy/MWCNT-COOH produced in Ethaline were studied in 1 M H_2SO_4 -ETH200 and in ETH200 monomer-free media, respectively.

3.3.2.3. The characterisation of the ion-Exchange Properties of the conductive Films

The ion-exchange properties of the conducting polymers have been discussed in detail in chapter 1. Here, we characterised the ion-exchange capability of each of the polymer and copolymer films synthesized in chapter 4 and 5. Initially, their defluoridation properties were explored in 0.1 M monomer-free electrolyte solutions at lower scan rates of 3, 5, and 10 mV s^{-1} . Furthermore, the defluoridation experiments were processed in different concentrations of NaF electrolyte solutions, at 0.1 M, 0.01 M, and 0.001 M NaF, respectively. To obtain a further information about the performance of the poly(aniline-co-o-aminophenol) and poly(aniline-co-o-toluidine) copolymer films, the fluoride ions were removed in presence of different ratios of chloride ions such as 90:10; 70:30, 50:50; 30:70 and 10:90 as F^- : Cl^- in 0.1 M concentration of F^- and Cl^- . Lastly, the regeneration of the copolymer films was also investigated in 1 M H_2SO_4 after treatment with a NaF electrolyte solution at different scan rates.

3.3.3. Surface Characterisation Techniques

3.3.3.1. Scanning electron microscopy and 3D Profiler

The surface examination of the polymer, copolymer and composite films were performed via scanning electron microscopy (SEM). For this, an FEI SIRION SEM was employed. The morphologies of the conducting films were studied under vacuum (10^{-5} Pa) with an accelerator voltage of between 12 keV and 20 keV; no gold sputter coating was required. The distance between sample and microscope was kept between 7 mm and 15 mm to acquire higher resolution images of the polymer, copolymer and composite films synthesized on a quartz crystal.

The 3D images of the conducting polymers, copolymer, and composite films were also examined using a 3D profiler in addition to the SEM studies.

3.3.4. FTIR

The copolymer films in this research were prepared from known ratios of monomer solutions, but it was not possible to be sure how much aniline, *o*-aminophenol and *o*-toluidine monomer participated in the copolymer films. Similarly, we cannot be sure how much aniline monomer and MWCNT were incorporated in the composite films. Therefore, the structural analysis of these copolymers and composite films is necessary to acquire more detailed information their structure and composition. For this reason, the Perkin Elmer Spotlight FTIR imaging system was used to record IR spectra between 4000 cm^{-1} and 750 cm^{-1} . The reflectance mode was selected with a resolution of 8 cm^{-1} (at $20 \pm 2^\circ\text{C}$).

3.3.5. Data Analysis

3.3.5.1. Surface coverage and thickness of the final films

The polymer, copolymer and composite films synthesized in this research show electroactivity in their doped state. However, this electroactivity is related to the existence of electroactive sites in these films. At this point, surface coverage (Γ , mol

cm⁻²) can be used as an indication of the electroactive species that are on the film¹⁰, which were calculated using equation 3.1

$$\Gamma = \frac{Q_{red}}{nFA} \quad 3.1$$

The density of the charged species (Q_{red} , coulomb) is referred to mostly the charge passed upon reduction, n is the number of electrons transferred during the redox reaction of the conducting polymer (n is 0.5 and 0.33 for the aniline and pyrrole monomer units, respectively)^{11, 12} and F is the Faraday constant (96485 Coulomb s⁻¹). A is the surface area of the working electrode, which was 0.018 cm² in this study during cyclic voltammetry experiments, and 0.23 cm² for EQCM experiments.

The other important feature of the conducting polymer, copolymer and composite films synthesized on the quartz crystals is their thickness, h , which can be calculated with the help of the surface coverage of the films via equation 3.2;¹³

$$h = \Gamma V \quad 3.2$$

where V is the volume of the polymer, which can be expressed using equation 3.3:

$$V = \frac{m}{\rho} \quad 3.3$$

where ρ is the density of the polymer ($\rho = 1.02$ g cm⁻³ for the aniline monomer and 0.97 g cm⁻³ for pyrrole monomer) and m is the mass of the polymer film. The volume V refers the volume of an unsolvated polymer film. During electrochemical reactions, the polymer films can swell or shrink with solvent transfer into/from the polymer film.¹⁴

3.3.5.2. The apparent molar mass (M_{app}) of the final films and the species transferred during redox cycling

The mass of polymer film coated on the quartz crystal can be found with the help of Faraday's law, which introduces the concept of the total charge (ΔQ) during oxidation or reduction of the polymer film being associated with the mass (Δm) of the polymer film deposited on the quartz crystal.¹⁵ This is expressed as shown in equation 3.4;

$$M_{app} = nF \frac{\Delta m}{\Delta Q} \quad 3.4$$

where M_{app} is the apparent molar mass of the polymer, n is the number of electrons transferred per ion during the redox reactions and F is the Faraday constant. $\Delta m/\Delta Q$ can be measured from the slope of a mass-charge curve. Δm can obtain from the equation $\Delta m = -c\Delta f$, where c is a constant; this can be achieved with the help of the value for Δf acquired from EQCM experiments.

During the oxidation and reduction reactions of the conducting polymers, ion-exchange occurs between the polymer film and electrolyte. Upon oxidation, the polymer film is positively charged and the anion (or cation ejected) would be incorporated to maintain electroneutrality. In the reverse scan, the anion releases in opposite site while polymer film turns out its insulating form. In this case, Δm take a negative or positive value, which is an indication of either a mass increase of the film for a positive value of Δm or a mass decrease for a negative value of Δm .¹⁶ This process also involves the transfer of solvent.¹⁵

M_{app} can be used as a tool to identify the species involved in the mass change.¹⁷ Ideally, the expected M_{app} value is unique to one type of ion species transferred during the electrochemical experiments. In other words, if the polymer films are positively charged, the transfer of anionic species can be expected. If the polymer film is negatively charged, the transfer of cations would similarly be expected. However, in a non-ideal situation, the sum of ions transferred, including solvent molecules, occurs between the polymer film and electrolyte solution.¹⁵

$$M_{app} = M_{anion} + \beta M_{cation} + \alpha M_{solvent} \quad 3.5$$

where M_{anion} , M_{cation} , and $M_{solvent}$ in equation 3.5 are the molar masses of the transferred anion, cation, and solvent molecules, respectively. α and β reflect the relative amount of solvent and cation transferred per anion.

3.3.5.3. The ohmic resistance of the polymer films

The ohmic resistance (Z) of the polymer films deposited on quartz crystal can be determined¹⁸ in liquid media by equation 3.6;

$$Z_{peak} = \frac{1}{Y_{peak}} \quad 3.6$$

where Y_{peak} is the admittance of the quartz crystal.

3.3.5.4. Mass specific capacitance from cyclic voltammetry

The molar specific capacitance (MSC , $F g^{-1}$) of the resultant polymer films can be determined from cyclic voltammograms of the polymer films in monomer-free solutions. When the area of curve is divided by the scan rate, the charge passed (Q_{red}) upon reduction can be found, and this value can be used in equation 3.7;^{19, 20}

$$MSC = \frac{Q_{red}}{\Delta V m} \quad 3.7$$

Where ΔV is the voltage variation during the redox cycling and m is total mass of polymer film on the quartz crystal.

3.4. References

- 1 A. P. Abbott, R. C. Harris and K. S. Ryder, *Journal of Physical Chemistry B*, 2007, **111**, 4910-4913 (DOI:10.1021/jp0671998).
- 2 E. L. Smith, A. P. Abbott and K. S. Ryder, *Chemical Reviews*, 2014, **114**, 11060-11082 (DOI:10.1021/cr300162p).
- 3 B. Yu, F. Zhou, G. Liu, Y. Liang, W. T. S. Huck and W. Liu, *Chemical Communications*, 2006, , 2356-2358 (DOI:10.1039/b603878f).
- 4 M. A. Atieh, O. Y. Bakather, B. Al-Tawbini, A. A. Bukhari, F. A. Abuilawi and M. B. Fettouhi, *Bioinorganic Chemistry and Applications*, 2010, , 603978 (DOI:10.1155/2010/603978).
- 5 D. J. Guo and H. L. Li, *Journal of Solid State Electrochemistry*, 2005, **9**, 445-449 (DOI:10.1007/s10008-004-0589-7).

- 6 J. E. Huang, X. H. Li, J. C. Xu and H. L. Li, *Carbon*, 2003, **41**, 2731-2736 (DOI:10.1016/S0008-6223(03)00359-2).
- 7 Q. Zhang, K. D. O. Vigier, S. Royer and F. Jerome, *Chemical Society Reviews*, 2012, **41**, 7108-7146 (DOI:10.1039/c2cs35178a).
- 8 A. D. Skoog, *Principles of Instrumental Analysis*, 1971.
- 9 M. Liu, M. Ye, Q. Yang, Y. Zhang, Q. Xie and S. Yao, *Electrochimica Acta*, 2006, **52**, 342-352 (DOI:10.1016/j.electacta.2006.05.013).
- 10 A. R. Hillman and M. A. Mohamoud, *Electrochimica Acta*, 2006, **51**, 6018-6024 (DOI:10.1016/j.electacta.2005.11.054).
- 11 G. Ciric-Marjanovic, *Synthetic Metals*, 2013, **177**, 1-47 (DOI:10.1016/j.synthmet.2013.06.004).
- 12 C. K. Baker and J. R. Reynolds, *Journal of Electroanalytical Chemistry*, 1988, **251**, 307-322 (DOI:10.1016/0022-0728(88)85192-1).
- 13 G. A. Snook, C. Peng, D. J. Fray and G. Z. Chen, *Electrochemistry Communications*, 2007, **9**, 83-88 (DOI:10.1016/j.elecom.2006.08.037).
- 14 S. Bruckenstein and A. R. Hillman, *Journal of Physical Chemistry*, 1988, **92**, 4837-4839 (DOI:10.1021/j100328a008).
- 15 A. Bund and S. Neudeck, *Journal of Physical Chemistry B*, 2004, **108**, 17845-17850 (DOI:10.1021/jp0469721).
- 16 M. MIRAS, C. BARBERO, R. KOTZ and O. HAAS, *Journal of Electroanalytical Chemistry*, 1994, **369**, 193-197 (DOI:10.1016/0022-0728(94)87098-5).
- 17 M. Grzeszczuk and M. Chmielewski, *Journal of Electroanalytical Chemistry*, 2012, **681**, 24-35 (DOI:10.1016/j.jelechem.2012.05.025).
- 18 M. GRZESZCZUK, *Electrochimica Acta*, 1994, **39**, 1809-1816 (DOI:10.1016/0013-4686(94)85169-7).
- 19 Y. Ju, G. Choi, H. Jung and W. Lee, *Electrochimica Acta*, 2008, **53**, 5796-5803 (DOI:10.1016/j.electacta.2008.03.028).
- 20 X. Wang, H. Li and P. Liu, *Electrochimica Acta*, 2014, **125**, 630-636 (DOI:10.1016/j.electacta.2014.02.015).

Chapter IV:

The growth dynamic of poly(aniline-co-o-aminophenol) copolymer film and the investigation of its defluoridation properties by means of EQCM

4.1. Introduction

4.1.1. Overview

Polyaniline (Pani) has emerged as one of the most common conducting polymers due to its high electroactivity, environmental stability, ease of preparation and the excellent reversibility between its oxidation and reduction reactions.^{1, 2} In addition, the presence of the chemically flexible -NH- group in its polymer backbone provides for both π -bond formation as well as mediating protonation and deprotonation.³

Pani also differs from other common conducting polymers, such as PPy and PEDOT, because it can be found in three different forms, those of leucoemeraldine, emeraldine and pernigraniline (detailed information about these was presented in chapter 1).^{1, 4, 5} There are many practical applications of Pani in rechargeable batteries, electrochromic devices, sensors, corrosion protection and supercapacitors.⁶⁻⁸

On the other hand, the electroactivity of Pani is reduced at $\text{pH} > 5$, at which point it behaves almost as an insulator.^{2, 9} The pH dependence of Pani restricts its applications in neutral and alkali media considerably. To overcome of this, one effective approach is to carry out the copolymerization of aniline in the presence of other monomers (copolymerization is presented in detail in chapter 1).^{2, 10} A copolymer can be considered analogous to a metallic alloy, which shows different properties to those of the individual metals used for its preparation.² In the case of copolymerization, the fact that copolymers have different electrochemical characteristics to the constituent homopolymers is only to be expected.² There are several studies on the copolymerization of aniline in the presence of other monomers, such as *p*-phenylenediamine,¹ pyrrole,¹⁰ and 2-amino-4-hydroxybenzenesulphonic acid (in ionic liquid),² which show that copolymerization is a convenient tool to achieve new

conducting materials with [more] desirable properties. Among these monomers, substituted aniline derivatives involving a functional group such as -OH, -SO₃H, -COOH are favourable because they decrease the pH dependence of aniline at higher pH values whilst retaining good redox activity.² Among these copolymers, poly(aniline-co-*o*-aminophenol) (Pani-PAP) is particularly promising, as its use in copolymerization shows good electroactivity in neutral and alkali media of Pani because of functional group (-OH, in this case) modulation of pH.^{9, 11} In addition to improved electroactivity in neutral and alkali media, the copolymerization of aniline with *o*-aminophenol (*o*-AP) has improved its solubility,¹² corrosion protection, environmental stability, and its capacity for energy storage.¹³ However, the ion-exchange properties have remained uncertain despite its promising properties. We focus on the ion-exchange properties of Pani-PAP during this research. Figure 4.1 shows the oxidized and reduced states of Pani-PAP.

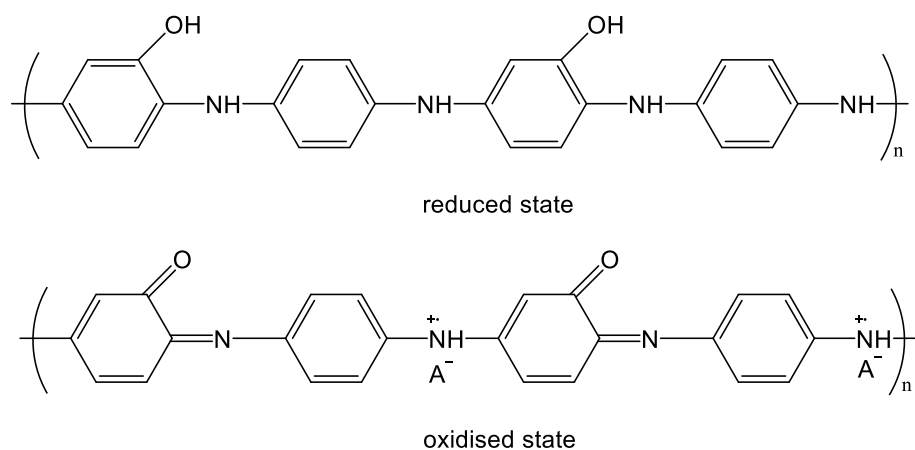


Figure 4.1. The oxidised and reduced states of Pani-PAP⁹

4.1.2. Defluoridation of Water by Conducting Polymer Films

The concentration of fluoride in drinking water in the UK is higher than the 1.5 mg/L that has been recommended level by World Health Organisation.¹⁴⁻¹⁶ For this reason, a variety of techniques have been developed to remove fluoride from drinking water such as chemical treatment,¹⁷ membrane separation,¹⁸ ion-exchange with adsorption¹⁹⁻²² and electrochemical ion-exchange techniques. Among these techniques, the electrochemical ion-exchange techniques,²³ which are mostly based on CPs, are remarkable due to their electrochemically reversible ion-exchange processes, being highly selective, being inexpensive, they are environmentally friendly and are easy to use.

The principle of electrochemical ion-exchange techniques is based on a doping/dedoping process in a polymer matrix.²⁴⁻²⁶ In the oxidized state of the polymer, the polymer film carries a positive charge with the application of an anodic potential (in figure 4.2). A positively charged polymer film shows a tendency to maintain neutrality with any accompanying anions (such as the fluoride ions in figure 4.2) in the electrolyte through their uptake into the polymer film matrix. In the case of applying a cathodic potential, the polymer film carries a negative charge, causing the expulsion of doped anions from the polymer matrix.²⁶ Because of this, conductive polymers are considered potential candidates for water purification without contamination of chemical properties.⁹ This exchange occurs during the transformation between the fully reduced states (leucoemeraldine) to the half-oxidised state (emeraldine) in Pani film.²⁶

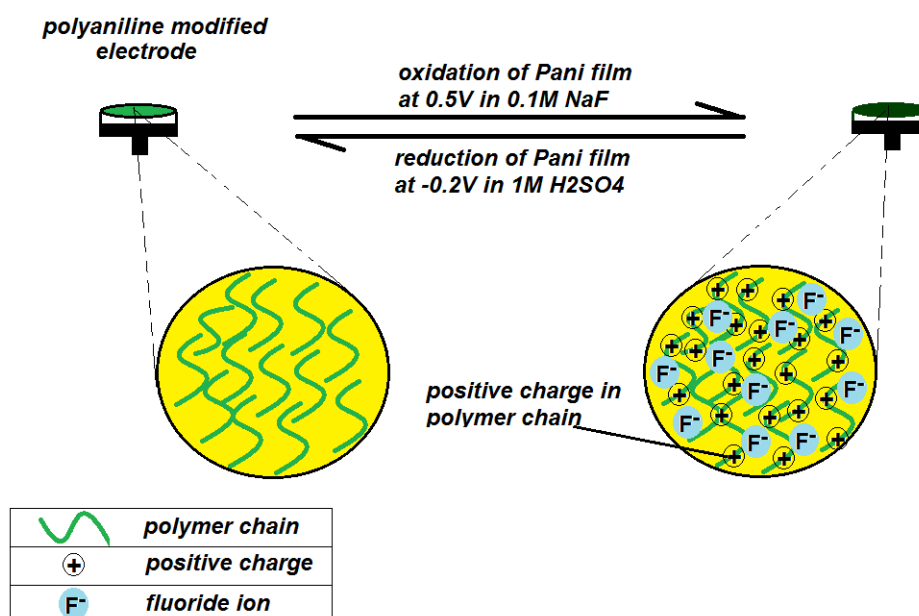


Figure 4.2. A representation of defluoridation by a polymer film (for example, Pani)

Although Pani itself is an excellent material for ion-exchange techniques in acidic systems, it loses its electroactivity in neutral and alkali media (pH 5 or greater). It is not suitable for defluoridation in drinking water because of the pH value of the medium, which is supported by the experimental results of Cui *et al.*¹⁶ However, copolymerization gives the opportunity to develop a new reactor for the removal fluoride ions from water in neutral medium.

In light of the above, we have studied the copolymerization of aniline with *o*-AP and *o*-OT, respectively, in order to gain a deeper understanding of their growth mechanisms and to improve their defluoridation properties for pH > 5. These studies were presented

separately in chapters 4 and 5; chapter 4 considers the study of Pani-PAP while chapter 5 will present electrochemical studies of the poly(aniline-co-*o*-toluidine) copolymer.

4.1.3. Aims and Objectives

The objectives of the studies reported in this chapter are (i) the understanding of the growth dynamics of Pani and poly-*o*-aminophenol (PAP) films; (ii) the copolymerization of Pani-PAP from different ratios of aniline and *o*-AP monomers in acidic medium; (iii) the effect of the different concentrations of monomers on the rate of copolymerization of Pani-PAP; (iv) the examination of their applications via the electrochemical ion-exchange technique, particularly as regards its defluoridation properties by means of the EQCM technique; (v) the characterisation of the acquired polymer and copolymer films via scanning electron microscope (SEM) and spectroscopic (FTIR) techniques.

4.1. Results and Discussions

4.2.1. The Growth Dynamic of Pani and PAP Films

4.2.1.1. Polyaniline film

Initially, the deposition of Pani films from a solution containing 0.1 M aniline monomer and 1 M H₂SO₄ on a gold working electrode (the surface area of the working electrode used was 0.018 cm²) were applied between -0.2 and 1.0 V vs. an Ag/AgCl reference electrode at over various numbers of cycles at 10 mV s⁻¹ with cyclic voltammetry. The acquired I-E curves show considerable similarity to those reported in the literature.²⁷⁻³⁰ During the redox reactions, the colour of Pani film changed to dark green (fully oxidized state, pernigraniline) from light green (fully reduced state, leucoemeraldine).

The increased cycling during the deposition of the Pani film not only the electroactivity but also physical properties such as thickness. The results show that the electroactive sites of the Pani film are enlarged with cycling. The other important outcome is that the thickness is significantly increased with cycling. The application of a slow scan rate and a high number of cycles generated a very thick film. However, these thick Pani films (deposited over 30 cycles) have undesirable properties such as poor adhesion in

comparison with thin Pani film (deposited over 5 cycles). This is an important issue because the thickness of modified electrodes must at some point be considered²⁵ when removing ions from solution, such as with the fluoride ions investigated herein. On the other hand, thick polymer films are not suitable for study with EQCM due to the validation of the Sauerbrey Equation mentioned in detail in chapter 2. This is because we have used the EQCM to acquire electroactivity with high-quality polymer films.

Later, the deposition of a Pani film via EQCM was carried out on a unpolished quartz crystal ($A = 0.23 \text{ cm}^2$) from a solution consisting 0.1 M aniline and 1 M H_2SO_4 between -0.2 and 0.9 V at 10 mV s^{-1} (to overcome the overoxidation problem of the Pani film, the upper potential was chosen to be lower than 1.0 V). The deposition of the Pani film was ended over 17 cycles. The current, mass, and charge density change during deposition of the Pani film as a function of applied potential is presented in figure 4.3. The anodic peak at 0.30 V, which is attributed to the redox reaction between leucoemeraldine and emeraldine, and is accompanied by the exchange of anions, SO_4^{2-} in this work, between the Pani film and the bulk solution.^{4, 5} As the deposition progresses, a second anodic peak appears at 0.6 V in the 10th scan. This second peak probably corresponds to the interconversion between quinone and hydroquinone or quinoneimine. Besides, the current density of the oxidation and reduction peaks increase rapidly with an increasing number of potential cycles. This is an indication of the autocatalytic effect of Pani described in early reports in the literature.^{4, 31} This can be explained by the existence of the Pani film on the working electrode surface ensuring a large redox active area for the deposition of the Pani film with each cycle. After the deposition of the Pani film, a thin light green Pani film was obtained on the quartz crystal, as shown in figure 4.4.



Figure 4.3. An image of the Pani film obtained from figure 4.4

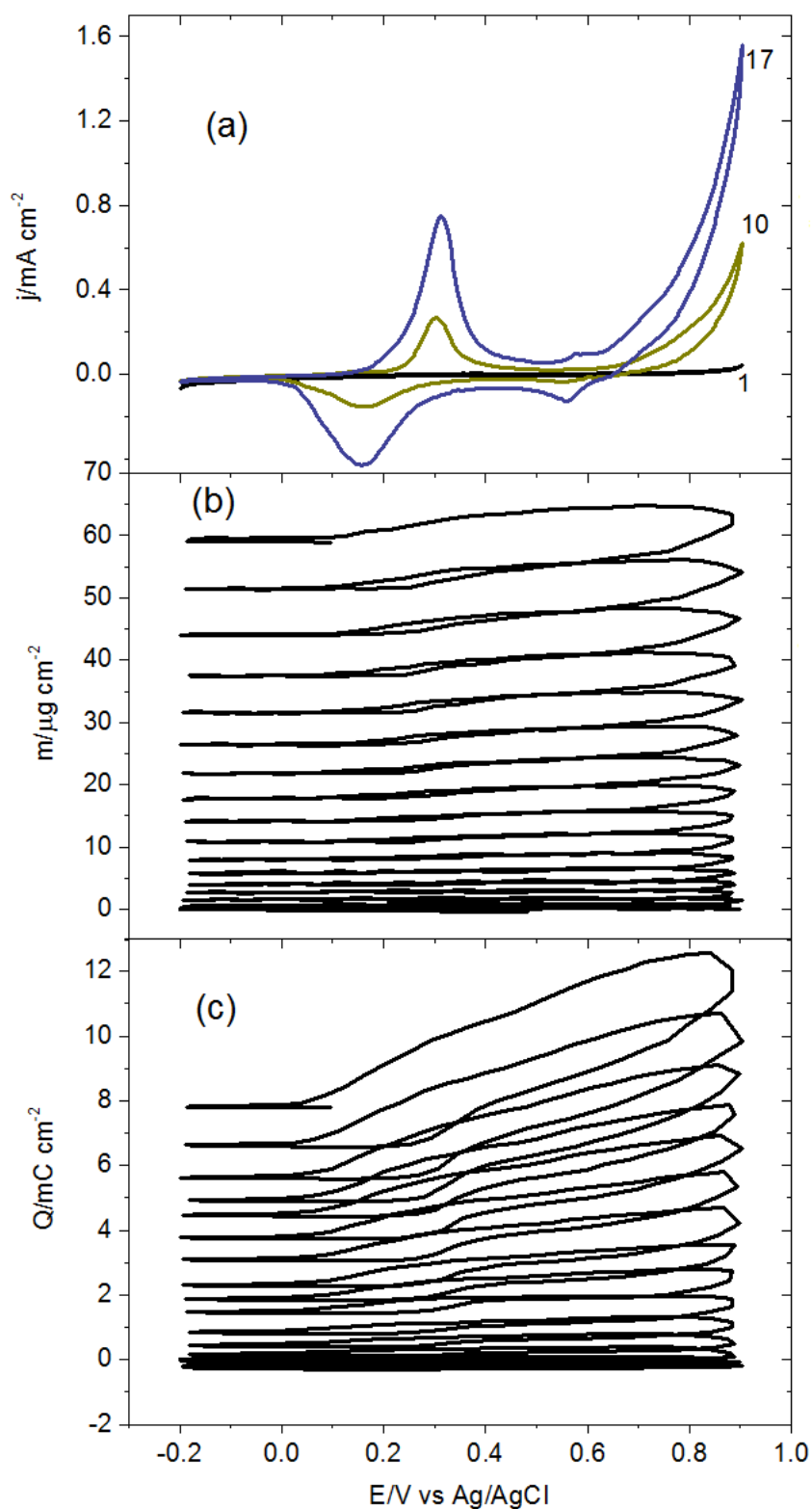


Figure 4.4. (a) The CV curve of the Pani film growth from 0.1 M aniline and 1 M H_2SO_4 crystal between -0.2 and 0.90 V (b) the mass and (c) the charge changes of the Pani film (Γ , $76.1\ nmol\ cm^{-2}$ for dimeric aniline units) (the numbers indicate the cycle numbers)

The mass loading in figure 4.4b rises gradually, reaching a maximum of about $60 \mu\text{g cm}^{-2}$ at the end of the 17th scan. The charge increases with each cycle at the same time. The mass and charge relationship of the Pani film synthesized using EQCM was explored by a mass-charge plot (in figure 4.5) obtained from figure 4.4. The mass of the quartz crystal increased with the cycling, demonstrating the formation of the Pani film on the quartz crystal. In the case of the reduction of the Pani film, the mass of the quartz crystals is not changed but the charge of the films decreases. From the ratio of the mass change to the charge passed, the apparent exchange of molar mass across the copolymer film can be calculated³² using equation 3.4.

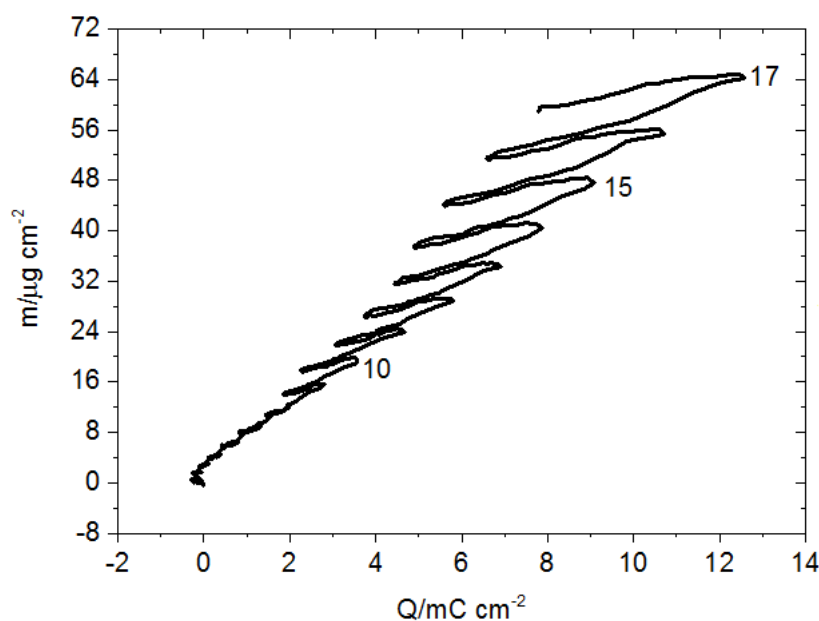


Figure 4.5. The mass-charge curve of the Pani film from figure 4.4 (the numbers indicate the cycle numbers)

The total mass density of the film is $59.5 \mu\text{g cm}^{-2}$ (synthesized in figure 4.7b) while the apparent molar mass is 475.0 g mol^{-1} (using equation 3.4). The molecular weight of two aniline monomers is 186.2 g mol^{-1} (n is 1 for dimeric aniline unit). The difference between these values can be derived the solvent molecules incorporated during the deposition of the Pani film mentioned in chapter 3. Regarding the transfer of solvent molecules, the solvent molecules (α) transferred into the Pani film was determined (using equation 3.5) as **16.0** per redox sites of the polymer. It can be concluded the Pani is a soft film due to the content of solvent.

Figure 4.6 reveals the crystal admittance spectra of the Pani film mentioned above. According to this data, the Pani film behaves as a rigid film when it is deposited under lower applied polymerization potentials, such as 0.90 V over a number of cycles. During EQCM experiments, we concluded that 30 % reducing (corresponding 1.7 mS) in admittance gives an acoustically thick film on the quartz crystal. In doing so, an appreciable thick Pani film was obtained, which is one of the most important aspects of ensuring good ion-exchange properties of modified electrodes.²⁵ Moreover, the ohmic resistance of the Pani film is considerably lower in an aqueous medium. The ohmic resistance of the quartz crystal is found as 575 Ω (calculated using equation 3.6).

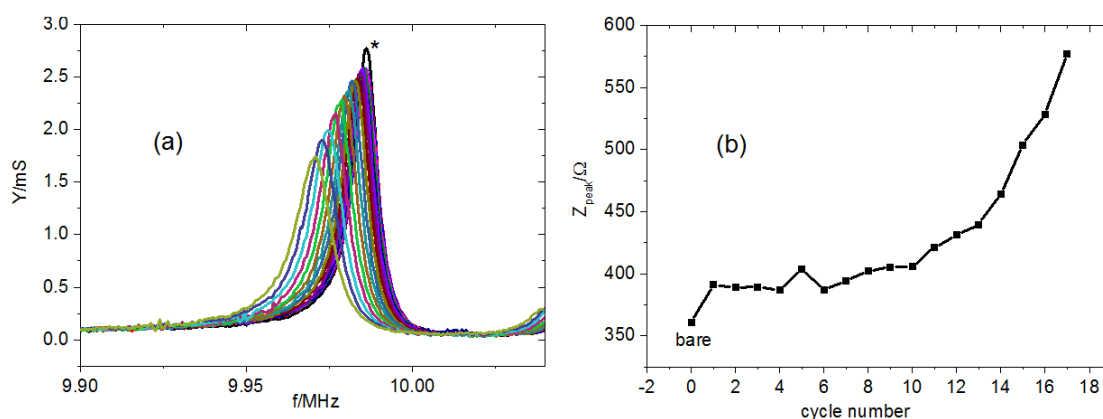


Figure 4.6. EQCM data acquired during deposition of the Pani film from figure 4.4 (a) the admittance change (b) the ohmic resistance of the Pani film from figure 4.6a

Surface coverage (Γ , mol cm⁻²) is an indication of the electroactive sites present on the polymer films,³³ which were calculated using equation 3.1 mentioned in chapter 3. The surface coverage of the Pani film is 76.1 nmol cm⁻² whilst the thickness is 138 nm for dimeric aniline unit. This also indicates the formation of an acoustically thin film with high electroactivity ($n = 1$ for dimeric aniline units and $A = 0.23$ cm²).

The electroactivity of the Pani film was characterised in 1 M H₂SO₄ monomer-free background solutions at different scan rates, will be presented in “regeneration of the polymer and the copolymer films” in this chapter.

4.2.1.2. Poly(*o*-aminophenol) film

Figure 4.7 reveals the polymerization of a PAP film in the presence of 0.1 M *o*-AP and 1 M H₂SO₄ between -0.2 and 1.0 V at 10 mV s⁻¹ over 18 cycles. It showed an anodic at 0.2 V and two cathodic peaks at 0.16/0.22 V, respectively. The polymerization peak

appears at 0.53 V corresponds to the oxidation of the amino group in the phenyl ring of *o*-AP. With an increasing number of scans, the peak currents show a small decrease, indicating the low electroactivity and poor reversibility of the PAP films. After each PAP film deposition, a visible film could not be found on quartz crystal even with 100 cycles despite observing redox reactions between -0.2 and 1.0 V at 10 mV s⁻¹. Thus, the PAP film is not suitable for ion-exchange because the thickness of the polymer film is more relevant.^{25, 34}

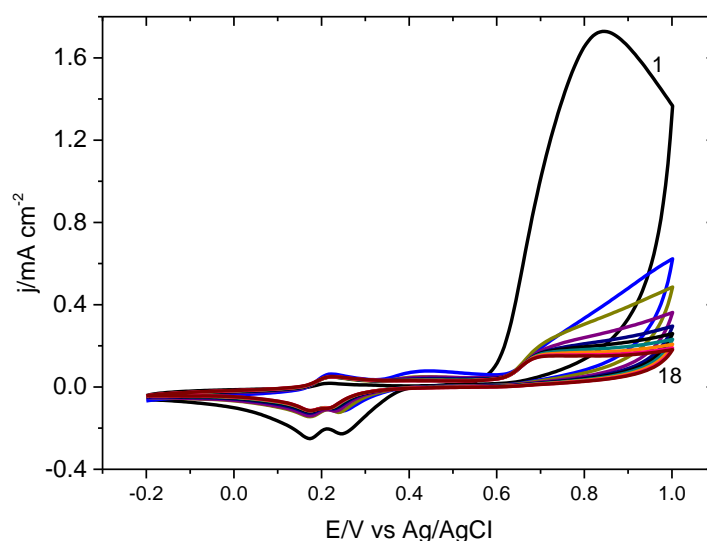


Figure 4.7. The CV curve of a PAP film growth from 0.1 M *o*-AP and 1 M H₂SO₄, $\nu = 10 \text{ mV s}^{-1}$ (Γ , 14.8 nmol cm⁻² for dimeric *o*-aminophenol units)

The simultaneous mass and charge change of the PAP film was revealed, as shown in figure 4.8. The mass loading of the PAP film is extremely slow compared with the Pani film synthesized under identical conditions.³³ The PAP film shows a higher current density in first five cycles, but this decreases gradually with an increasing number of cycles, despite the low scan rate used. The total mass density of the PAP film at the end of the deposition was 11.6 $\mu\text{g cm}^{-2}$.

Figure 4.9 shows the mass-charge curve of the PAP film during growth. Initially, the mass and charge of the PAP film increase slowly over 5 cycles, but the charge passed started to decrease while the mass continued to increase. This can be explained the overoxidation of the PAP film, indicating the decreasing of the electroactive sites. Also, the apparent molar mass of the PAP film was determined as 57.8 g mol⁻¹ for dimeric *o*-aminophenol units by equation 3.4 in chapter 3. The molecular weight of *o*-AP was

reported as 218.2 g mol^{-1} (for dimeric *o*-aminophenol units) in the literature. It means the electrochemical deposition of the PAP film occurred in lower efficiency.

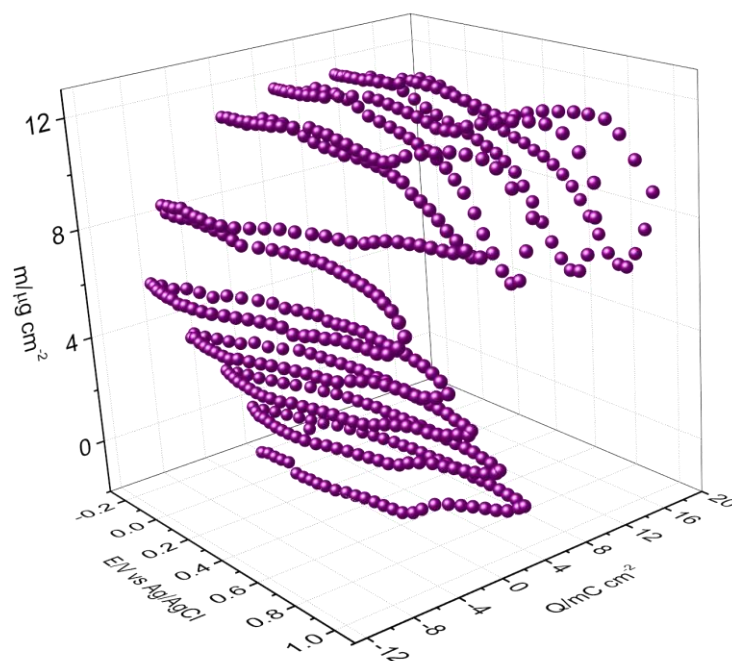


Figure 4.8. The simultaneous mass and charge change of the PAP film (from figure 4.7) as a function of applied potential, $v = 10 \text{ mV s}^{-1}$

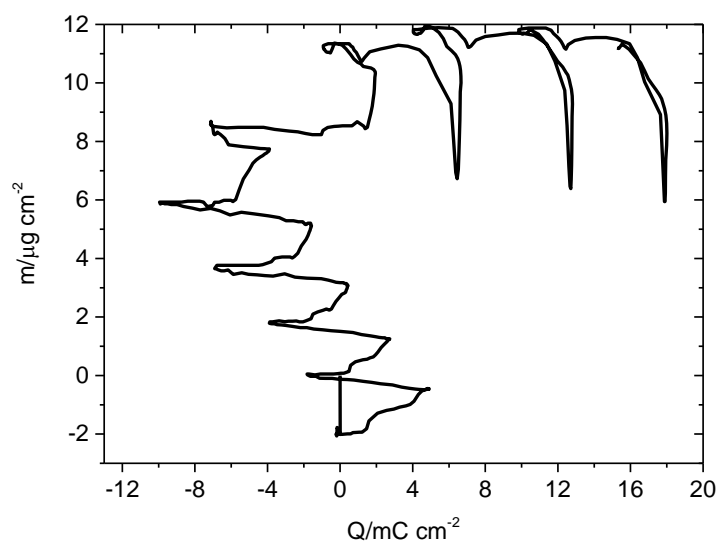


Figure 4.9. The mass-charge curve of the PAP film from figure 4.7. (h , 32 nm for dimeric *o*-aminophenol units)

4.2.1.3. Comparison of the Pani and the PAP polymer films

The electrochemical data for Pani and PAP from their voltammograms indicates that the electroactivity of PAP (Γ , $14.8 \text{ nmol cm}^{-2}$ for dimeric units) film is lower than that of

Pani film (Γ , 76.1 nmol cm⁻² for dimeric units). However, the thickness of the polymer films is a significant issue for ion-exchange techniques^{25,34} but there was no visible film on the quartz crystal even over 100 cycles at 10 mV s⁻¹. On the other hand, the deposition of a polyaniline film under identical conditions provides a thick film on the quartz crystal in just 7 cycles.

After the electrochemical deposition of Pani and PAP films, the films were transferred to a 1 M H₂SO₄ monomer-free solutions in order to characterise their electrochemical properties at 50 mV s⁻¹. Their redox peaks appear at distinctive potentials, as shown in figure 4.10. The anodic and cathodic peaks of the Pani film were observed at 0.34 V and 0.19 V, whilst the anodic and cathodic peaks of the PAP film appeared around 0.25 V. Also, in the case of the PAP film, the anodic and cathodic peaks were highly symmetric in shape, in terms of their potential positions and areas.

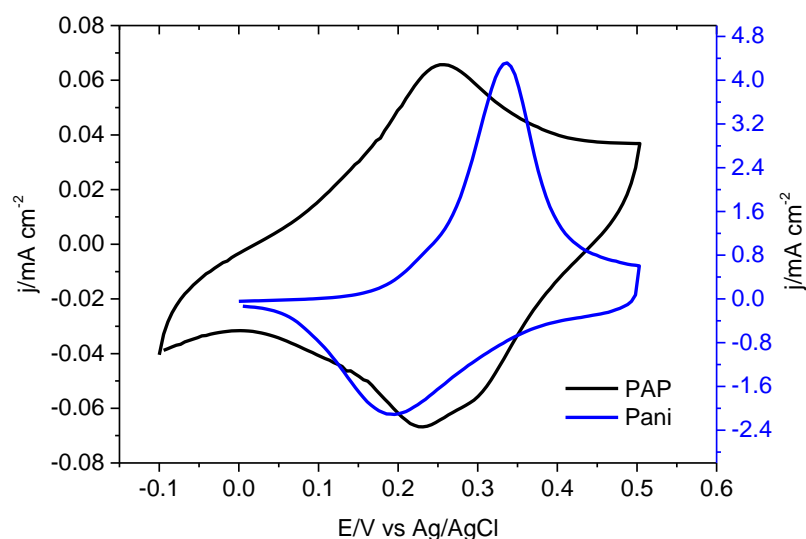


Figure 4.10. Characterisation of the Pani (figure 4.4) and the PAP (figure 4.7) films in 1 M H₂SO₄, $\nu = 50 \text{ mV s}^{-1}$

4.2.2. The Copolymerization of Pani-PAP Copolymer Films

4.2.2.1. Copolymerization of Pani-PAP copolymer films by chronoamperometry

The formation of copolymer films is occurred by head-to-tail coupling of the monomers like polymerization of aniline.³⁵ The electrochemical deposition of Pani-PAP films was

studied in the presence of different ratios of monomer, aniline and *o*-AP, in 1 M H₂SO₄ using the chronoamperometry technique. The results acquired are shown in figure 4.11.

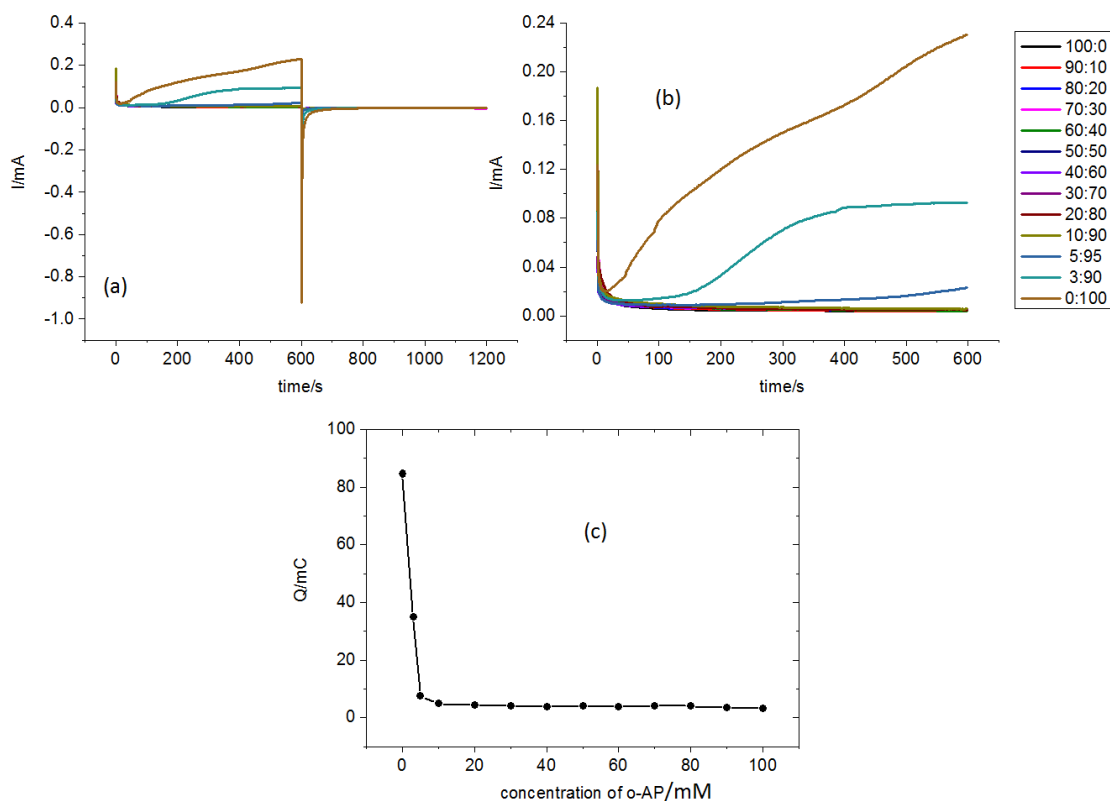


Figure 4.11. Chronoamperometry results of copolymerization of Pani-PAP; **(a)** the current change as a function of time during the electrochemical deposition of Pani-PAP copolymer films at E₁ = 1.0 V and E₂ = -0.2 V; **(b)** a detailed representation of the anodic deposition of the Pani-PAP copolymer films at 1.0 V; **(c)** the charge transport of the Pani-PAP films against the ratio of *o*-AP in 0.1 M monomer solution (from figure 4.11a) (The numbers indicate the ratio of monomers as *o*-AP:An)

The amount of *o*-AP plays a significant role the synthesis of electroactive Pani-PAP copolymer films, as can be seen in figure 4.11. The current density and the calculated charge values during the deposition at 1.0 V were raised with lower amounts of *o*-AP in 0.1 M monomer. 5 mM and 10 mM *o*-AP concentration were used, keeping a 0.1 M total monomer concentration to give an electroactive film. The Pani-PAP copolymer films from 95:5 and 90:10 as An:*o*-AP/mM give compact films, while other ratios involving higher amounts of *o*-AP did not reveal any visible copolymer film.

4.2.2.2. The growth of Pani-PAP copolymer films by means of EQCM

Initially the deposition of aniline and *o*-aminophenol were carried out for the ratios 50:50, 60:40, 70:30, and 80:20 (An:*o*-AP). Different redox peaks for pure Pani and pure

PAP film growth voltammograms appeared for 90:10 and 95:5 (An:*o*-AP) monomer ratios while giving similar current densities as a function of the applied potential. This shows that even the presence of a small amount of *o*-AP still dominates the copolymerization of the Pani-PAP, which are different from those homopolymers but showing a lower electroactivity. In the meantime, the visible film did not observe with a higher level of *o*-AP in monomer concentrations, showing the polymerization rate became significantly slow. Therefore, the total concentrations of monomers were increased to improve the effect of aniline in lower amounts of *o*-AP in further studies (via EQCM) to obtain a deeper understanding of the dynamic and the mass loading of the copolymerization of the Pani-PAP films.

Figure 4.12 shows the CVs of the Pani-PAP films from a solution consisting of different ratios of An:*o*-AP (90:10; 95:5; 160:40; 180:20; 190:10; 280:20; 290:10)/mM between -0.20 to 0.95 V (avoiding overoxidation) at either 5 or 10 mV s⁻¹. They give two anodic around 0.35 V and 0.50 V and two cathodic peaks around 0.32 and 0.45 V, implying the formation of copolymer films rather than a mixture of the monomer. However, many cycles caused a change in the electrochemical properties of the Pani-PAP copolymer films at a slow scan rate, 5 mV s⁻¹. In the case of large amount of aniline, such as with ratio 95:5 and 290:10 (An:*o*-AP/mM), the voltammograms appear essentially identical to that of pure Pani film, showing that a large amount of aniline starts to dominate the formation of the copolymer film. In the case of large amounts of *o*-AP, such as with a ratio of 160:40, the current density continued with subsequent cycling, such as with the deposition of pure PAP. The peak current densities of Pani-PAP copolymer films are smaller compared to that of Pani film but larger than those of PAP film.

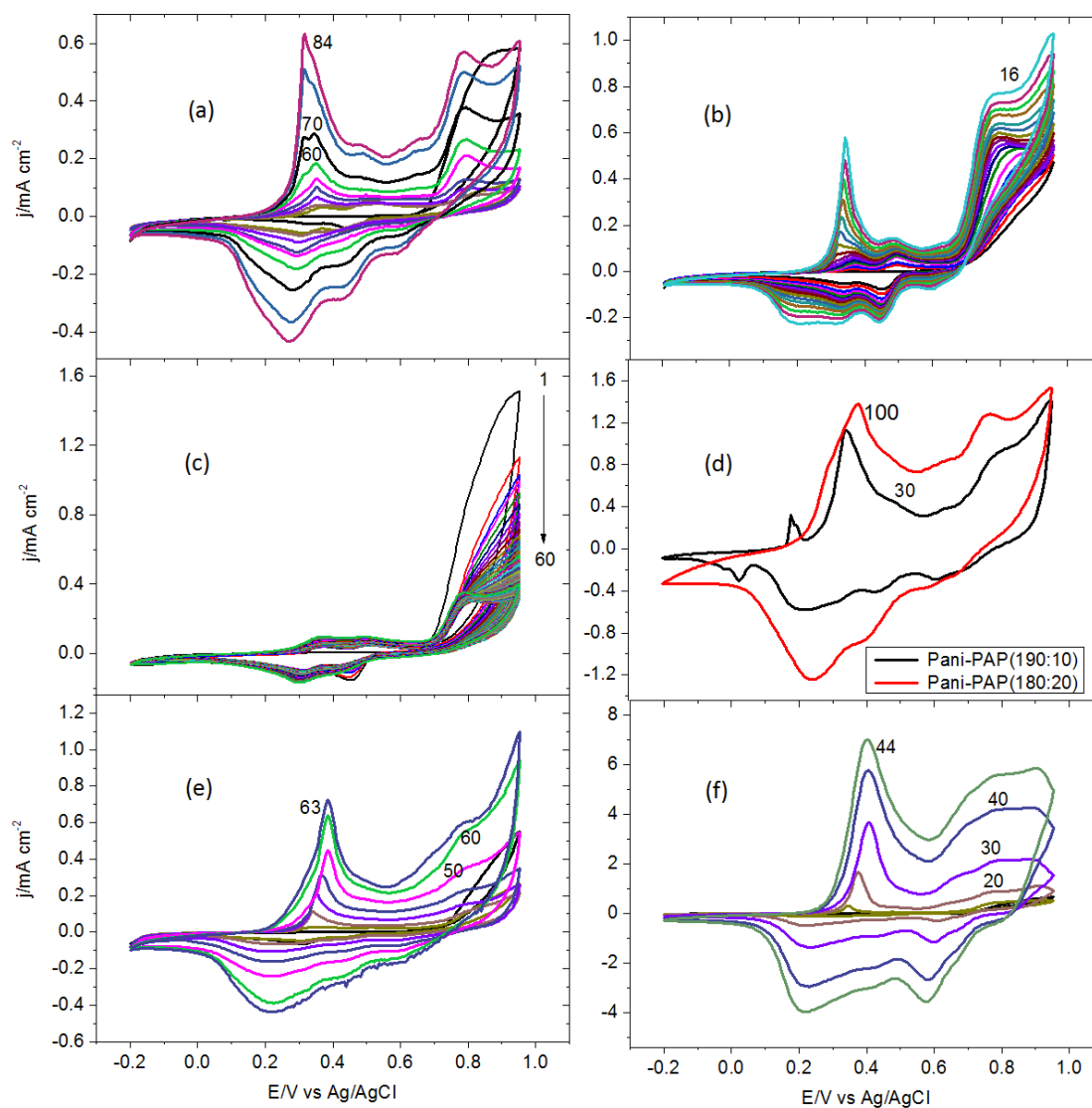
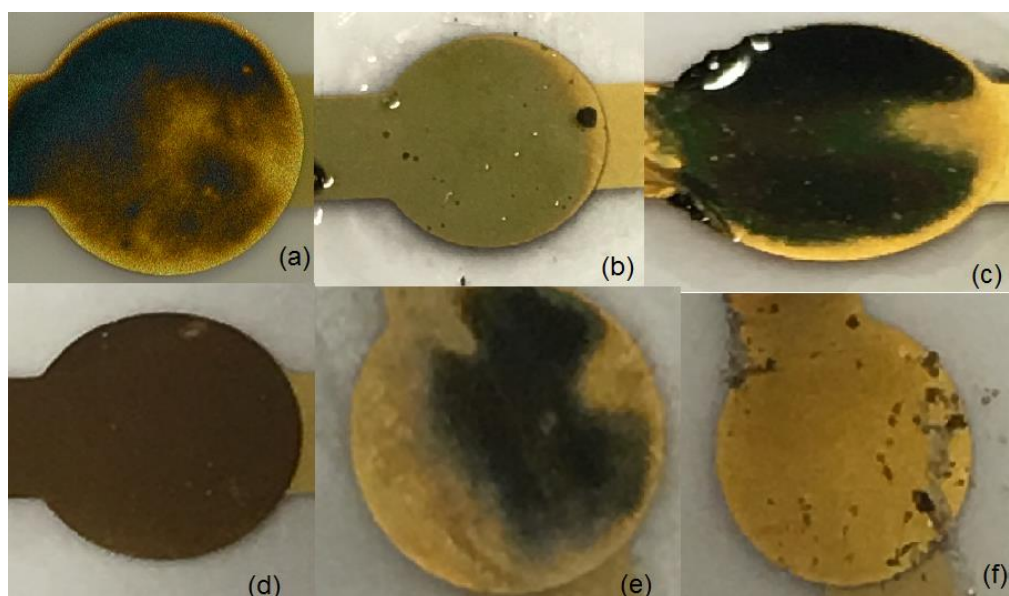


Figure 4.12. The CV curves of the Pani-PAP growth from different monomer concentrations (An:*o*-AP) (a) 90:10 at 5 mV s^{-1} (b) 95:5 at 5 mV s^{-1} (c) 160:40 at 10 mV s^{-1} (d) 180:20 and 190:10 at 10 mV s^{-1} (e) 280:10 at 10 mV s^{-1} , $v = 10 \text{ mV s}^{-1}$ and (f) 290:10 at 5 mV s^{-1} (the numbers indicates the number of cycles)

The surface coverage values of the Pani-PAP copolymer films are presented in table 4.1 (for dimeric units), showing the best electroactivity is obtained from 90:10 (An: *o*-AP/mM). Also, at the end of the deposition of the copolymer films from figure 4.12, the different colour copolymer films were observed on the quartz crystals, as shown in figure 4.13. The electrochemical deposition of the Pani-PAP (90:10) copolymer film give a sufficient and uniform film. Also, the different colour of the Pani-PAP (90:10) film is a significant indication of the formation of a new copolymer film as a different copolymer film reported in the literature.^{11, 36}

Table 4.1. Electrochemical data obtained from the voltammograms of the Pani-PAP copolymer films from figure 4.12 (n is 1 for dimeric units)

<i>An:o-AP</i> /mM	Γ /nmol cm ⁻²	h /nm	Colour of the film on quartz crystal	<i>An:o-AP</i> %
90:10	266.8	523	brown	90:10
95:5	136.4	267	light green	95:5
160:40	35.3	69	light brown	80:20
180:20	349.8	686	light green	90:10
190:10	151.9	297	light green	95:5
280:20	160.2	314	not visible	93.3:6.6
290:10	1548.2	303	dark green	96.6:3.3

**Figure 4.13.** The image of the Pani-PAP copolymer films synthesised over various numbers of cycles (in figure 4.12) (a) 180:20 at 10 mV s⁻¹ (b) 190:10 at 10 mV s⁻¹ (c) 290:10 at 5 mV s⁻¹ (d) 90:10 at 5 mV s⁻¹ (e) 95:5 at 5 mV s⁻¹ and (f) 160:40 as the ratio An:o-AP/mM at 5 mVs⁻¹

The admittance data obtained simultaneously during the deposition of the Pani-PAP copolymer films from figure 4.12 are plotted in figure 4.14, showing the formation of acoustically thin copolymer films on the quartz crystal, although a large number cycles did have to be used to achieve this in certain instances. The interesting thing from this figure is that the Pani-PAP films in ratios such as 290:10 (An:o-AP/mM) and 190:10 (An:o-AP/mM) that contained large amounts of aniline in the monomer solution gave acoustically thin films, because Pani film itself gives a thick film with as few as 7 cycles

in 0.1 M monomer and 1 M H₂SO₄ solution under identical conditions.³³ The addition of *o*-AP in aniline monomer solution significantly decreases the growth rate of the Pani film while at the same time providing compact, rigid films. A shift in frequency change was observed in the case of 90:10 and 180:20 ratios with continued cycling.

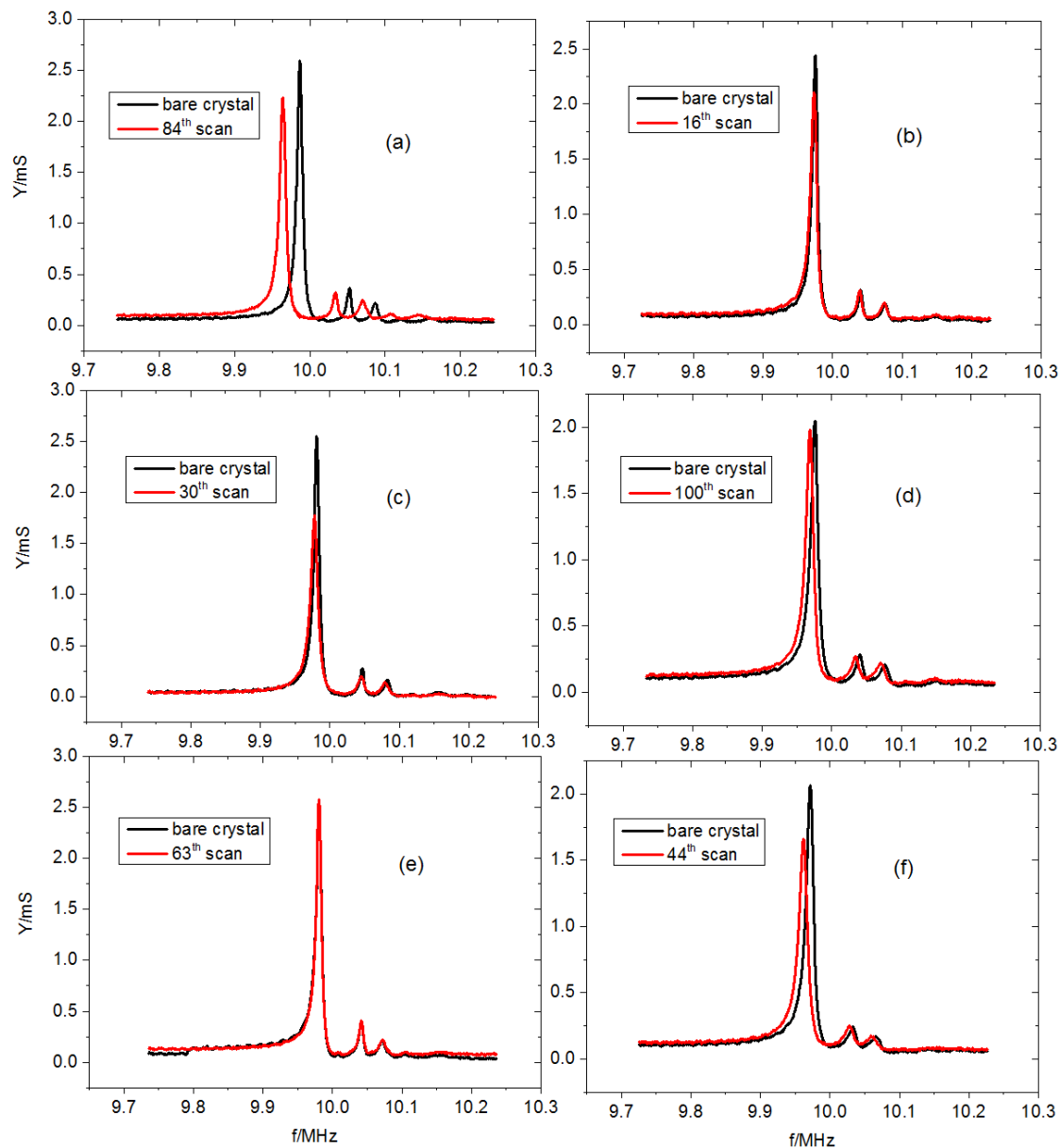


Figure 4.14. The admittance data of the Pani-PAP films deposited from different ratios of aniline and *o*-AP monomers at various scan rates (a) 90:10 at 5 mV s⁻¹ (b) 95:5 at 5 mV s⁻¹ (c) 160:40 at 10 mV s⁻¹ (d) 180:20 and 190:10 at 10 mV s⁻¹ (e) 280:10 at 10 mV s⁻¹, $v = 10$ mV s⁻¹ and (f) 290:10 (as An:*o*-AP/mM) at 5 mV s⁻¹ (from figure 4.12)

Of the Pani-PAP copolymer films deposited, the Pani-PAP (90:10) ratio seems most promising because it exhibited uniform deposition on the quartz crystal with high electroactivity. The mass-charge curves for this copolymer film as a function of applied

potential are plotted in figure 4.15. The mass loading is extremely slow for the first 20 cycles, though it did gradually increase over successive cycles. With a large number of cycles, the mass loading increases in rate. This could arise from the increasing ratios of aniline monomer consuming the *o*-AP monomers over the initial cycles. A similar phenomenon occurred during the change in charge of the Pani-PAP (90:10) copolymer film shown in figure 4.15b.

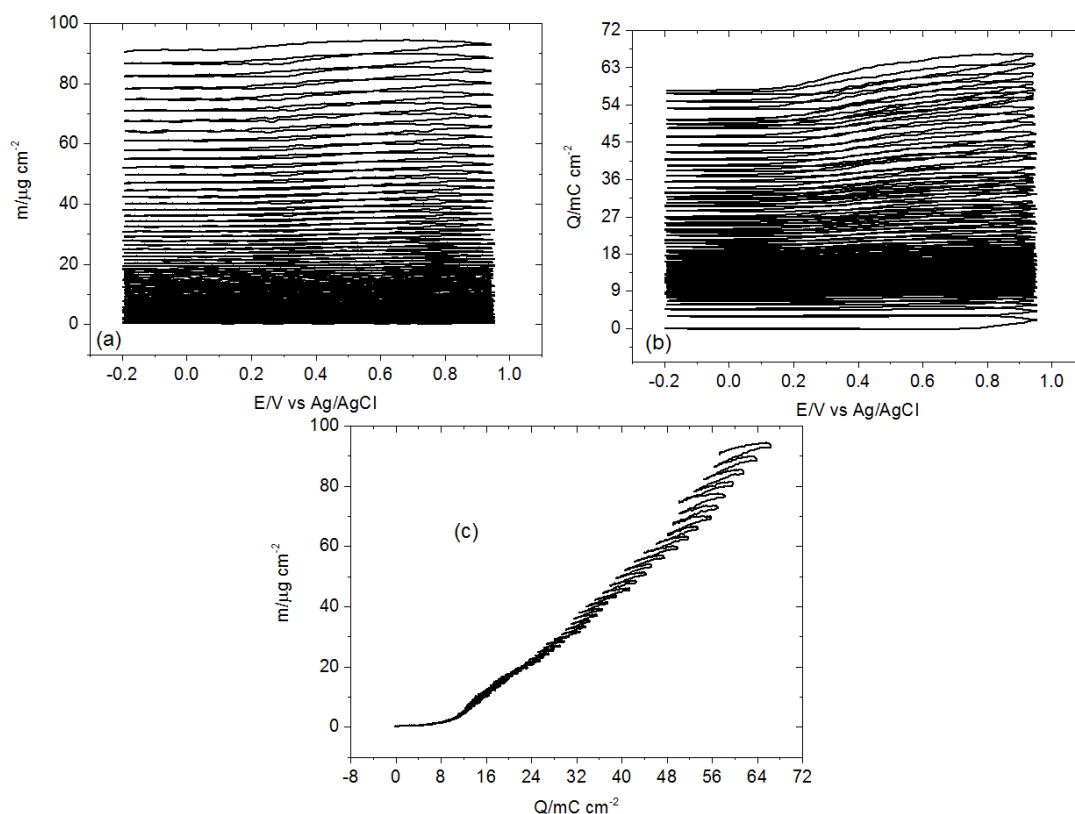


Figure 4.15. (a) the mass loading (b) the charge changes of the Pani-PAP film (90:10) as a function of applied potential, $v = 5 \text{ mV s}^{-1}$ (c) the mass-charge curves of the Pani-PAP growth

The apparent molar mass (M_{app}) of the Pani-PAP (90:10) film is 155.6 g mol^{-1} whilst the solvent content is 2.5 for dimeric units by equation 3.4 and 3.5. These findings indicate the copolymerization of aniline with *o*-aminophenol provides a firmer film because the solvent content of the Pani film is 16.0 mentioned above.

4.2.2.3. Characterisation of the Pani-PAP (90:10) copolymer film

The Pani-PAP copolymer films deposited in figure 4.12 were transferred to 1 M H_2SO_4 monomer-free background solution to explore their electroactivity. The associated cyclic voltammograms are displayed in figure 4.16. The redox peaks of the Pani-PAP

(90:10) film appears at 0.32/0.27 V, representing the distinctive than the other Pani-PAP films because they generally give around 0.35/0.24 V. This outcome also supports the formation of a new copolymer film from 90:10 (An:*o*-AP/mM).

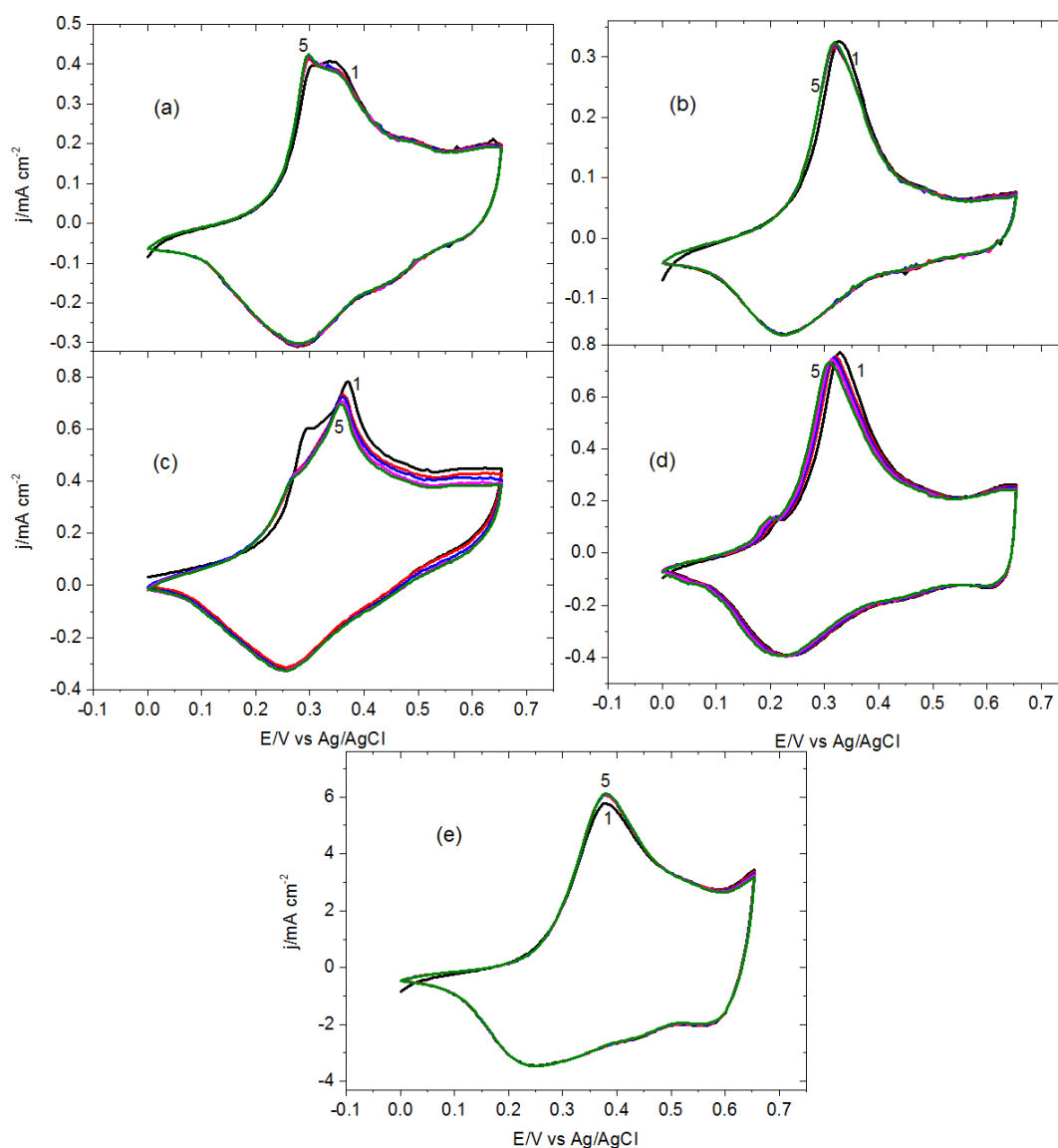


Figure 4.16. The CV curves of the Pani-PAP (An:*o*-AP) copolymer films in 1 M H₂SO₄ (a) 90:10 (b) 95:5 (c) 180:20 (d) 190:10 (e) 290:10 (as An:*o*-AP/mM) ; $\nu = 5 \text{ mV s}^{-1}$ (the numbers indicate the number of cycles)

The surface coverage of the Pani-PAP (90:10) copolymer films was found as 198.7 nmol cm⁻² whilst its thickness is 401 nm, indicating an acoustically thin film.

4.2.3. The Removal of Fluoride Ions

The removal of fluoride ions from drinking water is highly possible using the conducting polymer electrodes mentioned in the first part of this chapter. In the

following section, we will present the performance of the Pani film (in figure 4.4) and the Pani-PAP (90:10) copolymer film (in figure 4.12) synthesized in this regard.

4.2.3.1. Removal by the Pani Polymer film

Figure 4.17 shows the redox cycling of the Pani film in 0.1 M NaF at 5 mV s^{-1} . The film behaves in a reversible manner between its oxidation and reduction reactions in terms of mass and charge change in 1 M H_2SO_4 monomer-free solution. In the meantime, the Pani film uptakes anion into the film structures because the mass increase during the oxidation shows anion transfer to maintain the electroneutrality of the Pani film.

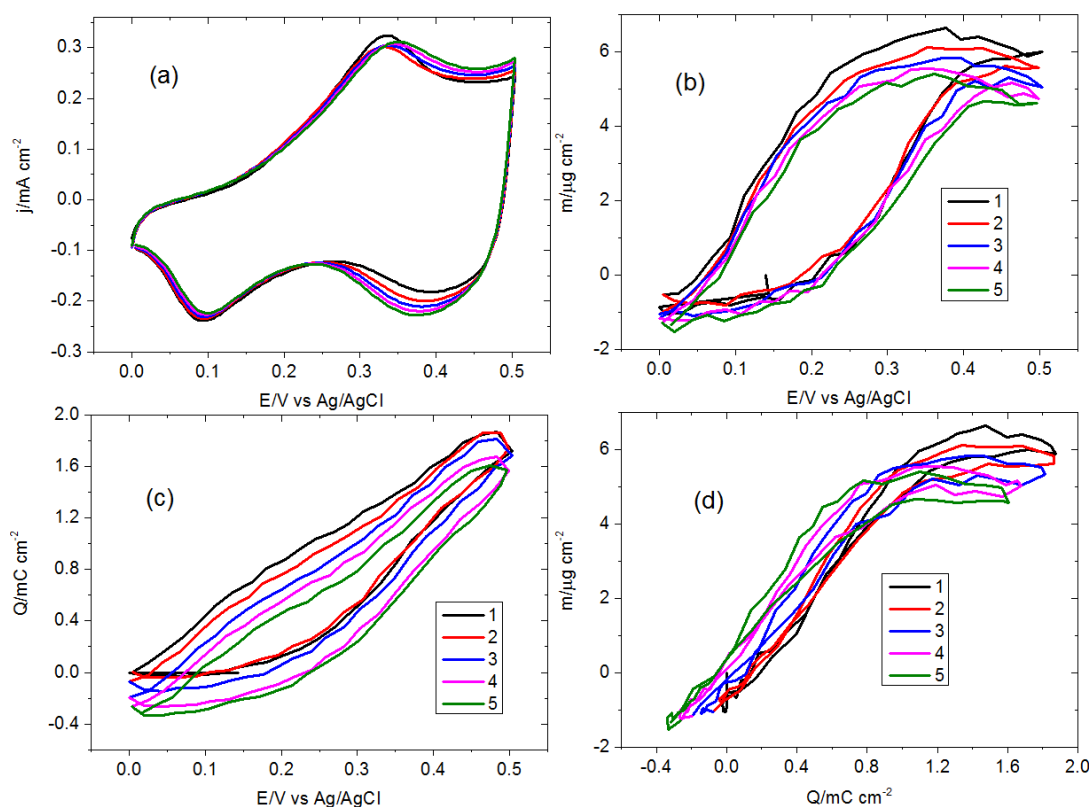


Figure 4.17. The removal of fluoride ions by the Pani film (a) the CV curve of the redox cycling of the Pani film in 0.1 M NaF (b) the mass change and (c) the charge change as a function of applied potential (d) mass-charge curve of the Pani film in 0.1 M NaF, the scan rate, $v = 5 \text{ mV s}^{-1}$ (the number indicates the cycle numbers)

Considering all the above, the molar mass of the incorporated anions and the number of transferred solvent molecules transferred (α) were found as reported in table 4.2 for the Pani film. According to these results, the ion exchange behaviour of the Pani film in 0.1 M NaF at different scan rates is reversible in terms of the apparent molar mass.

Table 4.2. Apparent molar mass (M_{app}) and number of transferred solvent molecules (α) during the redox cycling of the Pani film synthesised in figure 4.4

<i>Film</i>	<i>Scan rate/mVs⁻²</i>	<i>During oxidation</i>	<i>During reduction</i>	<i>During oxidation</i>	<i>During reduction</i>
		<i>M_{app}/gmol⁻¹</i>	<i>M_{app}/gmol⁻¹</i>	<i>α/per anion</i>	<i>α/per anion</i>
<i>Pani</i>	3	404.6	385.9	21.4	20
	5	305.0	305.0	15.8	15.8
	10	572	469	25	25

The Pani film uptakes **0.5** mol ion per redox sites of the polymer film as a theoretical. In the case of the Pani synthesized in figure 4.4, the Pani film takes **0.25** mol fluoride ions per redox sites of the polymer film at 0.3 V, corresponding **51.6 mg g⁻¹** fluoride ions from 0.1 M NaF upon oxidation and releases **50 mg g⁻¹** upon its reduction at pH 6.60. The performance of the Pani film is decreased practically. On the other hand, this amount is a considerably much greater than the available ion-exchange techniques the fluoride in the literature.^{14, 16}. They showed Pani films take 0.78 mg g⁻¹ and 20 mg g⁻¹ at 1.5 V. These films have taken a few fluoride ions while requiring a high potential, which can be resulted in the degradation of the film.

4.2.3.2. Removal by the Pani-PAP (90:10) copolymer film

The Pani-PAP (90:10) copolymer film deposited in figure 4.12 was transferred to 0.1 M NaF solutions at 5 mV s⁻¹ after the characterisation in 1 M H₂SO₄ monomer-free background solutions in figure 4.18a. The Pani-PAP (90:10) copolymer film give certain redox peaks (at 0.30/0.1 V), representing the ionic activity of the Pani-PAP (90:10) film in 0.1 M NaF at 6.60.

The simultaneous mass-charge change of the Pani-PAP (90:10) copolymer film is also plotted in figure 4.18b, showing the almost reversible change for the Pani-PAP (90:10) copolymer film while they behave as anion exchangers in 0.1 M NaF. The apparent molar mass of the incorporated ions is reported as 123.7 g mol⁻¹ during both oxidation and reduction. This means that the Pani-PAP (90:10) film is promising regarding the immediate uptake of fluoride ions from water and their immediate release at negative potentials.

As we mentioned earlier, the Pani-PAP (90:10) film must take **0.5** mol ions per redox sites of the copolymer film in theory. Here, the Pani-PAP (90:10) film takes **0.35** mol fluoride ions per redox sites of the copolymer film upon oxidation, which is much greater than the Pani film, taking 0.25 mol ion upon its oxidation. The corresponding amount of fluoride ions taken by Pani-PAP films were found as + **65.0 mg F⁻ g⁻¹** upon oxidation and **-64.3 mg F⁻ g⁻¹** upon reduction, showing the excellent ability for the Pani-PAP (90:10) film. Besides, the Pani-PAP (90:10) film makes possible the successive use without pre-treatment. The findings proved that the copolymerization of aniline with *o*-aminophenol enhanced markedly its defluoridation properties.

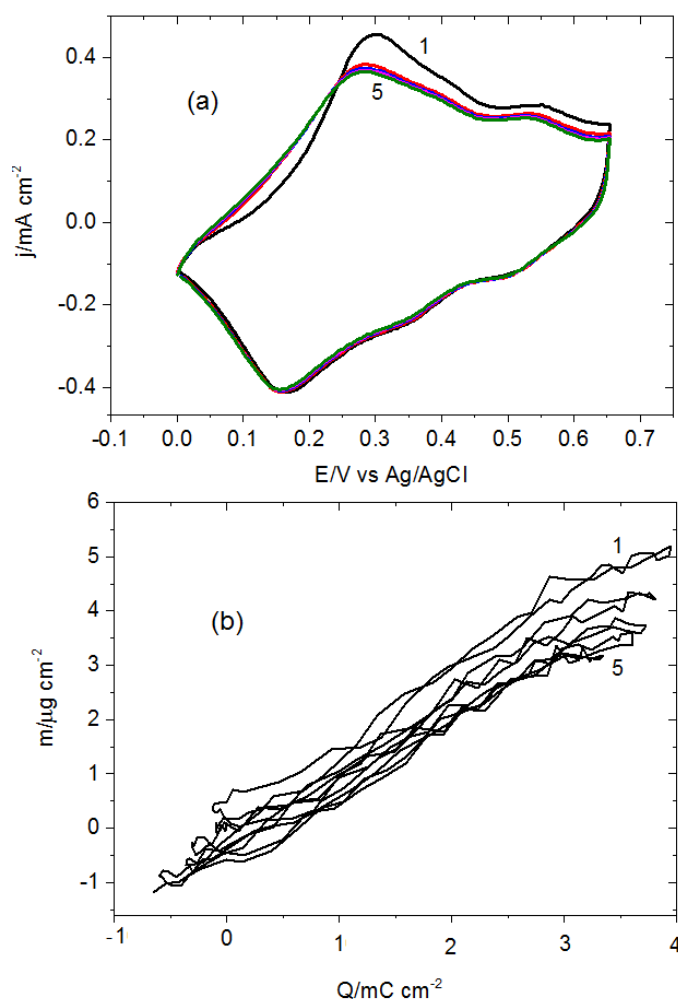


Figure 4.18. (a) The CV curves of the Pani-PAP (90:10) copolymer films in 0.1 M NaF (b) the mass-charge curve of the Pani-PAP (90:10) film in 0.1 M NaF, the scan rate, $\nu = 5 \text{ mV s}^{-1}$ (the numbers indicate the cycle numbers)

To explore the ionic activity of the Pani-PAP (90:10) film, this copolymer film was studied at different scan rates under otherwise identical conditions, as shown in figure 4.19. It shows the reversible behaviour of the Pani-PAP (90:10) film. Also, the

performance of the Pani-PAP (90:10) film was investigated in different concentrations of NaF, 0.01 and 0.001 M as shown in figure 4.20, showing a good ionic activity in even 0.001 M NaF with a reversible manner. The acquired gravimetric data was presented in table 4.3.

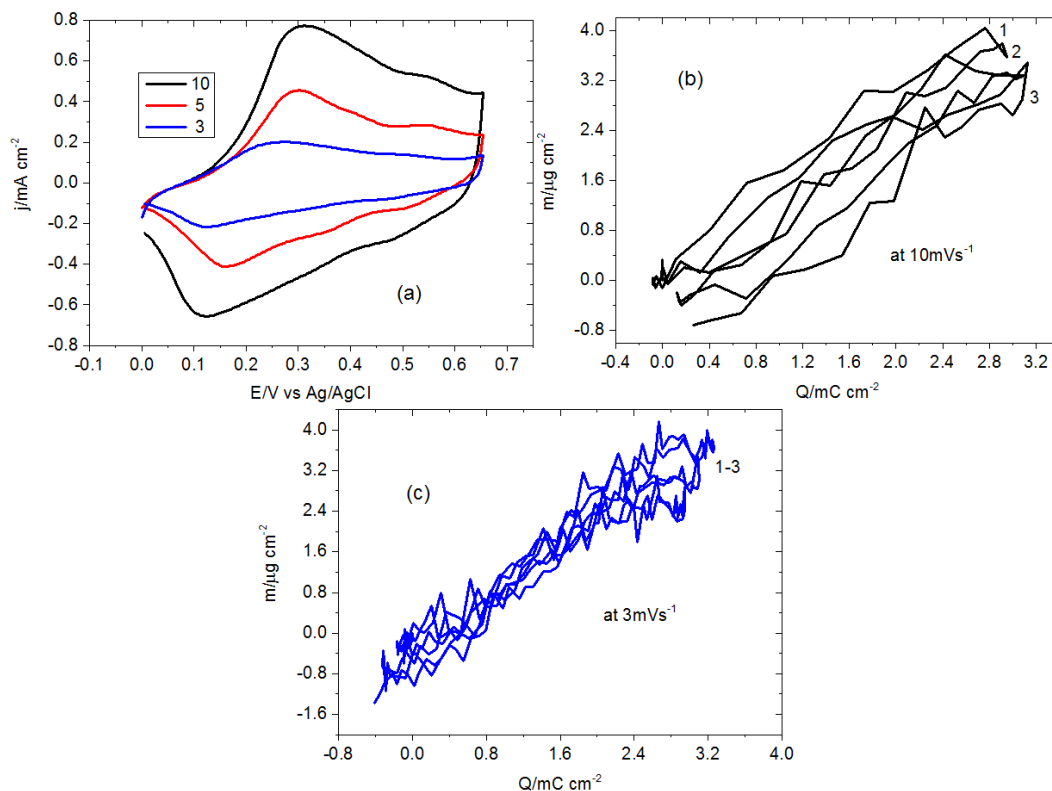


Figure 4.19. The removal of fluoride ions by Pani-PAP (90:10) film synthesised (see figure 4.12) NaF (a) the CV curves of the redox cycling of Pani-PAP (90:10) film at different scan rates of 3, 5 and 10 mV s⁻¹ in 0.1 M NaF (b) mass-charge change at 10 mV s⁻¹ (c) the mass-charge change at 3 mV s⁻¹

Table 4.3. Apparent molar mass (M_{app}) and number of transferred solvent molecules (α) during the redox cycling of the Pani-PAP (90:10) copolymer film

Scan rate/mVs ⁻¹	NaF/M	During oxidation	During reduction	During oxidation	During reduction
		M_{app}/gmol^{-1}	M_{app}/gmol^{-1}	$\alpha/\text{per anion}$	$\alpha/\text{per anion}$
3	0.1	106.5	106.5	4.9	4.8
	0.01	123.7	123.7	5.8	5.8
5	0.01	74.7	118.4	3.1	5.5
	0.001	185.2	185.2	9.2	9.2
10	0.1	119.2	119.2	5.6	5.6

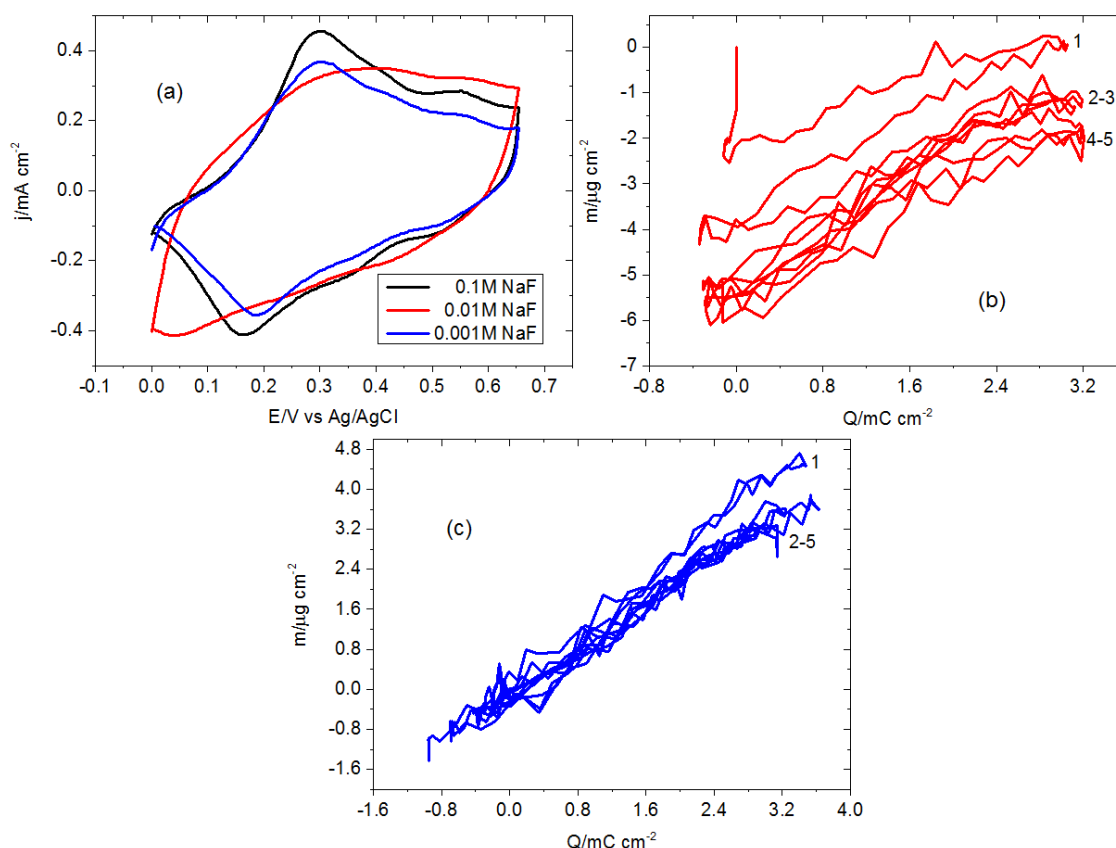


Figure 4.20. The removal of fluoride ions by Pani-PAP (90:10) film synthesised (see in figure 4.12) in the presence of different concentrations of fluoride ions, $v = 5 \text{ mV s}^{-1}$ (a) the CV curves of the redox cycling of Pani-PAP film in 0.1 M, 0.01 M and 0.001 M NaF (b) the mass-charge change in 0.01 M (c) the mass-charge change in 0.001 M NaF

The performance of the Pani-PAP (90:10) copolymer film was also explored in the presence of both chloride and fluoride ions at 5 mV s^{-1} , indicating the transfer of the same amounts of ions in different ratios, as shown in figure 4.21. The ionic-activity of the Pani-PAP (90:10) film in the NaF and NaCl electrolyte solution with a different ratio resulted in similar current densities. This can be explained the insertion of F^- and Cl^- can be together in terms of their ratios because of their small sizes. For instance, in the presence of 90 mM F^- and 10 mM Cl^- , the ions taken by the film can comprise 90% fluoride and 10% chloride ions in terms of the same current density values. The apparent molar mass values of the Pani-PAP (90:10) film determined by equation 3.4 showed in table 4.4. The solvent molecules transferred was determined by equation 3.5 considering the insertion of both ions, fluoride and chloride, in terms of their concentration ratios in electrolyte solutions.

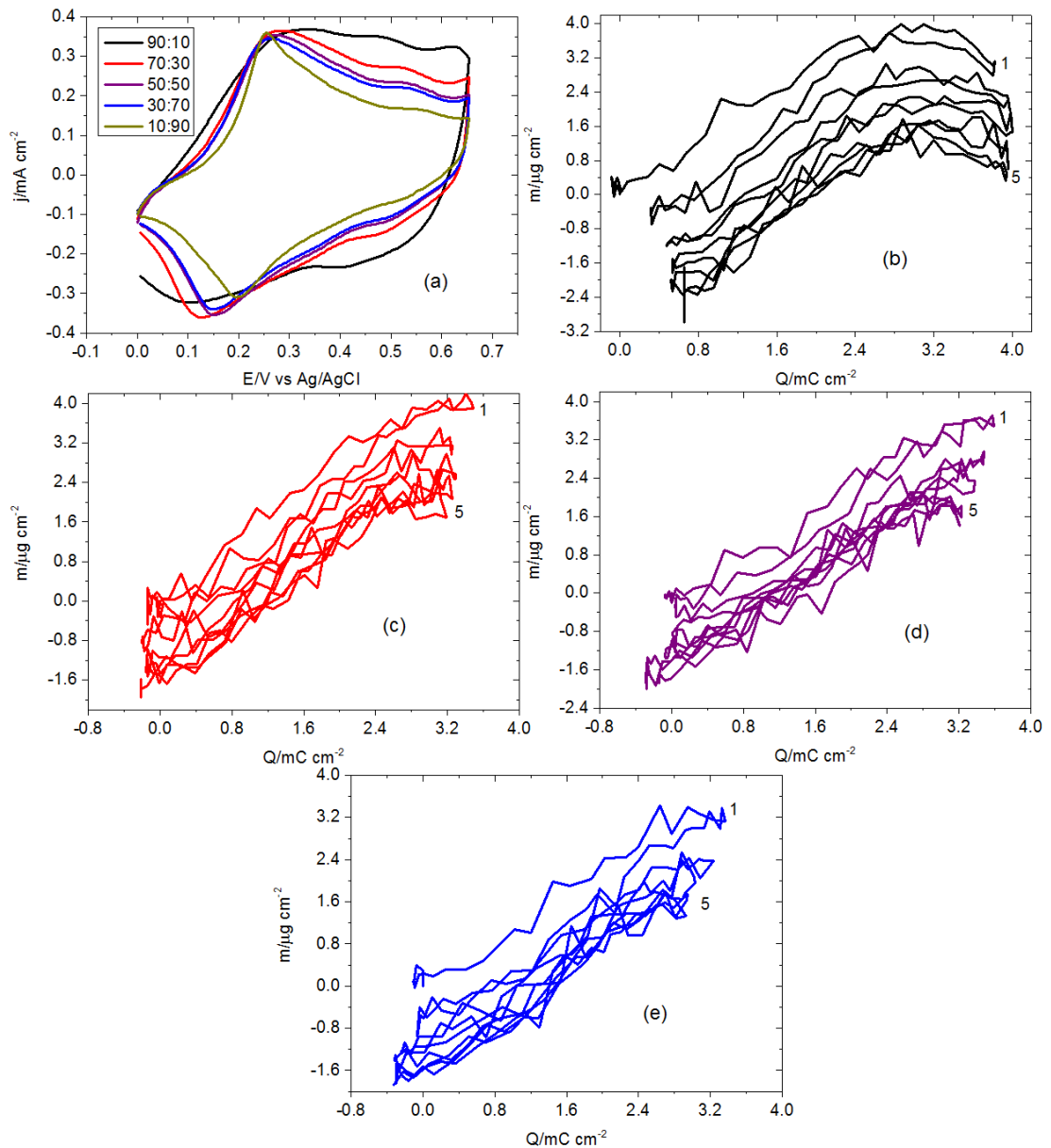


Figure 4.21. The removal of fluoride ions in the presence of F^- and Cl^- ions (total concentration of ions is 0.1 M) by the Pani-PAP (90:10) copolymer film (synthesised in figure 4.25a), $v = 5 \text{ mV s}^{-1}$ (a) the CV curves of the redox cycling of Pani film in different concentrations of F^- and Cl^- ions; the mass-charge curves of (b) in 90 mM F^- and 10 mM Cl^- (c) in 70 mM F^- and 30 mM Cl^- (d) in 50 mM F^- and 50 mM Cl^- (e) in 30 mM F^- and 10 mM Cl^- (f) in 10 mM F^- and 90 mM Cl^-

Table 4.4. Apparent molar mass (M_{app}) and number of transferred solvent molecules (α) during the redox cycling of the Pani-PAP (90:10) copolymer film in the presence of chloride ions, $v = 5 \text{ mV s}^{-1}$

<i>Ratio/mM F⁻: Cl⁻</i>	<i>During oxidation</i>	<i>During reduction</i>	<i>During oxidation</i>	<i>During reduction</i>
	<i>M_{app}/gmol^{-1}</i>	<i>M_{app}/gmol^{-1}</i>	<i>$\alpha/\text{per anion}$</i>	<i>$\alpha/\text{per anion}$</i>
90:10	76.4	96.9	3.1	4.2
70:30	107.7	110.1	4.6	4.8
50:50	96.4	96.2	3.8	3.8
30:70	91.1	109.1	3.4	4.4

4.2.4. Regeneration of the Polymer and the Copolymer Films

4.2.4.1. The Pani film

The electroactivity of the Pani film synthesized in figure 4.4 was explored in 1 M H_2SO_4 monomer-free background solution before and after treatment with a NaF electrolyte solution to obtain a better understating of the defluoridation on the properties of the Pani film. Cyclic voltammograms of the Pani film in 1 M H_2SO_4 at different scan rates and 5 mV s^{-1} are shown in figure 4.22a-b, indicating a higher current density with an increase in scan rate. After the treatment with NaF electrolyte solution, the Pani film was transferred to 1 M H_2SO_4 under identical conditions as those applied with NaF. As can be seen in figure 4.22c, the current density of the Pani film increases with each cycle, indicating the fluoride ions being released from the Pani film.

The $\log i_p$ - $\log v$ curves of the Pani film in 1 M H_2SO_4 are presented in figure 4.23 after NaF treatment, showing the reversibility of the Pani film was similar to when it was synthesized.

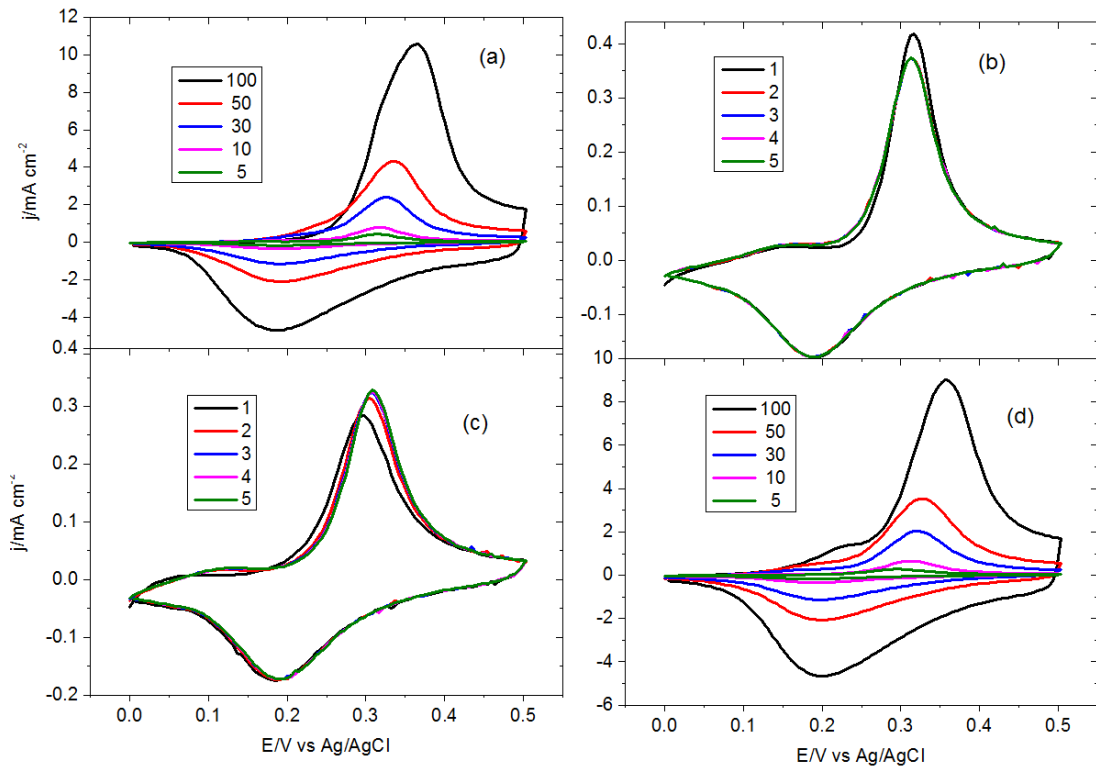


Figure 4.22. The electroactivity of the Pani film (from 4.4) in 1 M H_2SO_4 (**a**) the CV curves of the Pani film at different scan rates before treatment with NaF (**b**) the electroactivity of the Pani film in 1 M H_2SO_4 at 5 mV s^{-1} before treatment with NaF (**c**) the CV curves of the Pani film at different scan rates after treatment with NaF (**d**) the electroactivity of the Pani film in 1 M H_2SO_4 at 5 mV s^{-1} after treatment with NaF (the numbers indicate the scan rates in figure 4.22a-d, while representing cycle number in figure 4.22b-c)

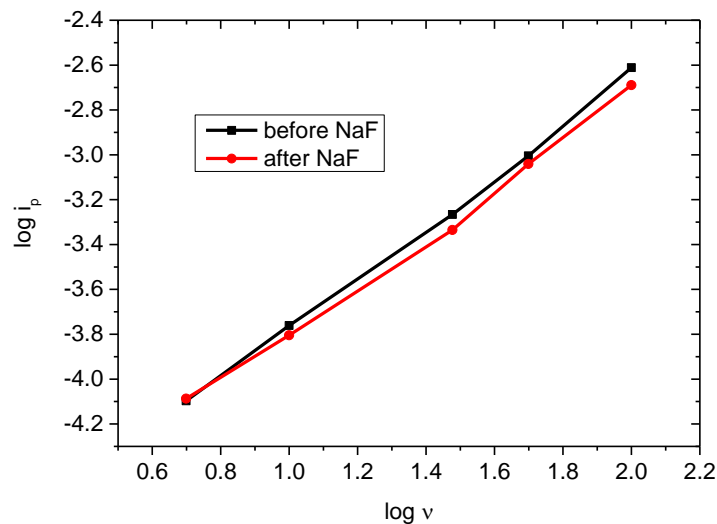


Figure 4.23. $\log i_p$ - $\log v$ curves of the Pani film in 1 M H_2SO_4 before and after treatment with NaF (from figure 4.22)

4.2.4.2. The Pani-PAP (90:10) copolymer film

The electroactivity of the Pani-PAP (90:10) copolymer film was examined in 1 M H_2SO_4 at different scan rates, as shown in figure 4.24a. The current densities of the copolymer film increase with increasing scan rate. The electroactivity of the copolymer film shows significant similarities after treatment with NaF electrolyte solution because there is no significant difference between figures 4.24b-c. However, the peak current densities increase after treatment with NaF, showing the release of fluoride ions from the film. Figure 4.25 displays the $\log i_p$ - $\log v$ curves of the Pani-PAP film in 1 M H_2SO_4 which were presented in figure 4.41 after treatment with NaF, showing the reversibility of the Pani-PAP copolymer film is similar to that when it was originally synthesized.

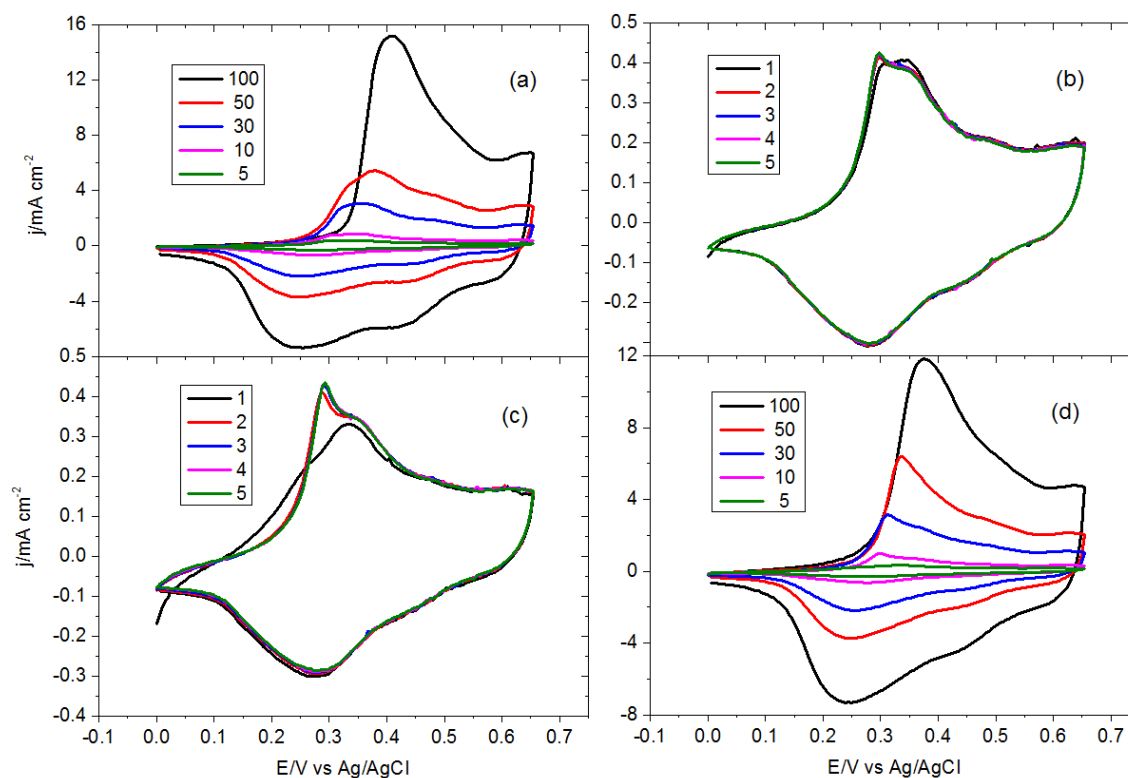


Figure 4.24. The electroactivity of the Pani-PAP (90:10) film in 1 M H_2SO_4 (a) the CV curves of the Pani-PAP film at different scan rates before treatment with NaF (b) the electroactivity of the Pani-PAP film in 1 M H_2SO_4 at 5 mV s^{-1} before treatment with NaF (c) the CV curves of the Pani-PAP film at different scan rates after treatment with NaF (d) the electroactivity of the Pani-PAP film in 1 M H_2SO_4 at 5 mV s^{-1} after treatment with NaF (the numbers indicate the scan rates in figure 4.24a-d while representing cycle number in figure 4.24b-c)

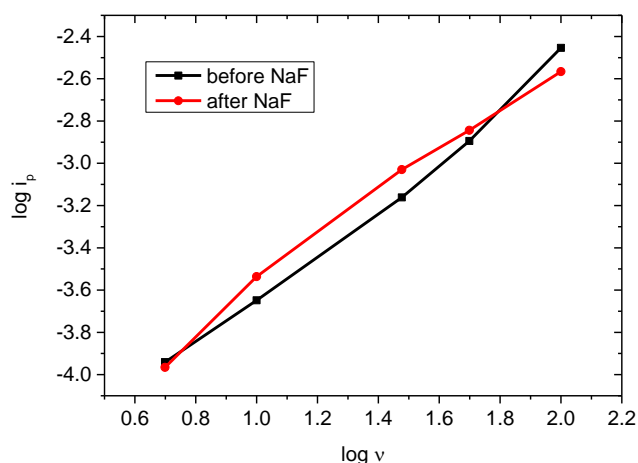


Figure 4.25. $\log i_p$ - $\log v$ curves of the Pani-PAP (90:10) film in 1 M H_2SO_4 before and after treatment with NaF (from figure 4.24)

4.2.5. The Surface Characterisation of the Polymer and the Copolymer Films

The characterisation of the morphologies of the polymer and copolymer films were carried out via scanning electron microscopy (SEM) to obtain detailed information about the morphologies of the resulting films on the quartz crystals.

4.2.5.1. Scanning electron microscopy

The SEM images of the copolymer and homopolymers are given in figure 4.26. As can be seen, there is a clear difference in the morphology of the copolymer, showing a highly porous surface. The SEM images presented to support the assumption of the deposition of a copolymer, rather than a mixture of monomers of aniline and *o*-AP. The Pani film has a highly porous surface compared to that of the Pani-PAP film. The Pani-PAP film shows a tight surface even at 1000x magnification. However, with higher magnifications, such as 4500x, the porous surface can be observed, but it is still firm in comparison to the Pani film. This can be explained by solvent transfer, which also explains why it is smaller for the Pani-PAP film during redox cycling.

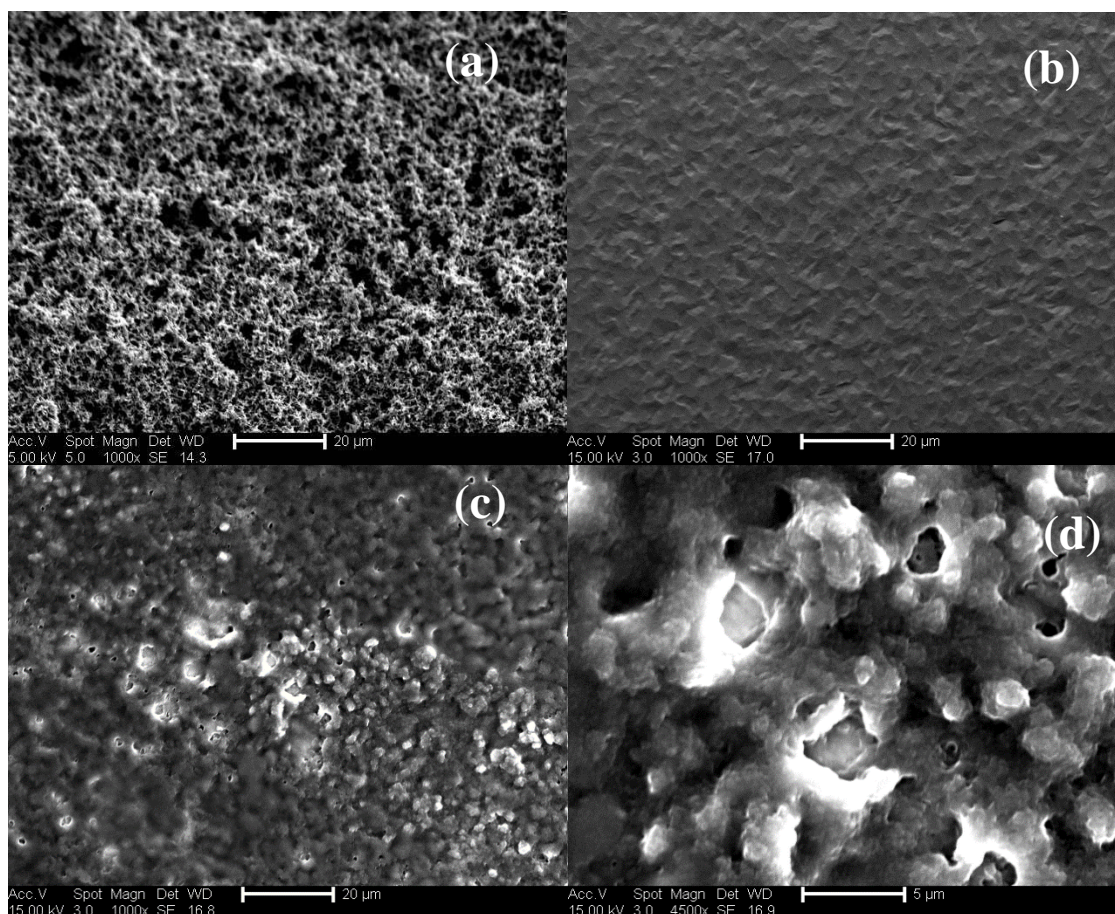


Figure 4.26. SEM images of (a) the Pani (b) the PAP (c-d) the Pani-PAP (90-10) films at different magnifications

4.2.6. FTIR

FTIR spectra of the Pani film and the Pani-PAP (90:10) copolymer film were presented in figure 4.27 and figure 4.28 while the corresponding possible vibrations were presented in table 4.5. The small peaks at 3782.8 cm^{-1} , 3321.3 cm^{-1} and 3642.8 cm^{-1} in both spectrums can be assigned to the -OH groups from water in the sample. The feature at 1637.4 cm^{-1} appeared in both spectrum can be assigned the C=C stretching and the deformation vibration of a primary -NH₂. Furthermore, the peaks also observed in both spectra around 1520 cm^{-1} are attributed to the C=C aromatic stretch vibration, which due to the absorption of a benzene ring and quinone ring vibrations, and the C=N stretching vibration produced from the formation of the polymer film. In addition, the peaks appeared in both spectrum around 1380 cm^{-1} is attributed to the O-C and C=N groups. These peaks are the indication of quinoid ring vibration involving C=N and C-N groups. The presence of the peak at 1280 cm^{-1} in both spectrums can be assigned to the O-C (which is the stretching vibrations of C-O in phenols generally appear 1200 cm^{-1})

and the C-N stretching vibrations (which can be arisen in aromatic amines are in the range 1280-1180 cm^{-1}). In the meantime, the feature around 1080 cm^{-1} , and 850 cm^{-1} are attributed to the C-N and N-H, =C-H for both spectrum.^{11, 35}

The similar spectrum of both the Pani and the Pani-PAP films exhibits the presence of aniline unit in both films. However, in figure 4.28, the shifting in spectrum band can be explained the participation of *o*-AP but cannot be obvious due to the low ratio in the polymer film.

Table 4.5. The absorption peaks of the Pani and the Pani-PAP films and corresponding functional group

<i>Absorption of Pani/cm⁻¹</i>	<i>Functional group</i>	<i>Absorption of Pani-PAP/cm⁻¹</i>	<i>Functional group</i>
3782.8	O-H (free)	3642.8	O-H (H-bonded)
3321.3	O-H (H-bonded)	1637.4	C=C, -NH ₂
1637.4	C=C, -NH ₂	1522	C=C, C=N
1519.5	C=C, C=N	1379.6	O-C
1389.4	O-C	1261.8	O-C, C-N
1274	O-C, C-N	1077.7	C-N
1082	C-N	910.7	=C-H
1011.4	C-N	854.3	N-H, =C-H
891.1	N-H, =C-H		

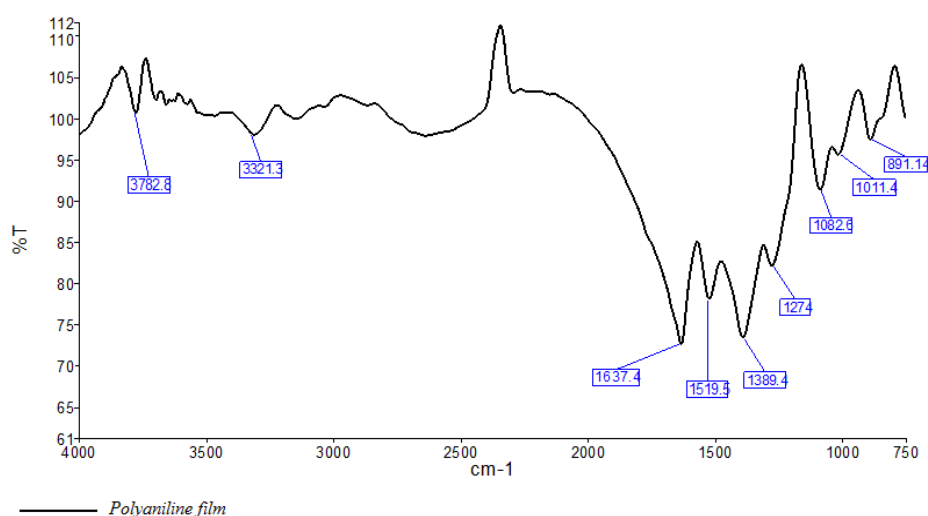


Figure 4.27. FTIR spectrum of the Pani film

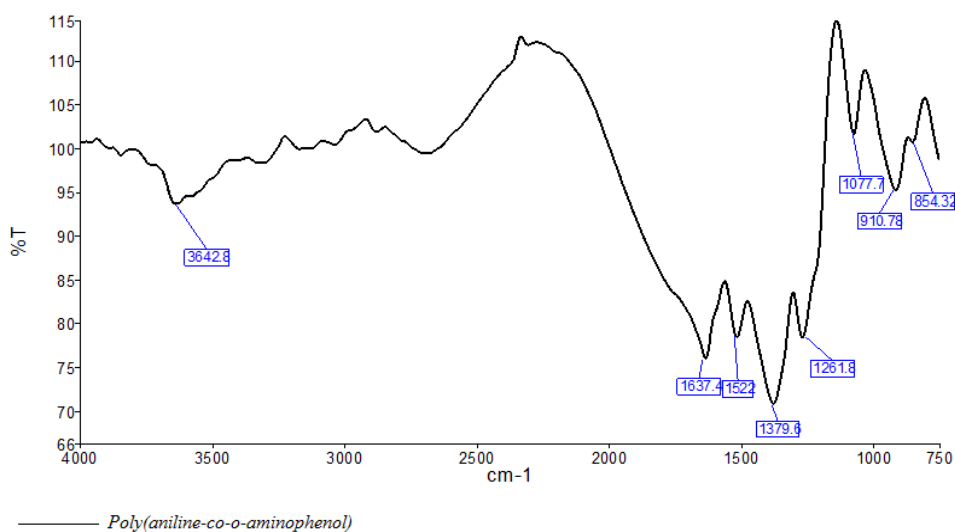


Figure 4.28. FTIR spectrum of the Pani-PAP film

4.3. Conclusion

In this study, we have studied three different aspects of conductive polymers, which were (i) the polymerization of Pani and PAP, (ii) the copolymerization of Pani-PAP films from their monomer solutions in various ratios and (iii) the defluoridation properties of the resultant Pani-PAP copolymer films.

In the first section, the electrochemical depositions of Pani and PAP films were presented, which showed considerable differences to each other, while the acquired voltammograms for both growth and characterisation show good agreement with similar reports in the literature.^{4, 35} Although the electrochemical deposition of Pani resulted in a thick film after only 7 cycles,³³ the electrochemical deposition of PAP did not provide a visible film, even over 100 cycles under otherwise identical conditions. This indicates that there is a huge difference between their growth rates. Afterwards, a Pani film was synthesised between -0.20 to 0.90 V over 17 cycles at 10 mV s⁻¹. This Pani deposition behaved as a rigid film (h , 138 nm) with a high electroactivity (Γ , 78.4 nmol cm⁻² for dimeric aniline units) in an acidic medium. Furthermore, the ionic activity of the Pani film was examined in 0.1 M NaF monomer-free solution (pH 6.60) at 5 mV s⁻¹. The redox cycling of the Pani film in NaF provides a particular anodic peak at 0.34 V and two cathodic peaks at 0.09 V and 0.38 V, while the mass of the Pani film increased upon oxidation. A quantitative evaluation of the Pani film showed it took 0.25 mol

fluoride ions per redox site of the film upon oxidation, which was attributed $51.6 \text{ mg} \pm 1.0 \text{ F}^{-1} \text{ g}^{-1}$ at pH 6.60. Theoretically, a Pani film should take 0.5 mol fluoride ions per redox site, accompanying $91.2 \text{ mg F}^{-1} \text{ g}^{-1}$. This indicates the efficiency of the Pani film synthesised in this study is significantly high. The amount of fluoride ions is much greater than the available techniques reported in the literature, which showed 0.78 mg g^{-1} by polyaniline¹⁴ and 20 mg g^{-1} at 1.5 V by polyaniline.¹⁶ Also, this techniques requires a high potential, which can result in the overoxidation of polyaniline.

Mu³⁵ reports that the electroactivity of polyaniline in a neutral medium was enhanced by the copolymerization of aniline with *o*-aminophenol, while the ionic activity of the final copolymer films became uncertain. Thus, we focused on the copolymerisation of Pani-PAP films in order to obtain information about their ion-activity in a neutral medium.

Several copolymer films were synthesised using different *o*-aminophenol and aniline monomer ratios, keeping the total monomer concentration constant at either 0.1 M or 0.2 M. The results showed that different anodic and cathodic peaks could appear in the presence of a small amount of *o*-aminophenol, such as in a 90:10 ratio (An:*o*-AP/mM). The presence of larger amounts of the *o*-aminophenol monomer results in a similar voltammogram to those observed for the PAP film, showing the domination of the *o*-aminophenol monomer regarding the film's resultant physical properties. The best copolymer composition was achieved from a solution of 90 mM aniline and 10 mM *o*-aminophenol in 1 M H₂SO₄ between -0.2 and 0.95 V at 5 mV s^{-1} over 84 cycles. This copolymer film, called Pani-PAP (90:10), formed as an adherent, smooth, thin film (h , 523 nm) on quartz crystal with a high electroactivity (Γ , $266.8 \text{ nmol cm}^{-2}$). This supports the notion that the copolymerisation of aniline with *o*-aminophenol enhanced the consequent electroactivity. The brown colour of this copolymer film was also distinctive in comparison with the other copolymer films synthesized in this research. Both the electrochemical and physical properties of the Pani-PAP (90:10) film confirmed the synthesis of a novel copolymer film with promising features. The admittance data for the Pani-PAP (90:10) film supported the formation of an acoustically thin film in figure 4.14a, showing rigid behaviour.

In the latter part, the removal of fluoride ions by the Pani-PAP (90:10) films synthesized in this study was explored in 0.1 M NaF electrolyte solutions at 5 mV s⁻¹. The Pani-PAP (90:10) took 0.35 mol fluoride ions per redox site of the polymer films, which indicated the efficiency of the polyaniline film had been increased by copolymerisation of aniline with *o*-aminophenol. The corresponding amount of the fluoride taken from this copolymer film was determined as 65.0 ± 0.6 mg F⁻ g⁻¹. Similarly, Karthikeyan *et al.*, studied the increase in capacitance of the polyaniline film to remove fluoride ions by polyaniline/alumina (Pani-AIO) and polypyrrole/alumina (PPy-AIO). The maximum amount of fluoride taken by Pani-AIO and PPy-AIO was 6.6 mg g⁻¹ and 8.0 mg g⁻¹, respectively, in acidic media.³⁷ The necessity for an acidic medium and a lower number of fluoride ions for these films showed that our copolymer film represents a promising means by which to remove fluoride ions. Additionally, the Pani-PAP (90:10) copolymer film shows reversible behaviour between its oxidation and reduction reactions at different scan rates in the absence/presence of NaCl at pH 6.60. Further, it can be used successively without compromising its chemical properties according to our regeneration experiments (figure 4.24).

Furthermore, it has been reported that the highest amount of fluoride in drinking water has been found as 2800 mg/L, whereas WHO recommends no more than 1.5 mg/L fluoride ions in drinking water.¹⁴⁻¹⁶ In this case, 2798.5 mg/L fluoride ions would have to be extracted to make this drinking water ‘safe’. When we consider the Pani-PAP (90:10) copolymer film obtained in this study for this process, we can categorically state that this copolymer is not able to absorb this amount. However, the capacitance of the Pani-PAP copolymer film can enhance such a process in two ways: *i*) we can synthesise a thicker Pani-PAP copolymer film or *ii*) we can use a large surface area to obtain a Pani-PAP copolymer film. In both ways, although the capacitance can increase easily, the thicker film might cause low loading and take a longer time to be effective. In the case of a large surface area, the Pani-PAP copolymer film can absorb fluoride ions in a relatively short time. On the other hand, the regeneration experiments showed we can use the Pani-PAP (90:10) copolymer film successively. This makes it possible to clean the electrode of fluoride ions after each process, and thus remove excessive fluoride ions with the same electrode.

In conclusion, the Pani and the Pani-PAP (90:10) films synthesised in this study represent a promising development in terms of the removal of fluoride ions in a straightforward and inexpensive way. Also, SEM suggested a firmer uniform surface for the Pani-PAP (90:10).

4.4. References

- 1 M. A. Shenashen, M. M. Ayad, N. Salahuddin and M. A. Youssif, *Reactive & Functional Polymers*, 2010, **70**, 843-848 (DOI:10.1016/j.reactfunctpolym.2010.07.005).
- 2 S. Mu, *Journal of Physical Chemistry B*, 2008, **112**, 6344-6349 (DOI:10.1021/jp7117828).
- 3 D. D. Borole, U. R. Kapadi, P. P. Mahulikar and D. G. Hundiware, *Material Letters*, 2004, **58**, 3816-3822 (DOI:10.1016/j.matlet.2004.07.035).
- 4 G. Ciric-Marjanovic, *Synthetic Metals*, 2013, **177**, 1-47 (DOI:10.1016/j.synthmet.2013.06.004).
- 5 A. A. Syed and M. K. Dinesan, *Talanta*, 1991, **38**, 815-837 (DOI:10.1016/0039-9140(91)80261-W).
- 6 T. K. Das and S. Prusty, *Polymer-Plastics Technology and Engineering*, 2012, **51**, 1487-1500 (DOI:10.1080/03602559.2012.710697).
- 7 G. A. Snook, P. Kao and A. S. Best, *Journal of Power Sources*, 2011, **196**, 1-12 (DOI:10.1016/j.jpowsour.2010.06.084).
- 8 C. Peng, S. Zhang, D. Jewell and G. Z. Chen, *Progress in Natural Science-Materials International*, 2008, **18**, 777-788 (DOI:10.1016/j.pnsc.2008.03.002).
- 9 Y. Zhang, S. Mu, B. Deng and J. Zheng, *Journal of Electroanalytical Chemistry*, 2010, **641**, 1-6 (DOI:10.1016/j.jelechem.2010.01.021).
- 10 H. R. Wasniki and D. S. Kelkar, *International Conference on Materials Science and Technology (Icmst 2012)*, 2015, **73**, 012026 (DOI:10.1088/1757-899X/73/1/012026).
- 11 M. Liu, M. Ye, Q. Yang, Y. Zhang, Q. Xie and S. Yao, *Electrochimica Acta*, 2006, **52**, 342-352 (DOI:10.1016/j.electacta.2006.05.013).
- 12 F. J. Hua and E. Ruckenstein, *Macromolecules*, 2004, **37**, 6104-6112 (DOI:10.1021/ma040070g).
- 13 S. L. Mu, *Synthetic. Metals*, 2004, **143**, 269-275 (DOI:10.1016/j.synthmet.2003.12.009).

- 14 M. Karthikeyan, K. K. Satheeshkumar and K. R. Elango, *Journal of Hazardous Materials*, 2009, **163**, 1026-1032 (DOI:10.1016/j.jhazmat.2008.07.057).
- 15 H. Cui, Y. Qian, H. An, C. Sun, J. Zhai and Q. Li, *Water Research*, 2012, **46**, 3943-3950 (DOI:10.1016/j.watres.2012.04.039).
- 16 H. Cui, Q. Li, Y. Qian, R. Tang, H. An and J. Zhai, *Water Research*, 2011, **45**, 5736-5744 (DOI:10.1016/j.watres.2011.08.049).
- 17 X. Fan, D. J. Parker and M. D. Smith, *Water Research*, 2003, **37**, 4929-4937 (DOI:10.1016/j.watres.2003.08.014).
- 18 P. I. Ndiaye, P. Moulin, L. Dominguez, J. C. Millet and F. Charbit, *Desalination*, 2005, **173**, 25-32 (DOI:10.1016/j.desal.2004.07.042).
- 19 M. Karthikeyan, K. K. Satheesh Kumar and K. P. Elango, *Journal of Fluorine Chemistry*, 2009, **130**, 894-901 (DOI:<http://dx.doi.org/10.1016/j.jfluchem.2009.06.024>).
- 20 M. Karthikeyan and K. P. Elango, *Journal of Environmental Sciences*, 2009, **21**, 1513-1518 (DOI:[http://dx.doi.org/10.1016/S1001-0742\(08\)62448-1](http://dx.doi.org/10.1016/S1001-0742(08)62448-1)).
- 21 M. Karthikeyan, K. K. Satheeshkumar and K. P. Elango, *Journal of Hazardous Materials*, 2009, **167**, 300-305 (DOI:<http://dx.doi.org/10.1016/j.jhazmat.2008.12.141>).
- 22 E. Subramanian and R. D. Ramalakshmi, *Journal of Scientific & Industrial Research*, 2010, **69**, 621-628.
- 23 Y. H. Lin, X. L. Cui and J. Bontha, *Environmental Science & Technology*, 2006, **40**, 4004-4009 (DOI:10.1021/es052148u).
- 24 Y. Kong, Y. Sha, S. Xue and Y. Wei, *Journal of Electrochemical Society*, 2014, **161**, H249-H254 (DOI:10.1149/2.088404jes).
- 25 R. M. Torresi, S. I. C. Detorresi, C. Gabrielli, M. Keddani and H. Takenouti, *Synthetic Metals*, 1993, **61**, 291-296 (DOI:10.1016/0379-6779(93)91275-7).
- 26 M. MIRAS, C. BARBERO, R. KOTZ and O. HAAS, *Journal of Electroanalytical Chemistry*, 1994, **369**, 193-197 (DOI:10.1016/0022-0728(94)87098-5).
- 27 N. Gospodinova and L. Terlemezyan, *Progress in Polymer Science*, 1998, **23**, 1443-1484 (DOI:10.1016/S0079-6700(98)00008-2).
- 28 D. Orata and D. A. Buttry, *Journal of American Chemical Society*, 1987, **109**, 3574-3581 (DOI:10.1021/ja00246a013).
- 29 A. F. Diaz and J. A. Logan, *Journal of Electroanalytical Chemistry*, 1980, **111**, 111-114 (DOI:10.1016/S0022-0728(80)80081-7).
- 30 H. N. Dinh and V. I. Birss, *Journal of Electroanalytical Chemistry*, 1998, **443**, 63-71 (DOI:10.1016/S0022-0728(97)00470-1).

-
- 31 Y. Wei, G. W. Jang, C. C. Chan, K. F. Hsueh, R. Hariharan, S. A. Patel and C. K. Whitecar, *Journal of Physical Chemistry*, 1990, **94**, 7716-7721 (DOI:10.1021/j100382a073).
- 32 A. Bund and S. Neudeck, *Journal of Physical Chemistry B*, 2004, **108**, 17845-17850 (DOI:10.1021/jp0469721).
- 33 A. R. Hillman and M. A. Mohamoud, *Electrochimica Acta*, 2006, **51**, 6018-6024 (DOI:10.1016/j.electacta.2005.11.054).
- 34 Q. Yang, Y. Zhang, H. Li, Y. Zhang, M. Liu, J. Luo, L. Tan, H. Tang and S. Yao, *Talanta*, 2010, **81**, 664-672 (DOI:10.1016/j.talanta.2009.12.051).
- 35 S. L. Mu, *Synthetic Metals*, 2004, **143**, 259-268 (DOI:10.1016/j.synthmet.2003.12.008).
- 36 J. Zhang, D. Shan and S. Mu, *Journal of Polymer Science Part A-Polymer Chemistry*, 2007, **45**, 5573-5582 (DOI:10.1002/pola.22303).
- 37 M. Karthikeyan, K. Kumar and K. Elango, *Journal of Fluorine Chemistry*, 2009; **130**, 894-901.

Chapter V:

The electrochemical deposition of poly(aniline-co-*o*-toluidine) copolymer film and film population changes in neutral medium

5.1. Introduction

5.1.1. Overview

Chapter 4 of this thesis presented the electrochemical copolymerization of aniline with *o*-aminophenol (*o*-AP) and its redox cycling in monomer-free NaF electrolyte solutions. Here, we will discuss the electrochemical characteristics of both the poly-*o*-toluidine (POT) polymer and its copolymer, poly(aniline-co-*o*-toluidine) (Pani-POT), as obtained from aniline and *o*-toluidine monomers in a strong acidic medium.¹

POT is one of the copolymers obtained the oxidation of *o*-toluidine monomers, which is a derivative of the aniline monomer that includes a methyl (-CH₃) substituent in its backbone chain, as different from the aniline monomer itself.¹ Although the structure of *o*-toluidine is similar to that of with aniline, the electroactivity of POT polymer film is significantly lower than Pani film. However, the copolymerization of *o*-toluidine with various monomers, such as aniline,²⁻⁴ *o*-phenylenediamine⁵ and *o*-aminophenol,⁶ reported in the literature provides for the improvement of the electrochemical properties of POT. The study reported Borole *et al.*² focus on the effect of the *o*-toluidine monomer on the growth of polyaniline (Pani), while Kumar³ was interested in the influence of *o*-toluidine on the solubility of Pani in an organic solvent. On the other hand, the ion-exchange properties of the resultant copolymer film have become uncertain. In this study, we focused on two important aspects of the Pani-POT copolymer films, which are the preparation of a high-quality copolymer with a high electroactivity, and the film population changes in monomer-free NaF electrolyte solutions as a different from the literature.

The addition of the *o*-toluidine monomer to an aniline monomer solution during electrochemical deposition can cause different sequences of monomers. Some possible

sequences of Pani-POT copolymer films are illustrated in figure 5.1. Among these, a possible sequence is the first, which is most commonly observed in the literature.¹

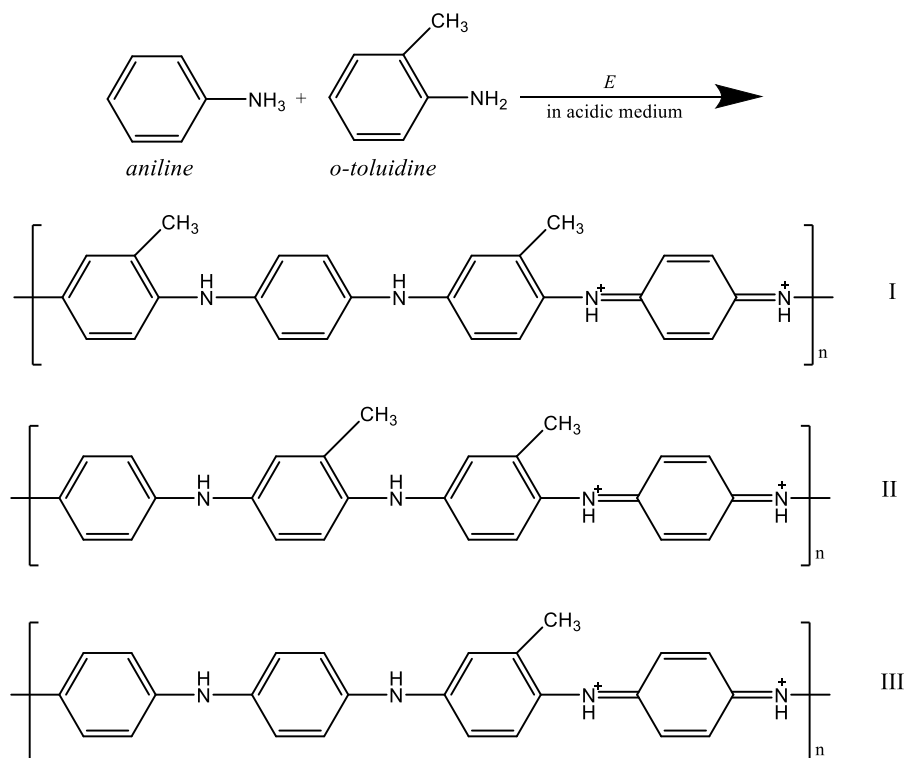


Figure 5.1. Some of the possible sequences of *o*-toluidine monomer in Pani chain (the literature shows the high possibility of I)

5.1.2. Aims and Objectives

The objectives of the studies undertaken in this chapter are, *(i)* the understanding of the growth dynamics of POT films; *(ii)* the copolymerization of Pani-POT between aniline and *o*-toluidine in acidic medium; *(iii)* the effect of the ratios of monomers on the copolymerization of the Pani-POT; *(iv)* the examination of their applications by means of the EQCM technique, such as defluoridation of water; *(v)* the characterisation of the morphologies of the acquired polymer and copolymer films via microscopic (SEM) and spectroscopic (FTIR) techniques.

5.2. Results and Discussion

5.2.1. Electrochemical Deposition of the Poly(*o*-toluidine) Film

The electrochemical deposition of POT films was initially studied using a solution consisting of 0.1 M *o*-toluidine and 1 M H₂SO₄ between -0.2 and 1.0 V at 10 mV s⁻¹

scan rate with several cycles of a gold working electrode (the surface area of the working electrode was 0.018 cm^2). However, the POT films easily degraded due to higher potential like Pani films. Thus, in further experiments, the deposition of the POT film via EQCM was carried out between -0.2 V and 0.95 V from $0.1 \text{ M } o\text{-toluidine}$ and $1 \text{ M } \text{H}_2\text{SO}_4$ at 10 mV s^{-1} scan rate over 20 cycles on a unpolished quartz crystal, as shown in figure 5.2.

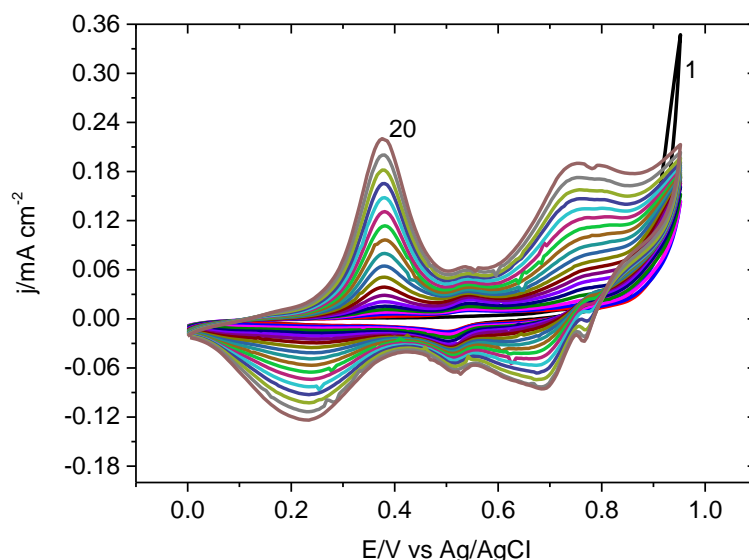


Figure 5.2. The CV curve of the deposition of a POT polymer film from $0.1 \text{ M } o\text{-toluidine}$ and $1 \text{ M } \text{H}_2\text{SO}_4$ as a function of applied potential, the scan rate, $v = 10 \text{ mV s}^{-1}$

There are three anodic peaks at 0.38 V , 0.54 V and 0.76 V , respectively, while the oxidation of monomers occurred at 0.81 V . In the reverse cycle, three cathodic peaks at 0.22 V , 0.50 V and 0.65 V , respectively, appear. The redox peak current densities increased with cycling but decreased with irreversible peak current densities. The redox couple at $0.39/0.42 \text{ V}$, which is either due to the dimer soluble products or to quinone/hydroquinone loosely surface-bound hydrolysis products.^{5, 6} The redox potential positions of the POT polymer films indicates the stability of them during a large number of cycles. In addition, the increase in the current densities shows a gradual increase in each peak over the 10 cycles. It then started to increase rapidly due to autocatalytic polymerization of POT.⁶ The quartz crystal was covered in a thin green film, as shown in figure 5.3.

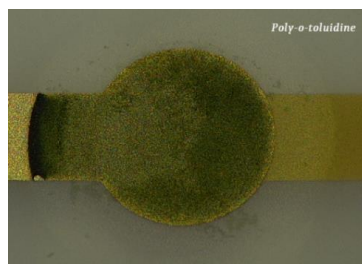


Figure 5.3. An image of the POT film synthesized from figure 5.2

The mass-charge curves were simultaneously acquired as a function of applied potential (from figure 5.2) are displayed in figure 5.4. The mass loading of the POT polymer film is extremely slow for the first 4 cycles, but started to increase, and continue with a gradual increase, with increased cycling. Simultaneously, the charge of the POT polymer film increased the polymerization potential until the 18th cycle but decreases thereafter. This is probably due to degradation of POT film causing the loss of electroactive sites. On the other hand, the mass loading continued with cycling.

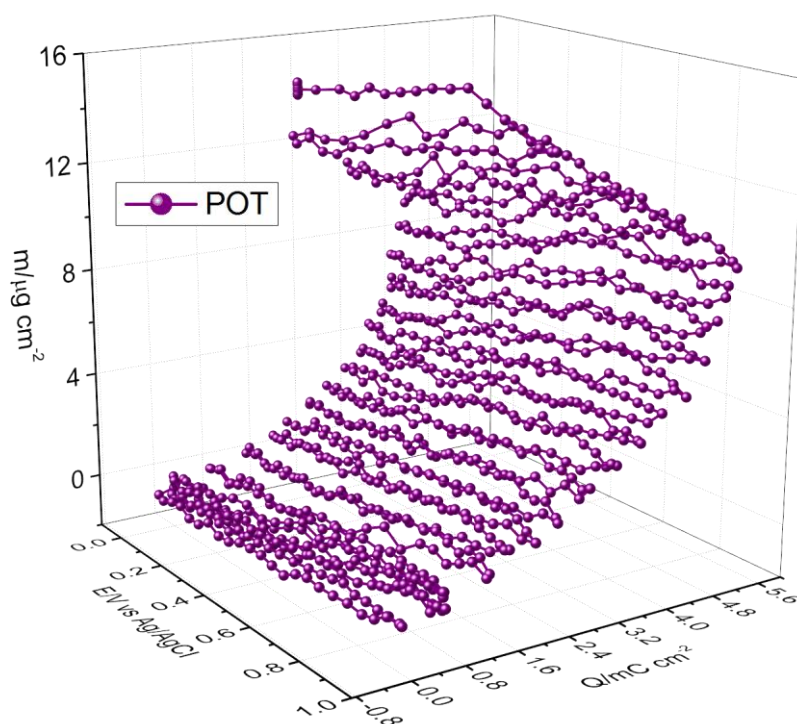


Figure 5.4. The mass-charge change of the POT (from figure 5.2) as a function of applied potential during the electrochemical deposition of POT from 0.1 M *o*-toluidine and 1 M H₂SO₄ with 20 cycles, the scan rate, $v = 10 \text{ mV s}^{-1}$

The charge passed (calculated from voltammograms areas) during the anodic and cathodic reactions can be determined as 0.55 mC and 0.54 mC, respectively. This indicates the overoxidation of the POT is not a serious issue between -0.20 and -0.95 V

but does become a significant problem after a large number of cycles. It was noted that the charge passed began to decrease after 18 cycles, and it was considered possible that the autocatalytic behaviour of POT accelerated the overoxidation of POT after a large number of cycles. The surface coverage of POT film in figure 5.2 was found to be $24.3 \text{ nmol cm}^{-2}$ using equation 3.1 for the dimeric o-toluidine unit, implying a lower electroactivity for the POT film.

The apparent molar mass of the POT film synthesized was found from the slope of the associated mass-charge curve (in figure 5.5b), using equation 3.4, at 91.1 g mol^{-1} . This value is quite close to 272.0 g mol^{-1} , showing the electrochemical deposition of POT polymer film happened with high efficiency. The solvent content of the POT film was determined as 3.2, showing the formation of the firmer film compare with the Pani film.

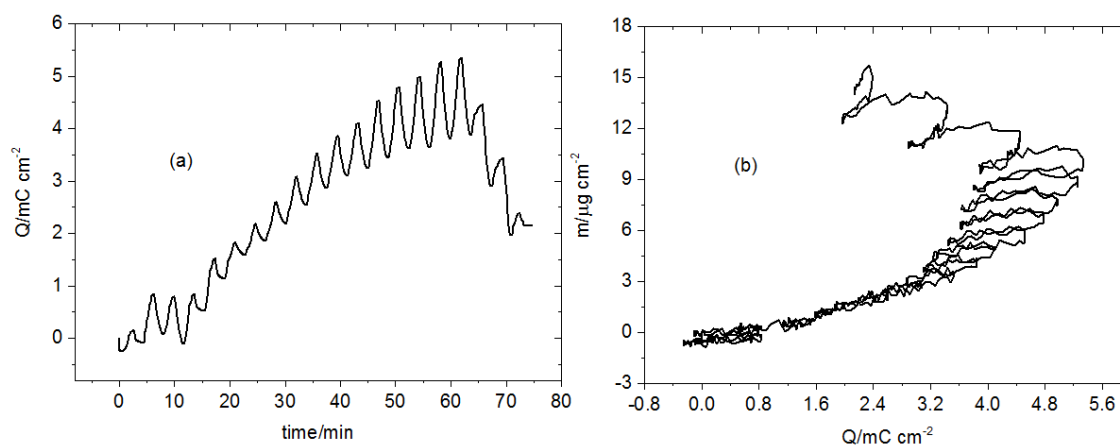


Figure 5.5. (a) the charge-time (b) the mass-charge curves of the POT film during electrochemical deposition from figure 5.2

The acquired EQCM admittance data for the POT film deposition is shown in figure 5.6, indicating a small decrease (about 30%) in admittance during the electrochemical deposition of the POT polymer film. The ohmic resistance of the POT film was obtained using the data from figure 5.6a, which increases steadily with continued cycling. At the end of the deposition, the impedance was found as 510Ω , while a rigid film had formed on the quartz crystal.

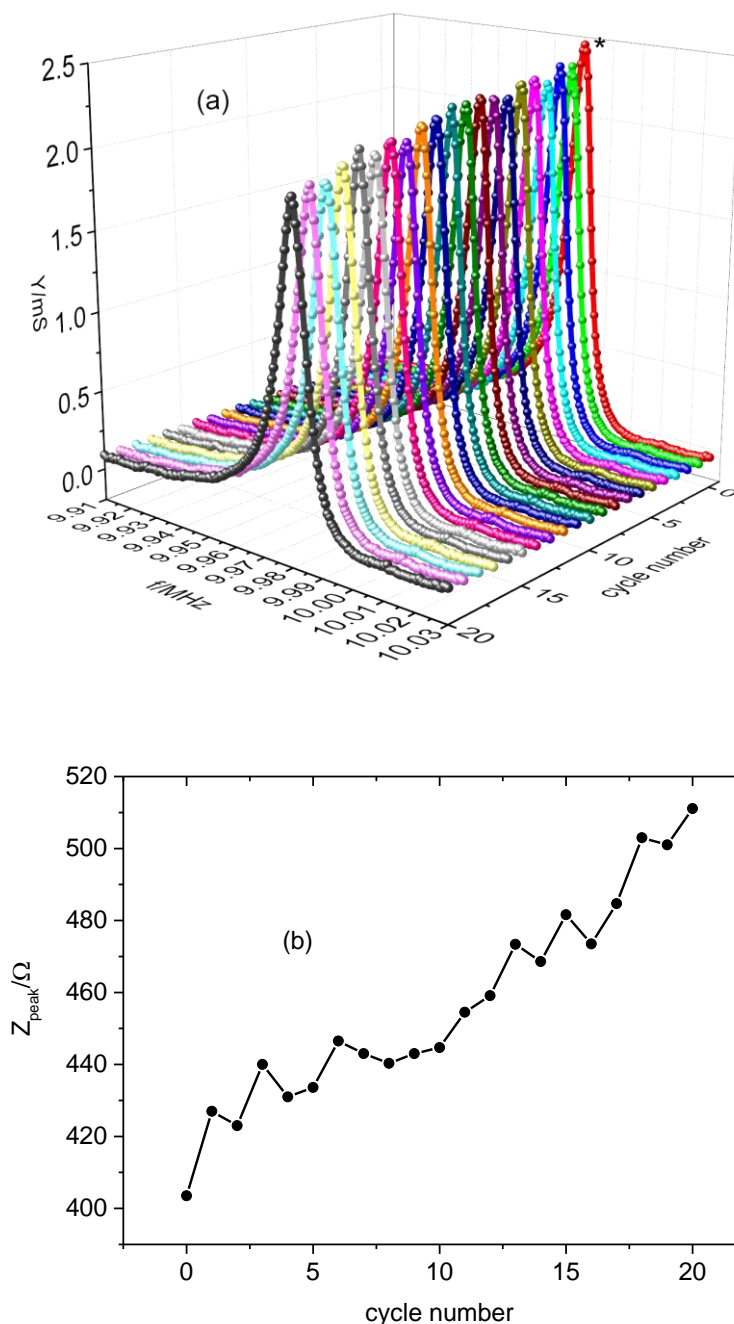


Figure 5.6. The EQCM data acquired simultaneously from the electrochemical deposition of the POT (see figure 5.2); (a) the admittance changes of the quartz crystal (b) the ohmic resistance of the POT film in aqueous medium (from figure 5.6a)

5.2.1.1. Comparison of the Pani, the PAP and the POT polymer films

The POT film synthesized in figure 5.2 was transferred to 1 M H_2SO_4 monomer-free solution in order to define the electrochemical activity at 5 mV s^{-1} . The oxidation peak of the POT appeared at 0.38 V, while for the Pani film synthesized in chapter 4 this value is 0.33 V, which are quite close each other (in figure 5.7). The reduction peaks of

the POT and the Pani films appear at 0.25 V and 0.19 V, respectively. The surface coverage of the POT is $24.3 \text{ nmol cm}^{-2}$ for dimeric *o*-toluidine units while it is $78.4 \text{ nmol cm}^{-2}$ for the Pani film (the surface coverage was calculated using the areas of voltammograms in figure 4.8). Moreover, the charge passed during the reduction of the POT film in 1 M H_2SO_4 is considerably lower than the charge passed during the oxidation. This indicates degradation of the POT film, which must be deposited at a lower potential than 0.95 V. The surface coverage of the POT is $24.3 \text{ nmol cm}^{-2}$, which is larger than the PAP ($14.8 \text{ nmol cm}^{-2}$) while the growth rate of the PAP is extremely smaller than the POT film. Among them, the electroactivity of the Pani film is much greater than both the PAP and the POT whilst the PAP has the lowest electroactivity (in figure 4.10 and 5.7).

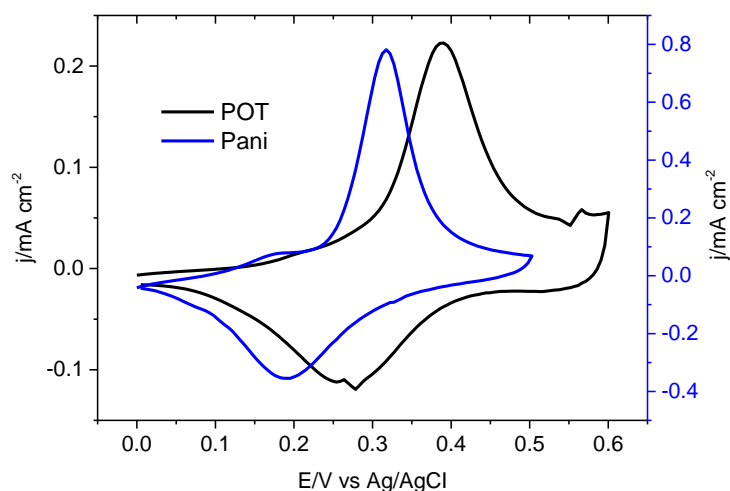


Figure 5.7. Characterisation of the Pani and the POT films (which were synthesised under identical conditions) in 1 M H_2SO_4 monomer-free solution, $\nu = 50 \text{ mV s}^{-1}$

Figure 5.8 shows the scan rate effects on the electroactivity of POT, which shows a reversible behaviour with happening by diffusionless at different scan rates due to a rapid charge transfer. It is supported the curve of $\log i_p / \log \nu$ plotted in figure 5.8.

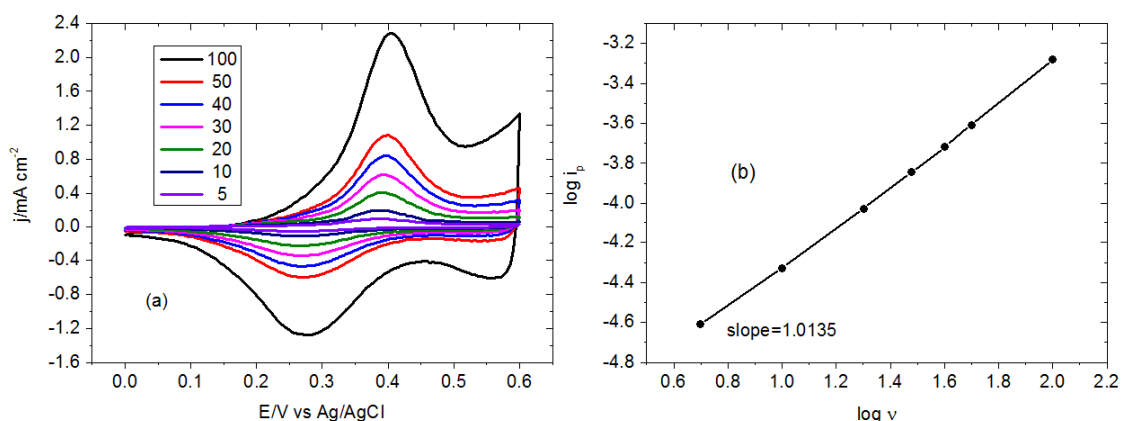


Figure 5.8. The electrochemical activity of the POT film (from figure 5.2) in 1 M H_2SO_4 at different scan rates, $v = 3, 5, \text{ and } 10 \text{ mV s}^{-1}$; **(a)** the CV curves of POT in 1 M H_2SO_4 ; **(b)** $\log i_p$ - $\log v$ curves from figure 5.8a (the number indicates the scan rates)

5.2.2. Copolymerization of the Pani-POT

5.2.2.1. The copolymerization of the Pani-POT by chronoamperometry

Although *o*-toluidine shows considerably lower electroactivity, as presented in first part of this chapter, the copolymerization of *o*-toluidine with aniline can improve the electrochemical properties while giving a different (co)polymer film. For this reason, the electrochemical deposition of Pani-POT films was applied by chronoamperometry using different monomer ratios of aniline and *o*-toluidine, while keeping the total concentration fixed at 0.1 M. Figure 5.9 indicates the result obtained using the chronoamperometry technique at 1.0 V for 600 s and for at -0.2 V at 600 s.

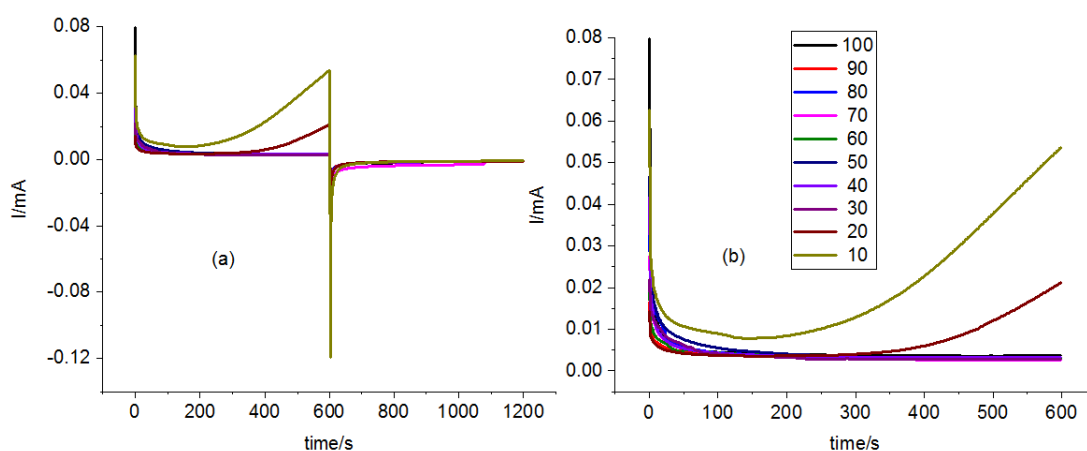


Figure 5.9. Electrochemical copolymerization of Pani-POT from 0.1 M monomer concentrations (*o*-OT: An) in 1 M H_2SO_4 by chronoamperometry; **(a)** the current-time curve at 1.0 V and -0.2 V; **(b)** the anodic deposition of Pani-POT film in detail at 1.0 V (the number indicates the ratio of (*o*-OT: An))

The current density during the deposition of the Pani-POT films was increased in presence of a small amount *o*-toluidine monomer in ratios such as 90:10 and 80:20 (An: *o*-OT). This is an indication of the major influence on the copolymerization rate. The charge passed whilst applying the potential at 1.0 V was plotted against the ratio of *o*-toluidine monomer in total monomer solutions, as shown in figure 5.10. It also gives supporting data as to the effect of the *o*-toluidine concentration on the copolymerization rate because it gradually decreases with an increasing amount of *o*-toluidine in the monomer solution.

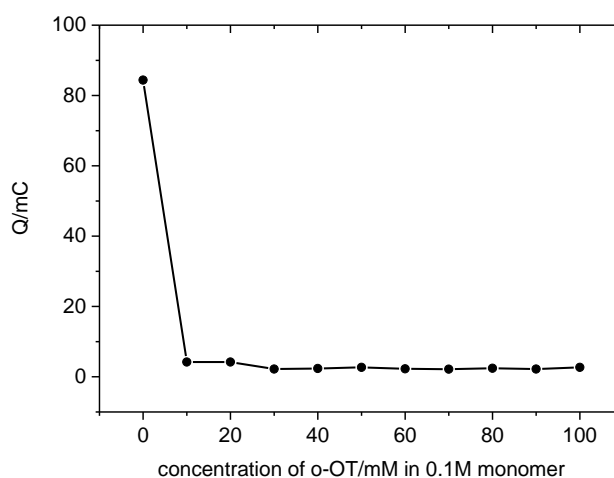


Figure 5.10. The charge passed of the Pani-POT films against the ratio of *o*-toluidine in 0.1 M monomer solution (from figure 5.9)

5.2.2.3. The electrochemical deposition of the Pani-POT copolymer films by means of EQCM

Several copolymer films of the Pani-POT deposited from various monomer concentration ratios of 50:50; 60:40; 70:30; 80:20; 90:10, as An:*o*-OT/mM, between -0.2 and 1.0 V at 50 mV s^{-1} in 1 M H_2SO_4 solution using cyclic voltammetry technique. In doing so, different voltammograms of the Pani-POT copolymer films to those of the homopolymers, Pani and POT, was obtained with a decreasing amount of *o*-toluidine (*o*-OT), such as 90:10 and 80:20 ratios. This indicates the domination of *o*-OT like *o*-AP (see chapter 4) in the growth of the Pani film. Similarly, the film formation did not occur during the 10 cycles for the higher ratios of *o*-OT monomer.

The results obtained from cyclic voltammetry experiments, showed two findings; (i) the Pani-POT copolymer films can be easily degraded above 0.9 V like the homopolymers

Pani and POT polymer films (ii) the percentage of *o*-OT in the monomer solutions can be held at some point while increasing the amount of aniline, which participated the increasing the electroactivity. For these reasons, several compositions of the aniline and *o*-OT monomers were prepared to 0.1 M or 0.2 M in monomer ratios of 80:20; 60:40; 170:30 and 150:50 as An:*o*-OT/mM composition. Figure 5.11 exhibits the CVs of the depositions of the Pani-POT copolymer films from these ratios between -0.2 V and 0.90 V with various cycle numbers at 5 mV s⁻¹.

All the CVs give one anodic around 0.36 V and two cathodic peaks around 0.51 V and 0.80 V, indicating similar electrochemical behaviour. The current densities of the electrochemical deposition of Pani-POT films are much greater for figure 5.11c-d than figure 5.11b in the 20th scan, showing the influence of the amount of aniline in the growth of the copolymer films.

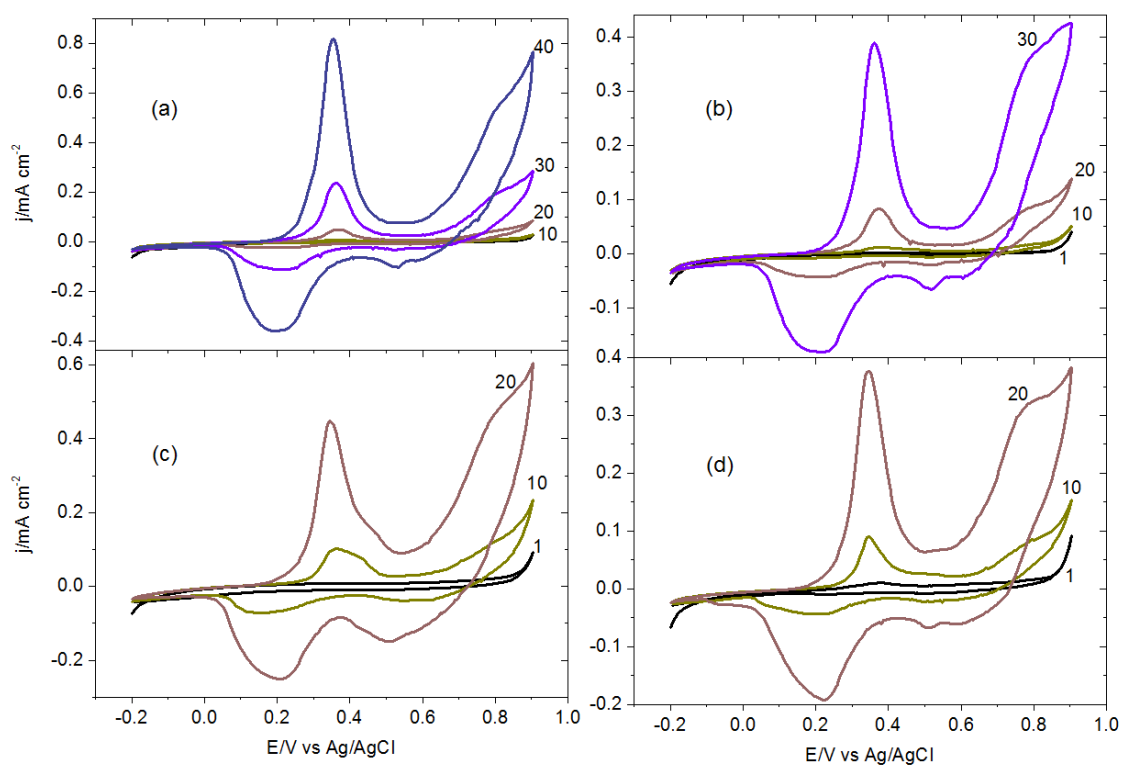


Figure 5.11. CV curves of the Pani-POT copolymer films from (a) 80 mM aniline and 20 mM *o*-OT (b) 60 mM aniline and 40 mM *o*-OT (c) 170 mM aniline and 30 mM OT (d) 150 mM and 50 mM *o*-OT in 1 M H₂SO₄, $v = 5 \text{ mV s}^{-1}$

The surface coverage of the Pani-POT copolymer films for dimeric units, calculated using equation 3.1, reveals that (in table 5.1) the electroactive sites are extremely large for Pani-POT (80:20) film despite the lower amount of aniline involves than Pani-POT

(170:30) film. This can arise from a large number of cycles from the increased participation of both monomers in the copolymer chain rather than aniline monomer by itself. The thickness of the Pani-POT films is an indication of an acoustically thin film with a high electroactivity. The colour of Pani-POT (80:20) film is also different from the other copolymer films synthesized in figure 5.12, implying different properties than for pure Pani and POT films besides the peak potential. After the electrochemical deposition of the Pani-POT copolymer films, green uniform films for the 80:20, 60:40, and 150:50 ratios, and dark green film for the 170:70 ratio, were observed on the quartz crystal, as presented in figure 5.12.

Table 5.1. Electrochemical data obtained from the voltammograms of the Pani-POT copolymer films synthesised in figure 5.11 using various monomer ratios

<i>Ratio of Pani-POT (An:o-OT)/mM</i>	<i>$\Gamma/nmolcm^{-2}$</i>	<i>h/nm</i>
80:20	198.2	393
60:40	109.5	144
170:30	192.9	260
150:50	119.8	152

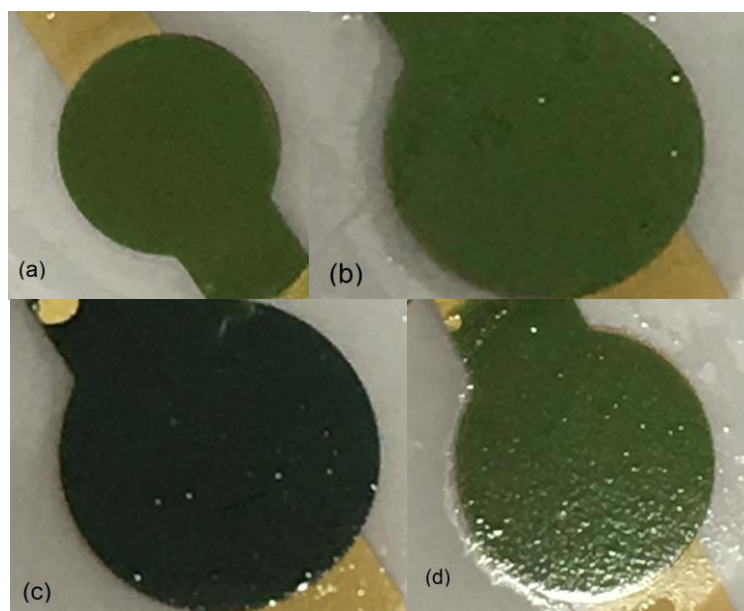


Figure 5.12. The images of the Pani-POT film deposited in figure 5.11 from (a) 170:30 (b) 60:40 (c) 80:20 (d) 150:50 as An:o-OT/mM ratio

The corresponding mass loading of the Pani-POT copolymer films during their depositions is plotted in figure 5.13a, indicating a rapid increase in mass at the same

time for the Pani-POT (170:30) and the Pani-POT (150:50) ratios because the amount of aniline increases the growth rate. However, when the cycling is continued for the Pani-POT (80:20), the growth of the copolymer film is increased due to an autocatalytic effect of both aniline and *o*-OT. On the other hand, the growth of the Pani-POT (60:40) copolymer film is slightly lower than Pani-POT (80:20) film. This could originate from the influence of the larger amount of *o*-OT monomer on the growth of the Pani-POT copolymer films, which results in the growth rate and surface coverage.

The apparent molar masses of the Pani-POT copolymer films are shown (calculated using equation 3.4 for a monomer unit from figure 5.13b) in table 5.2, showing results close to 93.13 g mol^{-1} (aniline) or 107.2 g mol^{-1} (*o*-OT) except the Pani-POT (60:40) film. This shows the efficiency of the copolymer films is mostly dependent on the small amount of *o*-OT to some degree. Also, the solvent content of the copolymer films, the Pani-POT (80:40, 170:30, 150:50) films are smaller than the Pani-POT (60:40) film, indicating the formation of a softer polymer film the existence of the higher ratios *o*-OT in the copolymer composition. As can be seen from this figure, the growth of Pani-POT (80:20) film is extremely low but becomes faster after 10 cycles. The reason for this increase must be due to the autocatalytic effect of both the aniline and *o*-OT monomers.

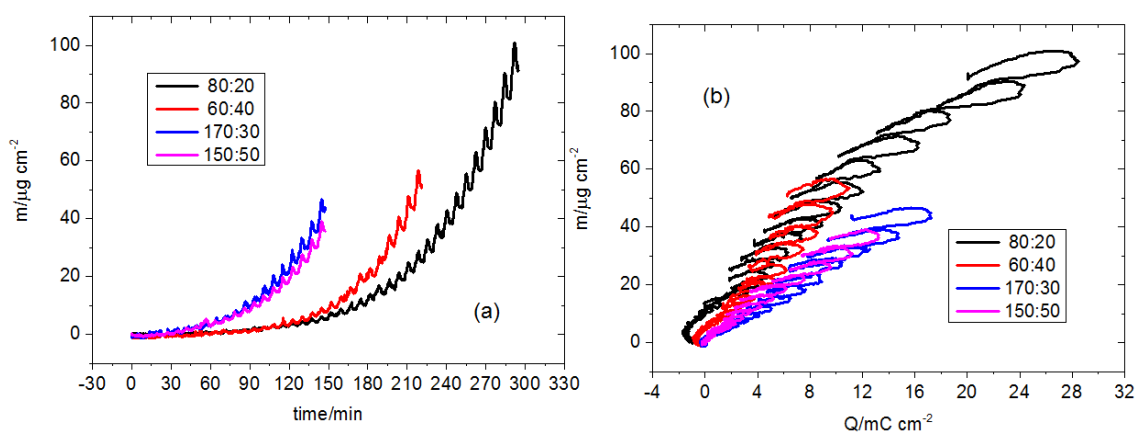


Figure 5.13. The mass loading of the Pani-POT films from figure 5.11 (a) as function of time (b) as a function of charge passed

Table 5.2. Apparent molar mass of the copolymer films obtained from the slope of the mass-charge graphs in figure 5.13 and the mass density after the deposition (α is the content of solvent in copolymer films determined by equation 3.5 in chapter 3)

<i>Ratio of Pani-POT An:o-OT/mM</i>	<i>M_{app}/gmol^{-1}</i>	<i>Mass density/$\mu\text{g cm}^{-2}$</i>	<i>$\alpha/\text{per redox site}$</i>
80:20	165.6	91.7	3.6
60:40	238.5	51.3	7.6
170:30	123.0	43.0	1.3
150:50	134.3	36.1	1.9

The admittance data for the electrochemical depositions of the Pani-POT film in various ratios in figure 5.11 were plotted in figure 5.14, showing the formation of the acoustically thin film while shifting the frequency of the quartz crystal. The admittance of the quartz crystal for all the Pani-POT copolymer films is around 1.7 mS, with a 588 Ω ohmic resistance of the Pani-POT copolymer films in the aqueous medium. This means that the Pani-POT copolymer films have a low resistance, despite using a large number of cycles for their deposition (the ohmic resistance values of the copolymer films were determined by equation 3.6 in chapter 3).

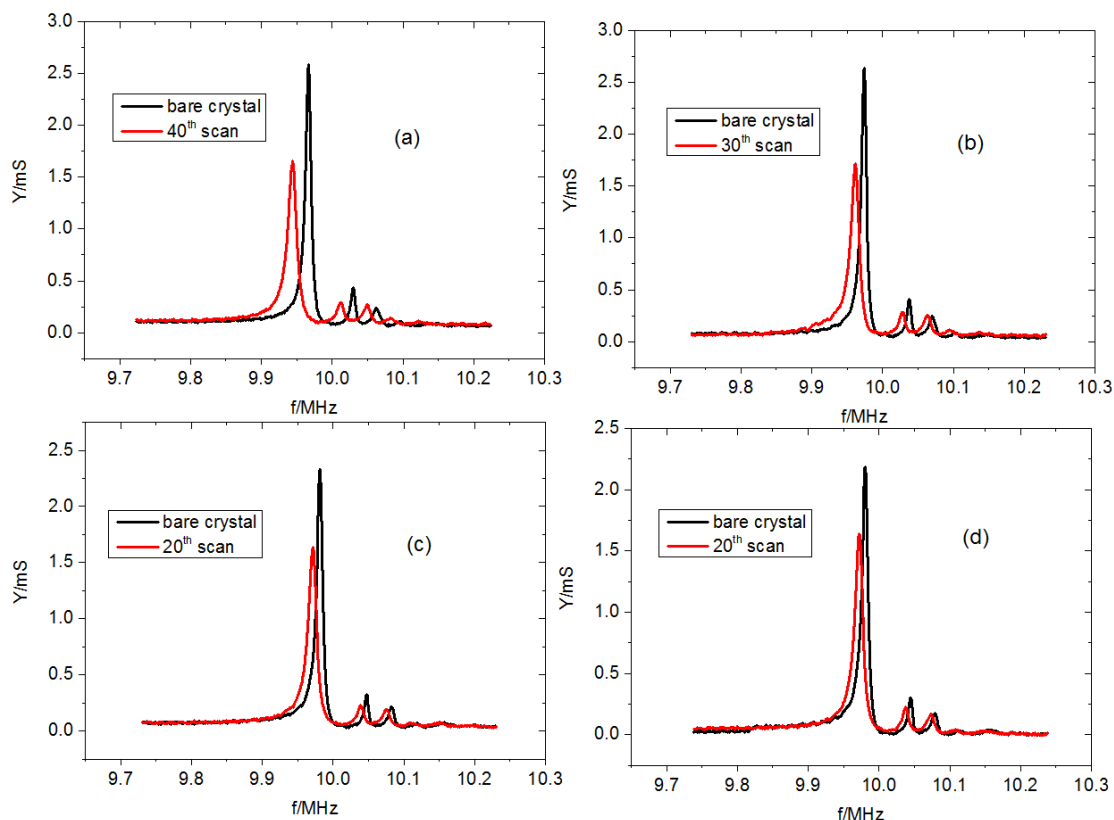


Figure 5.14. The admittance data of the electrochemical deposition of the Pani-POT copolymer films from figure 5.11 (a) the Pani-POT (80:20) (b) the Pani-POT (60:40) (c) the Pani-POT (170:30) (d) the Pani-POT (150:50)

5.2.2.4. Characterisation of the Pani-POT copolymer films

After the deposition of the Pani-POT copolymer films, the films were transferred in 1 M H_2SO_4 at 5 mV s^{-1} , showing a high electroactivity for Pani-POT (80:20) composition compared with others (in figure 5.15). In spite of the high aniline composition of the Pani-POT (170:30) and (150:50), the Pani-POT (80:20) copolymer films gave a high electroactivity at close peak potentials. This shows that the copolymerization of the Pani-POT films presents good electrochemical properties using many deposition cycles. The surface coverage of the Pani-POT (80:20) and the Pani-POT (170:30) films are $139.7 \text{ nmol cm}^{-2}$ and $130.7 \text{ nmol cm}^{-2}$, respectively.

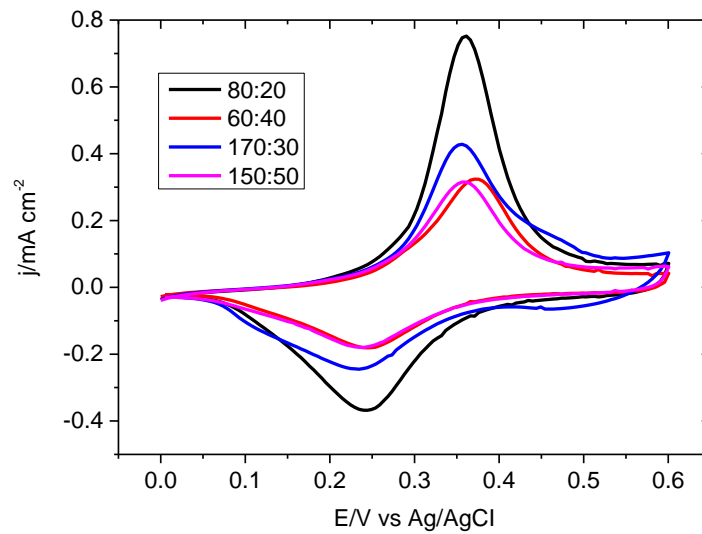


Figure 5.15. The CV curves of the Pani-POT films in 1 M H_2SO_4 , $v = 5 \text{ mV s}^{-1}$

When the mass changes of the Pani-POT copolymer films in 1 M H_2SO_4 were plotted as a function of applied potential, as seen in figure 5.16, the Pani-POT (80:20) and (170:30) films showed better reversibility compared to the Pani-POT (60:40) and (150:50) films.

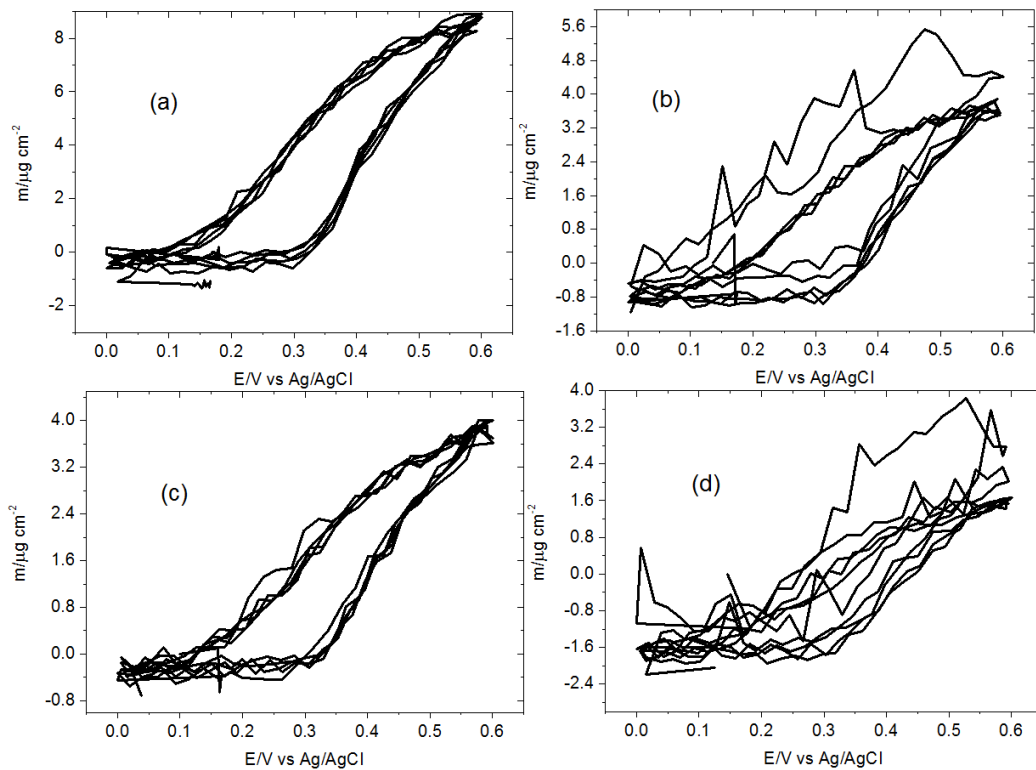


Figure 5.16. The mass and charge change of the Pani-POT copolymer films in 1 M H_2SO_4 (a) the Pani-POT (80:20) (b) the Pani-POT (60:40) (c) the Pani-POT (170:30) (d) the Pani-POT (150:50), $v = 5 \text{ mV s}^{-1}$

5.2.3. The Removal of Fluoride Ions

5.2.3.1. Using the POT polymer film

In this section, we will consider the ion-exchange properties of the POT (synthesized in figure 5.2) for the removal of fluoride ions from water. Figure 5.17 shows the ionic-activity of the POT in 0.1 M NaF at 5 mV s^{-1} . It indicates that the POT has a low ionic activity at pH 6.6 and it behaves unstable because it was decreasing cycles.

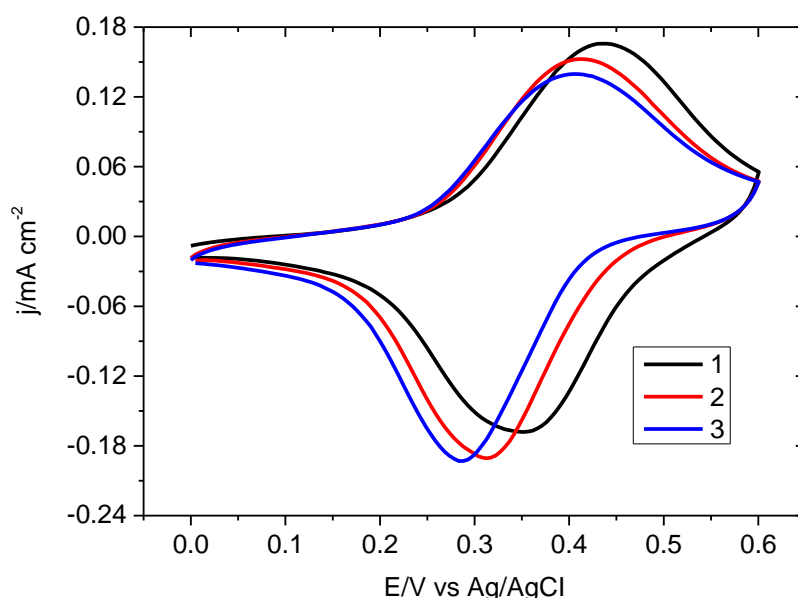


Figure 5.17. The CV of the POT film (deposited in figure 5.2) in 0.1 M NaF solutions, the scan rate, $v = 5 \text{ mV s}^{-1}$.

The corresponding mass change shows the mass of the POT increases upon oxidation but it was extremely small during the first cycle. Furthermore, this increase is getting smaller with each cycle. These results showed that the POT behaves as anion exchanger in irreversible manner. However, it is not capable to remove the fluoride ions.

5.2.3.2. Using the Pani-POT copolymer film

The defluoridation performance of the Pani-POT copolymer films deposited in figure 5.11 was examined in 0.1 M NaF (pH 6.60) solution at a slow scan rate, 5 mV s^{-1} , are shown in figure 5.18.

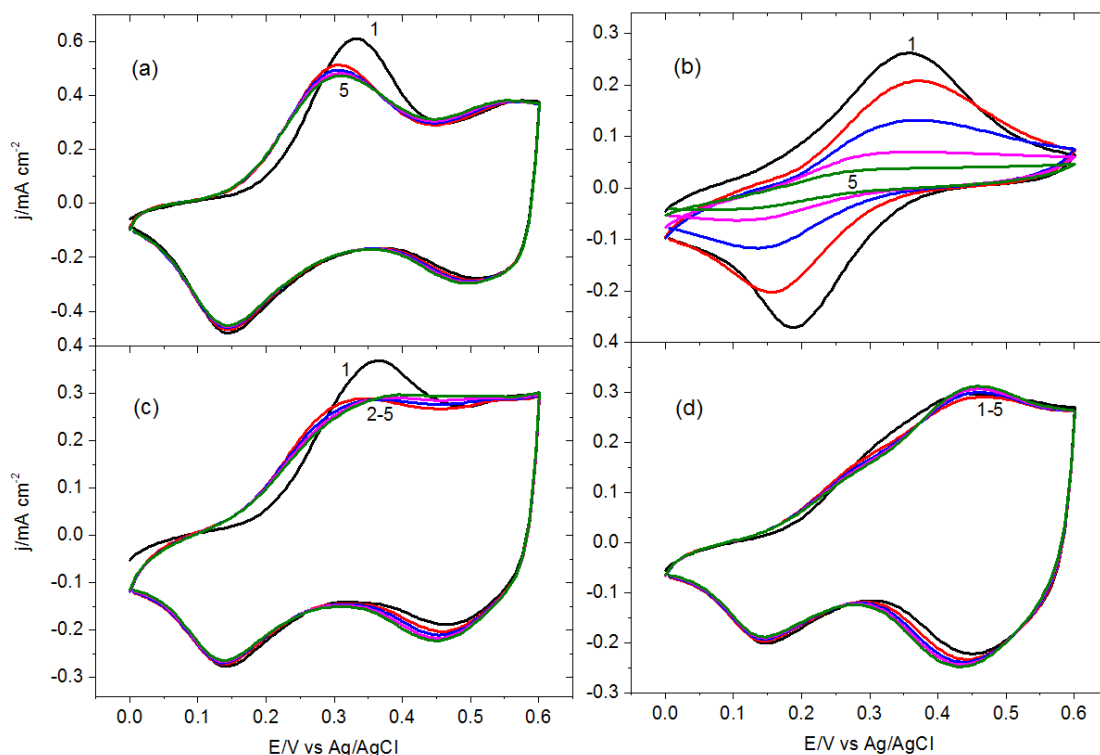


Figure 5.18. The CV curves of the Pani-POT copolymer films in 0.1 M NaF, $v = 5 \text{ mV s}^{-1}$ (a) the Pani-POT (80:20) (b) the Pani-POT (60:40) (c) the Pani-POT (170:30) (d) the Pani-POT (150:50)

The Pani-POT copolymer film shows ionic activity in monomer-free NaF solutions despite the neutral medium. Between the copolymer films, only the Pani-POT (60:40) film behaves in an unstable manner because its current density decreases with cycling. In the fifth scan, the redox peaks almost disappear. This copolymer film consists of much more of the *o*-OT monomer, which can cause unstable behaviour in comparison with other copolymer films, and it behaved in a highly stable manner with continued cycling.

The other ratios of the Pani-POT copolymer films show an excellent ability to remove fluoride ions. In ideal conditions, the Pani-POT copolymer film must 0.5 mol ion per redox sites of the copolymer as mention earlier in chapter 4. Here, the Pani-POT (80:20), the Pani-POT (170:30) and the Pani-POT (150:50) films take 0.35, 0.44 and 0.5 mol fluoride ion per redox sites of the copolymer films, respectively. This is a significant outcome because the efficiency is getting much greater when comparing the Pani film synthesized in chapter 4. The corresponding mass values of fluoride ions taken by the Pani-POT copolymer film is presented in table 5.3. However, the reversible

behaviour of the Pani-POT (80:20) copolymer film is better than the other compositions, which make an opportunity to use an ion-exchange modified electrode reversibly. This is evidence that the ions can be uptaken during oxidation and released again in opposite direction, during the reduction of the Pani-POT (80:20) film.

Table 5.3: The amount of fluoride anions taken by the Pani, and the Pani-PAP films, the scan rate, $v = 5 \text{ mV s}^{-1}$

<i>Film</i>	<i>The amount of fluoride ions/ mg F⁻ g⁻¹</i>	
	<i>Upon oxidation</i>	<i>Upon reduction</i>
<i>Pani</i>	+51.6	-50.2
<i>Pani-POT (80:20)</i>	+66.8	-64.4
<i>Pani-POT (60:40)</i>	+53.4	-42.4
<i>Pani-POT (170:30)</i>	+83.9	-94.0
<i>Pani-POT (150:50)</i>	+102.4	-96.4

The apparent molar masses of the incorporated ions during the redox cycling of the Pani-POT copolymer films are presented in table 5.4. A large number of ions uptaken by the Pani-POT (80:20) film is extremely high with respect to other the Pani-POT copolymer films. In addition, the reverse scans almost the same amount removed from the film during reduction.

Table 5.4. Electrochemical data obtained from the voltammograms of the Pani-POT copolymer films in 0.1 M NaF solutions, $v = 5 \text{ mV s}^{-1}$ (α is the solvent molecules transferred during redox cycling)

Pani-POT (An:o-OT)/mM	<i>Observed molar mass upon oxidation/gmol⁻¹</i>	<i>Observed molar mass upon reduction/g mol⁻¹</i>	<i>α/per anion during oxidation</i>	<i>α/per anion during reduction</i>
80:10	333.5	313.5	17.4	16.3
170:30	265.7	236.8	13.7	12.1
150:50	165.1	160.2	8.1	7.8

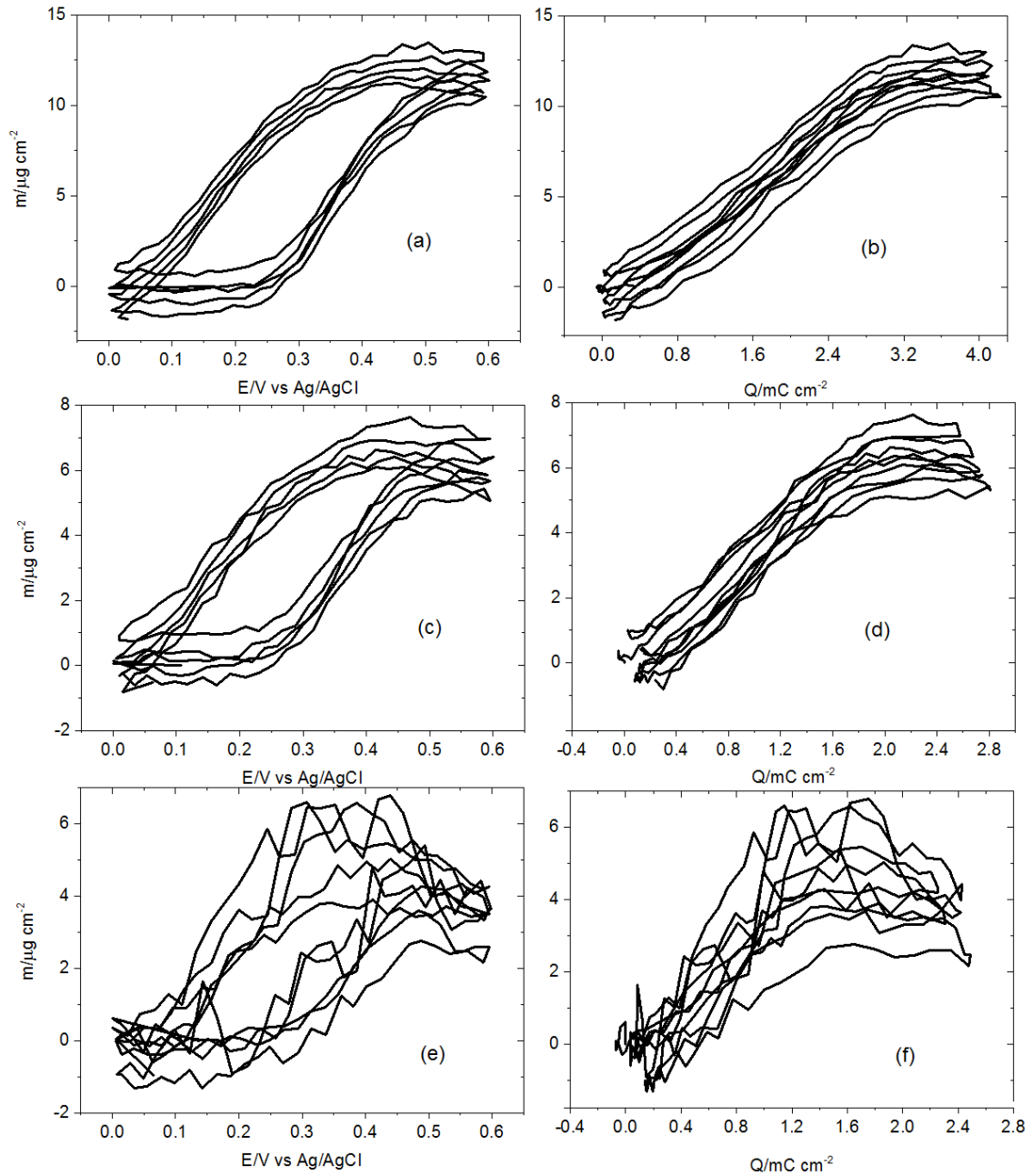


Figure 5.19. The mass change of the Pani-POT copolymer films in 0.1 M NaF, $v = 5 \text{ mV s}^{-1}$; the mass-E curves of (a) the Pani-POT (80:20) (c) the Pani-POT (170:30) (e) the Pani-POT (150:50) and the mass-charge curves of (b) the Pani-POT (80:20) (d) the Pani-POT (170:30) (f) the Pani-POT (150:50)

The effect of scan rate on the defluoridation of Pani-POT (80:20) copolymer film is examined in figure 5.20, which behaves reversibly at 10 mV s^{-1} but not at 3 mV s^{-1} . This most likely originates from the saturation of the film at slow scan rates. Furthermore, the redox peaks of the Pani-POT film appear at different potentials, and they disappear at 3 mV s^{-1} . This indicates the non-reversible behaviour because the peak potentials shift at different scan rates. It can be explained the slow charge transport between film and electrolyte.

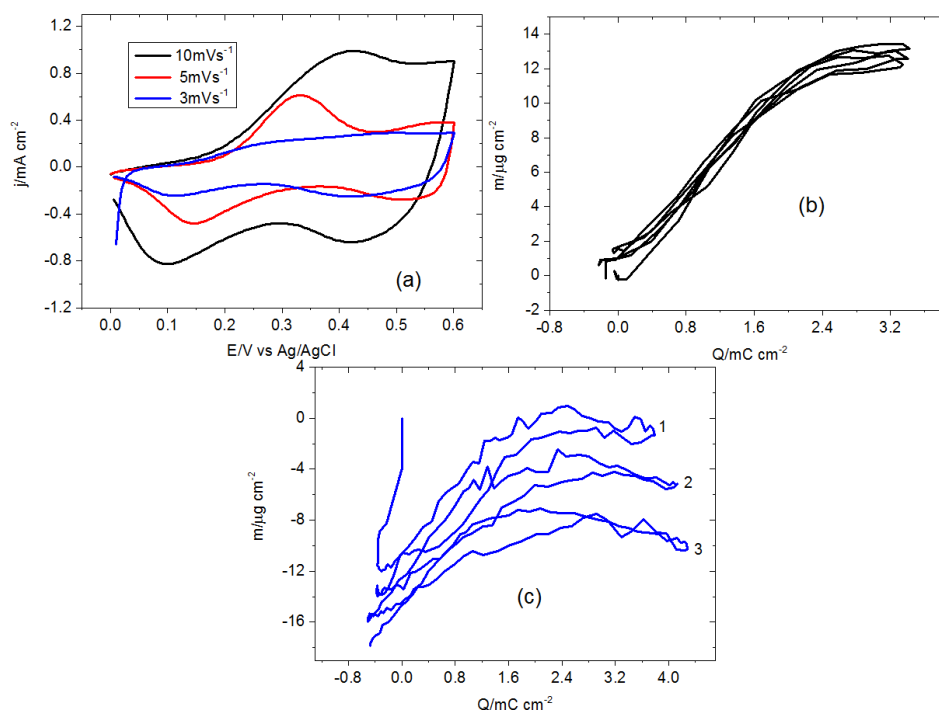


Figure 5.20. The removal of fluoride ions by the Pani-POT (80:20) copolymer film in 0.1 M NaF , at different scan rates $v = 10, 5$ and 3 mV s^{-1} ; (a) the CV curves (80:20) (b) the mass-charge curve at 10 mV s^{-1} (c) the mass-charge curve at 3 mV s^{-1}

The ability of the Pani-POT (80:20) film for defluoridation was examined in the presence of different fluoride concentrations, those of 0.1 M , 0.01 M and 0.0001 M NaF . The results obtained are presented in figure 5.22, indicating the existence of reversible behaviour of the Pani-POT copolymer films while taking fluoride ions even from a 0.001 M NaF electrolyte solution. The apparent molar masses of the incorporated ions from figure 5.20 and 5.21 are presented in table 5.5.

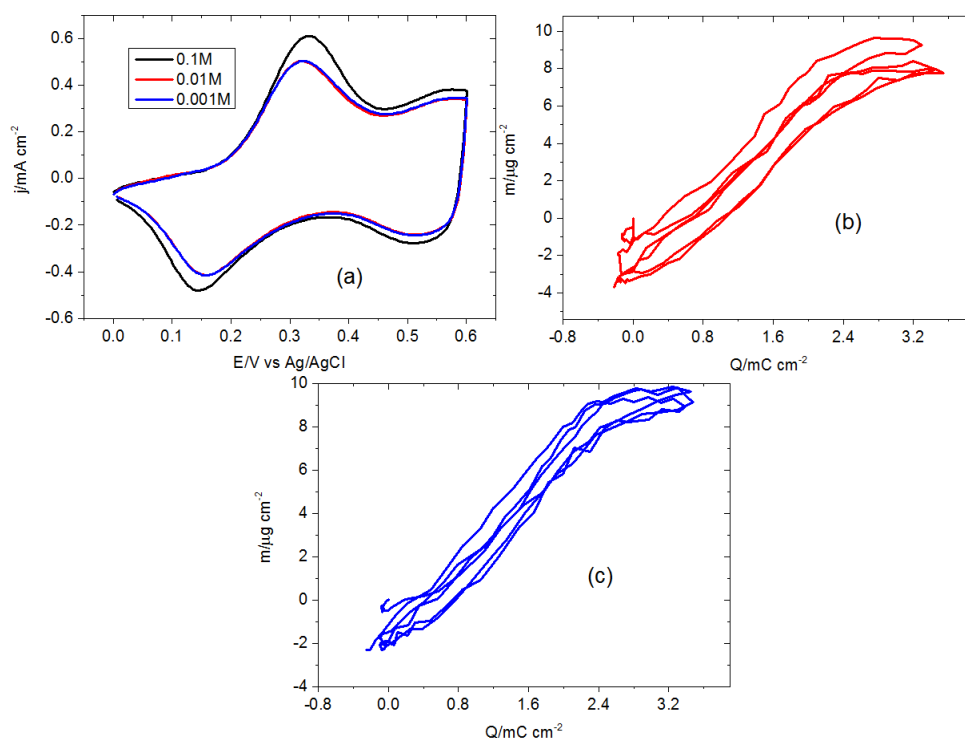


Figure 5.21. The removal of fluoride ions by the Pani-POT (80:20) film in 0.1 M, 0.01 M and 0.001 M NaF, $v = 5 \text{ mV s}^{-1}$; (a) the CV curves of the Pani-POT (80:20) (b) the mass-charge curve at 0.01 M NaF (c) the mass-charge curve in 0.001 M NaF

Table 5.5. Electrochemical data obtained from the voltammograms of the Pani-POT (80:20) film in NaF solutions (α is the solvent molecules transferred during redox cycling)

Scan rate/ mVs^{-1}	NaF/M	Observed molar mass upon oxidation/ g mol^{-1}	Observed molar mass upon reduction/ g mol^{-1}	α /per anion during oxidation	α /per anion during reduction
3	0.1	256.6	297.0	13.2	15.4
5	0.1	333.5	313.5	17.4	16.3
	0.01	303.3	323.5	15.8	16.9
	0.001	273.2	323.6	14.1	16.9
10	0.1	377.6	370.1	19.9	19.5

The removal of the fluoride ions by the Pani-POT (80:20) film in the presence of different ratios of chloride ions in 0.1 M electrolyte solutions of NaF and NaCl was performed. Figure 5.22 shows the associated cyclic voltammograms and mass-charge curves. In the cyclic voltammograms, the redox peaks are distinctive in their higher amounts of chloride ions (10F: 90Cl) while the number of ions taken by the copolymer decreases in figure 5.22f. The apparent molar mass of the incorporated ions is presented

in table 5.6 while considering the insertion of both ions (due to similar sizes) in terms of their ratio in the electrolyte solution. For instance, a solution involved 90 mM F^- and 10 mM Cl^- , the molar mass considered 20.65 g mol^{-1} .

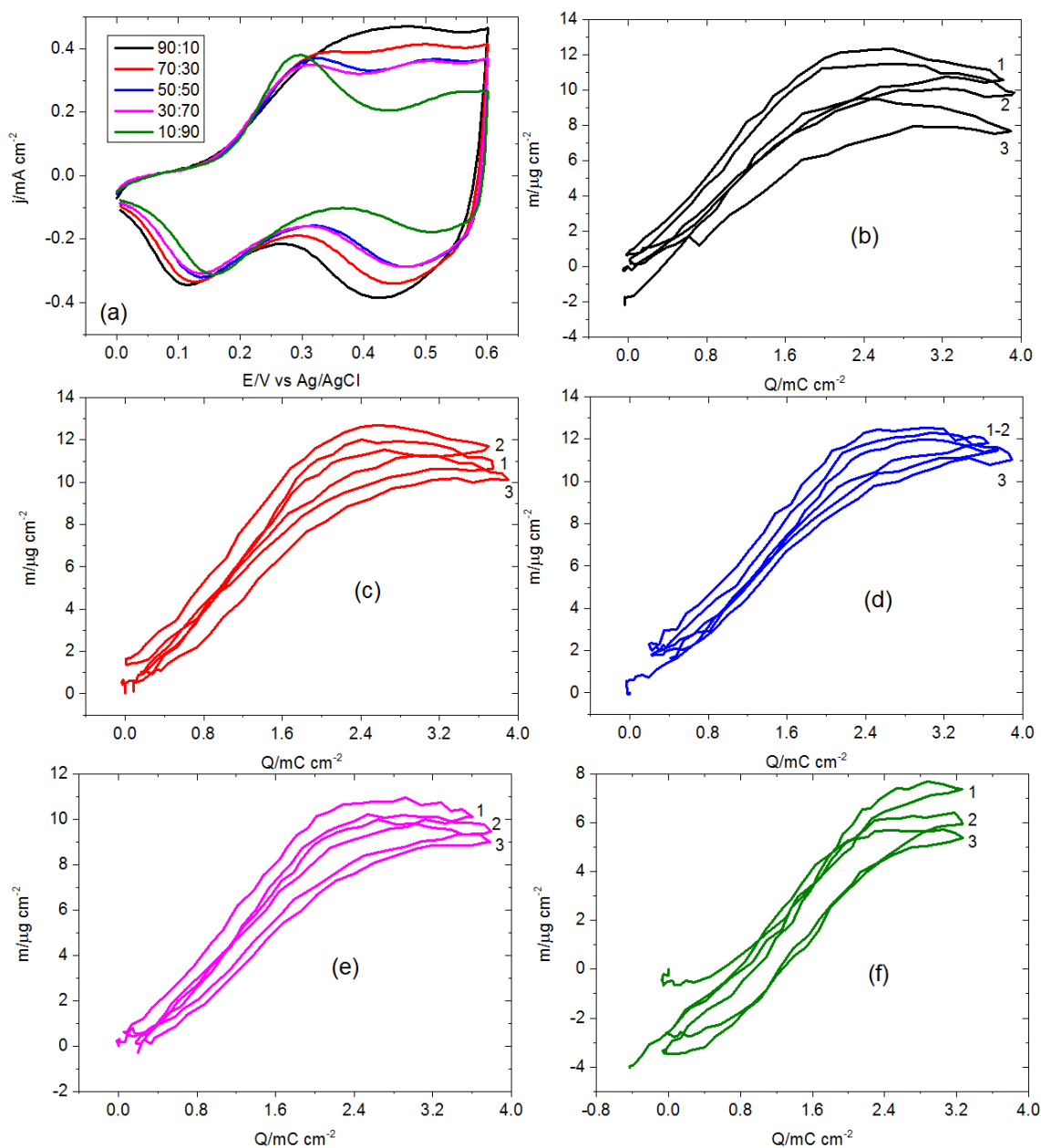


Figure 5.22. The removal of fluoride ions by the Pani-POT (80:20) copolymer film in 0.1 M of NaF and NaCl electrolyte solutions, $v = 5 \text{ mV s}^{-1}$, (a) the CV curves of them (b) in 90 mM NaF and 10 mM NaCl (c) in 70 mM NaF and 30 mM NaCl (d) in 50 mM NaF and 50 mM NaCl (e) in 30 mM NaF and 10 mM NaCl (f) in 10 mM NaF and 90 mM NaCl

Table 5.6 also shows the solvent molecules transferred during the redox cycling are quietly similar, showing the assumption is reliable, which suggested the insertion of both ions.

Table 5.6. Electrochemical data obtained from the voltammograms of the Pani-POT (80:20) copolymer film in the presence of different ratios of NaF: NaCl

NaF: NaCl/mM	Observed molar mass upon oxidation/gmol ⁻¹	Observed molar mass upon reduction/g mol ⁻¹	α /per anion during oxidation	α /per anion during reduction
90:10	268.6	268.6	13.7	13.7
70:30	277.6	275.2	14.1	13.9
50:50	296.6	290.1	14.9	14.6
30:70	272.0	270.3	13.4	13.3
90:10	219.0	218.6	10.2	10.2

5.2.4. Regeneration of the Pani-POT Copolymer Film

Figure 5.23 shows the electroactivity of Pani-POT (80:20) film in 1 M H₂SO₄ before and after NaF treatment.

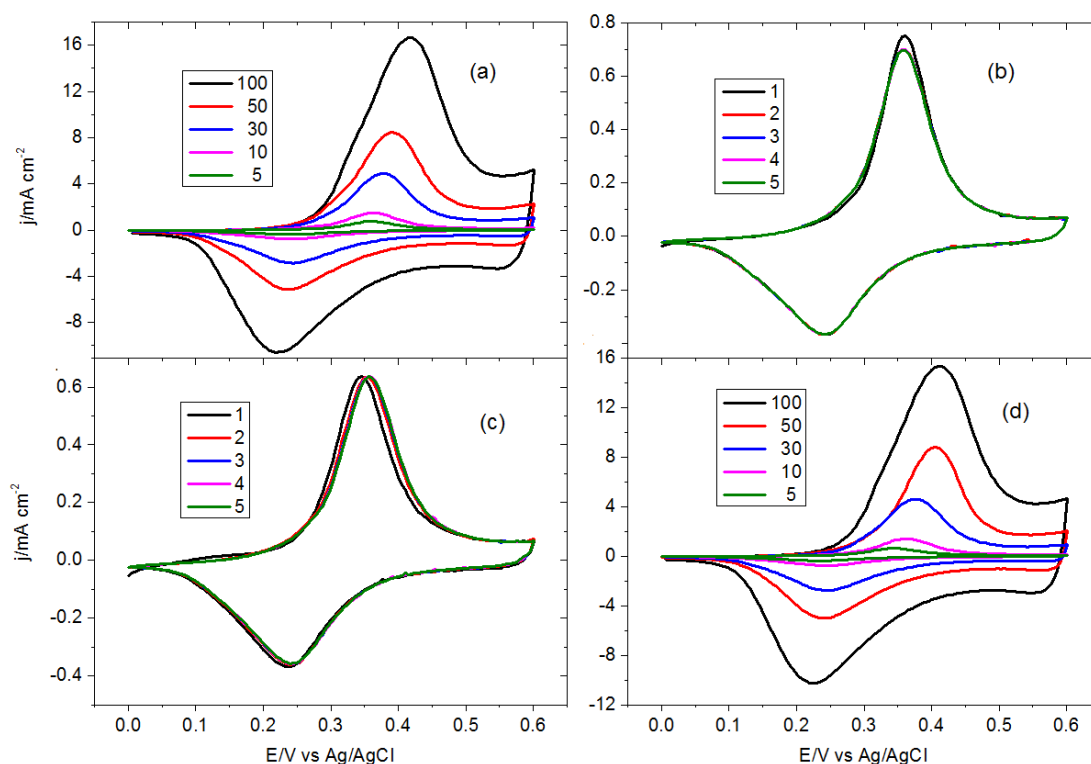


Figure 5.23. The electroactivity of the Pani-POT (80:20) film in 1 M H₂SO₄ (*a*) the CV curves of the Pani-POT at different scan rates before treatment of NaF (*b*) in 1 M H₂SO₄ at 5 mV s⁻¹ before treatment with NaF (*c*) the CV curves of Pani-POT at different scan rates after treatment of NaF (*d*) in 1 M H₂SO₄ at 5 mV s⁻¹ after treatment with NaF (the numbers indicate the scan rates in figure 5.23a-d, while representing cycle number in figure 5.23b-c)

After the NaF treatment at 5 mV s^{-1} in $1 \text{ M H}_2\text{SO}_4$, the current density started to increase with each cycle, showing the release of the ions taking place in the film. Similarly, the $\log i_p$ and $\log v$ curves of the Pani-POT copolymer films obtained from figure 5.23a-d, indicating the reversibility of the Pani-POT film does not affect the treatment of the NaF electrolyte solution, as shown in figure 5.24.

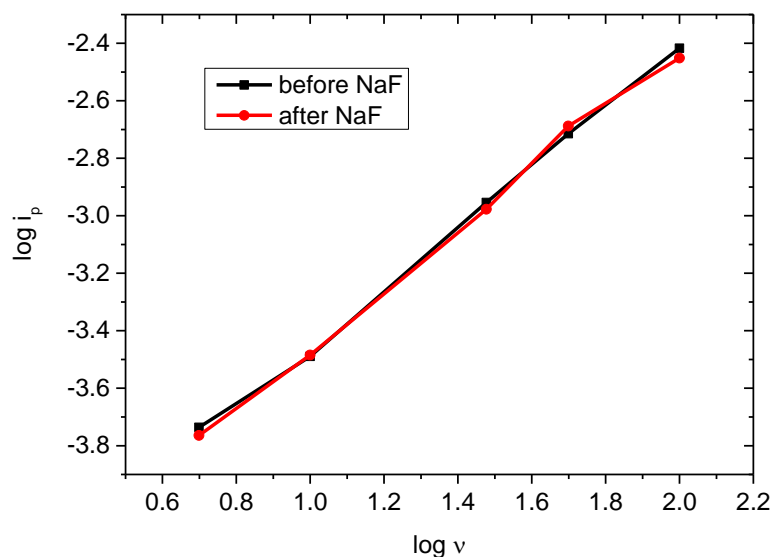


Figure 5.24. $\log i_p$ - $\log v$ curve of the Pani-POT (80:20) copolymer film in $1 \text{ M H}_2\text{SO}_4$ from figure 5.23a-d

5.2.5. The Surface Characterisation of the Polymer and the Copolymer Films

5.2.5.1. Scanning electron microscopy

The SEM images of the polymer and copolymer films are shown in figure 5.25, showing the significant difference between the homopolymers and their copolymer, the Pani-POT. Both the Pani and the POT films have more porous surfaces than the Pani-POT (80:20) copolymer film. It was structured a firm surface. This proved the formation of a copolymer rather than a mixture of homopolymers in addition to electrochemical experiments.

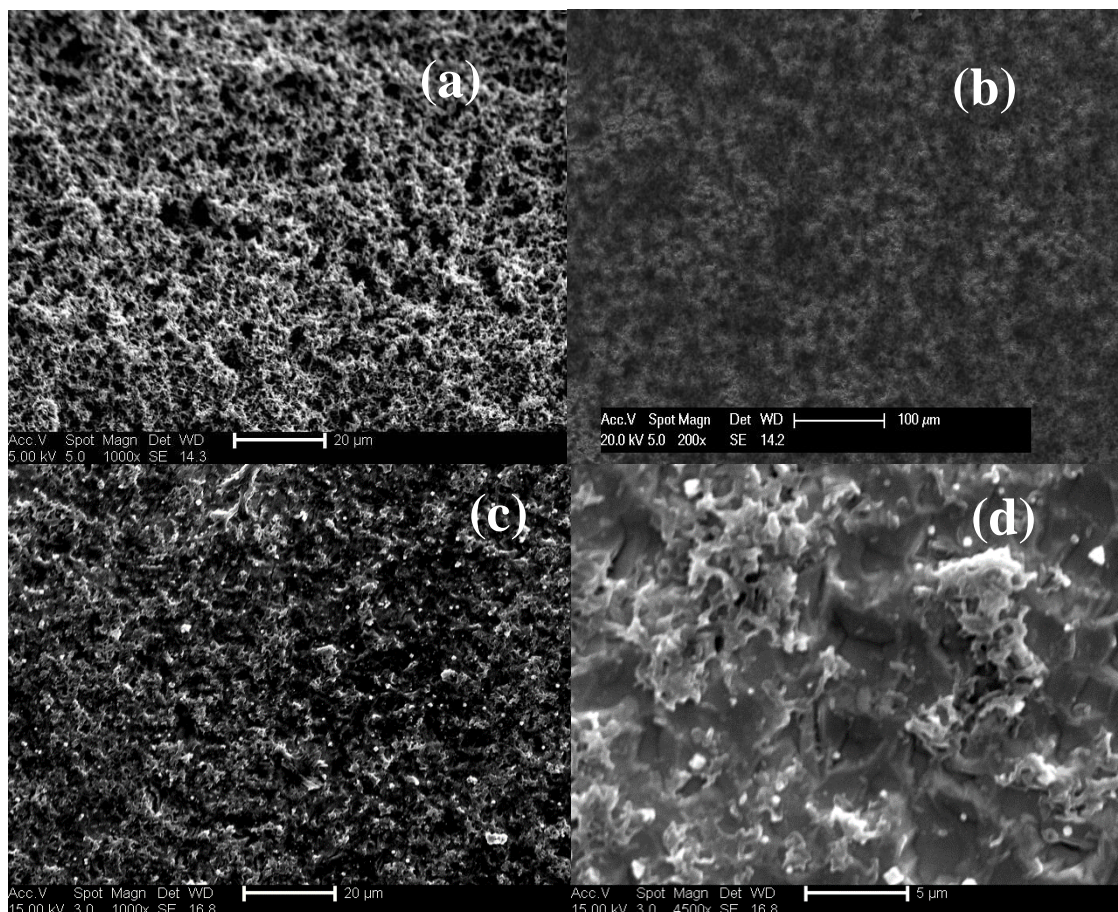


Figure 5.25. SEM images of (a) the Pani (b) the POT (c-d) the Pani-POT (80:20) films at different magnification

5.2.6. FTIR

The structural analysis of the POT and the Pani-POT films were performed with the help of the FTIR spectra shown in Figure 5.26. Absorption peak positions are presented in table 5.7 in order to compare peak positions of the homopolymers and the copolymer films.

The spectrums of the POT and the Pani-POT films show a quiet similarity because the peaks observed in the same region. The small peaks above 3440 cm^{-1} and 3200 cm^{-1} have attributed the vibration of primary amine, N-H and the -OH groups (can be from water in the sample), respectively. The peaks taken place between 2337.4 cm^{-1} and 2931 cm^{-1} are assigned the C=C aromatic vibration and the vibration of C-H. These peaks were observed for both spectra of POT and Pani-POT films, providing characteristic vibrations of Pani film presented in chapter 4. The peak observed at 1617.7 cm^{-1} in the spectrum of POT can be assigned the N-H stretching vibration, which appeared

characteristic peaks of aniline.^{7, 8} The feature at 1436 cm^{-1} and 1495 cm^{-1} are attributed the methylene group vibrations, which appeared in both spectra. This can a proof the existence of *o*-OT in copolymer film. In the meantime, the peaks also observed at 1166 cm^{-1} and 1315.8 cm^{-1} , 1031 cm^{-1} and 1153 cm^{-1} , and 873.9 cm^{-1} and 869.0 cm^{-1} are assigned the vibrations of C-N aromatic amine, and =C-H groups, which also characteristic peaks of Pani.^{7, 8}

Table 5.7. The absorption peaks of the POT and the Pani-POT films and corresponding functional group

<i>Absorption of POT/cm⁻¹</i>	<i>Functional group</i>	<i>Absorption of Pani-POT/cm⁻¹</i>	<i>Functional group</i>
3476.8	N-H, primary amine	3449	N-H, primary amine
3215.7	O-H (H-bonded)	3230.5	N-H, primary amine
2840.2	C=C, C-H	2931	C=C, C-H
2339.4	C=C, C-H	2337	C=C, C-H
1617.7	N-H	1535.8	C=C
1436	-C-H, methylene group	1495	C-H, methylene group
1166	C-N	1315.8	C-N, aromatic amine
1031	C-N	1153	C-N
873.9	=C-H	1033	C-N
		869.0	=C-H

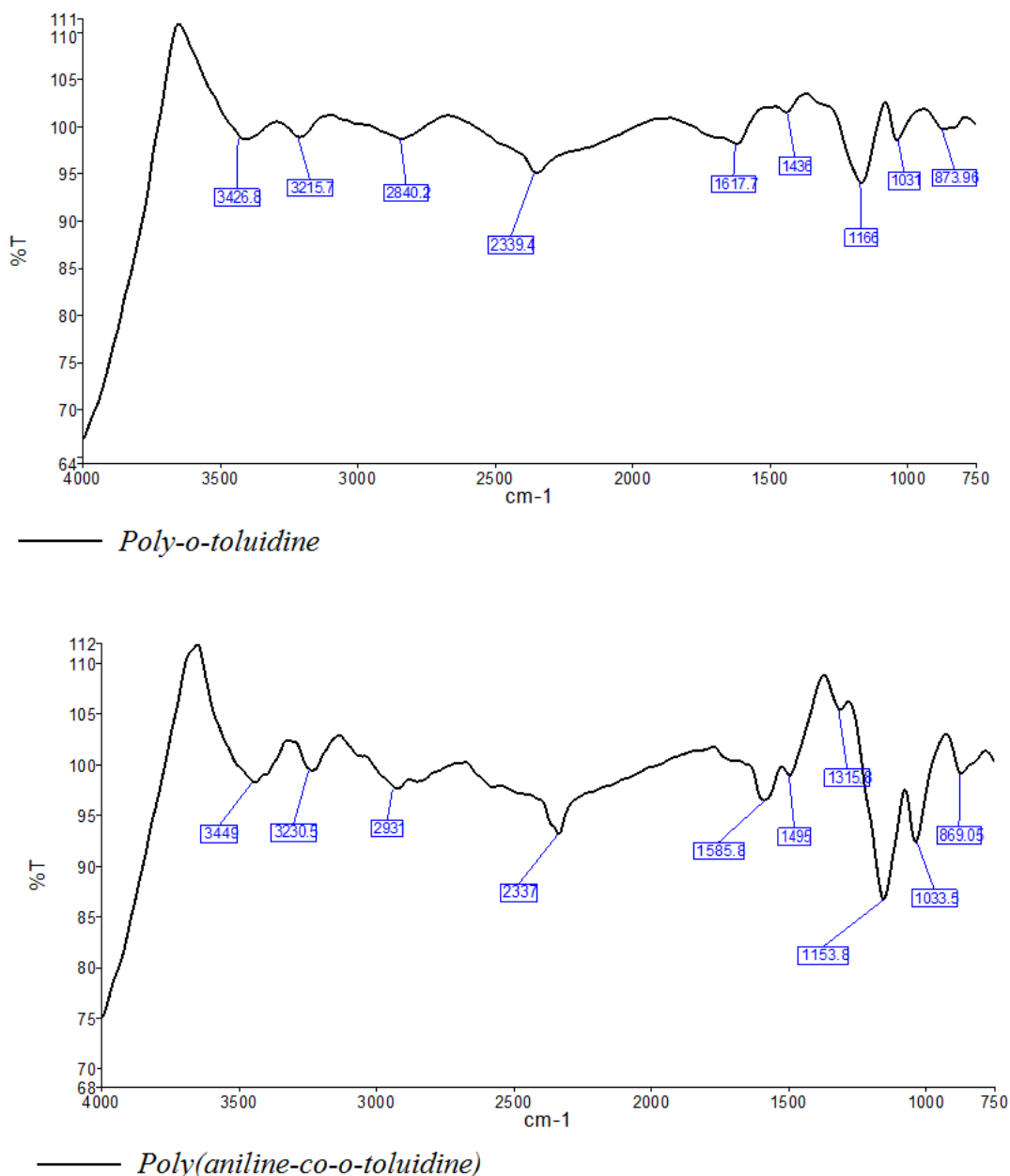


Figure 5.26. FTIR spectra of the POT and the Pani-POT (80:20) films

5.2.7. Comparison of the Pani-PAP and the Pani-POT copolymer films

The electrochemical properties of Pani-PAP (90:10) and Pani-POT (80:20) films were characterized in monomer-free 1 M H₂SO₄ solutions at 5 mV s⁻¹ (see figure 4.24 and 5.23). Their redox peaks appeared around 0.34/0.25 V, whilst the Pani-POT film provided a high current density upon redox cycling. The surface coverage of the Pani-PAP (90:10) and the Pani-POT (80:20) films were found in 266.8 nmol cm⁻² and 198.2 nmol cm⁻², respectively, which are great much greater than for the Pani film (Γ , 78.4

nmol cm⁻²) synthesized in chapter 4. This supports the observation that the copolymerization enhances the electroactivity of polyaniline. The thickness of the Pani-PAP (90:10) and the Pani-POT (80:20) copolymer films for dimeric units were determined as 523 nm and 393 nm, respectively. Furthermore, the copolymerisation of aniline and *o*-aminophenol/*o*-toluidine decreased the possibility of overoxidation of the resultant films because the redox peaks and irreversible peaks appeared at more negative potentials. Therefore, it is possible to remove fluoride ions without concern about possible degradation.

The defluoridation properties of the Pani-PAP (90:10) and the Pani-POT (80:20) films was also investigated in chapter 4 and 5. Both show an excellent ability to remove fluoride ions from 0.1 M NaF upon oxidation. Both copolymer films took 0.35 mol fluoride ions per redox site of the copolymer films compared to 0.25 mol fluoride ions per redox site of the polyaniline film obtained in chapter 4. This demonstrates that the copolymerization of polyaniline with *o*-aminophenol/*o*-toluidine increased the defluoridation ability of the polyaniline films at low potentials. The corresponding amounts of fluoride ions taken up by the Pani-PAP and the Pani-POT were determined as $65.0 \pm 0.6 \text{ mg F}^- \text{ g}^{-1}$ and $66.8 \pm 1.8 \text{ mg F}^- \text{ g}^{-1}$, respectively.

5.3. Conclusion

The present study describes two significant aspects of Pani-POT copolymer films, which are the preparation of a high-quality film with a high electroactivity via EQCM, and the ion-exchange properties in monomer-free NaF solutions.

First, we studied the growth rate of POT polymer film, which was extremely slow compared to the growth rate of the Pani film synthesised in chapter 4. The rate of growth increased when using a large number of cycles due to the autocatalytic effect of POT, though this results in overoxidation after a certain point. Besides, the resultant POT film had a low electroactivity in monomer-free 1 M H₂SO₄, as reported in the literature.² On the other hand, we also studied the ionic activity of the POT film in 0.1 M NaF monomer-free solution, which showed a low ionic activity and unstable behaviour during its redox reactions; clearly, these are undesirable properties for ion exchange modified electrodes. Thus, we can state that POT is not a good candidate for

the development of an ion exchange electrode. However, the copolymers of *o*-toluidine with aniline enhanced its electrochemical properties as reported in the literature.² This leads us to the development of a novel ion exchange modified electrode based on a Pani-POT copolymer film.

We employed EQCM to obtain both gravimetric and electrochemical information about the copolymerization of the Pani-POT films. Electrochemical data obtained from the growth voltammograms of the Pani-POT copolymer film reveal that the electroactivity and growth of the copolymer films are largely dependent on the ratio of the *o*-toluidine monomer in the monomer solution, which causes a decrease in both electroactivity and growth rate on addition of a large amount *o*-toluidine (such as 60 mM aniline and 40 mM OT composition in 1 M H₂SO₄). On the other hand, the small ratio of *o*-toluidine in the monomer solutions results in a similar voltammogram to that observed for pure Pani growth. For this reason, the ratio of *o*-toluidine was kept in a specific range in the monomer solutions. Pani-POT (80:20) and (170:30) films showed different peak positions to those of their homopolymers, with high electroactivity. In the case of Pani-POT (80:20) film, it is obvious that the participation of *o*-toluidine is slow, but increases with the application of a large number of cycles at 5 mV s⁻¹. Furthermore, the admittance data was evaluated that the decrease in admittance demonstrated the formation of acoustically thick and rigid copolymer films. Also, the ohmic resistance of each copolymer film synthesised was found to be 588 Ω whilst the thickness was 393 nm, showing the formation of a thin electroactive film (Γ , 198.2 nmol cm⁻² for dimeric units).

The Pani-POT (80:20) film had a higher electroactivity when it was reversibly cycled in monomer-free 1 M H₂SO₄ solution at different scan rates. This is a significant outcome, because the reports in the literature mentioned the different characteristics of Pani-POT copolymer films as compared to their homopolymers, but we were able to synthesise a highly electroactive copolymer film with new properties. This showed that the ratios of the monomers and the conditions are particularly important for the synthesis of the copolymers. The overoxidation of the Pani-POT (80:20) film is negligible when considering the POT and Pani films because the redox peaks appeared around 0.33/0.25 V, which allows the study of low potentials.

Furthermore, the ionic activity of the Pani-POT (80:20) film was performed in monomer-free NaF electrolyte solutions (pH 6.60), which gave redox peaks with high current densities. The Pani-POT (80:20) film also shows excellent reversible behaviour while taking up ions during its oxidation. A quantitative evaluation of the Pani-POT (80:20) film was determined from cycling in 0.1 M NaF at 5 mV s^{-1} . The Pani-POT (80:20) copolymer film takes 0.35 mol fluoride ion per redox site of the copolymer film, which is much greater than the Pani film synthesised in chapter 4. However, there are a number of similar electrochemical properties between the Pani-PAP (90:10) (discussed in chapter 4) and the Pani-POT (80:20) films, showing copolymerization is an excellent means by which to enhance the properties of polyaniline. Also, they showed different colours and thicknesses, offering the possibility of some electrochromic device in addition to their high electroactivities. The corresponding amount of fluoride ions taken up by the Pani-PAP and the Pani-POT films were determined as $65.0 \pm 0.6 \text{ mg F}^{-} \text{ g}^{-1}$ and $66.8 \pm 1.8 \text{ mg F}^{-} \text{ g}^{-1}$, respectively. Both show higher capacitances than currently available techniques (discussed in chapter 4) in the literature.^{10, 11}

Similarly, the Pani-POT (80:20) film behaves in a reversible manner in 0.1 M NaF (pH 6.60) at different scan rates, while it allows for successive usage according to our regeneration experiments.

The surface characterization of Pani-POT film and its homopolymers was also investigated via SEM, showing a highly porous surface for the Pani film, and a firm surface for the Pani-POT (80:20) film, supporting the formation of a copolymer rather than a mixture of homopolymers.

This chapter has shown that co-polymers of aniline with substituted anilines produce more even films. The issue with these materials is that despite their improved stability, repeated cycling still leads to decomposition of the polymer. Other researchers have studied composite materials with carbon-based and metal oxide-based dispersed phases, and these have shown significantly improved stability. In the next chapter, the applicability of composites with polymers will be investigated.

5.4. References

- 1 Y. Wei, G. W. Jang, C. C. Chan, K. F. Hsueh, R. Hariharan, S. A. Patel and C. K. Whitecar, *Journal of Physical Chemistry*, 1990, **94**, 7716-7721 (DOI:10.1021/j100382a073).
- 2 D. D. Borole, U. R. Kapadi, P. P. Mahulikar and D. G. Hundiwale, *Material Letters*, 2006, **60**, 2447-2452 (DOI:10.1016/j.matlet.2006.01.014).
- 3 D. Kumar, *Synthetic Metals*, 2000, **114**, 369-372 (DOI:10.1016/S0379-6779(00)00270-8).
- 4 D. D. Borole, U. R. Kapadi, P. P. Mahulikar and D. G. Hundiwale, *Material Letters*, 2004, **58**, 3816-3822 (DOI:10.1016/j.matlet.2004.07.035).
- 5 S. Bilal and R. Holze, *Journal of Electroanalytical Chemistry*, 2006, **592**, 1-13 (DOI:10.1016/j.jelechem.2006.03.039).
- 6 Q. Yang, Y. Zhang, H. Li, Y. Zhang, M. Liu, J. Luo, L. Tan, H. Tang and S. Yao, *Talanta*, 2010, **81**, 664-672 (DOI:10.1016/j.talanta.2009.12.051).
- 7 S. L. Mu, *Synthetic Metals*, 2004, **143**, 259-268 (DOI:10.1016/j.synthmet.2003.12.008).
- 8 M. Liu, M. Ye, Q. Yang, Y. Zhang, Q. Xie and S. Yao, *Electrochimica Acta*, 2006, **52**, 342-352 (DOI:10.1016/j.electacta.2006.05.013).
- 9 J. Lippe and R. Holze, *Journal of Electroanalytical Chemistry*, 1992, **339**, 411-422 (DOI:10.1016/0022-0728(92)80465-G).
- 10 H. Cui, Q. Li, Y. Qian, R. Tang, H. An and J. Zhai, *Water Research.*, 2011, **45**, 5736-5744 (DOI:10.1016/j.watres.2011.08.049).
- 11 M. Karthikeyan, K. K. Satheeskumar and K. R. Elango, *Journal of Hazardous Materials*, 2009, **163**, 1026-1032 (DOI:10.1016/j.jhazmat.2008.07.057).

Chapter VI:

The electrochemical deposition of Pani film in the presence of MWCNTs and its redox switching in Ethaline

6.1. Introduction

6.1.1. Overview

In recent times, there has been a growing interest in the combination of conducting polymers (CPs), in particular, polyaniline (Pani) and polypyrrole (PPy), and carbon nanotubes (CNTs), because of both their fundamental and potential applications in energy storage devices.^{1, 2} The combination of these two unique materials results in a material that displays the characteristics properties of each, such as the electroactivity, reversibility and chemical stability of the polymer film³ and the excellent mechanical, electrical properties of CNTs.⁴⁻⁷ In addition, CNTs also provide a large surface area due to their small dimensions,^{4, 8, 9} making these composites potentially useful to many applications within the field of energy storage devices, such as pseudo-capacitors.^{4, 10-13} Also, CNTs can behave as a dopant anion^{14, 15} because of their negatively-charged walls when they are functionalised¹⁶ in concentrate HNO₃, as shown in figure 6.1.

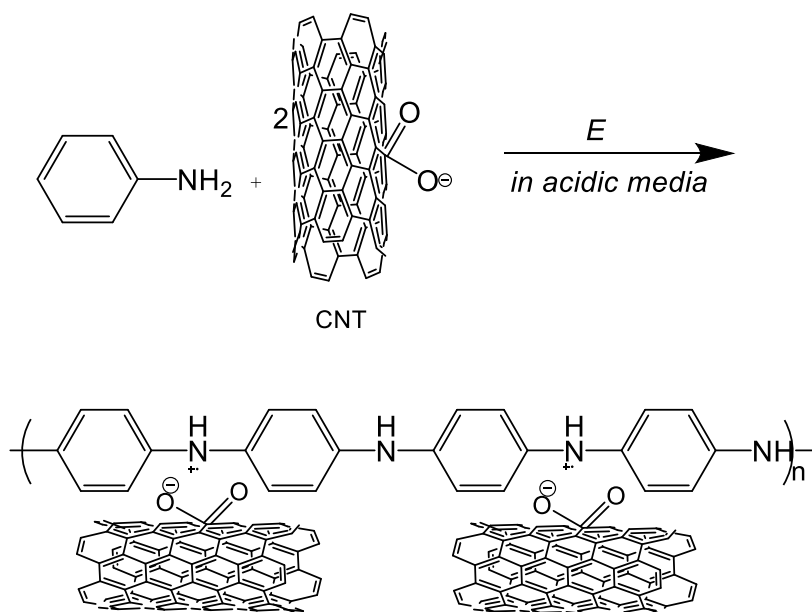


Figure 6.1. The behaviour of CNTs as dopant anions during the deposition of a Pani film

There are a variety of methods, such as chemical and electrochemical polymerization, that can be used to prepare the composites of polymer and CNTs mentioned in detail in chapter 1. Amongst these, electrochemical polymerization is commonly used to monitor the electrochemical properties of composites of CPs and CNTs.¹⁷ The literature studies reported for Pani/CNTs^{5, 6} and PPy/CNTs¹⁸ in aqueous medium show the attendant improvements in their electrical properties. On the other hand, the dispersion of CNTs in aqueous solution show non-proper, causing the poor interaction between monomer and CNTs.⁶ On the other hand, deep eutectic solvents, discussed in detail in chapter 1, are favourable solvents for the electrochemical polymerization of CPs such as polyaniline,¹⁹ polypyrrole and PEDOT^{20, 21} because they have high ionic strengths and large electrochemical windows. They provide for the synthesis of high-quality conducting polymers.²² In addition, they are excellent media for well-dispersion of CNTs in monomers solution due to their high viscosity. Thus, we focused on Ethaline as a DESs for the electrochemical deposition of the composite films in order to improve the charge transport process of the Pani/CNTs and PPy/CNTs composite films.

There are two types of CNTs, which are known as multiwall carbon nanotubes (MWCNT) and single wall carbon nanotubes (SWCNT),²⁴ and which are again discussed in detail in chapter 1. Here, our studies used MWCNTs. Moreover, several methods of preparation have been used to obtain the CP/CNTs composites mentioned in detail in chapter 1. In the present study, we used EQCM via electrochemical deposition to obtain a better understanding as to the dynamic growth of composite films.

6.1.2. Aims and Objectives

The objectives of this chapter are: *(i)* the electrochemical deposition of aniline in the presence of different ratios of MWCNTs in aqueous acidic medium of varying concentrations; *(ii)* the investigation of the growth dynamics of Pani and Pani/MWCNT composite films by means of EQCM; *(iii)* the characterisation of the charge transport process of the Pani and Pani/MWCNTs films in 1 M H₂SO₄ monomer-free electrolyte solutions; *(iv)* to define the charge and discharge characteristics of the resultant composite films; *(v)* the electrochemical deposition of aniline in the presence of different ratios of MWCNTs in Ethaline; *(vi)* the investigation of the growth dynamics of Pani and Pani/MWCNT composite films by means of EQCM in Ethaline; *(vii)* the

characterization of the charge transport process of the Pani and Pani/MWCNTs films in 1 M H₂SO₄ monomer-free background solutions; (viii) to define the charge and discharge characteristics of the resultant composite films; (ix) identification of the surface morphologies of the composite films resulting from Pani/MWCNT from aqueous and non-aqueous media by means of SEM and 3D microscopy techniques; (x) the structural analysis of the resulting polymer and composite film via FTIR.

6.2. Results and Discussions

6.2.1. Electrochemical Deposition of the Pani Film in the Presence of MWCNTs in Aqueous Solution

6.2.1.1. Cyclic voltammetry experiments

MWCNTs are inert materials, and which allow only for a weak interaction with aniline monomer molecules.¹⁸ To form a strong interaction between aniline monomers and MWCNTs, the walls of the MWCNTs need to be functionalised¹⁶ in concentrate HNO₃ (as mentioned in more detail in chapter 3). In further experiments, we preferred the MWCNT-COOH for the synthesis of Pani/MWCNTs composite films due to its favourable contribution to the electroactivity, as mentioned above.

Initially, we studied the electrochemical deposition of Pani films via cyclic voltammetry from 0.1 M aniline and 1 M H₂SO₄ solutions between -0.2 V and 1.2 V at 50 mV s⁻¹ in the presence/absence of 20 wt% MWCNTs. As mention earlier, CNTs behave as dopant anions during the polymerisation of Pani, but the process still requires the addition of a different dopant anion in an acidic medium such as SO₄²⁻. On the other hand, the presence of CNTs in the monomer solution provides a means of stabilisation for the electrochemical deposition of Pani because it acts a source of electrons, thus preventing the overoxidation of polyaniline at higher potentials.

The charges passed during the electrochemical experiments on the Pani film growth in the presence/absence of MWCNTs are found as 0.21 mC and 78 mC, respectively. This shows the enhancement of the charge transport characteristics of the Pani film. Figure 6.2 shows the SEM images of the Pani/MWCNTs composite film.

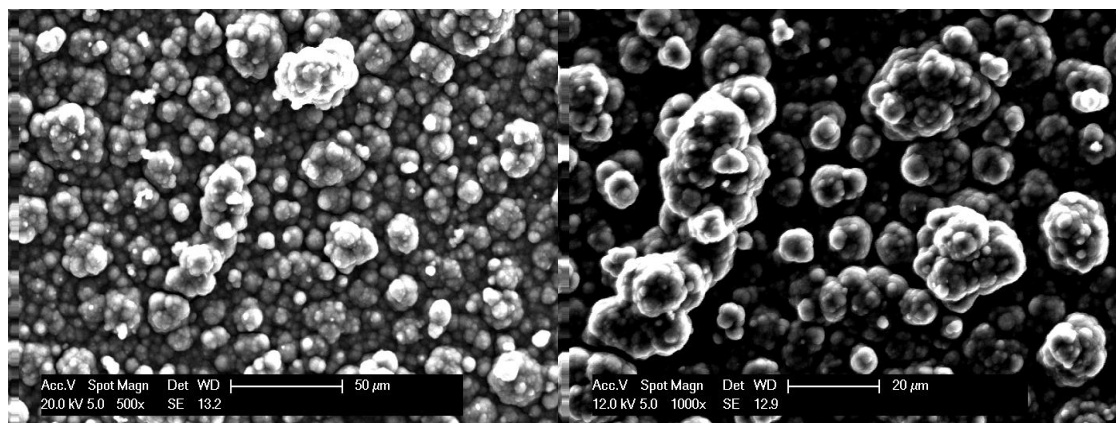


Figure 6.2. SEM images (at various magnifications) of the Pani/MWCNTs film

Later, several Pani and Pani/MWCNTs films were synthesised using EQCM technique under identical conditions at various acid concentrations in order to obtain the effects of MWCNTs on the growth of Pani and Pani/MWCNTs films as well as the charge transport properties of the final films.

6.2.1.2. EQCM experiments on the electrochemical deposition of the Pani/MWCNTs films

The electrochemical deposition of a Pani film requires a strongly acidic medium. However, the strong acid medium reduces the solubility of MWCNTs in an aqueous medium,⁸ diminishing the interaction between the monomer and MWCNTs. To obtain detailed information regarding MWCNTs on the electrochemical deposition of a Pani film, various aniline and MWCNTs solutions using different concentrations of H₂SO₄ were prepared and were subsequently deposited at 10 mV s⁻¹. Figure 6.3 shows CVs of Pani growth in the absence/presence of MWCNTs in 1 M and 0.1 M H₂SO₄, respectively.

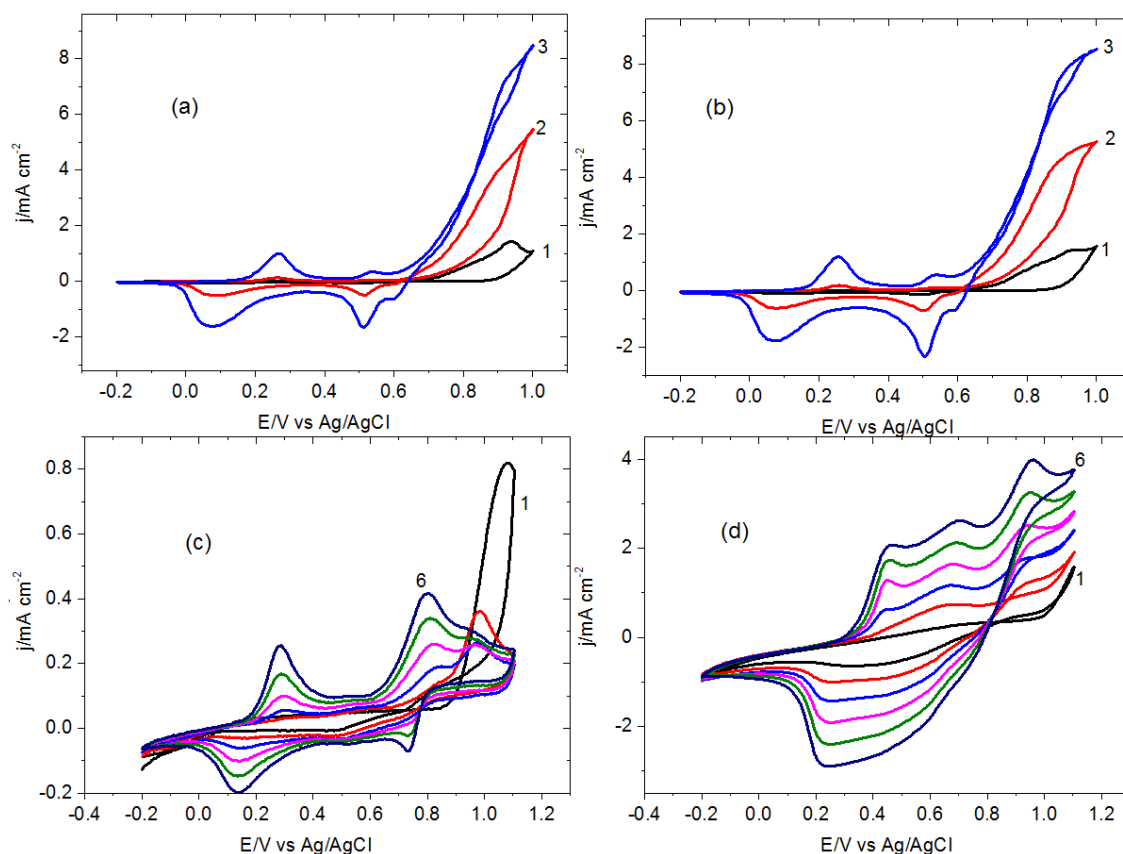


Figure 6.3. The CV curves of the Pani film growth from 0.1 M aniline in the absence/presence of MWCNTs in at various acidities, the scan rate, $v = 10 \text{ mV s}^{-1}$ (a) in 1 M H_2SO_4 (b) in 1 M H_2SO_4 and 5 wt% MWCNTs (c) in 0.1 M H_2SO_4 (d) in 0.1 M H_2SO_4 and 5 wt% MWCNTs

The results revealed that the addition of MWCNTs to the monomer solution does not influence the polymerization of aniline at higher acidities. This support our assumption that the weak interaction between the monomer and MWCNTs is due to the precipitation of MWCNTs at higher acidities. On the other hand, the effects of MWCNTs on the growth of the Pani film is remarkable at lower acidities, i.e., 0.1 M H_2SO_4 , because it increases the current density by more than a factor of four.

Additionally, the electrochemical properties of Pani film in the presence of MWCNTs at lower concentrations of H_2SO_4 (0.1 M) were significantly affected. We deduce this from the broad anodic and broad cathodic peaks observed in the associated cyclic voltammogram, rather than the three discrete redox peaks seen in figure 6.3c. This could arise from the kinetic effects of MWCNTs because of the small separation and strong interaction between aniline and MWCNTs. The redox peaks almost appeared at the same potential for figure 6.3a-b whilst the charge passed for the Pani/MWCNTs

(figure 6.3b) film upon redox reactions is much more than the Pani film (figure 6.3a). On the other hand, in the case of the lower acidity, the differences between redox peak potentials of the Pani and the Pani/MWCNTs films is getting increase by shifting to more positive potential in the presence of MWCNTs. the irreversible peak of the Pani film (figure 6.3c) appears at 0.86 V while it is 0.98 V for the Pani/MWCNTs film (figure 6.3d). Electrochemical data from the growth voltammograms are reported in table 6.1. The peak positions in figure 6.3d are shifted to more positive potentials, while the current density is considerably increased over that seen in figure 6.3c. Furthermore, the cathodic peak appears as a single broad peak between 0.1 and 0.8 V, indicating overlapped peaks otherwise identical to those seen in figure 6.3c. The charge passed is also developed about 50 times greater than in the smaller acid concentrations.

Table 6.1. Electrochemical data obtained from the growth voltammograms of the Pani film in absence/presence of 5 wt% MWCNTs in different acid concentrations

<i>Film</i>	<i>E/V</i>						<i>Q/mC</i>	
	<i>E_{ox,1}</i>	<i>E_{ox,2}</i>	<i>E_{IR}</i>	<i>E_{red,1}</i>	<i>E_{red,2}</i>	<i>E_{red,3}</i>	<i>Q_{anodic}</i>	<i>Q_{cathodic}</i>
<i>Pani</i> (figure 6.3a)	0.26	0.53	0.86	0.07	0.51	0.60	3.39	10.6
<i>Pani/MWCNTs</i> (figure 6.3b)	0.25	0.53	8.60	0.06	0.50	0.59	4.38	14.17
<i>Pani</i> (figure 6.3c)	0.28	0.79	0.86	0.13	0.53	0.72	0.28	0.14
<i>Pani/MWCNTs</i> (figure 6.3d)	0.45	0.70	0.98	0.23	--	--	45.9	32.1

The corresponding mass and charge of the Pani/MWCNTs film (in figure 6.3d) as a function of the applied potential are presented in figure 6.4, which shows a gradual increase in the mass of the composite film. In the case of the charge, this increases during anodic oxidation but is otherwise significantly decreased. This can be explained by increased levels of MWCNTs being encapsulated during anodic oxidation and then released during reduction, rather than participating in the growth of the polymer film.

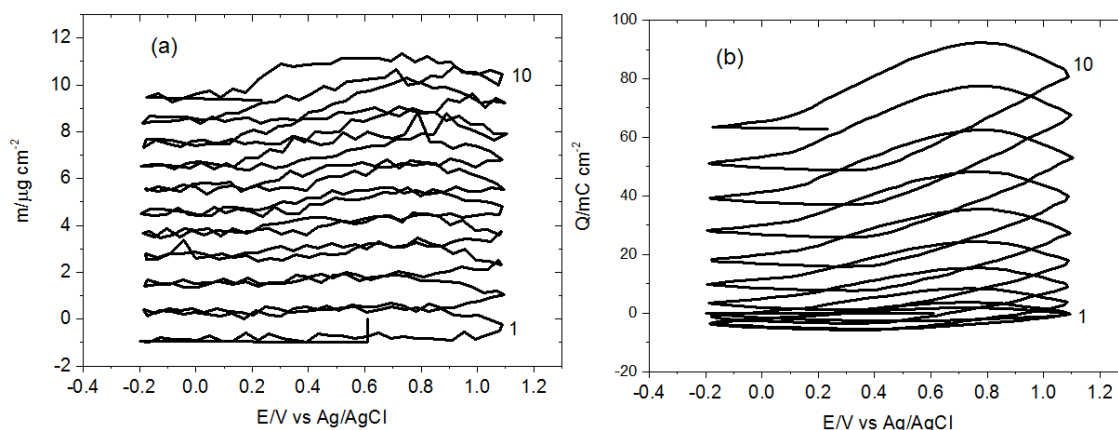


Figure 6.4. (a) Mass and (b) charge change of the Pani film in the presence of 5 wt% MWCNTs (from figure 6.7d)

The mass-charge curves of the Pani (see figure 6.3c) and the Pani/MWCNTs (see figure 6.3d) films are plotted in figure 6.5. The addition of MWCNTs decreases the efficiency of the deposition of the Pani film in otherwise identical conditions. The amount of charge passed is higher for the Pani/MWCNTs film contrary to the Pani film during growth as seen in table 6.3, which supports the hypothesis of the presence of trapped MWCNTs during deposition rather than participating the polymer chain. The apparent molar masses of the polymer and the composite films calculated using equation 3.4 (see chapter 3) were presented in table 6.2. The molar mass of the Pani film is determined as 63.1 g mol^{-1} for an aniline unit experimentally while it is 5.8 g mol^{-1} for Pani/MWCNTs film (in figure 6.7d). This is the indication of low efficiency in the MWCNTs.

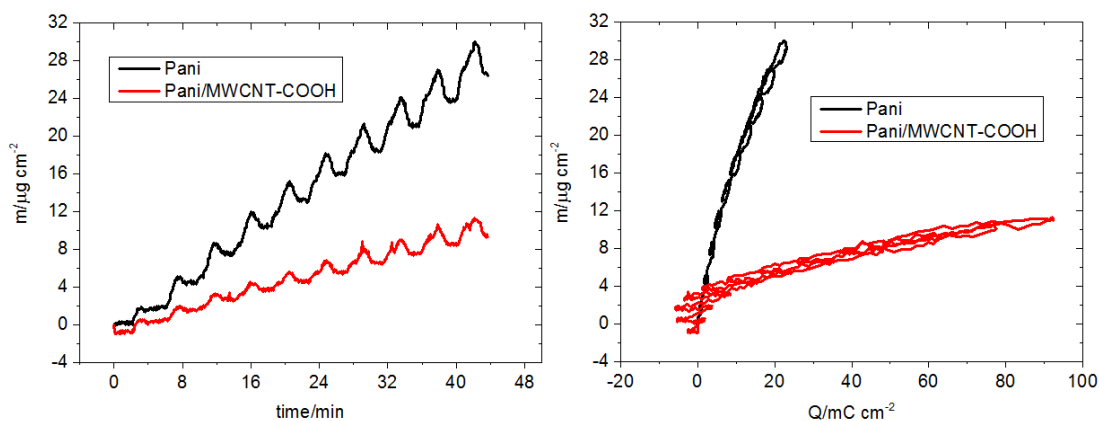


Figure 6.5. (a) mass-time (b) mass-charge curves of the Pani and the Pani/MWCNTs films (from figure 6.3c-d)

The surface coverage of the Pani/MWCNTs film is $2068.3 \text{ nmol cm}^{-2}$, which is considerably greater than that observed for pure Pani film synthesised under identical conditions. However, this may not reflect the existence of electroactive sites in the case

of the Pani/MWCNTs film because of trapped MWCNTs upon oxidation. These trapped MWCNTs would release upon reduction, which contributes the charge passed but does not reflect MWCNTs taking place polymer chain. Therefore, the redox cycling in 1 M H₂SO₄ monomer-free background solution was applied presented in the following section.

Table 6.2. Gravimetric and electrochemical data for the growth of the Pani and the Pani/MWCNTs films ($n = 1$ for dimeric aniline units for surface coverage but $n = 0.5$ for per aniline unit for the apparent molar mass)

<i>Film</i>	M_{app}/gmol^{-1} (figure 6.5b)	$M/\mu\text{g cm}^{-2}$ (figure 6.4a)	$Q/\text{mC cm}^{-2}$ (figure 6.4)	$\Gamma/\text{nmol cm}^{-2}$
<i>Pani</i>	63.1	29.8	22.8	12.6
<i>Pani/MWCNTs</i>	5.8	11.4	92.7	2068.3

The admittance data describing the Pani and the Pani/MWCNTs films is shown in figure 6.6. Both indicate rigid (acoustically thin) behaviour due to the narrow peak observed when admittance decreases.

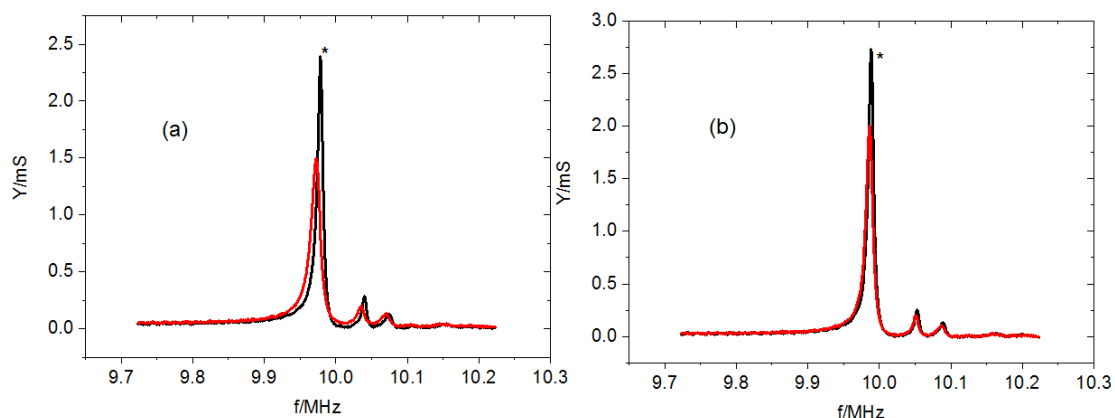


Figure 6.6. Admittance decrease of (a) the Pani (b) the Pani/MWCNTs films during their growth from figure 6.3c-d (* indicates bare crystal frequency)

As can be seen in the results presented above, the presence of MWCNTs enhances the amount of charge while reducing the mass loading of Pani film in 0.1 M H₂SO₄.

The effects of MWCNTs on the growth of Pani films were investigated in the presence of various concentrations of MWCNTs using the chronoamperometry technique. For

this end, several Pani films were grown from 0.1 M aniline and 0.1 M H₂SO₄ in the presence of MWCNTs (at 0, 1, 3, 6, 10, and 15 wt%, respectively) at 1.3 V. They were then reduced at -0.2 V, as shown in figure 6.7a. During their growth, the amount of charge passed was plotted against the concentration of MWCNTs in 0.1 M monomer solution, as can be seen in figure 6.7c, which showed a rapid increase in larger amounts of MWCNTs.

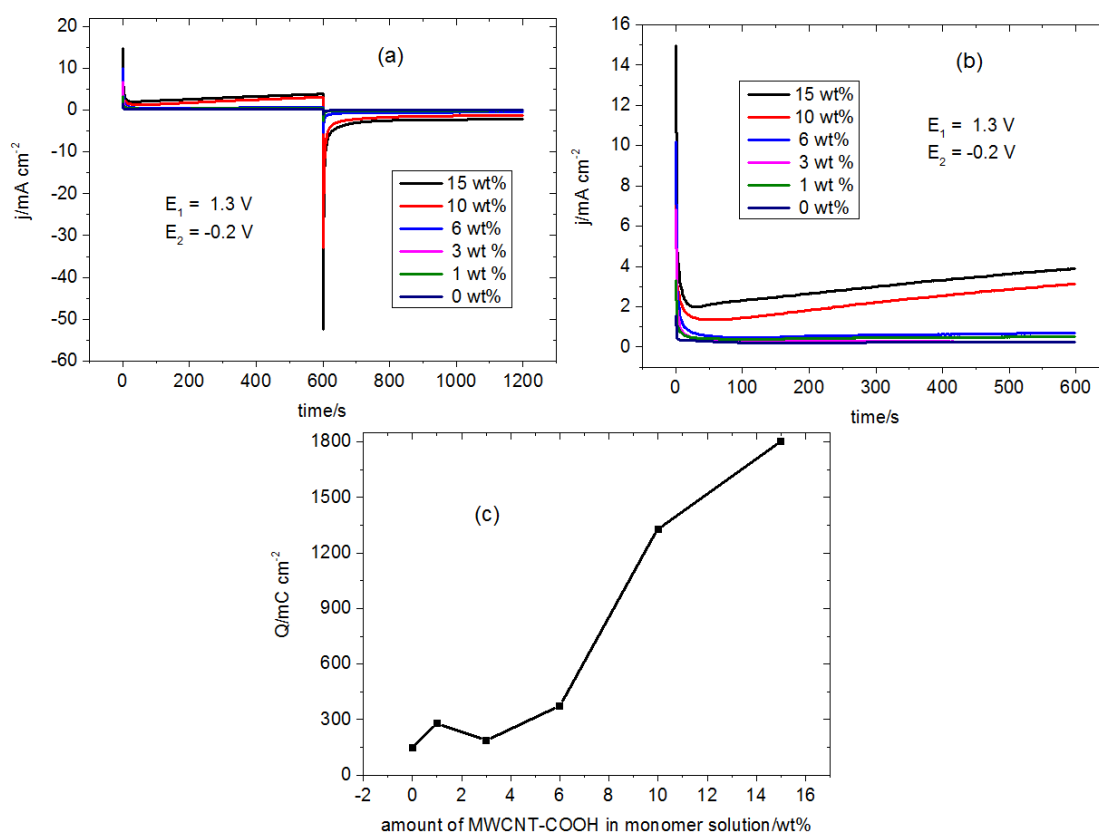


Figure 6.7. (a) Electrochemical deposition of Pani films from 0.1 M aniline and 0.1 M H₂SO₄ in the presence of various concentrations of MWCNTs (0, 1, 3, 6, 10, and 15 wt% respectively) by chronoamperometry at 1.3 V and reduction of the deposited composite films at -0.2 V (b) a detailed representation of the anodic oxidation of the Pani films in the presence of MWCNTs (c) the amount of charge passed during the electrochemical deposition of the Pani films from figure 6.7b

6.2.1.3. Characterisation of the Pani/MWCNTs composite films

The electrochemical activity of the Pani and the Pani/MWCNTs films synthesised in otherwise identical conditions were performed in 1 M H₂SO₄ and 0.1 M NaF, monomer-free solutions, respectively, at a slow scan rate of 5 mV s⁻¹. The voltammograms thus acquired are displayed in figure 6.8. In H₂SO₄, both the Pani and the Pani/MWCNTs films show redox peaks at similar positions, but with a higher current density in

Pani/MWCNTs film. In NaF, both show redox peaks around 0.4/0.2 V while the Pani/MWCNTs film again shows a higher current density.

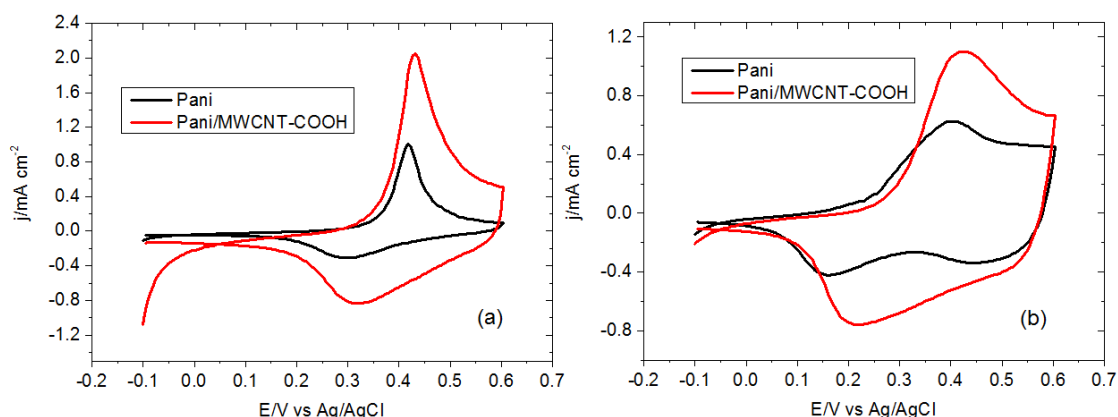


Figure 6.8. Electroactivity of the Pani (from figure 6.7c) and Pani/MWCNTs (5 wt%) (from figure 6.7d) films in monomer-free solutions, the scan rate, $\nu = 5 \text{ mV s}^{-1}$ (a) in 1 M H_2SO_4 (b) 0.1 M NaF

The charge passed is still much greater for the Pani/MWCNTs composite film in each of these two electrolytes but smaller than that required for the growth voltammograms. The surface coverage values for the Pani and the Pani/MWCNTs films in 1 M H_2SO_4 are $135.1 \text{ nmol cm}^{-2} \text{ mC}$ and $441.6 \text{ nmol cm}^{-2}$, respectively. In this case, we can eliminate the possibility trapped MWCNTs because it is released to solution again during growth. However, here there is no monomer and MWCNTs in 1 M H_2SO_4 and the produced current density occurred from oxidation and reduction of the Pani/MWCNTs composite film. Therefore, the surface coverage is $441.6 \text{ nmol cm}^{-2}$, which is considerably smaller than the $2068.3 \text{ nmol cm}^{-2}$ obtained from the growth voltammogram of Pani/MWCNTs film. Furthermore, the ionic activity of the Pani film in the presence of MWCNTs was developed according to figure 6.8b because the charge passed (6.9 mC for the Pani/MWCNT) film is six times bigger than the Pani film (1.6 mC).

The corresponding mass and charge change of the Pani and Pani/MWCNTs films in monomer-free solutions is shown in figure 6.9, showing the anion-exchange feature (in figure 6.9c) because the mass of the composite film increases upon oxidation. However, this increase is much smaller in the Pani/MWCNTs film, which is thinner than the Pani film. The thickness is a significant feature for the ion-exchange properties of polymer and composite films reported in the literature.²⁵ In the meantime, the charging and discharging of the Pani and the Pani/MWCNTs film were compared in figure 6.9b-d,

showing a superior result for the Pani/MWCNTs film despite the thinner film contrary to the Pani film. At this point, the Pani/MWCNTs film requires a numerous of cycles to achieve a compose film with desirable properties. Additionally, the Pani/MWCNTs film give a certain redox couple peak at 0.45/0.22 V, indicating a development not only charging-discharging of the Pani film but also its ion-exchange behaviour at pH 6.6 with the addition of MWCNTs. This can be explained the enlarged surface of the films due to MWCNTs.

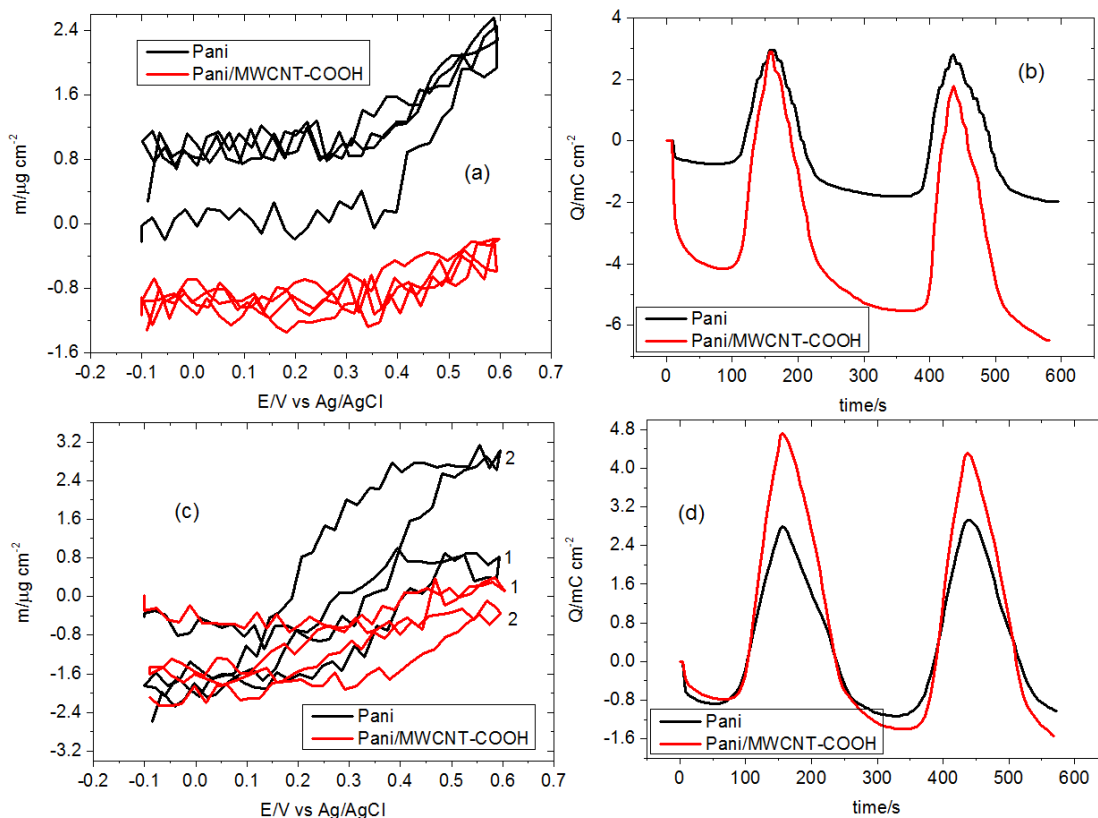


Figure 6.9. The mass change of the Pani and the Pani/MWCNTs films in monomer-free solutions (a) in 1 M H₂SO₄, (c) in 0.1 M NaF; charging and discharging of the Pani and the Pani/MWCNTs films at identical conditions (b) in 1 M H₂SO₄, (d) in 0.1 M NaF

6.2.1.4. Surface characterisation of the Pani and the Pani/MWCNTs films

The morphologies of the dried Pani polymer and Pani/MWCNTs films from the aqueous medium were investigated using SEM. The acquired SEM images of the Pani film was revealed in figure 6.10, showing a high porous but uniform surface.

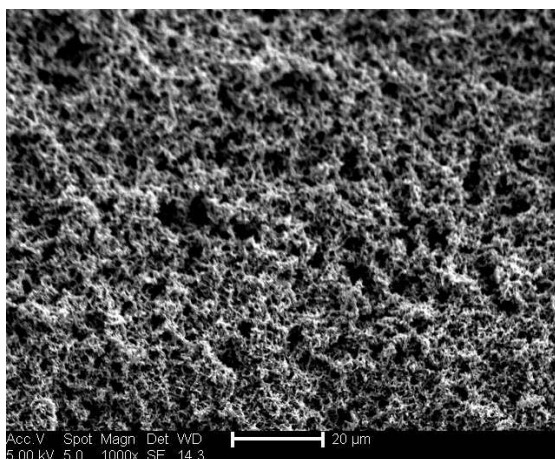


Figure 6.10. A SEM image of the Pani film obtained over 7 cycles at 10 mVs^{-1}

The SEM images of the Pani film synthesised with MWCNTs from aqueous medium were taken at various magnifications, as shown in figure 6.11. It shows a highly porous surface with a degree of roughness. It appears like the growth is taking place on the wall of the MWCNTs because the film was not coated properly on the quartz crystal. The building is like happening around of MWCNTs.

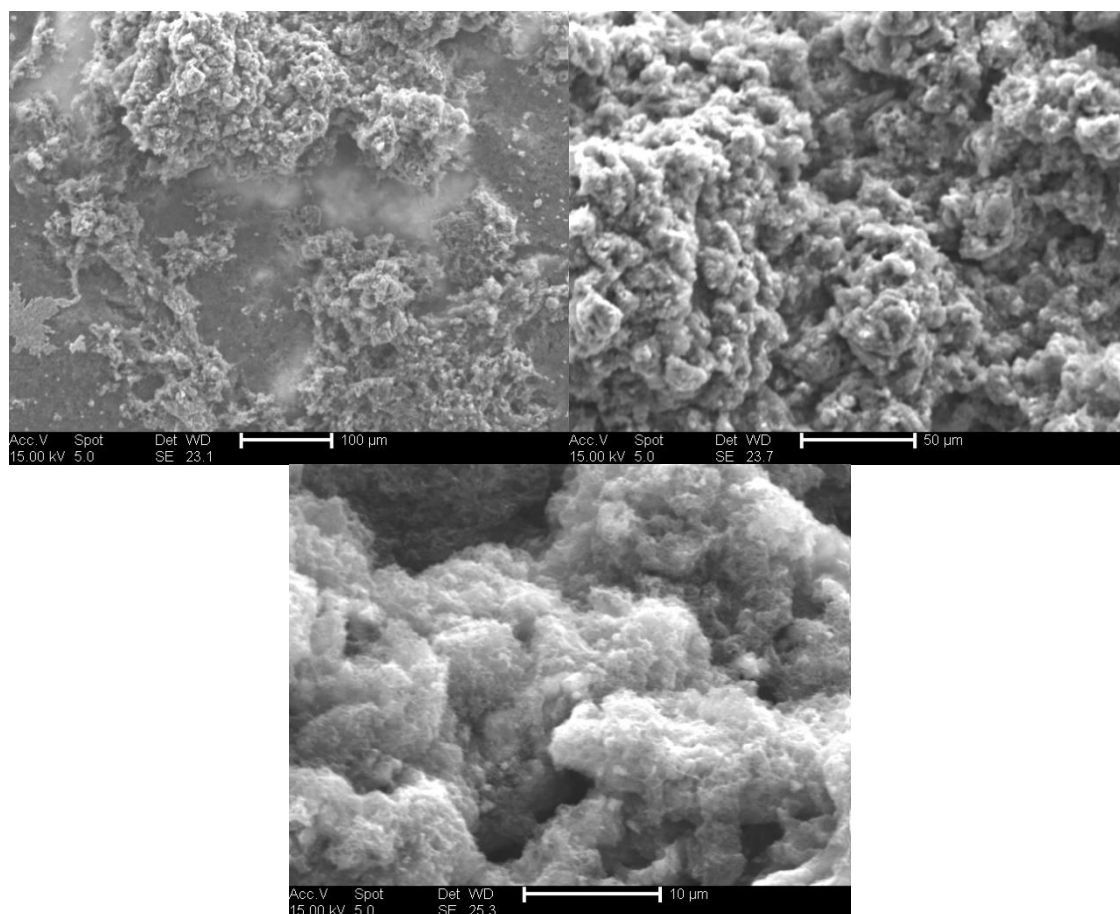


Figure 6.11. The SEM images of the Pani/MWCNTs composite film

The surface of the Pani and Pani/MWCNTs films synthesised from aqueous medium also were investigated via a 3D profiler. Figure 6.12 reveals that there is a significant difference between them. The Pani film was deposited as a green film whilst the Pani/MWCNTs film grew as a blue film with a rough surface.

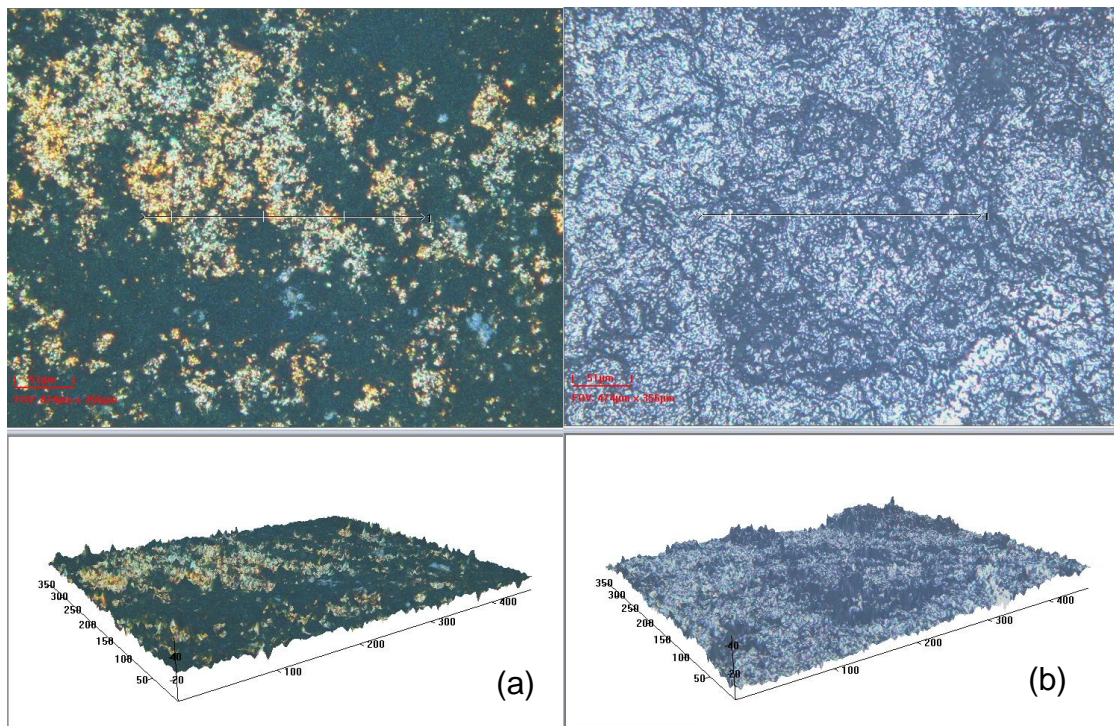


Figure 6.12. 3D images of (a) the Pani and (b) the Pani/MWCNTs films from the aqueous medium

6.2.2. Electrochemical Deposition of the Pani/MWCNTs in Ethaline

By this time, the electrochemical deposition of Pani films in the absence/presence of MWCNTs had been performed in aqueous medium. The results showed an improvement in the electroactivity of the Pani film, but the resultant films show non-homogenous formation on the quartz crystal, at a lower efficiency than the loading polymer film. This can be overcome by polymerization of aniline from Ethaline, which is one of the DESs discussed in detail in chapter 1. DESs can provide for the uniform dispersion of MWCNTs in the solvent during electrochemical experiments, and so can increase the participation of MWCNTs in composite films. Abbott *et al.* report that when the species are suspended, such as MWCNTs, they remain stable over a long period of time, the results of which is that this can increase the participation of the particulates in the deposition of the composites.²⁶ In our case, MWCNTs were

suspended for a long time (about a week), which might result in an increase in the participation of MWCNTs in the polymer films.

Initially, the electrochemical deposition of Pani films from 1 M aniline and 1 M H₂SO₄ was performed in the absence/presence of 10 wt% MWCNTs in ETH200 between 0.0 and 1.3 V at 100 mV s⁻¹. The CV curves of the Pani and the Pani/MWCNTs films thus acquired are displayed in figure 6.13.

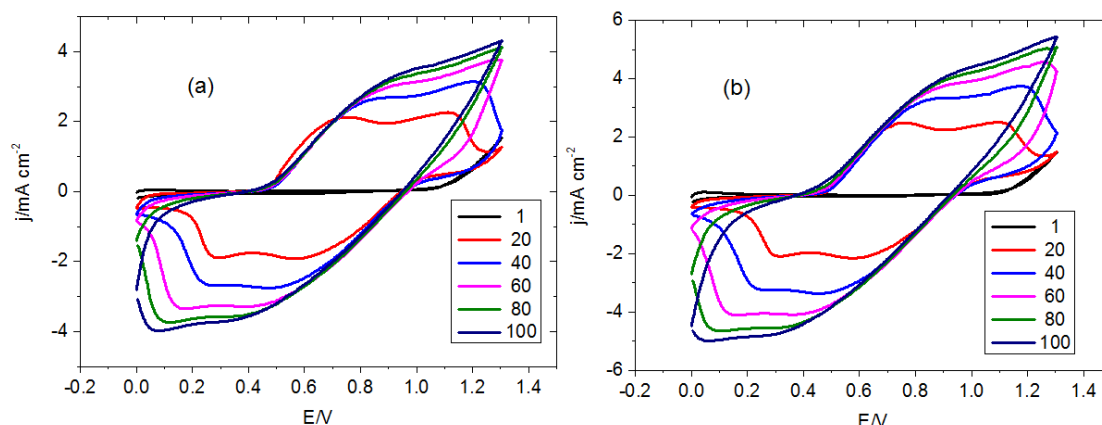


Figure 6.13. The CV curves of the electrochemical deposition of (a) a Pani film from 1 M aniline and 1 M H₂SO₄ (b) a Pani/MWCNTs film from 1 M aniline and 1 M H₂SO₄ in 10 wt% MWCNTs, the scan rate, $\nu = 100 \text{ mV s}^{-1}$

The growth of the Pani film gives two anodic peaks at 0.60 V and 1.00 V, and two cathodic peaks at 0.27 V and 0.60 V in ETH200. These shifts towards more positive potentials with cycling, and disappear altogether when a large number of cycles has been applied. A black film was observed after the deposition of the Pani film. Similar behaviour was observed in the presence of 10 wt% MWCNTs with higher current densities. This is an indication of the enhancement of the charge transport process in the Pani film with MWCNTs. On the other hand, ETH200 is somewhat inconvenient in this instance, because it is frozen in this solvent at room temperature (as shown in figure 6.14a) after preparation, which makes the processability of the aniline monomer solution for its electrochemical deposition impossible. Therefore, we used ETH400 instead, which is constituted of a 1:4 mixture of choline chloride and ethylene glycol. It provides for the solubility of the aniline monomer at room temperature, as shown in figure 6.14b.

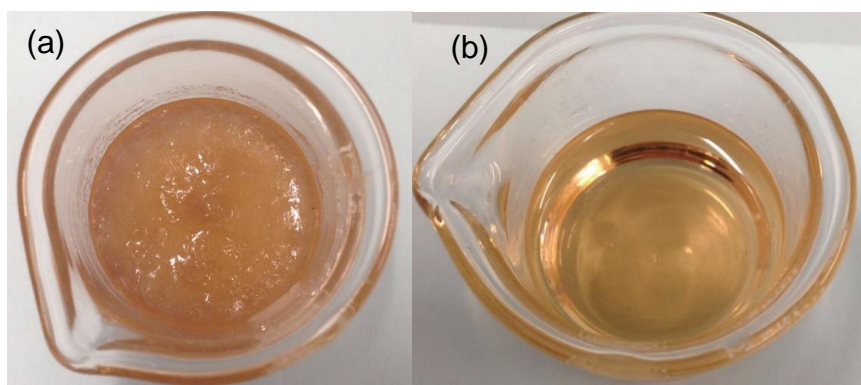


Figure 6.14. 1 M aniline and 1M H₂SO₄ (a) in ETH200, (b) in ETH400

In order to understand the effects of the ratios of MWCNTs on the growth of the Pani films, we studied the electrochemical deposition of the Pani films from a solution consisting of 1 M aniline and 0.5 M H₂SO₄ (acid concentration reduced to 0.5 M to allow for a strong interaction between the aniline monomer and MWCNTs) using various concentrations of MWCNTs was performed at 1.3 V over 600 s and reduced at -0.3 V using the chronoamperometry technique.

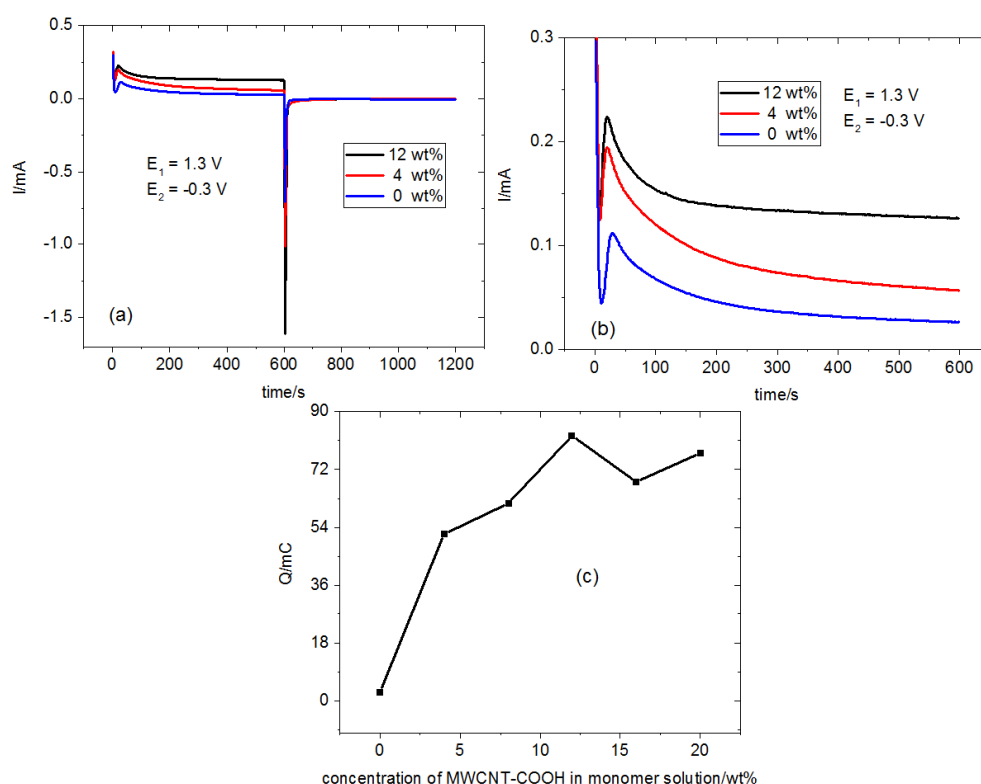


Figure 6.15. (a) Electrochemical deposition of Pani films from 1 M aniline and 0.5 M H₂SO₄ in the presence of various concentrations of MWCNTs (0, 4, 12 wt%) at 1.3 V, and the reduction of the deposited film at -0.3 V (b) a detailed representation of the anodic deposition of the Pani film from figure 6.15a (c) the amount of charge passed during the electrochemical deposition of Pani film against the concentration of MWCNTs in monomer solution at 1.3 V

The results indicate the presence of MWCNTs increases the amount of charge passed during the electrochemical deposition of the Pani film in ETH400 like in aqueous medium. Thus, we applied the electrochemical deposition of the Pani film from 1 M aniline and 0.5 M H₂SO₄ was applied via EQCM between -0.2 and 0.9 V at a slow scan rate of 5 mV s⁻¹ in ETH400 to obtain a detailed information about electrochemical and gravimetric information about the Pani/MWCNT film growth.

In figure 6.16a, Pani film gave an anodic peak at 0.10 V and a cathodic peak -0.05 V, which are shifted to more positive potentials with continued cycling. In the meantime, the irreversible peak at 0.73 V in the first scan, corresponding to the oxidation of the aniline monomer, is shifted to a more negative potential with continued cycling. This indicates that the oxidation of aniline monomer requires a lower potential when increasing redox sites on quartz crystal due to the autocatalytic effect of the Pani film as mentioned earlier.

The mass and charge change in the Pani film during its growth was also analysed, as shown in figure 6.16b. The mass of the Pani film began to increase at the polymerization potential (around 0.73 V), while positively charged in the first anodic oxidation. In the reversible scan, the charge of the film decreases, which turns into its insulating form. With sufficient cycles, the mass increase is accelerated, which is an indication of the autocatalytic effect of the Pani film deposited on the quartz crystal as mentioned above. The surface coverage and the thickness of unsolvated Pani film were determined by equation 3.1 and equation 3.2 mentioned in chapter 3 ($n = 1$ for the dimeric aniline unit). The surface coverage is 333.4 nmol cm⁻² whilst the thickness is 609 nm for the Pani film. Both value rapidly increases, indicating the electroactivity of the Pani film while it is getting an enlarger.

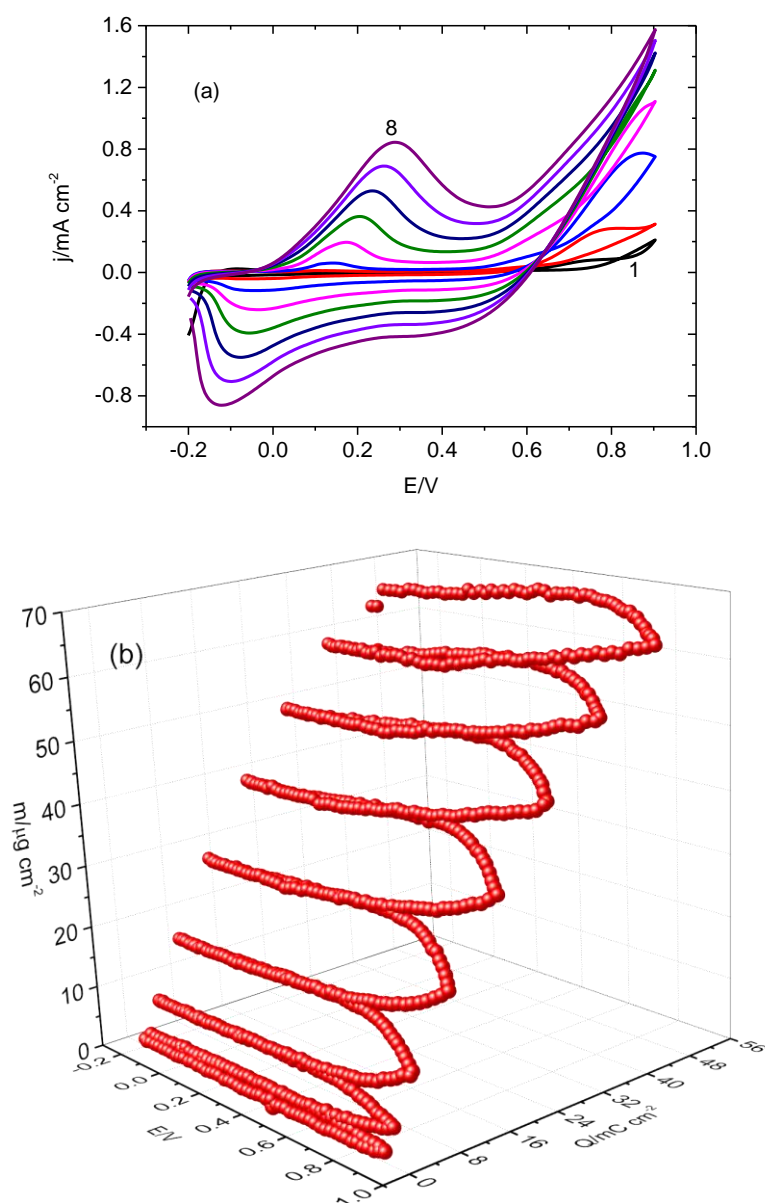


Figure 6.16. Electrochemical deposition of the Pani film from 1 M aniline and 0.5 M H_2SO_4 , the scan rate, $\nu = 5 \text{ mV s}^{-1}$ (a) the CV curve of the Pani film (b) the corresponding mass-charge change as a function of applied potential (Γ , $333.4 \text{ nmol cm}^{-2}$ for dimeric units)

A homogenous green film was observed at the end of deposition, as shown in figure 6.17.

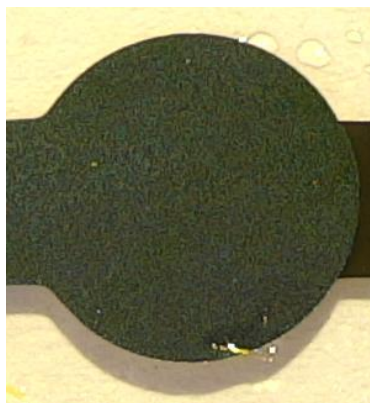


Figure 6.17. An image of the Pani film on Pt quartz crystal from figure 6.16

The mass-charge curves for the electrochemical deposition of the Pani film from figure 6.16 are plotted in figure 6.18, which show an almost linear increase in cycling. This indicates happening the electrochemical deposition of the Pani film in ETH400 with a high efficiency. The apparent molar mass, M_{app} , of the Pani film at the end of each scan is presented in table 6.3 (the apparent molar mass of the film was determined by equation 3.4 in chapter 3).

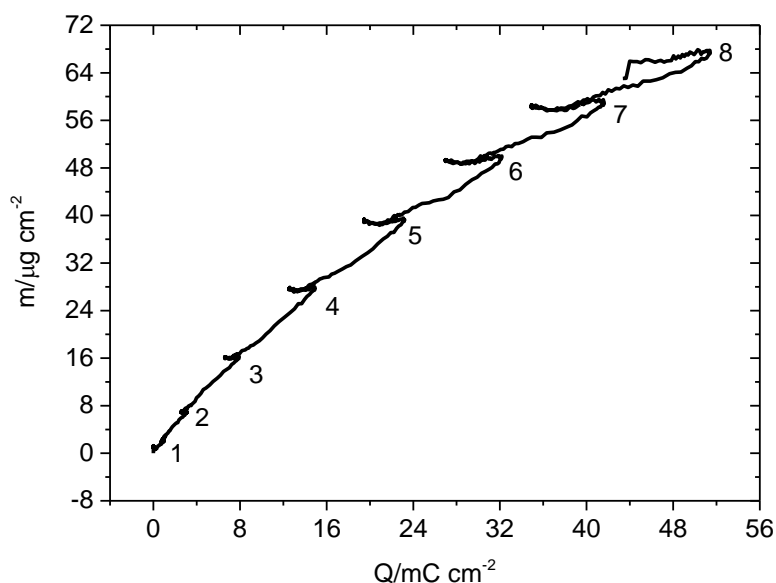


Figure 6.18. The mass-charge curve of the Pani film synthesised in ETH400 in figure 6.16 (the number indicates the cycle number)

The apparent molar mass values indicate a decrease with cycling while the mass density increases considerably. This is thought to arise due to the insertion of solvent molecules. As it can be seen in table 6.3, the content of the solvent in the Pani film decreases with

cycling. This can be explained that the formation of the Pani film is getting firm with cycling.

Table 6.3. Gravimetric data (obtained figure 6.18) for the Pani film growth in ETH400 (α is the solvent molecules taking place per redox sites of Pani film)

<i>Pani growth</i>	$M_{app}/gmol^{-1}$	α	$M/\mu g\ cm^{-2}$	$Q/mC\ cm^{-2}$
<i>scan 1</i>	89.9	0.5	1.9	1.02
<i>scan 2</i>	146.4	0.6	7.06	2.72
<i>scan 3</i>	83.8	0.5	15.9	7.81
<i>scan 4</i>	83.8	0.5	27.7	14.6
<i>scan 5</i>	65.6	0.4	39.4	23.2
<i>scan 6</i>	64.5	0.4	49.7	31.9
<i>scan 7</i>	45.7	0.4	58.7	41.4
<i>scan 8</i>	43.4	0.4	67.7	51.4

Furthermore, the acoustic data obtained for the Pani film deposition via EQCM were analysed. The admittance data for the growth of the Pani film in Ethaline is shown in figure 6.19, which suggests an approximate 44 % decrease in admittance after eight scans. A further 30% decrease results in the formation of a non-rigid film as we mentioned in chapter 4. At the same time, the ohmic resistance calculated by equation 3.6 mentioned chapter 3 was determined as 2100 Ω in the 8th scan, indicating high resistance behaviour with increasing cycling.

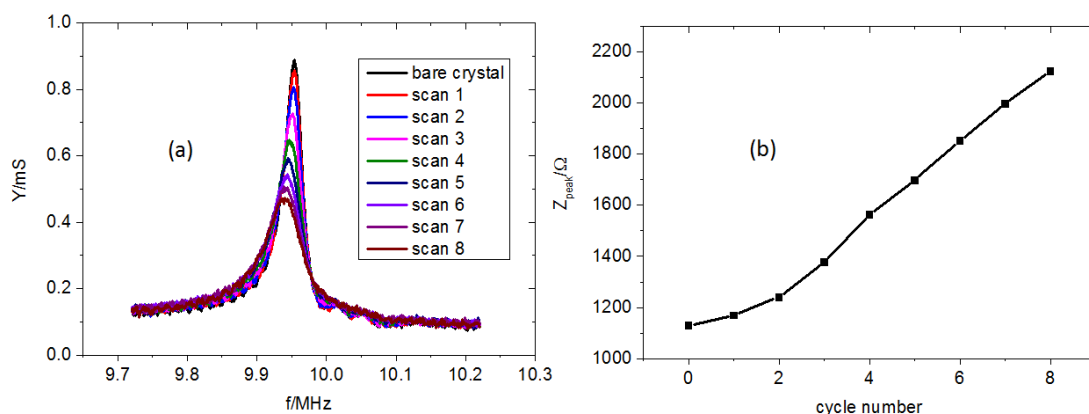


Figure 6.19. (a) Admittance data of the Pani film during growth (from figure 6.16) (b) the ohmic resistance of quartz crystal during the growth of the Pani film in ETH400

In further experiments, the electrochemical deposition of Pani film was performed with the addition of various concentrations of MWCNTs (0, 0.1, 0.2, 0.3, and 0.6 wt%) between -0.20 and 0.85 V at 5 mV s^{-1} . The acquired cyclic voltammograms are presented in figure 6.20 together with the corresponding mass-charge curves. Although the presence of MWCNTs enhances the current density of Pani film, the growth of Pani film occurs with lower efficiency in higher concentrations of MWCNTs (e.g., 0.6 wt%), as for the aqueous medium mentioned in the first part of this chapter. However, the addition of a small amount of MWCNTs not only improved the electroactivity but also provided for higher efficiency in the growth of Pani film compared to Pani/MWCNTs (0.1 wt%) and Pani/MWCNTs (0.2 wt%) films. The electrochemical and gravimetric data for Pani and Pani/MWCNTs films are presented in tables 6.4 and 6.5.

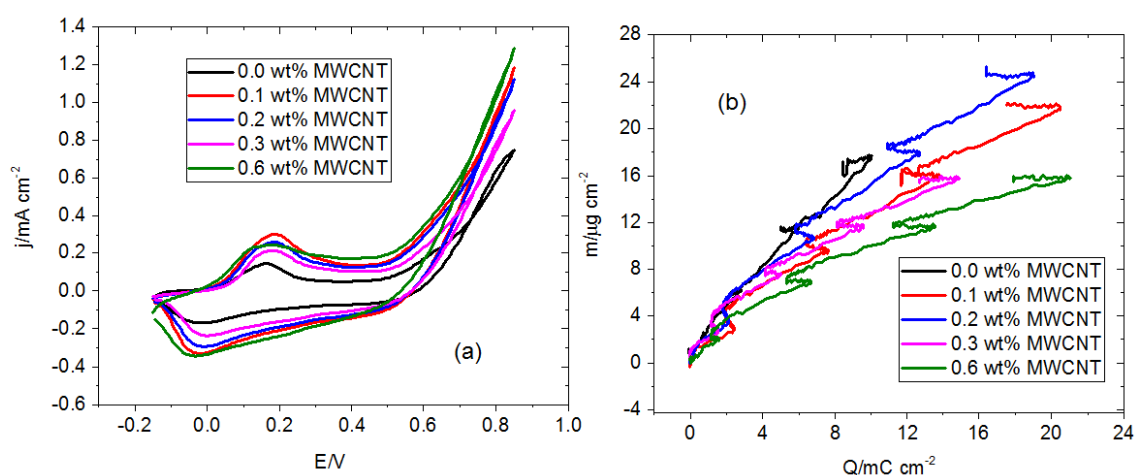


Figure 6.20. (a) CV curves of Pani film growth in the presence of various concentrations of MWCNTs, the scan rate, $v = 5 \text{ mV s}^{-1}$ (b) the corresponding mass-charge curves for the Pani films from figure 6.20a

Table 6.4. Electrochemical data obtained from 4th scans of Pani and Pani/MWCNTs films from figure 6.20

MWCNTs wt%	E/V			Q/mC		Γ/nmol cm^{-2}	h/nm
	E_{ox}	E_{red}	E_{IR}	Q_{anodic}	$Q_{cathodic}$		
0.0	0.16	-0.01	0.49	0.81	0.99	162.2	296
0.1	0.18	-0.01	0.51	3.68	4.80	337.9	617
0.2	0.17	-0.01	0.53	3.76	4.32	332.5	607
0.3	0.17	0	0.53	2.07	3.32	266.6	488
0.6	0.15	-0.03	0.51	4.26	5.36	239.7	438

Table 6.5. Gravimetric data obtained from curves of the Pani and the Pani/MWCNTs films from figure 6.20 (α is the solvent molecules taking place per redox sites of Pani)

<i>MWCNTs wt%</i>	<i>M_{app}/gmol⁻¹</i>	<i>α</i>	<i>M/$\mu\text{g cm}^{-2}$</i>	<i>Q/mC cm⁻²</i>
0.0	86.3	0.5	17.7	9.9
0.1	51.5	0.4	21.9	20.5
0.2	62.3	0.4	24.4	18.9
0.3	51.2	0.4	15.7	14.8
0.6	36.7	0.4	15.9	20.9

The surface coverage of Pani/MWCNTs composite films is much greater than pure Pani film synthesised under identical conditions in figure 6.20. This can arise from the dopant effect of MWCNT besides their electrical properties. The lower content of MWCNTs in the polymer film (0.1 wt%) provides both much more electroactive sites with an efficient deposition. However, the increasing level of MWCNTs (0.6 wt%) in the Pani film resulted in the low mass gaining but higher electroactive sites, implying lower efficiency than the Pani/MWCNTs film (0.1 wt%) but still much greater pure Pani synthesized under identical conditions. In the meantime, the apparent molar mass presented in table 6.5 decreased with the increasing level of MWCNTs whilst the content of solvent remained in the composited film, which is 0.4. The insertion of solvent decreases with the addition of MWCNTs, implying the change of structure of Pani film with MWCNTs such as porosity.

The detailed electrochemical data for the growth of the Pani/MWCNTs (0.2 wt%) film is shown in figure 6.21, showed a gradual increase in mass and charge of the Pani/MWCNTs composite film while the mass-charge curve is a linear change, implying an efficient coating of the composite film.

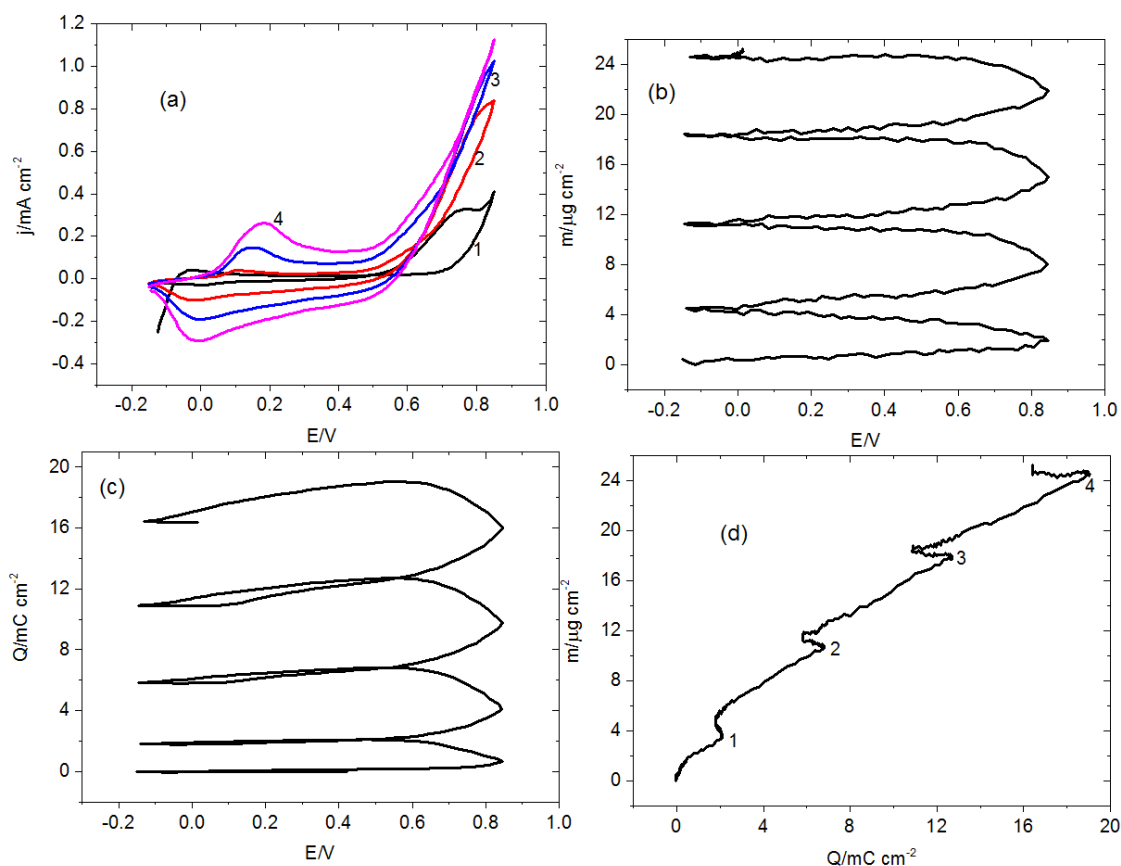


Figure 6.21. EQCM data of the Pani/MWCNTs (0.2 wt%) film growth (a) The CV curve of the Pani film from 1 M aniline and 0.5 M H₂SO₄ with 0.2 wt% MWCNTs, $v = 5 \text{ mV s}^{-1}$ (b) mass (c) charge change as a function of applied potential (d) the mass-charge curve

Admittance data for the growth of the Pani/MWCNTs (0.2 wt%) composite film is shown in figure 6.22, indicating the formation of a rigid composite film on the quartz crystal with a decrease of 28.1% in admittance. After the electrochemical deposition of Pani/MWCNTs (0.2 wt%) film, the admittance and ohmic resistance were measured as 0.69 mS and 1450 Ω , respectively in Ethaline.

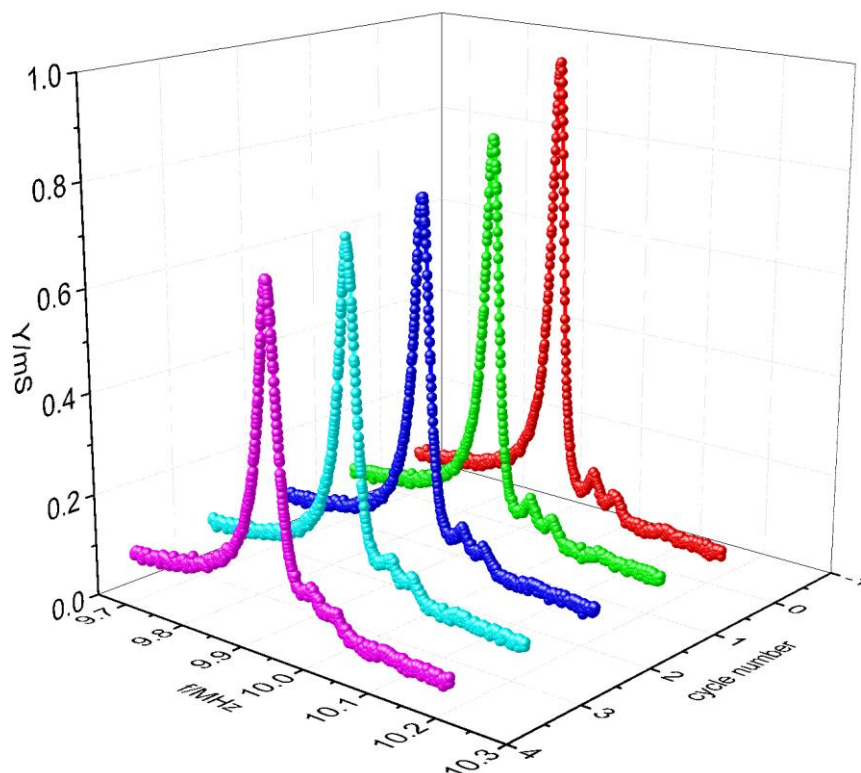


Figure 6.22. Admittance change against the quartz crystal frequency during the electrochemical deposition of the Pani/MWCNTs (0.2 wt%) film from figure 6.21

6.2.2.1. Charge and discharge characterisation of Pani/MWCNTs films

After deposition, the Pani and Pani/MWCNTs films were transferred to monomer-free 1 M H₂SO₄ in ETH200 and monomer-free ETH200 solutions in order to identify their electrochemical properties. Figure 6.23 shows the CV curves of the Pani film in 1 M H₂SO₄-ETH200. Over 19 cycles, there is a shift in the redox peaks (0.37/0.11V) to more positive potentials. This shift is greater for the first six cycles but reduces with continued cycling. On the other hand, when looking at the charge passed values (in table 6.10), there is a reversible change between the redox reactions. In the case of ETH200 without acid, cyclic voltammetry shows two distinctive peaks around at 0.1/0.4V that do not shift over 12 cycles. It behaves in a stable manner whilst showing electroactivity.

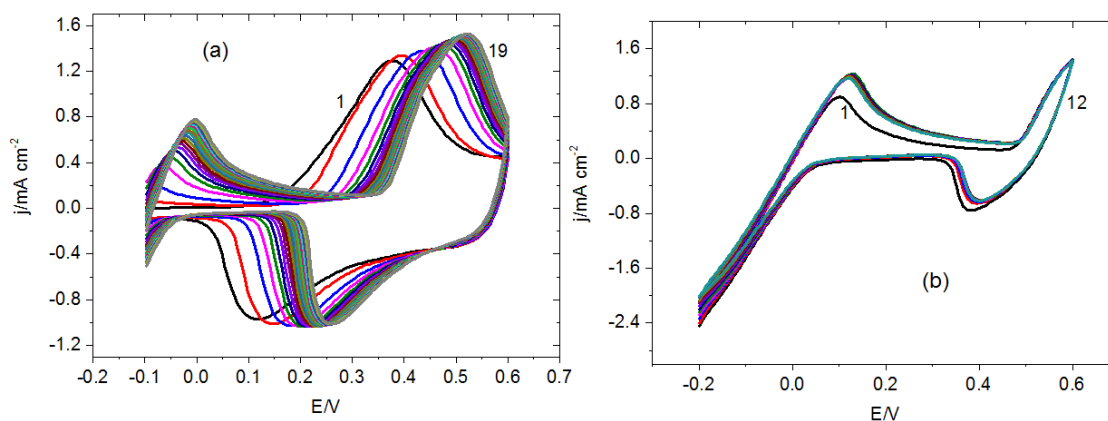


Figure 6.23. The electroactivity of the Pani film (a) in 1M H₂SO₄-ETH200 (b) in ETH200, the scan rate, $\nu = 5 \text{ mV s}^{-1}$

The corresponding mass change as a function of the applied potential is plotted in figure 6.24a, indicating a sudden increase over the first few cycles that subsequently reduces. This can be explained the insertion of a large number of anions but releases the small of them upon reduction. With continued cycling, they accumulated causing the saturation of the film sites. In the meantime, the change in charge over time was plotted, showing the charging, and discharging of the Pani film. The charging of the Pani film is reduced with continued cycles.

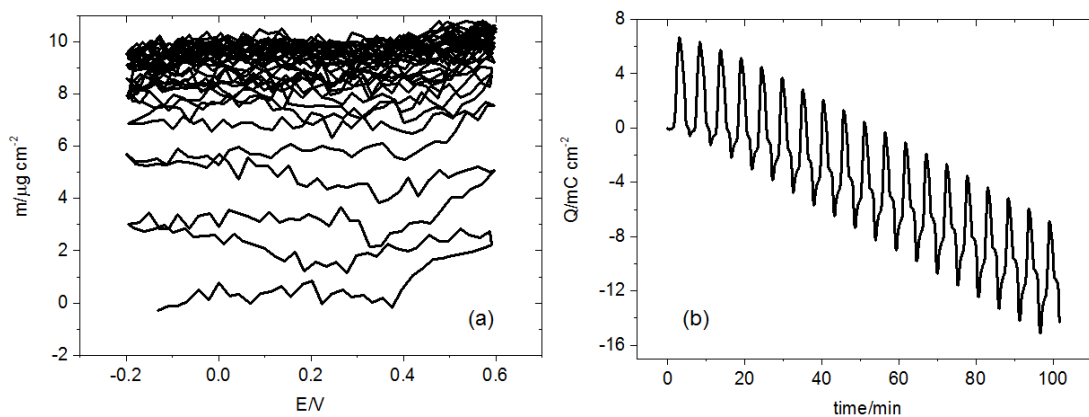


Figure 6.24. (a) the mass-E curves of the Pani film in 1M H₂SO₄-ETH200 (b) charge-discharge curve of the Pani film in 1M H₂SO₄-ETH200 (from figure 6.23a)

The electroactivity of the Pani and the Pani/MWCNTs (0.2 wt%) films synthesised between -0.2 to -0.85 V in figure 6.24 was represented in figure 6.25 for comparison. Although they are deposited under identical conditions, the Pani/MWCNTs film exhibit a stable electroactivity with higher current density. This gives supporting evidence as to the improvement of electroactivity and stability of the Pani film with the addition of MWCNTs. In addition, their redox peaks appear at different potentials. The Pani film

gives 0.38/0.35 V, while Pani/MWCNTs film gives 0.45/0.38 V. Electrochemical data obtained from figure 6.25 is presented in table 6.6. The surface coverage of Pani/MWCNTs film synthesised with 4 cycles in the presence of 0.2 wt% MWCNTs is smaller than Pani film synthesised with 8 cycles in figure 6.16 but much greater than Pani film synthesised under identical conditions. Plus, mass specific capacitance (MSC) determined by equation 3.7 mentioned in chapter 3 exhibits the improvement the capability of the Pani film with the addition of MWCNTs even than the Pani film synthesised with much more cycles (8 cycles in figure 6.16).

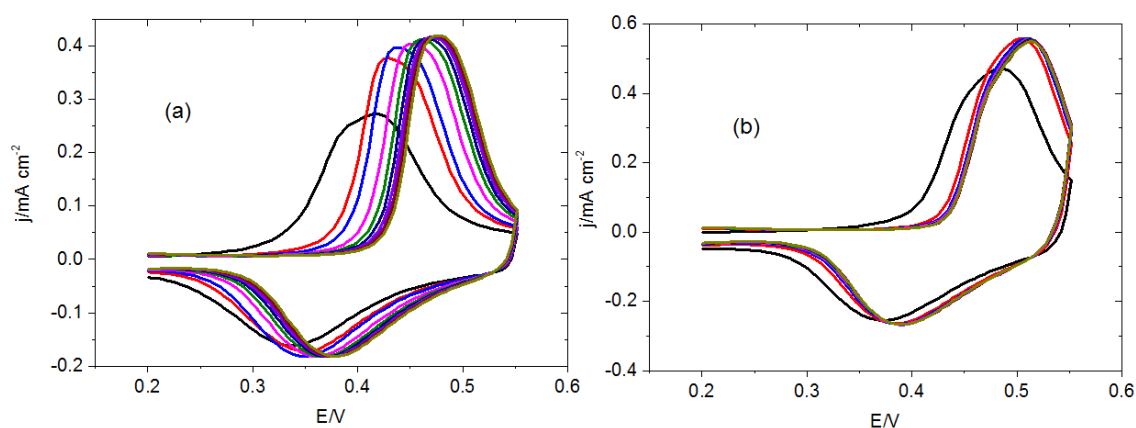


Figure 6.25. The electroactivity of the Pani and the Pani/MWCNTs (0.2 wt%) films synthesised under identical conditions (a) in 1 M H₂SO₄-ETH400 (b) in ETH400

Table 6.6. Electrochemical data obtained from voltammograms of the Pani and the Pani/MWCNTs films

<i>Electrolyte</i>	<i>Film</i>	<i>E/V</i>		<i>Q/mC</i>		<i>Γ/nmol cm⁻²</i>	<i>MSC/F g⁻¹</i>
		<i>E_{ox}</i>	<i>E_{red}</i>	<i>Q_{anodic}</i>	<i>Q_{cathodic}</i>		
<i>In 1M H₂SO₄-ETH200</i>	<i>Pani</i> (in figure 6.28)	0.37	0.11	8.98	8.12	401.9	805.9
	<i>Pani</i> (in figure 6.30)	0.41	0.33	1.18	1.11	50.0	792.8
	<i>Pani/MWCNTs</i> <i>Film</i> (in figure 6.30)	0.46	0.37	2.26	2.06	92.8	1170.1

The corresponding gravimetric data was presented in figure 6.26. The interesting point is here the behaviour of the Pani film because the mass decreases with cycling. On the other hand, the mass of the Pani/MWCNTs film increases with cycling. This increase is considerably greater over the first cycles but reduces with a large number of applied

cycles. This is an evidence of the influence of the MWCNTs on the electrochemical properties of the final films.

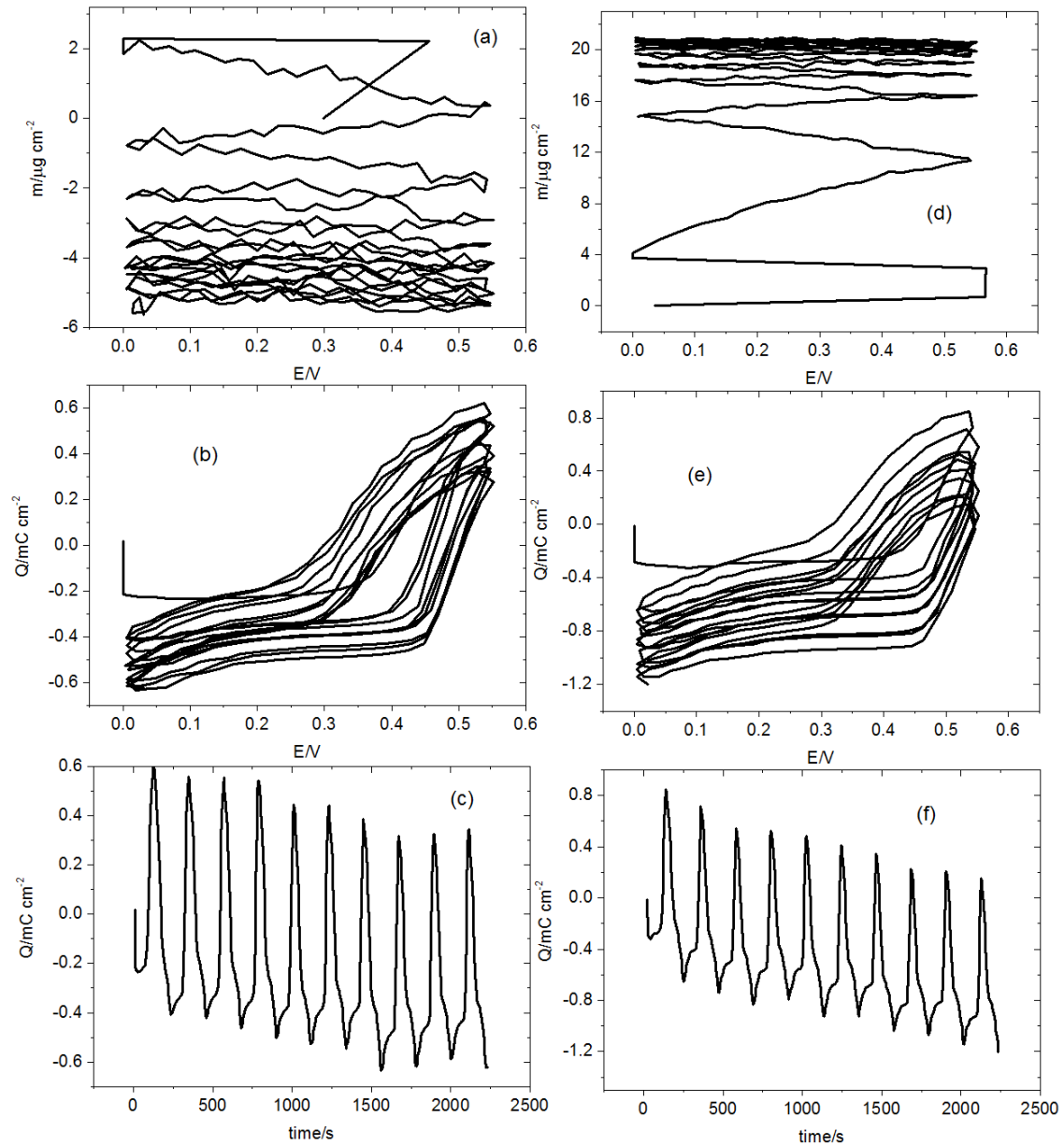


Figure 6.26. (a) the mass-E curves of the Pani and the Pani/MWCNTs (0.2 wt%) films in 1M H₂SO₄-ETH200 (b) charge-discharge curve of Pani and Pani/MWCNTs (0.2 wt%) films in 1 M H₂SO₄-ETH200 (c) mass-E curves of Pani and Pani/MWCNTs (0.2 wt%) films in ETH200 (d) charge-discharge curve of the Pani and the Pani/MWCNTs (0.2 wt%) films in ETH200

The ion activity of the Pani and the Pani/MWCNTs films were also investigated in monomer-free ETH200 without acid. Figure 6.27 shows the EQCM data for both films, indicating the Pani/MWCNTs film not only behaves in a stable manner but is also more ionic activity in comparison with pure Pani film. Furthermore, the reversible behaviour between charging and discharging of the Pani/MWCNTs film is quite remarkable. Here,

the Pani film exhibits higher current density but there are no obvious redox peaks. On the other hand, the Pani/MWCNTs film provides both certain redox peaks at 0.3/0.25 V and reversible change charging and discharging between redox reactions.

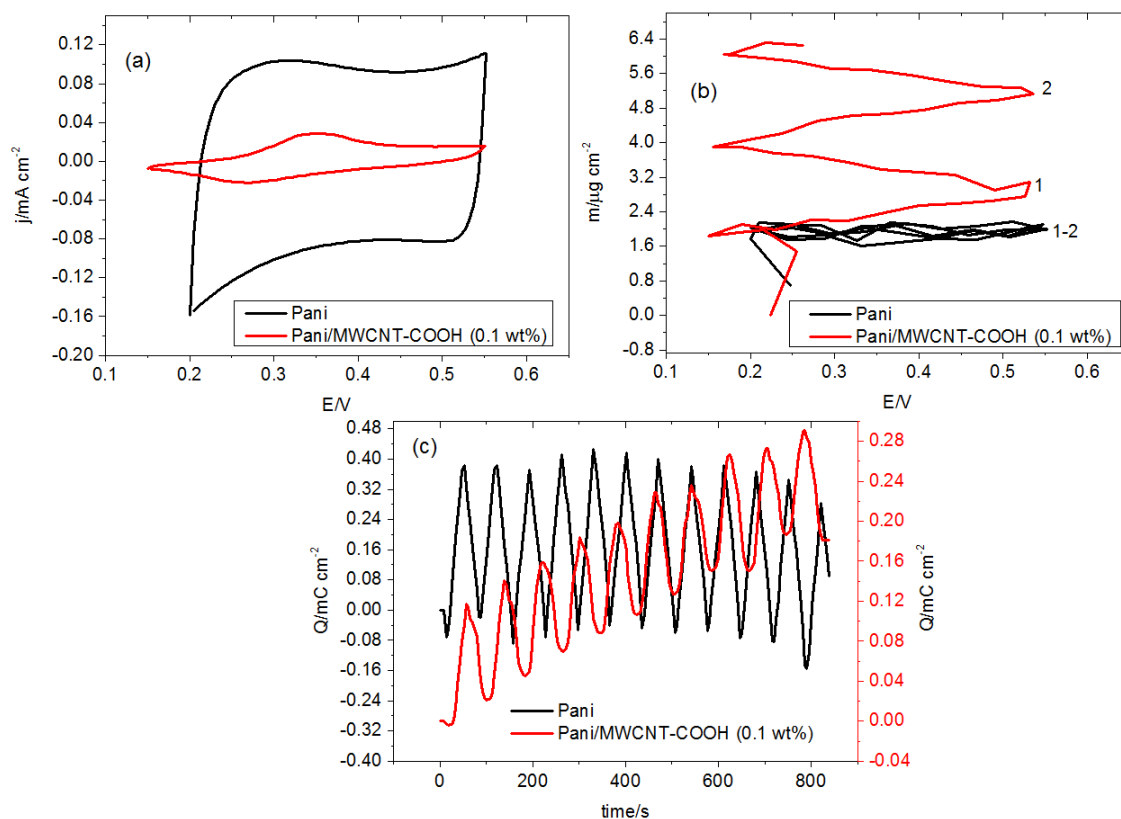


Figure 6.27. EQCM data for the Pani and the Pani/MWCNTs (0.2 wt%) films in monomer-free ETH200, the scan rate, $v = 5\ mV\ s^{-1}$ (a) the CV curves (b) mass change of the films as a function of applied potential (c) charging and discharging of the films under identical conditions

6.2.3.2. Surface characterisation of the Pani and the Pani/MWCNTs films

The surfaces of the Pani and Pani/MWCNTs films synthesised from Ethaline were also explored using SEM, as shown in figures 6.32 and 6.33. The Pani film gives an image that shows the existence of ‘starfish-like’ growths at various points on the quartz crystal.

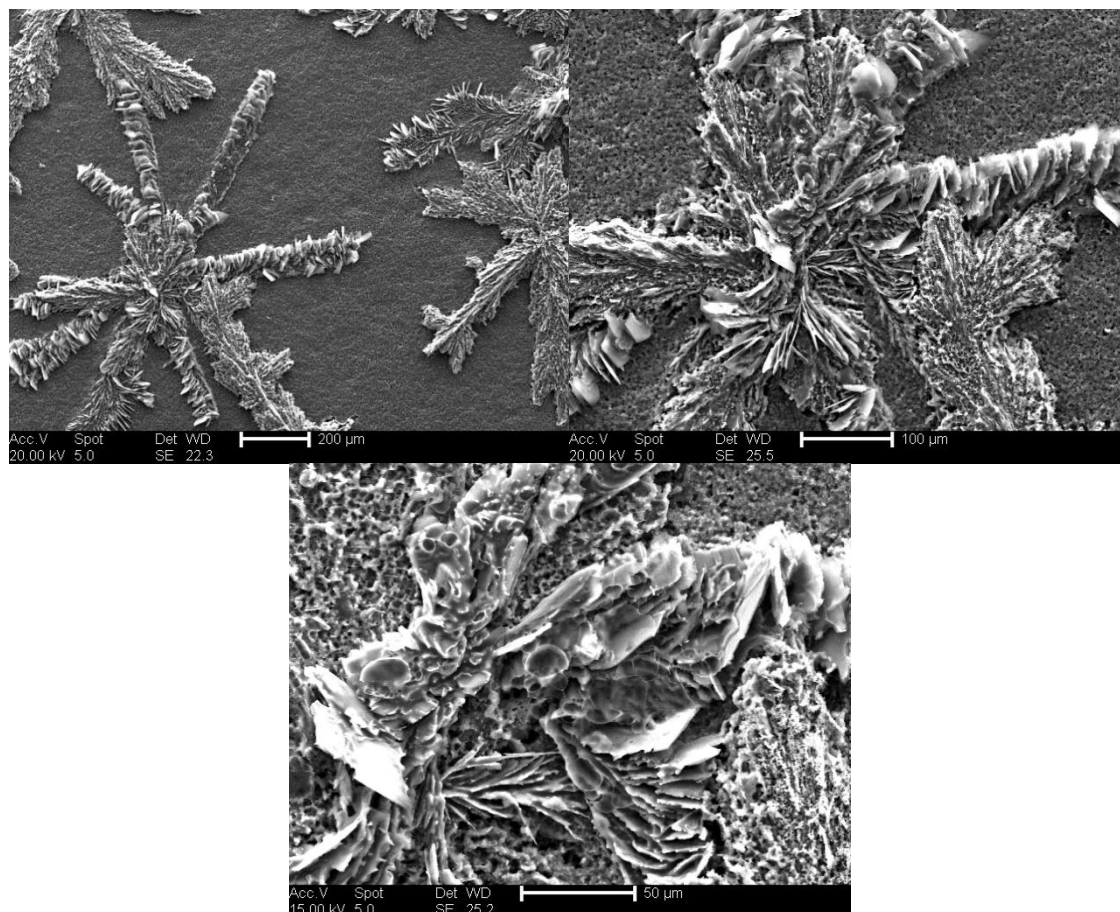


Figure 6.28. SEM images of the Pani film at different magnifications

The addition of MWCNTs to the aniline monomer solution affects the surface of the resultant composite film as shown in figure 6.29. The composite film gives a uniform surface with a high porosity. This is an indication of the strong interaction between the monomer and MWCNTs, resulting in a different distribution of polymer film through the quartz crystal.

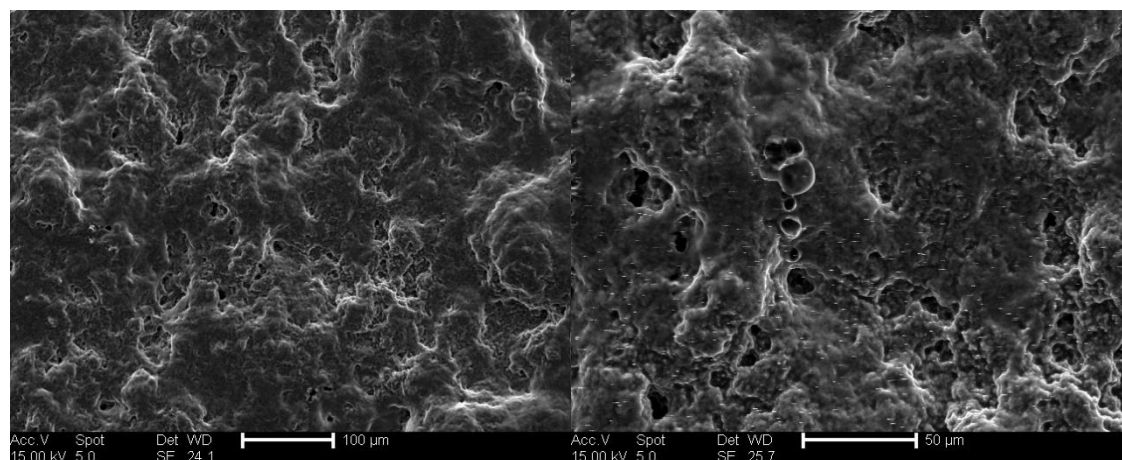


Figure 6.29. SEM images of the Pani/MWCNTs film at different magnifications

Figure 6.30 shows 3D images of the Pani and the Pani/MWCNTs films grown in Ethaline. There is a clear difference between them in terms of their colour and surface.

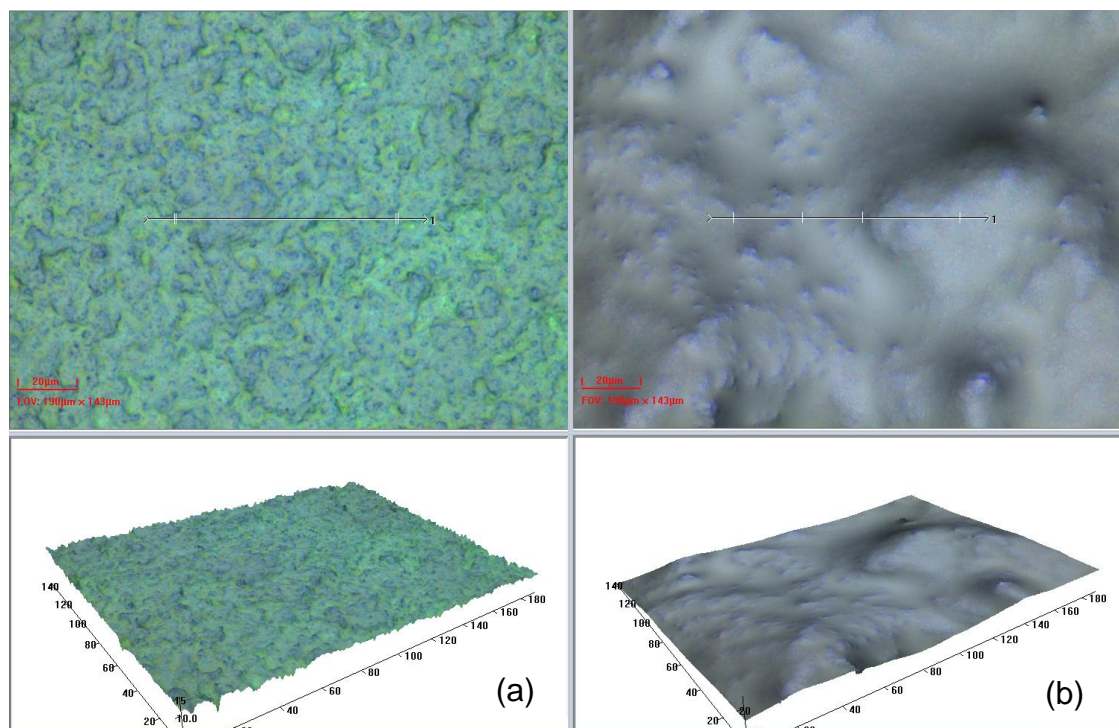


Figure 6.30. 3D images of (a) the Pani and (b) the Pani/MWCNTs films grown in Ethaline

6.2.3. FTIR

Since the discovery of CNTs, several studies have been devoted to the investigation of the vibrational properties via infrared techniques. However, both SWCNT and MWCNT do not have permanent dipole moments, with the infrared activity instead related to the dynamic dipole moments arising from non-symmetric vibrations.

Figure 6.31 shows the FTIR spectrum of the Pani and Pani/MWCNT films. In the case of the Pani film, the absorptions at 1583.5 and 1500.3 cm^{-1} are attributed to C-C aromatic stretching vibrations, which are common to all films. The absorption at 1310.3 cm^{-1} is assigned to the vibrational modes of C-N aromatic amines while the absorption at 1156.0 cm^{-1} is attributed to C-H in alkyl halides and C-C aliphatic amines. The final absorption band appears at 820.0 cm^{-1} and is attributed to aromatic C-H vibrations, and are also common to all films. In the case of the Pani/MWCNTs film, the absorptions at 1369.3 cm^{-1} and at 1275.0 cm^{-1} are attributed to alkene C-H vibrations and the C-O in carboxylic acid, respectively. The latter vibrational modes at 1082.7 cm^{-1} and 924.7 cm^{-1}

¹ are associated with the C-N vibration of aliphatic amines and O-H of a carboxylic acids, respectively. This shows the content of the MWCNTs, providing by the appearance of vibrational features specific to C-O (carboxylic acid).

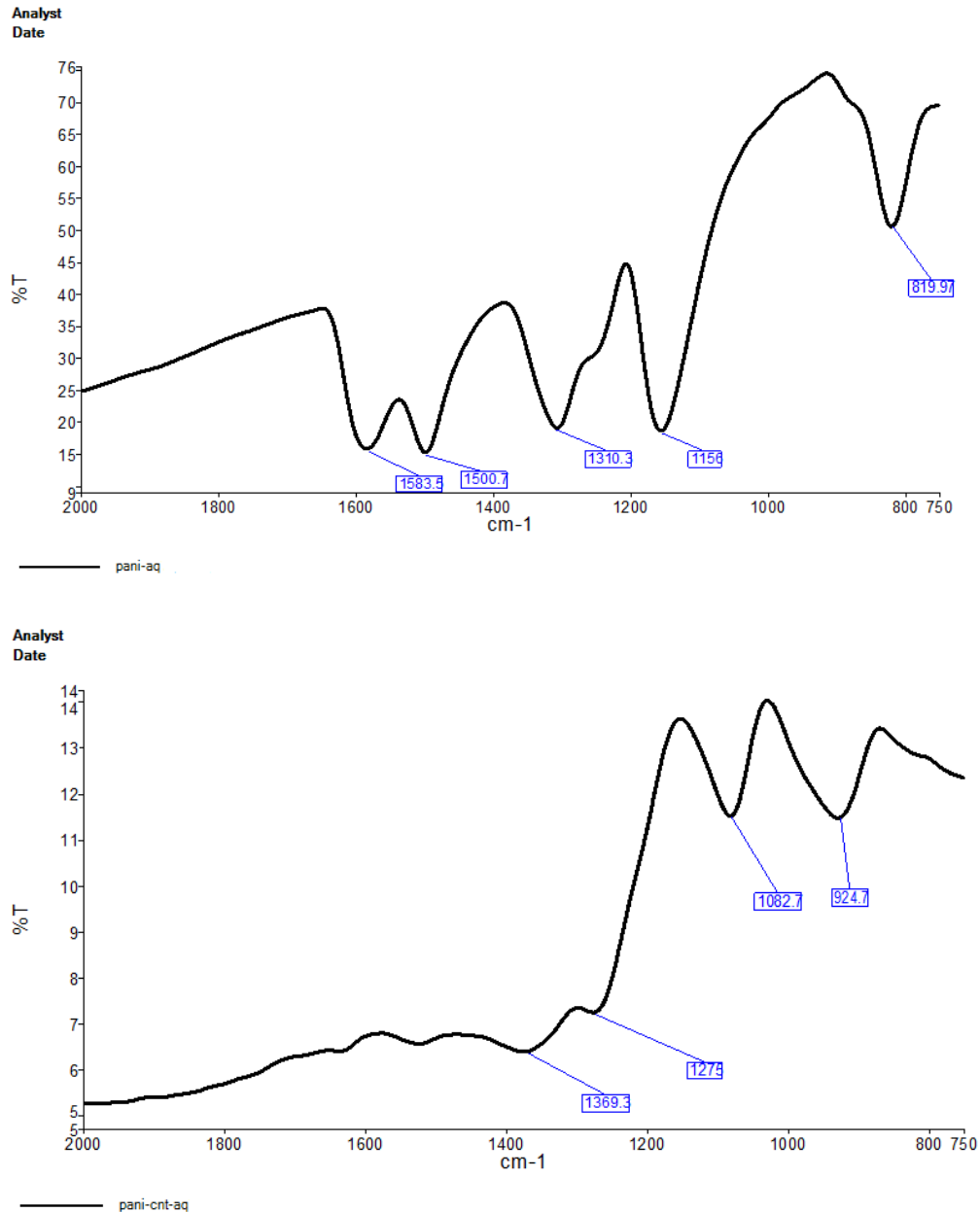


Figure 6.31. The FTIR spectra of the Pani and the Pani/MWCNTs films from aqueous medium

Figure 6.32 shows the FTIR spectra of the Pani and the Pani/MWCNTs films generated in Ethaline. The absorptions at $1800\text{--}1700\text{ cm}^{-1}$, at $1300\text{--}1200\text{ cm}^{-1}$ and $1100\text{--}1000\text{ cm}^{-1}$ are attributed to C=O, C-H, and C-N, respectively which are commonly observed in the other films vibrational modes. There is no significant difference between the spectra for

the Pani and the Pani/MWCNT films, reflecting MWCNTs does not show any IR activity.

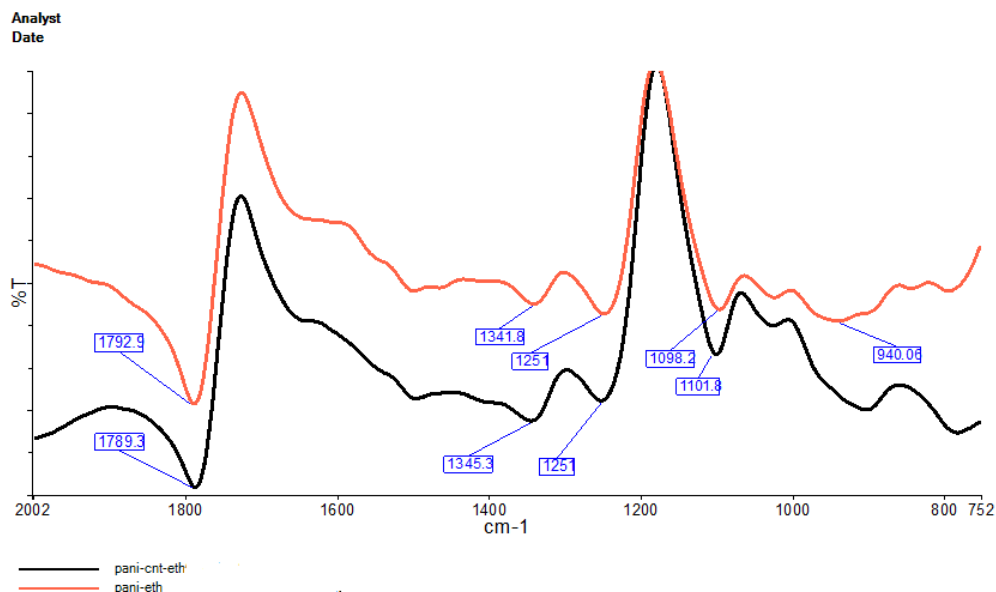


Figure 6.32. The FTIR spectra of the Pani and the Pani/MWCNTs films formed from Ethaline

6.3. Conclusion

In this chapter, the effects of MWCNTs on the electrochemical polymerization of aniline and the electrochemical properties of the resultant composite films in aqueous and non-aqueous (Ethaline) media were investigated. Initially, we functionalized the walls of the MWCNTs in concentrated HNO₃ to provide a strong interaction with aniline monomers.

We first studied the electrochemical polymerization of aniline in an aqueous medium to gain information on the growth dynamics of Pani/MWCNTs composite films. The results show good agreement with the literature,^{5, 6} which implied a considerable improvement in electroactivity compared to the pure Pani film. However, we found significant evidence of the decreasing mass loading of polyaniline in the presence of MWCNTs. Additionally, the concentration of H₂SO₄ plays a significant role in increasing the effects of MWCNTs. At higher concentrations of H₂SO₄ (1 M), the interaction between the aniline monomer and MWCNTs is extremely weak. Lower concentrations of H₂SO₄ provide for an increase in this interaction, resulting in an increase in the amount of charge passed. Both the Pani and the Pani/MWCNTs films

were deposited on a quartz crystal via EQCM under optimal conditions. The Pani and the Pani/MWCNTs films generated in aqueous medium show lower efficiency because the apparent molar masses of the Pani and the Pani/MWCNTs films are 63.1 g mol^{-1} and 5.8 g mol^{-1} , respectively.

In further experiments, the electrochemical deposition of Pani and Pani/MWCNTs films was studied in Ethaline via cyclic voltammetry, chronoamperometry and EQCM. The results of these studies show the electrochemical behaviour of Pani film in the presence of MWCNTs was influenced in a similar manner. The apparent molar masses of the Pani and the Pani/MWCNTs (0.2 wt%) film generated from Ethaline with 4 (figure 6.20) were determined to be 86.3 g mol^{-1} and 51.5 g mol^{-1} , respectively. Also, the addition of the sulphuric acid (99.9 %) also adds a small amount water to the Ethaline, decreasing its viscosity.²⁷ The percentage of water in the monomer solution in ETH400 was determined as 11.2%.

The characterisation of the electrochemical properties of the Pani and the Pani/MWCNTs (0.2 wt%) films generated from Ethaline were explored in their background solutions. The Pani/MWCNTs (0.2 wt%) film in a monomer-free acidic medium (figure 6.25) showed more stable behaviour and high electroactivity with respect to the Pani film generated from Ethaline. Additionally, the electroactivity of the Pani/MWCNTs (0.2 wt%) film in ETH200 was examined, suggesting a superior electroactivity with obvious redox peaks. The surface coverage of Pani was enlarged from $162.2 \text{ nmol cm}^{-2}$ to $332.5 \text{ nmol cm}^{-2}$ with the addition of 0.2 wt% MWCNTs under identical conditions, while they show reversible behaviour between their redox reactions. The mass-specific capacitance (MSC) values of the Pani and the Pani/MWCNTs (0.2 wt%) films synthesised from Ethaline were determined to be $792.8 \pm 10.5 \text{ F g}^{-1}$ and $1170.1 \pm 44.7 \text{ F g}^{-1}$, respectively. The reports in the literature suggest that the theoretical specific capacitance of polyaniline is 750 F g^{-1} , but was actually found to be 240 F g^{-1} when synthesized from an aqueous medium.²⁸ Similarly, the mass-specific capacitance of the Pani/MWCNTs composite film synthesised from aqueous medium is reported as being 670 F g^{-1} .²⁹ Additionally, the maximum specific capacitance of graphene materials such as supercapacitors was reported to be 205 F g^{-1} in the literature.³⁰ All the above cases demonstrate that the addition of MWCNTs to

polyaniline film in Ethaline enhanced the mass-specific capacitance, which is promising for future energy storage devices.

The morphologies of the resultant Pani/MWCNTs films produced from aqueous medium were also different to that of pure Pani film, showing a non-homogenous coating over the quartz crystal with a rough surface. The existence of this roughness at certain regions of the quartz crystal and the SEM images may indicate that electrochemical polymerization had taken place on the walls of the MWCNTs. The lower efficiency of the mass loading and the poor quality of the resultant films were enhanced by the Ethaline solvent; Ethaline provides a high-quality Pani/MWCNTs composite film coating with higher electroactivity (figure 6.29 and 6.30)

Finally, we investigated the effects of MWCNTs on the structure of polyaniline via FTIR. FTIR revealed that the existence of MWCNTs in polymer films can be demonstrated by the vibrational features at 1082.7 cm^{-1} and 924.7 cm^{-1} , which are attributed to the carboxylic acid group on the Pani/MWCNTs film generated in an aqueous medium. However, the spectra of the Pani and Pani/MWCNTs films synthesized in Ethaline were highly similar, and there is no specific vibration by which to determine the presence of MWCNTs. This could mean that the MWCNTs might not show IR activity in this medium.

6.4. References

- 1 C. C. Hu and C. H. Chu, *Material Chemistry Physics*, 2000, **65**, 329-338 (DOI:10.1016/S0254-0584(00)00254-6).
- 2 R. V. Salvatierra, M. M. Oliveira and A. J. G. Zarbin, *Chemistry of Materials*, 2010, **22**, 5222-5234 (DOI:10.1021/cm1012153).
- 3 N. Gospodinova and L. Terlemezyan, *Progress in Polymer Science*, 1998, **23**, 1443-1484 (DOI:10.1016/S0079-6700(98)00008-2).
- 4 C. Peng, S. Zhang, D. Jewell and G. Z. Chen, *Progress in Natural Science-Materials International*, 2008, **18**, 777-788 (DOI:10.1016/j.pnsc.2008.03.002).
- 5 J. E. Huang, X. H. Li, J. C. Xu and H. L. Li, *Carbon*, 2003, **41**, 2731-2736 (DOI:10.1016/S0008-6223(03)00359-2).

- 6 D. J. Guo and H. L. Li, *Journal of Solid State Electrochemistry*, 2005, **9**, 445-449 (DOI:10.1007/s10008-004-0589-7).
- 7 X. Luo, A. J. Killard, A. Morrin and M. R. Smyth, *Analytica Chimica Acta*, 2006, **575**, 39-44 (DOI:10.1016/j.aca.2006.05.064).
- 8 M. Q. Wu, G. A. Snook, V. Gupta, M. Shaffer, D. J. Fray and G. Z. Chen, *Journal of Materials Chemistry*, 2005, **15**, 2297-2303 (DOI:10.1039/b418835g).
- 9 R. B. Mathur, S. Chatterjee and B. P. Singh, *Composites Sci. Technol.*, 2008, **68**, 1608-1615 (DOI:10.1016/j.compscitech.2008.02.020).
- 10 C. Zhong, Y. Deng, W. Hu, J. Qiao, L. Zhang and J. Zhang, *Chemical Society Review*, 2015, **44**, 7484-7539 (DOI:10.1039/c5cs00303b).
- 11 P. Pieta, G. M. Venukadasula, F. D'Souza and W. Kutner, *Journal of Physical Chemistry C*, 2009, **113**, 14046-14058 (DOI:10.1021/jp903891v).
- 12 S. K. Mondal, K. Barai and N. Munichandraiah, *Electrochimica Acta*, 2007, **52**, 3258-3264 (DOI:10.1016/j.electacta.2006.09.067).
- 13 Y. Ju, G. Choi, H. Jung and W. Lee, *Electrochimica Acta*, 2008, **53**, 5796-5803 (DOI:10.1016/j.electacta.2008.03.028).
- 14 H. Zengin, W. S. Zhou, J. Y. Jin, R. Czerw, D. W. Smith, L. Echegoyen, D. L. Carroll, S. H. Foulger and J. Ballato, *Advanced Materials*, 2002, **14**, 1480-+ (DOI:10.1002/1521-4095(20021016)14:203.0.CO;2-O).
- 15 G. Z. Chen, M. S. P. Shaffer, D. Coleby, G. Dixon, W. Z. Zhou, D. J. Fray and A. H. Windle, *Advanced Materials*, 2000, **12**, 522-+ (DOI:10.1002/(SICI)1521-4095(200004)12:73.0.CO;2-S).
- 16 M. A. Atieh, O. Y. Bakather, B. Al-Tawbini, A. A. Bukhari, F. A. Abuilawi and M. B. Fettouhi, *Bioinorganic Chemistry and Applications*, 2010, , 603978 (DOI:10.1155/2010/603978).
- 17 P. Gajendran and R. Saraswathi, *Pure and Applied Chemistry*, 2008, **80**, 2377-2395 (DOI:10.1351/pac200880112377).
- 18 J. Wang, J. H. Dai and T. Yarlagadda, *Langmuir*, 2005, **21**, 9-12 (DOI:10.1021/la0475977).
- 19 P. M. V. Fernandes, J. M. Campina, C. M. Pereira and F. Silva, *Journal of Electrochemical Society*, 2012, **159**, G97-G105 (DOI:10.1149/2.059209jes).
- 20 K. P. Prathish, R. C. Carvalho and C. M. A. Brett, *Electrochemistry Communications*, 2014, **44**, 8-11 (DOI:10.1016/j.elecom.2014.03.026).
- 21 A. R. Hillman, K. S. Ryder, V. C. Ferreira, C. J. Zaleski and E. Vieil, *Electrochimica Acta*, 2013, **110**, 418-427 (DOI:10.1016/j.electacta.2013.07.120).

22 Q. Zhang, K. D. O. Vigier, S. Royer and F. Jerome, *Chemical Society Review*, 2012, **41**, 7108-7146 (DOI:10.1039/c2cs35178a).

23 G. A. Snook, P. Kao and A. S. Best, *Journal of Power Sources*, 2011, **196**, 1-12 (DOI:10.1016/j.jpowsour.2010.06.084).

24 H. Miyagawa, M. Misra and A. K. Mohanty, *Journal of Nanoscience and Nanotechnology*, 2005, **5**, 1593-1615 (DOI:10.1166/jnn.2005.181).

25 M. Miras, C. Barbero, R. Kotz and O. Haas, *Journal of Electroanalytical Chemistry*, 1994, **369**, 193-197 (DOI:10.1016/0022-0728(94)87098-5).

26 AP. Abbott, K El. Taaib, G. Fresh, KJ. McKenzie and K. Ryder, *Physical Chemistry, and Chemical Physics*, 2009, **11**, 4269-4277 (DOI: 10.1039/b81788tj)

27 E. L. Smith, A. P. Abbott and K. S. Ryder, *Chemical Reviews*, 2014, **114**, 11060-11082 (DOI:10.1021/cr300162p).

28 A. Snook, Pon Kao, and Adam S. Best, *Journal of Power Sources*, 2011, **196**, 1-12

29 C. Peng, S. Zhang, D. Jewell, and G. Chen, *Progress in Natural Science*, 2008, **18**, 777-788

30 Y. Wang, Z. Shi, Y. Huang, Y. Ma, C. Wang, M. Chen, and Y. Chen, *American Chemical Society*, 2009, **113**, 13103-13107 (DOI: 10.1021/jp902214f).

Chapter VII:

The enhancement of electrochemical stability of PPy with MWCNTs in aqueous and non-aqueous media

7.1. Introduction

7.1.1. Overview

The previous study is related the electrochemical deposition of aniline in MWCNTs in chapter 6. Here, we utilized another conducting polymer, polypyrrole (PPy), obtained from the pyrrole monomer shown in figure 7.1, which shows excellent reversibility between redox reactions, and chemical stability. In contrast to Pani, an acidic medium is not required for the deposition of PPy to proceed.^{1, 2} Therefore, the MWCNTs are well dispersed through the solution, allowing for a stronger interaction between the monomer and CNTs.

As mentioned in chapter 7, MWCNTs were functionalised³ in concentrated HNO₃ before conduction the electrochemical experiments for PPy/MWCNTs (the functionalisation of the wall of MWCNT was mentioned in detail in chapter 3). Therefore, MWCNTs can behave as a dopant anion during the electrochemical polymerization of pyrrole,⁴ as illustrated in figure 7.1.

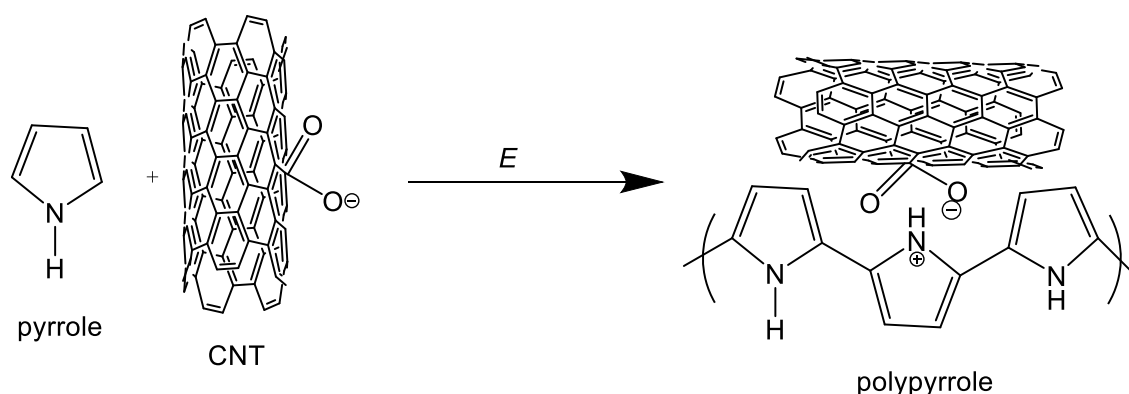


Figure 7.1. An illustration of MWCNTs as a dopant anion during the electrochemical deposition

7.1.2. Aims and Objectives

The objectives of this chapter are: (i) the electrochemical deposition of pyrrole in the presence of different ratios of MWCNTs in aqueous medium; (ii) investigation of the growth dynamics of PPy and PPy/MWCNT films by means of EQCM; (iii) the characterisation of the charge transport process of the PPy and PPy/MWCNTs films in monomer-free electrolyte solutions; (iv) defining the charge and discharge characteristics of the resultant composite films; (v) the electrochemical deposition of pyrrole in the presence of different ratios of MWCNTs in Ethaline; (vi) investigation of the growth dynamics of PPy and PPy/MWCNT films by means of EQCM in Ethaline; (vii) characterisation of the charge transport process of the PPy and PPy/MWCNTs films in monomer-free Ethaline; (viii) defining the charge and discharge characteristics of the resultant composite films; (ix) identifying of the surface morphologies of the resulting composite films of PPy/MWCNT from aqueous and non-aqueous media by means of SEM and 3D microscopy techniques; (x) structural analysis of the resulting polymer and composite film via FTIR.

7.2. Results and Discussions

7.2.1. Electrochemical deposition of PPy films in the presence of MWCNTs in aqueous medium

The electrochemical deposition of PPy films can proceed in the presence of counterions, and NaCl without acid, differently from Pani. Figure 7.2 shows the CV curves of the growth of PPy film in the absence/presence of MWCNTs from a solution consisting of 0.1 M pyrrole and 0.2 M NaCl without/with 5 wt% MWCNTs between -0.6 and 0.7 V over 13 cycles at 10 mV s⁻¹. Both display a broad anodic and a broad cathodic peak between -0.4 V and 0.4 V in their respective voltammograms, whilst showing irreversible peaks at 0.62 V and 0.56 V, respectively. These potentials are attributed to the oxidation of the pyrrole monomer on the surface of the working electrode. As can be seen, the oxidation of the pyrrole monomer occurs at a more positive potential in the presence of MWCNTs but at a higher current density. The charge passed is calculated from the voltammograms of PPy and PPy/MWCNTs films are 2.46 mC and 18.3 mC, respectively, upon oxidation (A is 0.23 cm² and $n = 0.33$ for pyrrole). This indicates the

huge influence of MWCNTs on the amount of charge passed during PPy film growth. These results show good agreement with the literature.⁴

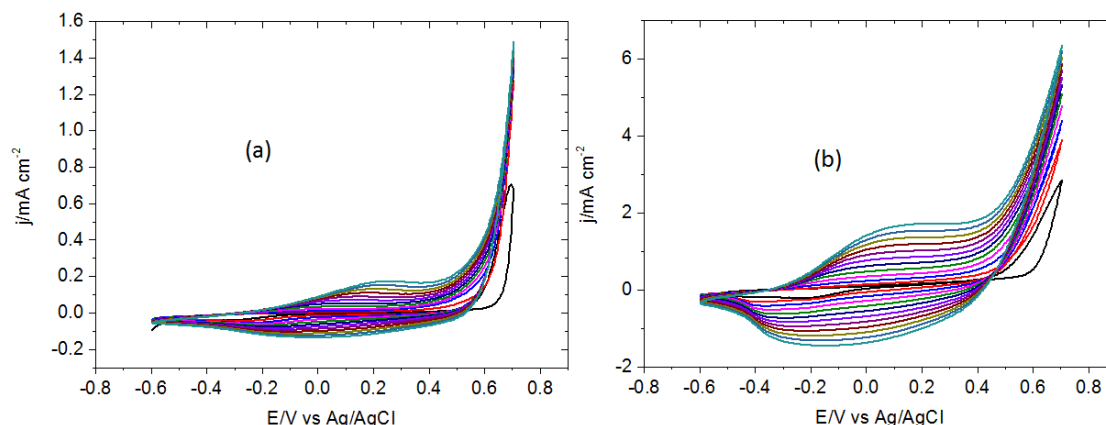


Figure 7.2. Electrochemical deposition of PPy film from (a) 0.1 M PPy and 0.1 M NaCl; (b) 0.1 M PPy and 0.2 M NaCl in presence of 5 wt% MWCNTs; $v = 10 \text{ mV s}^{-1}$

To obtain a deeper understanding of the effects of MWCNTs on the growth of PPy film, the electrochemical deposition of PPy films was studied via chronoamperometry in the presence of the different ratios of MWCNTs (0, 1, 3, 6, 10 and 15 wt%, respectively). Figure 7.3 shows the results of the chronoamperometry experiments.

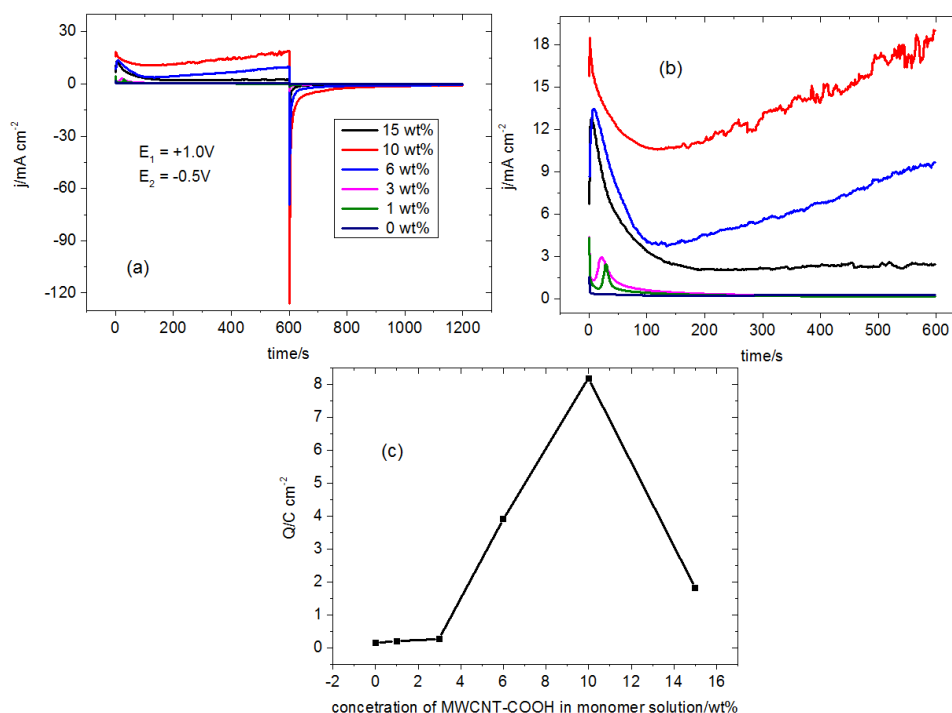


Figure 7.3. (a) Electrochemical deposition of PPy films from 0.1 M pyrrole and 0.1 M NaCl in presence of various concentrations of MWCNTs at 1.0 V and reduction of the coated films at -0.5 V (b) a detailed representation of anodic deposition of PPy film at 1.0 V (c) the charge passed during the electrochemical deposition of PPy films against the concentration of MWCNTs in monomer solution from figure 7.3a

Regarding the results, the charge passed rapidly increases with the amount of MWCNTs until some critical point, after which it begins to reduce. This suggests that the amount of MWCNTs should fix at some point to increase its contribution to electrochemical properties. On the other hand, the reason for this decrease after a certain concentration of MWCNTs is present can be explained through the prevention of the migration of monomers to the surface of the working electrode.

As can be seen from the results obtained by each of these two different techniques – cyclic voltammetry and chronoamperometry – the electrochemical polymerization of pyrrole was affected by the presence of MWCNTs. The addition of MWCNTs enhances the amount of charge passed during the growth of PPy film. However, the mass loading of the PPy/MWCNTs film still remains uncertain. In order to gain information on the mass loading and charge change of the growth of PPy/MWCNTs, film the EQCM technique was employed.

Figure 7.5 shows the EQCM data for the electrochemical deposition of PPy films from a solution consisting 0.1 M pyrrole and 0.1 M NaCl in the absence/presence of 5 wt% MWCNTs from between -0.5 V and 1.0 V at 10 mV s⁻¹. There is a significant outcome to this experiment in that the lower concentrations of NaCl cause the polymerization potential and the peak potentials to shift more positive potential. Meanwhile, the effects of MWCNTs exhibit certain similarities in terms of the mass and charge change of the polymer and composite film during their growth. After the deposition of the PPy film, a homogenous black film was observed on the quartz crystal, as shown in figure 7.5. The surface coverage of the PPy film was determined as 539.4 nmol cm⁻² while it is 2396.4 nmol cm⁻² for the PPy/MWCNTs film using equation 3.1.

The corresponding mass and charge change also revealed certain characteristics of the PPy and the PPy/MWCNTs film growth. The mass density of the PPy film is about 330 μg cm⁻², while it is around 20 μg cm⁻² for the PPy/MWCNTs film under same experimental conditions. This means the addition of MWCNTs (5 wt%) reduces the efficiency of PPy film deposition while increasing the charge passed by around a factor of two.

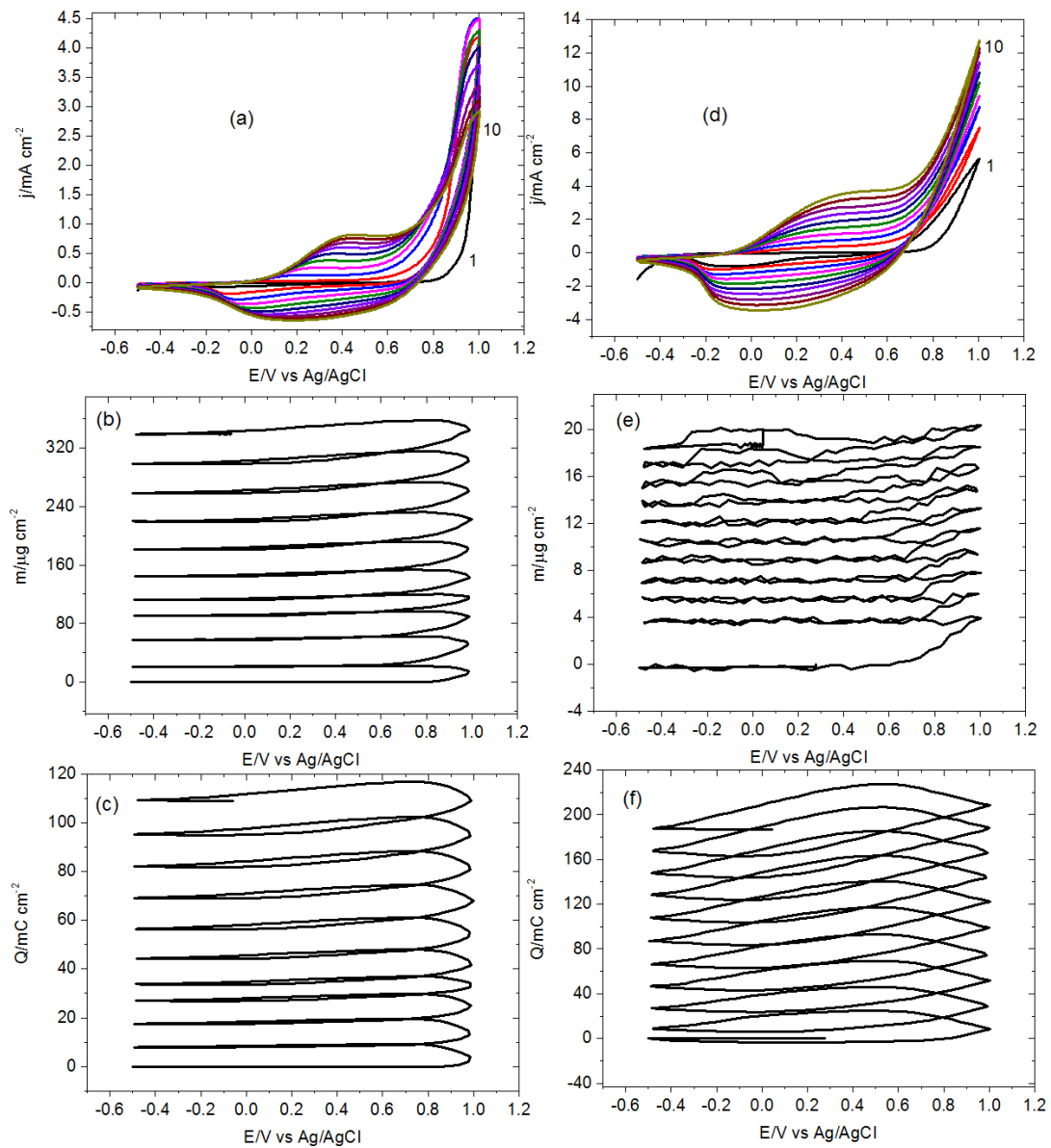


Figure 7.4. (a) electrochemical deposition of PPy film from 0.1 M pyrrole and 0.1 M NaCl (b) mass and (c) charge change of PPy film during its deposition from figure 7.5a, the scan rate, $\nu = 10 \text{ mV s}^{-1}$; (d) electrochemical deposition PPy/MWCNTs (5 wt%) film from 0.1 M pyrrole, 0.1 M NaCl and (e) mass and (f) charge change of PPy/MWCNTs composite film during its deposition from figure 7.6d, the scan rate, $\nu = 10 \text{ mV s}^{-1}$



Figure 7.5. An image of the PPy without MWCNTs

The mass-charge curves of the PPy and the PPy/MWCNTs (5 wt%) films were plotted to understand the relationship between mass and charge change during the associated electrochemical experiments. Both show a linear increase, but the gradient for the PPy film is much larger, indicating a higher efficiency for the deposition of PPy film. On the other hand, it also means that the continued cycling provides a much more electroactive and allows for the synthesis of an acoustically thick PPy/MWCNTs film. The molar masses calculated by equation 3.4 for the PPy and the PPy/MWCNTs films. The theoretical molar mass of pyrrole is 67.09 g mol^{-1} , which is a highly different the experiment finding, 98.9 g mol^{-1} . This difference, 31.8 g mol^{-1} , can be originated the content of the solvent in polymer film attributed 1.8 solvent molecules. In the case of PPy/MWCNTs film, 47.6 g mol^{-1} is lower than 67.06 g mol^{-1} , showing the lower efficiency for its deposition.

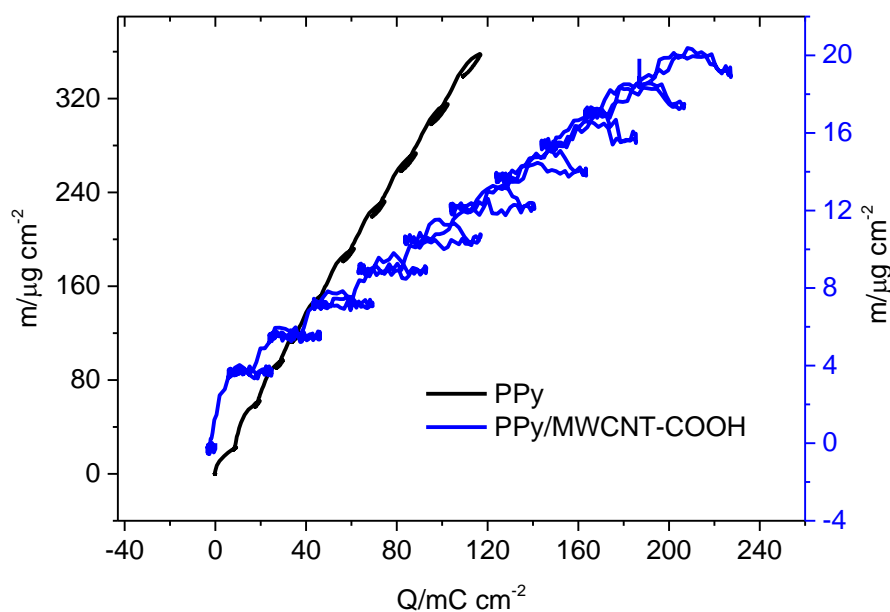


Figure 7.6. The mass-charge curves of the electrochemical deposition of the PPy (black) and the PPy/MWCNTs (blue) films, respectively from figure 7.5

The admittance data for the PPy and the PPy/MWCNTs film growth is presented in figure 7.7, showing the formation of rigid films. On the other hand, the coating of PPy film causes a shift in frequency of the quartz crystal, indicating the viscoelastic property of the polymer film. The admittance of the PPy film was 2.08 mS whilst it was 1.50 mS for the PPy/MWCNTs film. This shows the formation of an acoustically thick PPy/MWCNTs film with comparing the PPy film. The ohmic resistance (determined by

equation 3.6 mentioned in chapter 3) of the PPy/MWCNTs (666.6 Ω) composite films is much greater than the PPy (480.7 Ω) film synthesised under identical conditions.

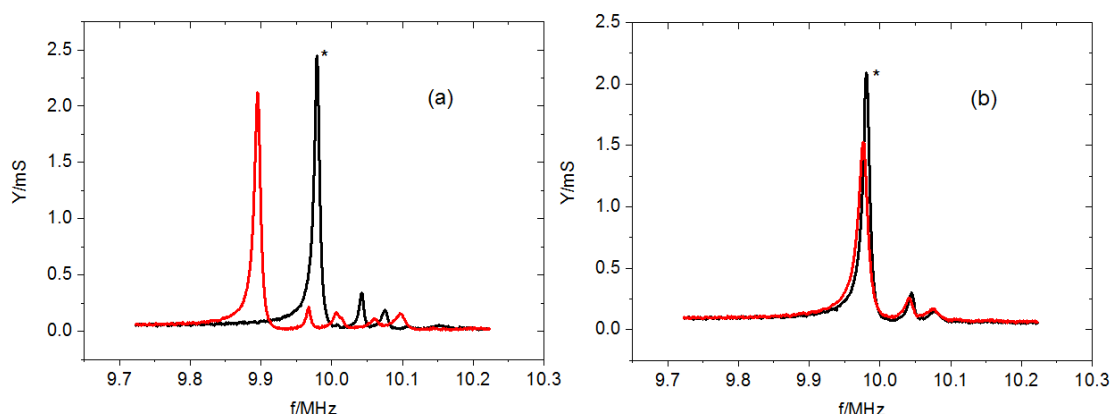


Figure 7.7. Admittance data for (a) the PPy and (b) the PPy/MWCNTs film growth from figure 7.4

7.2.1.1. Characterisation of the PPy/MWCNTs composite films

The PPy and PPy/MWCNTs (5 wt%) films were transferred to monomer-free 0.1 M NaF to obtain information regarding their electroactivity. The CV curves of such are shown in figure 7.8.

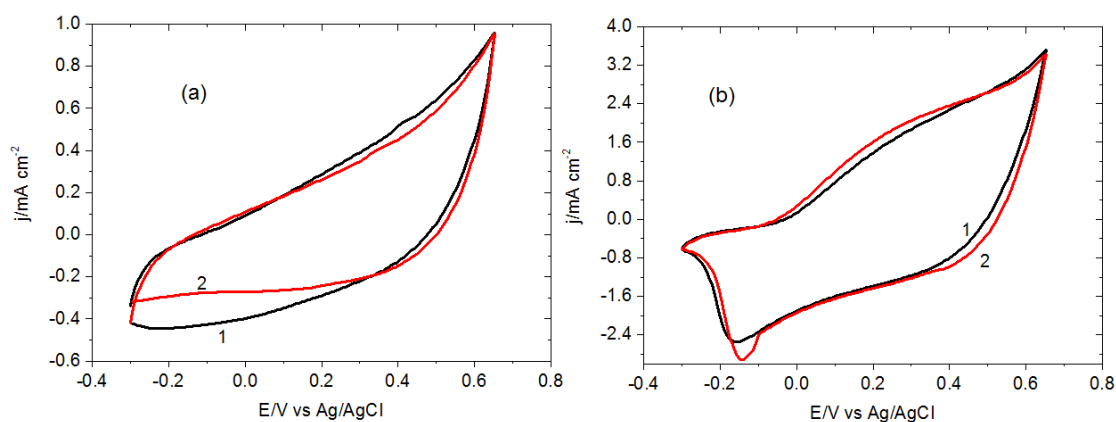


Figure 7.8. Electroactivity of (a) the PPy and (b) the PPy/MWCNTs films in monomer free 0.1 M NaF solutions, the scan rate, $v = 5 \text{ mV s}^{-1}$ (the numbers indicate the cycle number)

The existence of MWCNTs in the PPy film enhances the electroactivity significantly, as it allows for an increase in current density by a factor of four, as can be seen in figure 7.8. The corresponding EQCM data for PPy and PPy/MWCNT films in monomer-free NaF solution are also shown in figure 7.9, showing increases in their mass during the oxidation of the films, but in different amounts. This can arise due to the different thicknesses of the film, which play an important role in the ion-exchange properties of

the polymer and composite films.⁵ On the other hand, charging and discharging characteristics of the film under identical conditions are compared in figure 7.9d, which illustrate an important development in the charging and discharging characteristics for PPy/MWCNTs film. This is a valuable outcome in terms of the development of energy storage devices. Electrochemical and gravimetric data obtained from the curves are presented in table 7.1.

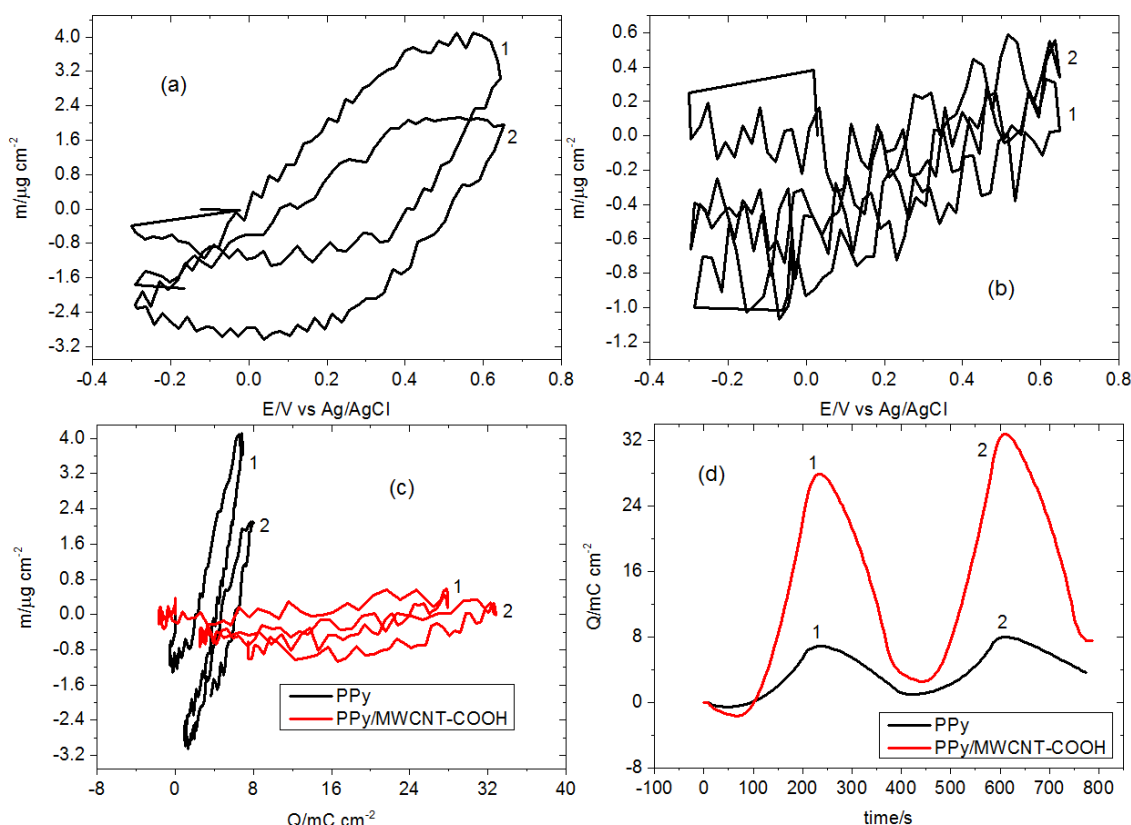


Figure 7.9. EQCM data of PPy and PPy/MWCNTs film in monomer free 0.1 M NaF, the scan rate, $\nu = 5 \text{ mV s}^{-1}$ (a) mass change of PPy film (b) mass change of PPy/MWCNTs (c) mass-charge curves for PPy and PPy/MWCNTs (d) comparison of charging and discharging characteristics of PPy and PPy/MWCNTs films under identical conditions

Table 7.1. Electrochemical data obtained from the voltammograms of the PPy and the PPy/MWCNTs films in monomer-free 0.1 M NaF (figure 7.8 and 7.9)

Film	Q/mC		$M_{app}/g \text{ mol}^{-1}$		$\Gamma/nmol \text{ cm}^{-2}$
	Q_{anodic}	$Q_{cathodic}$	during oxidation	during reduction	
PPy	13.7	11.2	72.3	125.5	764.6
PPy/MWCNTs	56.4	53.0	1.2	3.4	3618.6

7.2.1.2. Surface characterisation of the PPy and the PPy/MWCNTs films

The surface properties of the resultant polymer and composite films were investigated using two different techniques, scanning electron microscopy (SEM) and a 3D profiler (see detailed descriptions in chapters 2 and 3).

Figures 7.10 and 7.11 display the SEM images recorded for the PPy and the PPy/MWCNTs films synthesised from an aqueous medium. There is a clear difference between them, reflecting the significance of the effect of MWCNTs on the growth of the PPy film. In the case of the PPy film, in figure 7.10 a homogenous coating with a highly porous surface was observed. Conversely, the PPy/MWCNTs film has a surface roughness and a non-homogenous coating. The growth seems to occur around the walls of the MWCNTs.

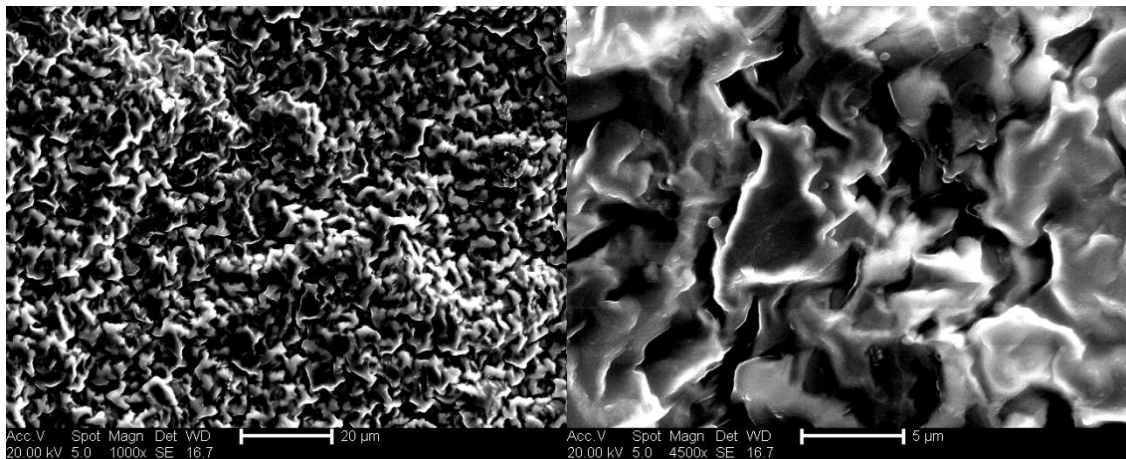


Figure 7.10. SEM images of the PPy film from aqueous medium

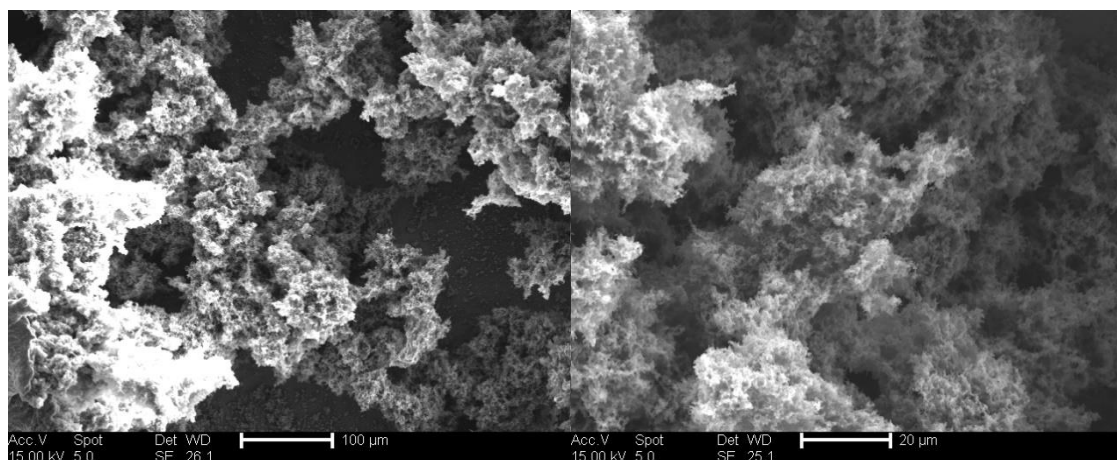


Figure 7.11. SEM image of the PPy/MWCNTs film deposited aqueous medium

3D images of the PPy and the PPy/MWCNTs films were also obtained. Figure 7.12 shows the surfaces of the PPy and the PPy/MWCNTs films obtained from an aqueous medium. While the PPy film shows a homogenous but non-uniform green surface, the PPy/MWCNTs film has a non-homogenous surface.

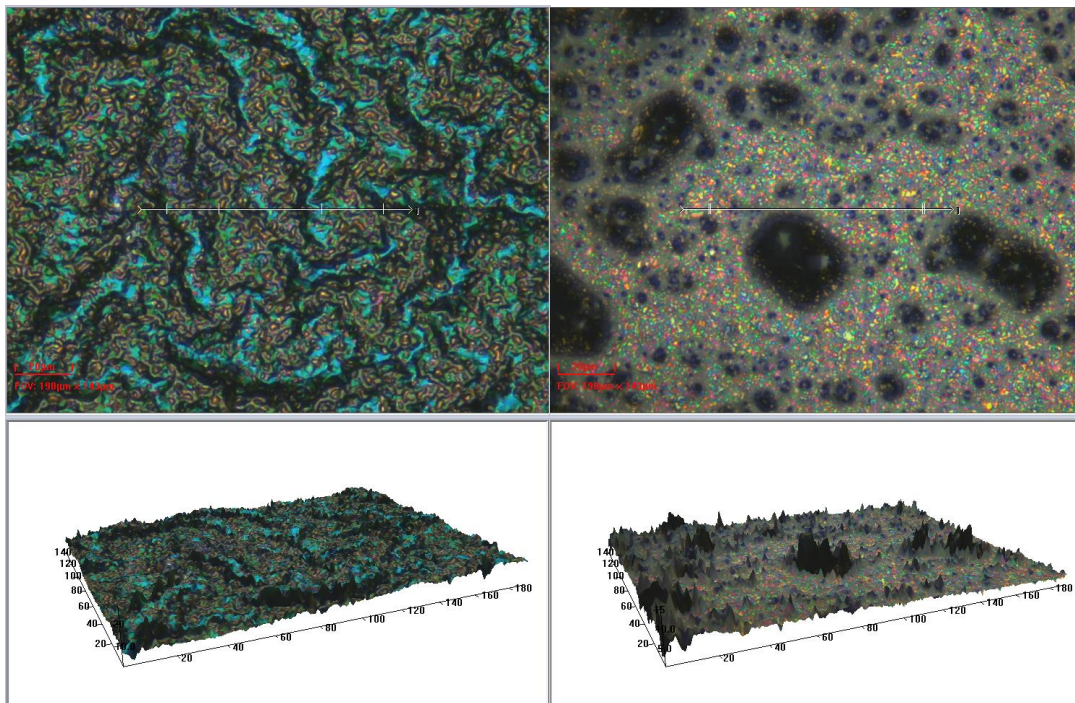


Figure 7.12. 3D images of the PPy and the PPy/MWCNTs films from aqueous medium

The findings from the electrochemical deposition of the PPy/MWCNTs film show the development of the electroactivity of the PPy film but it resulted in the lower efficiency and a poor-quality coating. This implies a novel medium, such as Ethaline, can enhance the electrochemical and physical properties of the PPy/MWCNTs film. Therefore, we focus on majorly the electrochemical deposition of the PPy/MWCNTs film in ETH200 in the second part of this chapter.

7.2.2. Electrochemical deposition of PPy film in the presence of MWCNTs in Ethaline

In the electrochemical deposition of PPy film in an aqueous medium with MWCNTs, the participation of MWCNTs in the growth of PPy film provides for the enhancement of the electrochemical properties of the PPy film but also results in lower formation efficiency and the formation of non-uniform composite films. To overcome these

difficulties, and to synthesise high-quality PPy/MWCNTs composite films, the use of Ethaline as a DES was evaluated because of the unique properties of such medium.⁶

The electrochemical deposition of PPy and PPy/MWCNTs films were applied first in 0.7 M pyrrole in ETH200 and 0.7 M pyrrole with 5 wt% MWCNTs in ETH200 between -0.4 and 1.1 V at a high scan rate of 100 mV s⁻¹. The acquired cyclic voltammograms of the PPy and the PPy/MWCNTs film growth are displayed in figure 7.13. As can be seen, the addition of MWCNTs effects the size and shape of the redox peaks of the PPy film as occurred for the PPy film deposited from an aqueous medium. The calculated cathodic charge values from the voltammograms are 0.24 mC and 0.55 mC for PPy and PPy/MWCNTs films, respectively. This means that the charge passed improves with the addition of MWCNTs in Ethaline.

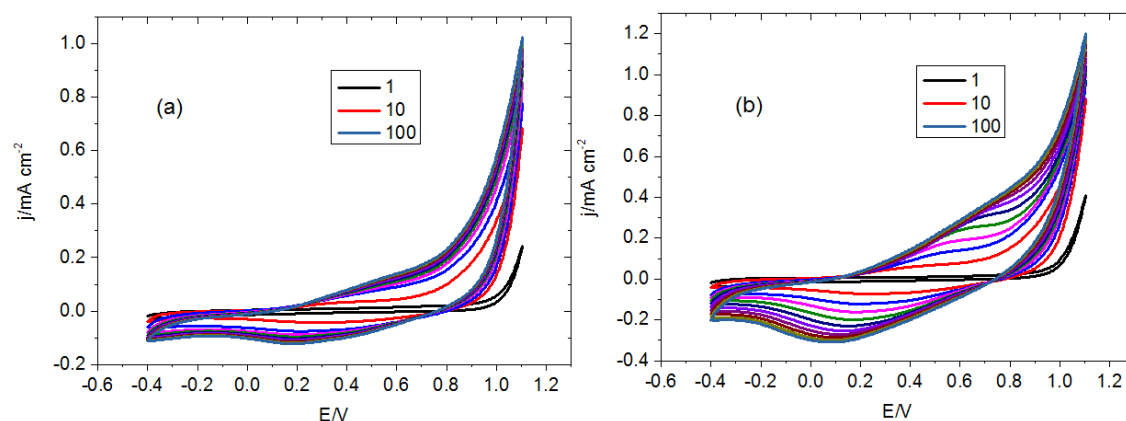


Figure 7.13. The CV curves of growth (a) the PPy film from 0.7 M pyrrole in ETH200 and (b) the PPy/MWCNTs film from 0.7 M pyrrole and 5 wt% MWCNTs in ETH200 $v = 100 \text{ mV s}^{-1}$ (the numbers indicate the number of cycles)

The effect of MWCNTs on the growth of PPy films in Ethaline was also investigated in the presence of a variety of concentrations of MWCNTs using the chronoamperometry technique. Figure 7.14 shows the results obtained from these experiments.

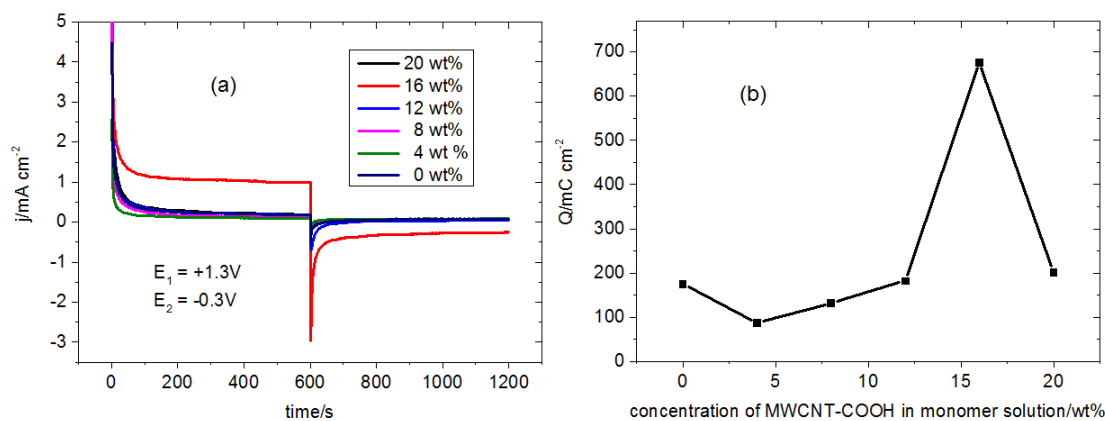


Figure 7.14. (a) Electrochemical deposition of PPy films in the presence of various concentrations of MWCNTs at 1.3 V, and the reduction of the coated films at -0.3 V (b) the charge passed during the electrochemical deposition of the PPy film versus the concentration of MWCNTs in pyrrole monomer solution in ETH200 from figure 7.14a

Initially, the charge passed decreased with the addition of MWCNTs (4 wt%) but subsequently began to increase with increasing MWCNTs until the concentration of MWCNTs was relatively high (16 wt%), at which point it suddenly decreased again. It may be noted that this is a similar outcome to that observed for aqueous medium.

Indeed, generally speaking, similar results were obtained in the Ethaline medium as had been found in the aqueous medium. The electrochemical deposition of PPy film was performed in conjunction with the EQCM technique to find the effects of mass loading with charge change. The EQCM data of the PPy/MWCNTs (5 wt%) film synthesised at the slow scan rate of $5\ mV\ s^{-1}$ is shown in figure 7.15. The resultant the PPy and the PPy/MWCNTs films were observed as homogenous black films on the quartz crystal, as shown in figure 7.16. PPy/MWCNTs film was observed as non-homogeneous from an aqueous medium.

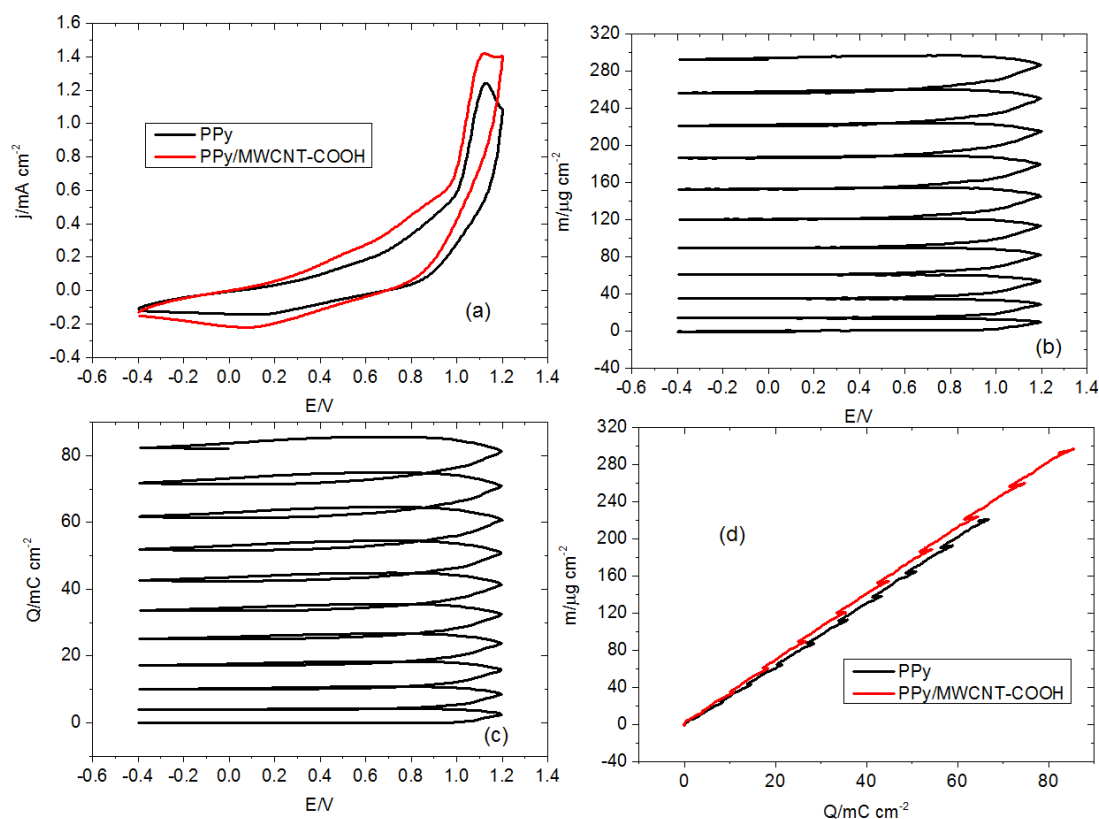


Figure 7.15. EQCM data for the electrochemical deposition of the PPy and the PPy/MWCNTs films, the scan rate, $v = 5 \text{ mV s}^{-1}$ (a) 10th scan of PPy and PPy/MWCNTs (5 wt%) film growth under identical conditions (10 cycles were applied to induce growth) (b) the mass change and (c) the charge change of PPy/MWCNTs film growth and (d) mass-charge curves of the PPy and the PPy/MWCNTs films,



Figure 7.16. Images of the PPy and the PPy/MWCNTs films synthesised in Ethaline

Both the PPy and the PPy/MWCNTs films were obtained over 10 cycles in figure 7.15. Figure 7.15a shows the 10th scan of their growth to compare their current densities. As can be seen, the current density is much greater for the PPy/MWCNTs film without shifting the peak positions to any great degree. The important outcomes of these experiments, the mass-charge curves of the PPy and the PPy/MWCNTs films in figure 7.15d, showing a high efficiency for them with compare to in aqueous medium. This is an evidence that Ethaline medium is superior to aqueous medium regarding mass

loading. The electrochemical and gravimetric data for the PPy and the PPy/MWCNTs films is reported presented in table 7.2, as are obtained from the curves shown in figure 7.15. The solvent content (α) of the PPy and the PPy/MWCNTs films determined by equation 3.5 is 0.8 per redox site of the films. This means the addition of the MWCNTs does not affect the insertion of solvent molecules into a PPy film.

Table 7.2. Electrochemical data obtained from the voltammograms of the PPy and the PPy/MWCNTs films from figure 7.15

<i>Film</i>	<i>Q/mC</i>		<i>M_{app}/g mol⁻¹</i>	<i>Γ/nmol cm⁻²</i>	<i>h/nm</i>
	<i>Q_{anodic}</i>	<i>Q_{cathodic}</i>			
<i>PPy</i>	5.17	5.22	106.0	356.4	531
<i>PPy/MWCNTs</i>	7.02	7.54	110.8	514.8	767

The admittance data for the electrochemical deposition of the PPy and the PPy/MWNCT-COOH films was also analysed in figure 7.17. The formation of both films results in a shift in frequency of the quartz crystal, with the formation of the PPy/MWCNTs film resulting in a much greater decrease in admittance. The admittance of the PPy and the PPy/MWCNTs films at the end of the respective deposition experiments were found as 0.64 (decrease from 0.69) and 0.44 (decrease from 0.80), respectively.

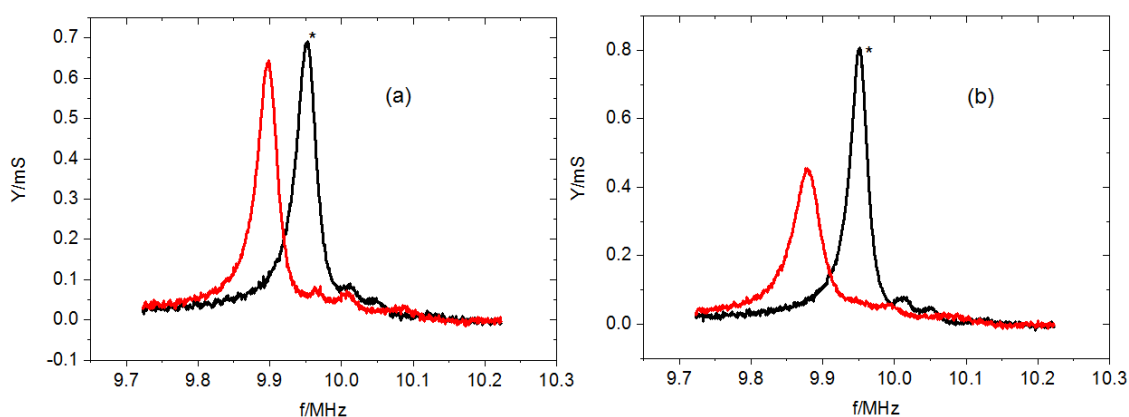


Figure 7.17. Admittance data for (a) the PPy and (b) the PPy/MWCNTs (5 wt%) films from figure 7.15

As it can be seen, the presence of 5 wt% MWCNTs raises the mass loading of the PPy film, in contrast to Pani which lowers it (see chapter 6). At this point, it is important to know the effect of the ratios of MWCNTs on the growth of PPy film in Ethaline.

Consequently, we deposited various PPy/MWCNTs composite films, namely PPy/MWCNTs (0.5 wt%), PPy/MWCNTs (1 wt%) and PPy/MWCNTs (16 wt%), as shown by the associated voltammograms in figure 7.18. They were each deposited over 4 cycles under identical conditions, the only difference in each case being the different ratio of MWCNTs in the 0.7 M pyrrole in ETHH200 medium. The cyclic voltammograms (only the 4th growth scan is shown for each) did not display any significant differences, despite the use of a wide range of the concentrations of MWCNTs (ranging from 1 to 16 wt%). On the other hand, larger amounts of MWCNTs caused a decrease in the mass loading of a PPy film, as can be seen in figure 7.18d, while a small amount increased the amount of a PPy film, as can be seen in figure 7.18c.

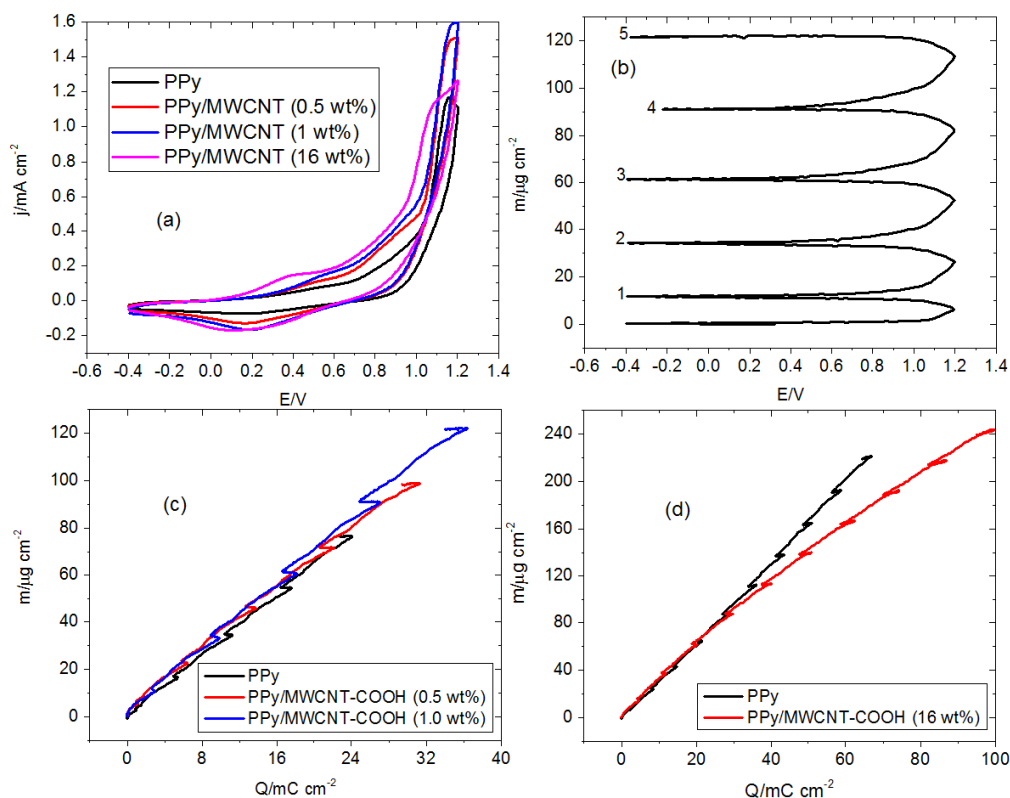


Figure 7.18. EQCM data for PPy growth in the presence of different ratios MWCNTs, $v = 5 \text{ mV s}^{-1}$ (a) CV curves of the PPy and the PPy/MWCNTs growth (4th scan showed as their last growth cycle) (b) mass-charge change for the PPy/MWCNTs (1 wt%) composite film (c) comparison of mass-charge curves of the PPy and the PPy/MWCNTs synthesised under identical conditions (d) comparison of mass-charge curves of the PPy and the PPy/MWCNTs (16 wt%) film

Table 7.3 presents the gravimetric data obtained the curves shown in figures 7.18c-d. The molar masses of the PPy/MWCNTs composite films reduce with larger amounts of MWCNTs as it provides higher surface coverage at the electrode.

Table 7.3. Electrochemical and gravimetric data for the PPy and the PPy/MWCNTs films from figure 7.18 (α is the content of the solvent molecules in the films)

<i>wt % MWCNTs in pyrrole</i>	<i>$M_{app}/g\ mol^{-1}$</i>	<i>$\alpha/per\ redox\ site$</i>	<i>$\Gamma/nmol\ cm^{-2}$</i>
0.0	100.5	0.8	344.5
0.5	100.3	0.8	520.1
1.0	107.1	0.8	664.2
16.0	77.97	0.7	676.9

7.2.2.1. Characterisation of the PPy and the PPy/MWCNTs films

The PPy and the PPy/MWCNTs films were transferred to a monomer-free ETH200 solution in order to characterise their electroactivity under identical conditions. The acquired EQCM data are presented in figure 7.19.

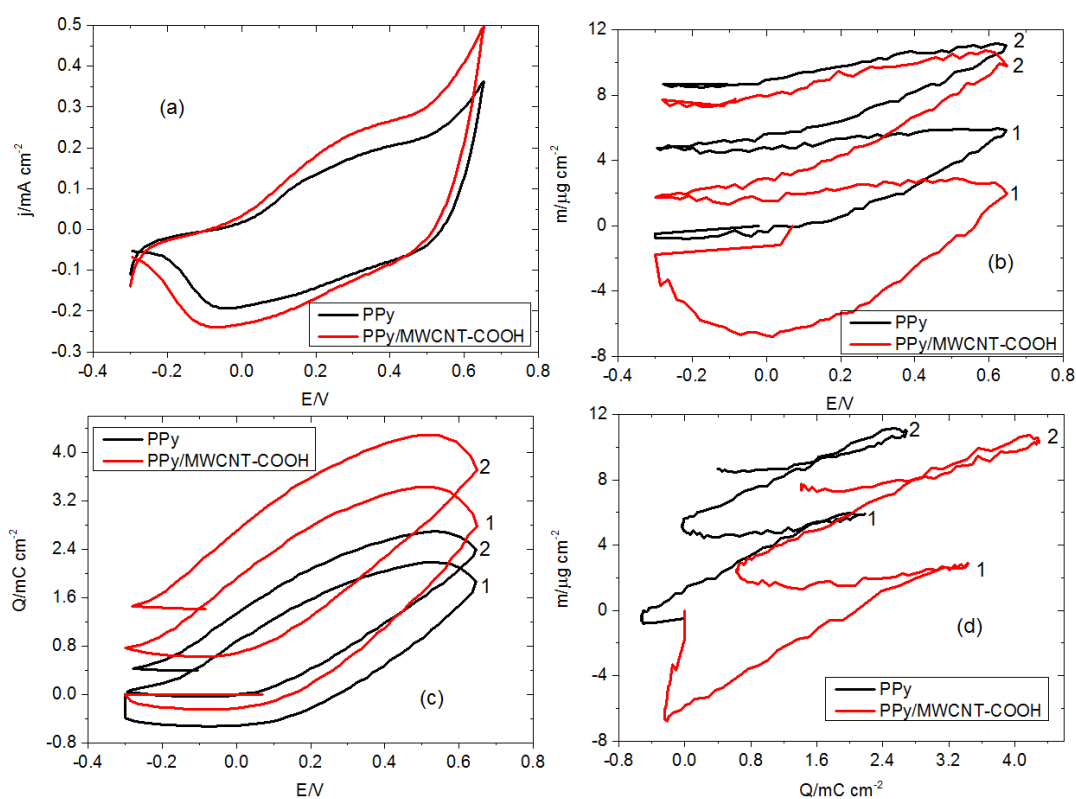


Figure 7.19. Electroactivity of the PPy and the PPy/MWCNTs (5 wt%) films in monomer-free ETH200, $v = 5\text{ mV s}^{-1}$ (a) CV curves of the PPy and the PPy/MWCNTs films in ETH200 (b) mass and (c) charge changes in the PPy and the PPy/MWCNTs films as a function of applied potential (d) mass-charge curves for the PPy and the PPy/MWCNTs films

The current density of the PPy/MWCNTs (5 wt%) film is larger than that of the PPy film, though both species otherwise present essentially similar redox peak potentials between -0.2 and 0.5 V. However, neither film shows a reversible change for their mass and charge values between their redox reactions. The electrochemical and gravimetric data obtained from these curves is presented in table 7.4. The ionic-activity of the PPy/MWCNTs film is much greater than the PPy film under identical conditions. The solvent molecules transferred during redox cycling of the PPy and the PPy/MWCNTs film was determined as 1.1 and 1.3 upon oxidation and 0.5 and 0.4 upon reduction, respectively. The mass specific capacitance (MSC) of the PPy and the PPy/MWCNTs film were evaluated, which showed the higher capacity for the PPy/MWCNTs film compared with the PPy film.

Table 7.4. Electrochemical and gravimetric data obtained from the voltammograms of the PPy and the PPy/MWCNTs film from figure 7.15

<i>Film</i>	<i>Q/mC</i>		<i>M_{app}/g mol⁻¹</i>		<i>Γ/nmol cm⁻²</i>	<i>MSC/F g⁻¹</i>
	<i>Q_{anodic}</i>	<i>Q_{cathodic}</i>	<i>During oxidation</i>	<i>During reduction</i>		
PPy	5.27	4.56	197.1	27.9	311.3	100.1
PPy/MWCNTs (5 wt%)	7.0	5.74	246.9	13.6	391.9	120.5

The charging and discharging characteristics of the PPy and the PPy/MWCNTs (5 wt%) films were compared in figure 7.20. They display quasi-reversibility but considerably increased charging for the PPy/MWCNTs film.

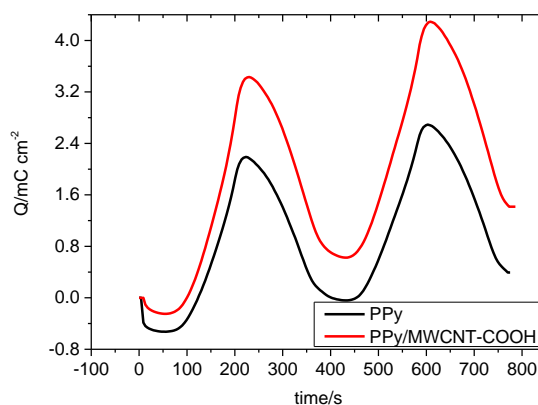


Figure 7.20. Charging and discharging properties of the PPy and the PPy/MWCNTs (5 wt%) films under identical conditions

The characterisation of the other PPy/MWCNTs composite films can be seen in figure 7.21. As it can be seen, the PPy/MWCNTs (1 wt%) film shows an improvement in current density without causing any attendant shifts in peak positions. Also, it provides a reversibility between charging and discharging for the PPy/MWCNTs film; the PPy film is not reversible, despite being synthesised under the same conditions as the PPy/MWCNTs (1 wt%) film.

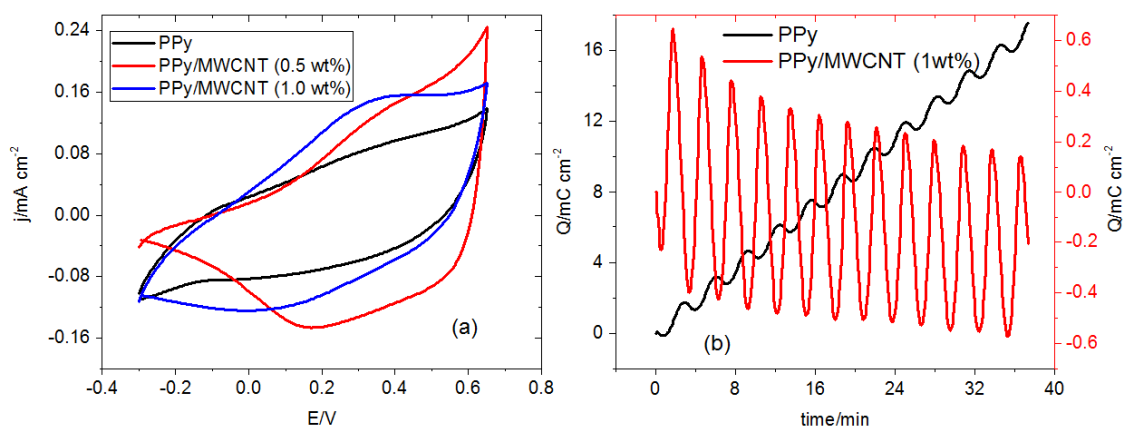


Figure 7.21. Electroactivity of the PPy/MWCNTs film synthesised with various concentrations of MWCNTs in monomer-free ETH200, $v = 5 \text{ mV s}^{-1}$ (a) CV curves of the PPy and the PPy/MWCNTs film (b) charging and discharging of the PPy and the PPy/MWCNTs films

7.2.2.2. Surface Characterisation of the PPy and the PPy/MWCNTs Films

Figures 7.22 and 7.23 reveal the surfaces of the PPy and the PPy/MWCNTs films synthesised from the non-aqueous medium, Ethaline. The PPy film has a different surface than the PPy film synthesised from an aqueous medium. It is still homogeneous, but its roughness is lower with high adherence to the quartz crystal. Similarly, the effect of MWCNTs on the surface of pyrroles is obvious, which provides the formation of firm composite films but that is still homogenous.

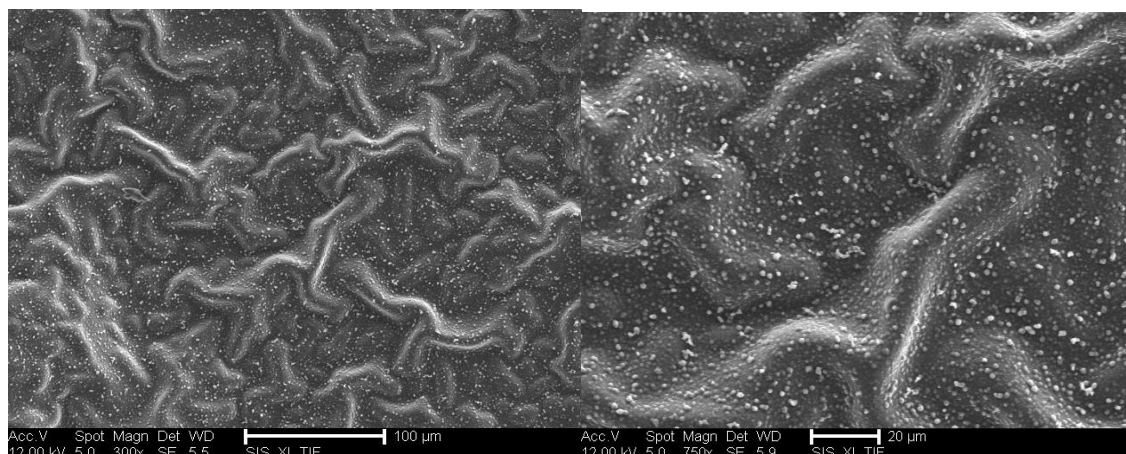


Figure 7.22. SEM images of the PPy film from ETH200

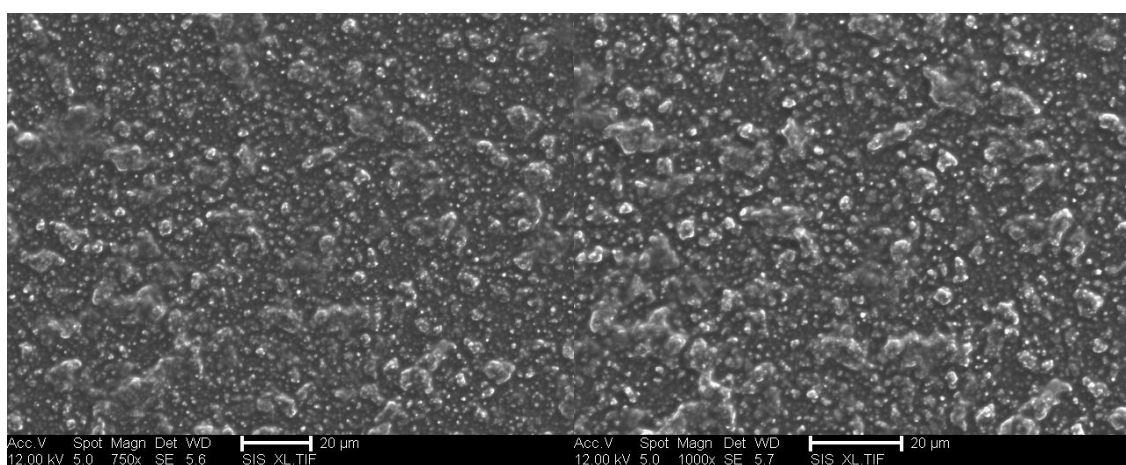


Figure 7.23. SEM images of the PPy/MWCNTs film from ETH200

In figure 7.24, the PPy film synthesised from Ethaline exhibits a uniform and homogenous surface. Conversely, the PPy/MWCNTs film formed from Ethaline shows a more ‘compact’ surface than the PPy film.

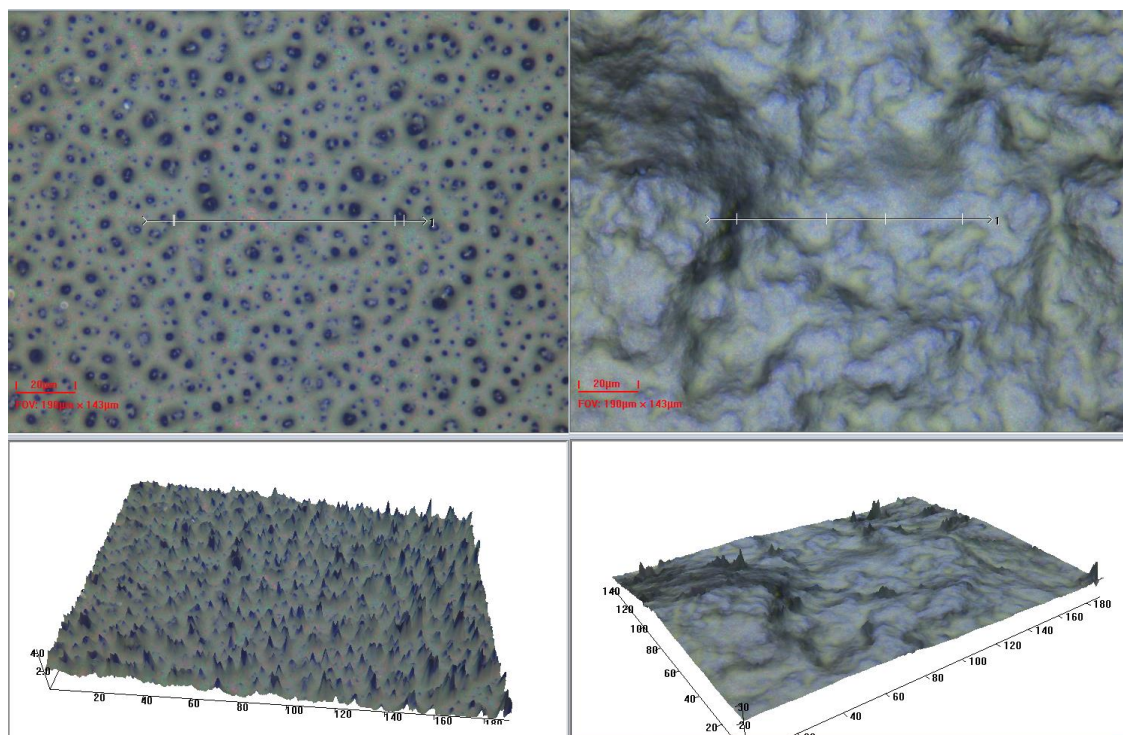


Figure 7.24. 3D images of the PPy and the PPy/MWCNTs film from Ethaline

7.2.3. FTIR

Figure 7.25 shows the FTIR spectra of the PPy and the PPy/MWCNT films from an aqueous medium. In the case of the PPy film, the features observed at 1711, 1555, and 1315 cm^{-1} are attributed to a carboxylate C=O, aromatic (in-ring) C-C, and nitro N-O functional group stretching modes, respectively. The features at 1156, 1039, and 907.56 cm^{-1} are attributed to aliphatic amines C-N, aliphatic amine C-N, and a carboxylic O-H motion, respectively. In the case of the PPy/MWCNT film, absorption was mostly observed for the same vibrational modes, with the exception the feature at 1309.3 cm^{-1} , which has been assigned to a carboxylic C-O vibration in accord with the presence of MWCNTs in the film.

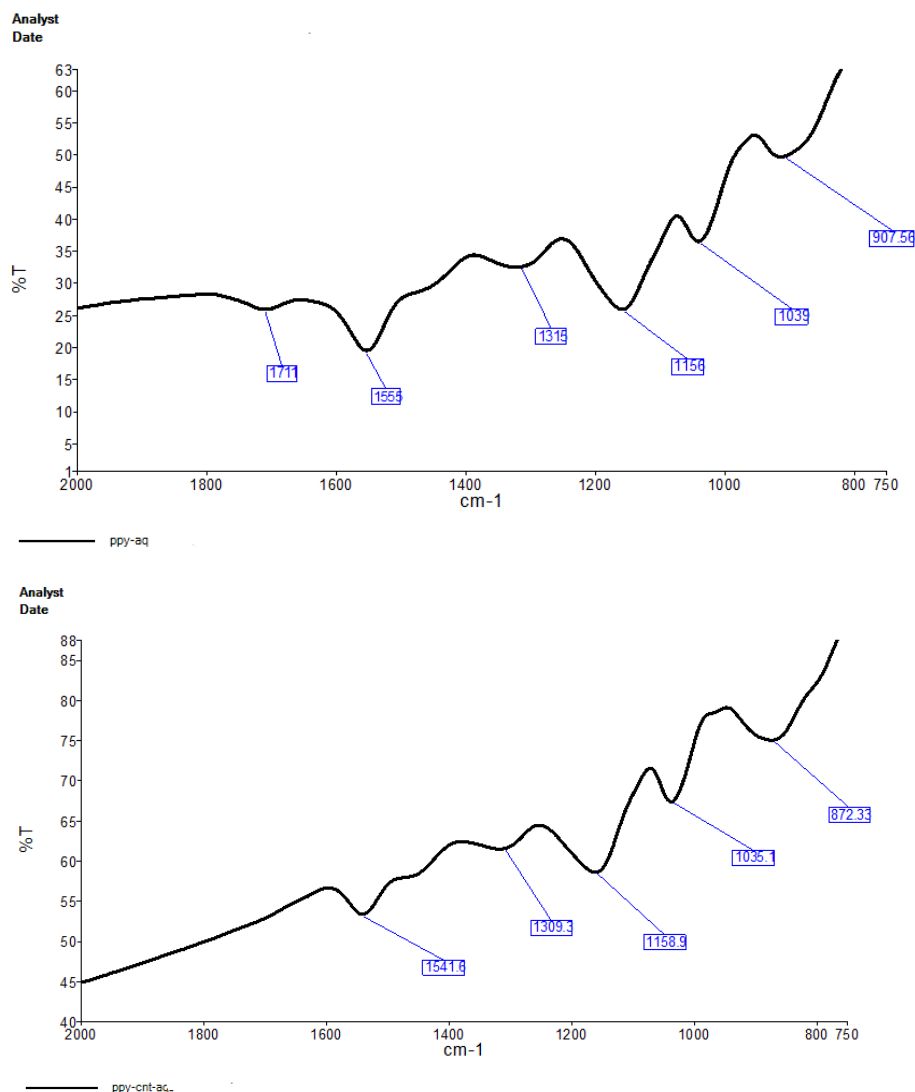


Figure 7.25. The FTIR spectra acquired for the PPy and the PPy/MWCNT films from aqueous medium

The latter examination of the FTIR was applied to the PPy film and the PPy/MWCNT composite films generated in Ethaline, as shown in figure 7.26. The feature at 1800-1700 cm⁻¹ is assigned to a C=O stretching mode and the feature at 1650-1600 cm⁻¹ to an amine N-H mode. The features at 1482, 1250 and 1176.4 cm⁻¹ are assigned to aromatic C-C, C-H, and C-N vibrational modes, respectively. The vibrational modes give almost same region; however, the peak at 1250 cm⁻¹ for the PPy film appears quite flat, which can be explained by delocalisation being much improved in the presence of MWCNTs.

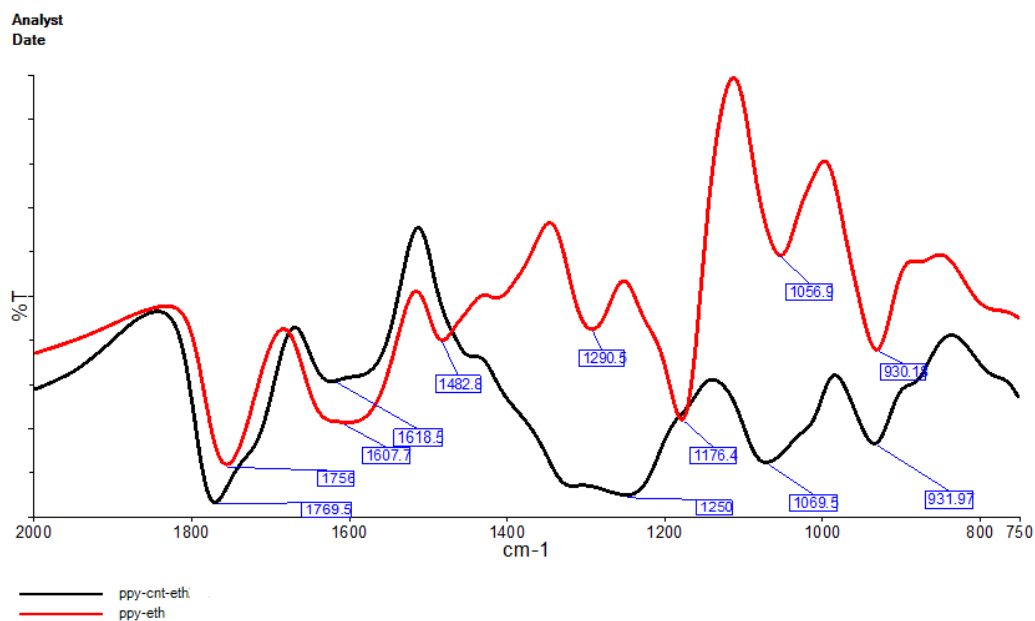


Figure 7.26. The FTIR spectrum of the PPy and the PPy/MWCNTs film from Ethaline

7.3. Conclusion

In this study, the electrochemical deposition of PPy film in different solvents, both aqueous and Ethaline media, in the absence and presence of MWCNTs, was studied. In doing so, the effects of MWCNTs on the growth of PPy film in both media was explored using the EQCM technique. During the experimental studies, several electrochemical techniques, chronoamperometry, cyclic voltammetry and EQCM, were employed. All experimental conditions were otherwise kept constant, with only the amount of MWCNTs being varied.

Initially, we performed the deposition of PPy film in the absence/presence of MWCNTs in an aqueous medium. The results showed that the presence of MWCNTs enhanced the charge transport between the film and solution during the electrodeposition of PPy film, as previously reported in the literature.^{7,8} However, it also decreases the amount of film loaded on the quartz crystal. At this point, Ethaline, as a non-aqueous medium, was used for the electrochemical deposition of PPy/MWCNTs film to enhance the electrochemical properties and the efficiency of PPy film loading on the quartz crystal. This showed the development of the mass loading and electrochemical properties of PPy/MWCNTs film with good physical properties, as subsequently determined via SEM and 3D microscopy. This outcome also supported the work of Abbott *et al.*, who

reported the species suspended in the solvent increases the participation of the particulates in the deposition.⁹ In the case of PPy, the suspended MWCNTs can stay in the monomer solution for a long time (about a week) and contribute to increasing of the ratio of MWCNTs in the composite film.

The electrochemical characterisation of the final PPy/MWCNTs composite film was applied in its background solutions. The surface coverage of the PPy and the PPy/MWCNTs (5 wt%) film synthesised in Ethaline were determined to be 311.3 nmol cm⁻² and 391.6 nmol cm⁻², while their mass-specific capacitance was found to be 100.1 ± 3.9 F g⁻¹ and 120.5 ± 5.4 F g⁻¹, respectively. In the literature, the mass-specific capacitances of PPy and PPy/MWCNTs (20 wt%) film synthesised in aqueous medium were reported to be 530 g F⁻¹ and 506 g F⁻¹, respectively.^{10,11} This indicates that Ethaline is not a suitable medium for the deposition, which is probably due to decreased charge transport.

Additionally, the spectral analysis of the composite films via FTIR showed the existence of the MWCNTs is obvious due to the spectral feature at 1309 cm⁻¹ which can be assigned to a carboxylic C-O vibration in aqueous medium. On the other hand, PPy/MWCNTs films generated in Ethaline gave a similar spectrum to PPy, except for the peak shape at 1250 cm⁻¹ which showed a narrower peak in MWCNTs. This can arise due to the participation of MWCNTs in the polymer chain.

7.4. References

- 1 A. F. Diaz, J. I. Castillo, J. A. Logan and W. Y. Lee, *Journal of Electroanalytical Chemistry*, 1981, **129**, 115-132 (DOI:10.1016/S0022-0728(81)80008-3).
- 2 C. K. Baker and J. R. Reynolds, *Journal of Electroanalytical Chemistry*, 1988, **251**, 307-322 (DOI:10.1016/0022-0728(88)85192-1).
- 3 M. A. Atieh, O. Y. Bakather, B. Al-Tawbini, A. A. Bukhari, F. A. Abuilawi and M. B. Fettouhi, *Bioinorganic Chemistry and Applications*, 2010, , 603978 (DOI:10.1155/2010/603978).
- 4 G. Z. Chen, M. S. P. Shaffer, D. Coleby, G. Dixon, W. Z. Zhou, D. J. Fray and A. H. Windle, *Advanced Materials*, 2000, **12**, 522-+ (DOI:10.1002/(SICI)1521-4095(200004)12:73.0.CO;2-S).

5 M. Miras, C. Barbero, R. Kotz and O. Haas, *Journal of Electroanalytical Chemistry*, 1994, **369**, 193-197 (DOI:10.1016/0022-0728(94)87098-5).

6 Q. Zhang, K. D. O. Vigier, S. Royer and F. Jerome, *Chemical Society Review*, 2012, **41**, 7108-7146 (DOI:10.1039/c2cs35178a).

7 J. Wang, J. H. Dai and T. Yarlagadda, *Langmuir*, 2005, **21**, 9-12 (DOI:10.1021/la0475977).

8 M. Hughes, G. Chen, M. Shaffer, D. Fray, A. Windle, *Composites Science and Technology*, 2004, **64**, 2325-2331.

9 AP. Abbott, K El. Taaib, G. Fresh, KJ. McKenzie and K. Ryder, *Physical Chemistry, and Chemical Physics*, 2009, **11**, 4269-4277 (DOI: 10.1039/b81788tj)

10 A. Snook, Pon Kao, and Adam S. Best, *Journal of Power Sources*, 2011, **196**, 1-12

11 C. Peng, S. Zhang, D. Jewell, and G. Chen, *Progress in Natural Science*, 2008, **18**, 777-788

Chapter VIII:

Conclusions and Future Work

8.1. Conclusions

In this thesis, comprehensive information regarding electroactive polymers, particularly Pani and PPy, and their applications were presented in chapter one, while the methods used in this research were described in chapter two.

The research motivations considered the growth dynamics and properties of the electroactive polymers Pani and PPy and their redox cycling. Two significantly different studies were undertaken to these ends, which demonstrated: *i*) the copolymerization of aniline with its derivatives, *o*-aminophenol, and *o*-toluidine, and the defluoridation properties of the resultant copolymer films, and *ii*) the polymerization of aniline and pyrrole in the presence of various concentrations of MWCNTs at optimum conditions in both aqueous and non-aqueous (Ethaline) media, and the enhancement of the charge transport of the final films.

In the first part of this research, *i*) the growth dynamics of Pani, PAP, and POT, and the investigation of the electrochemical properties of the final polymer films, *ii*) the growth dynamics of the Pani-PAP and the Pani-POT copolymer films using various ratios of monomers whilst maintaining total concentrations of either 0.1 M and 0.2 M, depending on experiment, *iii*) the removal of fluoride ions by the Pani-PAP and the Pani-POT film in monomer-free 0.1 M NaF electrolyte solutions (pH 6.60), were investigated.

Initially, the polymerizations of the Pani, PAP and POT films was carried out under otherwise identical conditions. The growth rate of the Pani film was much greater than those of the PAP and POT films, whilst they give different redox peaks to each other in their respective voltammograms. In particular, the peak positions of the PAP film are distinct in comparison to both the Pani and the POT film when characterized in monomer-free 1 M H₂SO₄ solutions under identical conditions. The redox peaks of the PAP film appeared around 0.25/0.24 V, while the Pani and the POT film redox peaks appeared around 0.4/0.2 V in monomer-free 1 M H₂SO₄ at 50 mV s⁻¹ (figure 4.10 in

chapter 4 and figure 5.7 in chapter 5). The growth rate of the PAP film was also lower than that found for POT. This can be explained as being due to the presence of -OH groups in the polymer backbone of *o*-aminophenol, which is more negative than the -CH₃ group in the polymer backbone of *o*-toluidine.

In the later stages, the copolymerization of the Pani-PAP and the Pani-POT films were carried out under optimal conditions. The results of this show that the *o*-aminophenol/*o*-toluidine ratio plays a significant role in the copolymerization of the Pani-PAP and the Pani-POT films because their small ratios, such as 5 mM AP in 100 mM monomer solution and 10 mM OT in 100 mM monomer solution, produced novel voltammograms that are entirely different to the voltammograms of their respective monomers. Surface coverage was increased with a decreasing amount of *o*-aminophenol/*o*-toluidine. However, applying a large number of cycles during the growth of the copolymerization experiments increased the surface coverage and the mass of the films, indicating the effect of the autocatalytic effect of Pani film.^{1, 2} In light of these results, we studied the copolymerization of the Pani-PAP and the Pani-POT films in 0.1 and 0.2 M total monomer concentrations via EQCM, keeping the ratios of *o*-aminophenol and *o*-toluidine with a certain range, such as 80-90% *o*-aminophenol/*o*-toluidine total monomer concentrations. The best copolymer composition for the Pani-PAP film was found to be (90:10) as An:*o*-AP/mM, and (80:20) as An:*o*-OT/mM for the Pani-POT film. Furthermore, in the case of the Pani-POT film, overoxidation is a negligible because the electrochemical performance of the Pani-POT film does not require a high potential because of its redox peaks positions (0.4/0.2 V) after it is synthesised at 0.90 V. This was a significant problem for POT film during the deposition and redox cycling experiments due to its high polymerization potential.³

EQCM studies were conducted for the Pani-PAP (90:10) and the Pani-POT (80:20) films at a slow scan rate of 5 mV s⁻¹ under optimal conditions to obtain high quality, electroactive and acoustically thick copolymer films. Here, the thickness is the key feature regarding the ion-exchange of the conducting polymers during their redox cycling because it increases the capacity for the removal of ions, such as fluoride, from solution.⁴ In doing so, the surface coverage values of the Pani-PAP (90:10) and the Pani-POT (80:20) films synthesised were determined to be 266.8 nmol cm⁻² and 198.2 nmol cm⁻², respectively, while their thicknesses were determined as 523 nm and 393

nm, respectively. Both copolymer films show higher electroactivity than the Pani film (I , 78.4 nmol cm⁻²). Additionally, acoustic data obtained via EQCM (see chapter 4-5) shows that continuous cycling causes a rise in the resistance of the Pani, the Pani-PAP (90:10) and the Pani-POT (80:20) films, besides which the admittance also decreases. However, the ohmic resistance of the Pani-PAP (90:10) (444.4 Ω) film is lower than that of polyaniline film (575 Ω). This showed that the copolymerization not only changes the electrochemical properties of Pani film, but also decreases the ohmic resistance through the formation of a rigid copolymer film.

The polymer and copolymer films were transferred to 1 M H₂SO₄ monomer-free background solutions in order to identify their electrochemical properties. The results show that the redox peaks of the Pani-PAP (90:10) and the Pani-POT (80:20) films appeared in different potential regions than those of polyaniline, indicating the formation of copolymer films rather than a mixture.

In a further step, the defluoridation properties of the Pani, POT, Pani-PAP (90:10) and Pani-POT (80:20) films were explored in 0.1 M NaF monomer-free solutions at pH 6.60. The defluoridation characteristics of these polymer and copolymer films are based on the ion-exchange principle related to the doping/dedoping process in the polymer matrix.⁵ This exchange occurs during the transformation of the fully reduced state (leucoemeraldine) to the half-oxidised state (emeraldine).⁶ The defluoridation properties of the PAP film were not studied because there was no a visible film on the quartz crystal after deposition, even when conducting over 100 cycles. Moreover, the POT film showed unstable behaviour with low ionic activity in monomer-free 0.1 M NaF (figure 5.17 in chapter 5). Consequently, the defluoridation experiments were mostly employed for the Pani, Pani-PAP (90:10) and Pani-POT (80:20) films in various concentrations of NaF in the absence/presence of NaCl at slow scan rates of 3, 5, and 10 mV s⁻¹.

Upon oxidation, the mass of all the films increased, which was due to the insertion of anions. Between the redox reactions, the mass changes of the films as a function of applied potential were found to be reversible. The significant ionic activity of the films in 0.1 M NaF at pH 6.60 represents a promising outcome for the development of a novel technique to remove fluoride anions from water and waste eaters without chemical contaminants. Additionally, the effect of scan rate on the defluoridation of the

copolymer film was measured in 0.1 M NaF solutions at 3, 5 and 10 mV s⁻¹, revealing a reversible change between oxidation and reduction.

The quantitative evaluation of this transfer between the copolymer and the electrolyte solution can be achieved by determining the number of electrons transferred during the redox cycling in 0.1 M NaF at 5 mV s⁻¹. In theory, a Pani film and its copolymers, the Pani-PAP and the Pani-POT films, must take 0.5 mol ion per redox site of the polymer film, attributing 91.2 mg F⁻ g⁻¹. The Pani, Pani-PAP (90:10), and Pani-POT (80:20) films synthesised in this study took 0.25, 0.35 and 0.35 mol fluoride ion per redox site, respectively. The copolymer films take the same amount, but much more than the Pani film. This proves that the copolymerization of aniline with *o*-aminophenol/*o*-toluidine enhances the ion exchange capability of polyaniline. The corresponding mass values of fluoride ions taken up by the Pani, Pani-PAP and Pani-POT films were determined to be 51.6 ± 1.0 mg g⁻¹, 65.0 ± 0.6 mg g⁻¹ and 66.8 ± 1.8 mg g⁻¹, of fluoride ions, respectively, in 0.1 M NaF. In all cases, however, the amount of fluoride removed is much greater than the capacities of the available techniques reported in the literature^{7, 8} to date, which are 0.78 mg g⁻¹ and 20 mg g⁻¹ at 1.5 V for pure Pani. Additionally, Karthikeyan *et al.* reported the removal of fluoride ions by polyaniline/alumina and polypyrrole/alumina as being 6.6 mg/g and 8 mg/g in acidic media, respectively.⁹ Both techniques take up a smaller amount of fluoride despite utilizing a high potential and acidic media. Also, films reported in the literature are severely hampered by being one-time usage only, while the copolymer films synthesised in this research can be used repeatedly. Regeneration experiments showed the copolymer films can be used successively without chemical contamination.

In the last stage of this section, the morphologies of the acquired copolymer films and their corresponding homopolymers were explored using SEM, as described in chapter 2. The Pani film exhibits a uniform and highly porous surface, whilst the Pani-PAP (90:10) film was formed of interwoven fibres (with spherical particulates). The different morphology of the copolymer compared to the morphologies of the homopolymers strongly support the assumption of the formation of a true copolymer instead of a mix of homopolymers.

The next study considered the development of the charge transport process of Pani and PPy film with the addition of MWCNTs in Ethaline medium, rather than in an aqueous medium. For this purpose, the walls of the MWCNTs were functionalised in concentrate HNO_3 , providing a strong interaction between monomers and MWCNTs (see chapter 3).

The effects of MWCNTs on the growth of Pani and PPy films in an aqueous medium by cyclic voltammetry and chronoamperometry were considered. A higher concentration of MWCNTs in the monomer solutions caused an increase in the current densities of the redox peaks, resulting in shifts to more positive potentials. In a similar manner, EQCM experiments revealed the enhancement of the current densities of the redox peaks with an increasing amount of MWCNTs in the monomer solutions, but a decrease in the mass loading of the polymer films, while they gave non-homogenous films with high roughness. Considering the above, Ethaline was used instead of the aqueous medium due to its high ionic strength, which made it possible to have large amounts of the dopant anions in solution, as well as its low volatility, low toxicity, wide potential window, and cost-effectiveness.

In the case of Ethaline, similar results were acquired as for the aqueous medium, showing a larger amount of MWCNTs resulted in a lower efficiency for both polymer films, though this was increased with lower amounts of MWCNTs; when the level of MWCNTs was decreased in the monomer solutions, this resulted in a much more efficient coating. This probably occurred due to the high viscosity of Ethaline, providing an increase in the participation of MWCNTs in the polymer films. This assumption was also supported by the work of Abbott *et al.*, who reported the suspended species increases the composition of composite materials.¹⁰

The characterisation of the electroactivity of the composite films synthesised in Ethaline was carried out in 1 M H_2SO_4 -ETH200 and ETH200 monomer-free solutions, respectively. The results indicated the development of a charge transport process in monomer-free solutions. Furthermore, the PPy/MWCNTs showed a reversible change between the oxidation and reduction reactions that also demonstrated high electroactivity.

The mass-specific capacitance of the composite films synthesised in Ethaline was determined by cyclic voltammetry, which were $1170.1 \pm 44.7 \text{ F g}^{-1}$ for Pani/MWCNTs, $792.8 \pm 10.5 \text{ F g}^{-1}$ for Pani under identical conditions, and $120.5 \pm 5.4 \text{ F g}^{-1}$ for PPy/MWCNTs, and $100.1 \pm 3.9 \text{ F g}^{-1}$ for PPy under identical conditions. The reports in the literature show that the theoretical specific capacitance of pure Pani and PPy films are 750 F g^{-1} and 620 F g^{-1} , whilst their measured mass specific capacitance has been determined to be 240 F g^{-1} and 530 F g^{-1} , respectively.¹¹ Additionally, the mass-specific capacitance of Pani/MWCNTs and PPy/MWCNTs films obtained in aqueous medium were found to be 670 F g^{-1} and 530 F g^{-1} , respectively.¹² Also, the maximum specific capacitance of graphene materials was reported to be 205 F g^{-1} in the literature.¹³ Consequently, we can conclude the mass-specific capacitance of Pani/MWCNTs film was significantly improved in Ethaline but it resulted in a decrease in the mass-specific capacitance of PPy/MWCNTs film.

The findings showed that the enhancement in the capacitances of both Pani and Pani/MWCNTs films was considerable in Ethaline, which offers a promising technique for the development of the capacitance of energy storage devices.

8.2. Future Work

The results presented above regarding Pani-PAP and Pani-POT copolymer films are promising in the sense of the removal of fluoride ions from drinking water and wastewater because they represent a cost-effective, easy to use solution that does not result in chemical contamination. This gives an excellent opportunity for the future design of water purification systems, and so on.

In the meantime, the results presented regarding the studies of the Pani/MWCNT and PPy/MWCNT in an Ethaline medium indicate interesting behaviour in terms of their surface and electrochemical characteristics. This could be further investigated in the presence of various DESs in order to obtain an in-depth understanding of the mechanisms of formation and charge transport processes. Also, this could lead to the emergence of novel pseudo-capacitors based on polymer composite films.

8.3. References

- 1 Y. Wei, R. Hariharan and S. A. Patel, *Macromolecules*, 1990, **23**, 758-764 (DOI:10.1021/ma00205a011).
- 2 Y. Wei, G. W. Jang, C. C. Chan, K. F. Hsueh, R. Hariharan, S. A. Patel and C. K. Whitecar, *Journal of Physical Chemistry*, 1990, **94**, 7716-7721 (DOI:10.1021/j100382a073).
- 3 J. Lippe and R. Holze, *Journal of Electroanalytical Chemistry*, 1992, **339**, 411-422 (DOI:10.1016/0022-0728(92)80465-G).
- 4 R. M. Torresi, S. I. C. Detorresi, C. Gabrielli, M. Keddad and H. Takenouti, *Synthetic Metals*, 1993, **61**, 291-296 (DOI:10.1016/0379-6779(93)91275-7).
- 5 Y. Zhang, S. Mu, B. Deng and J. Zheng, *Journal of Electroanalytical Chemistry*, 2010, **641**, 1-6 (DOI:10.1016/j.jelechem.2010.01.021).
- 6 M. Miras, C. Barbero, R. Kotz and O. Haas, *Journal of Electroanalytical Chemistry*, 1994, **369**, 193-197 (DOI:10.1016/0022-0728(94)87098-5).
- 7 H. Cui, Q. Li, Y. Qian, R. Tang, H. An and J. Zhai, *Water Research*, 2011, **45**, 5736-5744 (DOI:10.1016/j.watres.2011.08.049).
- 8 M. Karthikeyan, K. K. Satheeskumar and K. R. Elango, *Journal of Hazardous Materials*, 2009, **163**, 1026-1032 (DOI:10.1016/j.jhazmat.2008.07.057).
- 9 M. Karthikeyan, K. Kumar, K. Elango, *Journal of Fluor Chemistry*, 2009, **130**, 894-901.
- 10 AP. Abbott, K El. Ttaib, G. Frish, KJ. McKenzie and K. Ryder, *Physical Chemistry, and Chemical Physics*, 2009, **11**, 4269-4277 (DOI: 10.1039/b81788tj)
- 11 C. Peng, S. Zhang, D. Jewell and G. Z. Chen, *Progress in Natural Science-Materials International*, 2008, **18**, 777-788 (DOI:10.1016/j.pnsc.2008.03.002).
- 12 A. Snook, Pon Kao, and Adam S. Best, *Journal of Power Sources*, 2011, **196**, 1-12
- 13 Y. Wang, Z. Shi, Y. Huang, Y. Ma, C. Wang, M. Chen, and Y. Chen, *American Chemical Society*, 2009, **113**, 13103-13107 (DOI: 10.1021/jp902214f).